



THE UNIVERSITY *of* EDINBURGH

This thesis has been submitted in fulfilment of the requirements for a postgraduate degree (e.g. PhD, MPhil, DClinPsychol) at the University of Edinburgh. Please note the following terms and conditions of use:

This work is protected by copyright and other intellectual property rights, which are retained by the thesis author, unless otherwise stated.

A copy can be downloaded for personal non-commercial research or study, without prior permission or charge.

This thesis cannot be reproduced or quoted extensively from without first obtaining permission in writing from the author.

The content must not be changed in any way or sold commercially in any format or medium without the formal permission of the author.

When referring to this work, full bibliographic details including the author, title, awarding institution and date of the thesis must be given.

A Study of Regulatory Mechanisms of Glycolytic and Gluconeogenic Enzymes

by

Meng Yuan

Thesis Presented for the Degree of Doctor of Philosophy



School of Biological Sciences

University of Edinburgh

Edinburgh, UK

2016

Abstract

Many diseases correlate with abnormal glucose metabolism in cells and organisms. For instance, the human M2 isoform of the glycolytic enzyme pyruvate kinase (M2PYK) plays an important role in metabolic reprogramming of tumour cells whereby aerobic glycolysis or the ‘Warburg effect’ supports cell proliferation by accumulating necessary biomass. By contrast, gluconeogenesis may play an important role, as observed in certain types of trypanosomatid parasites (e.g. the amastigote form of *Leishmania major*) where anabolism is essential for infectious properties. Hence, these glucose metabolising enzymes are important potential drug targets for cancer and trypanosomiasis. However, many aspects of their regulatory mechanisms are still poorly understood.

This thesis describes biochemical and structural studies on M2PYK and on *L. major* fructose-1,6-bisphosphatase (*LmFBPase*), providing insights into allosteric mechanisms and structure-based drug design for both enzymes. Human PYKs and *LmFBPase* were expressed and purified from *Escherichia coli*, and their kinetics were fully characterised. It was shown that certain amino acids regulate the activity of M2PYK allosterically, but in opposite ways, with some being inhibitors and others activators. X-ray crystallographic structures and biophysical data of M2PYK complexes with alanine, phenylalanine, serine or tryptophan reveal an R-/T-state oscillating model of M2PYK involving a 11° rotation of each subunit. In addition, M2PYK was demonstrated to be a redox-sensitive enzyme. Reducing reagents were shown to help maintain the tetramer and prevent its dissociation, and thereby to activate M2PYK, whereas oxidation and nitrosylation reagents functioned in the opposite sense. Nitrosylation assays showed that the main nitrosylated residue is Cys326 of M2PYK, which is located on the tetramer interface. Dynamics and modulator effects of PYKs were further studied by hydrogen–deuterium exchange by mass spectrometry. These observations highlight the important effects of amino acids on M2PYK regulation. M1PYK by contrast, was demonstrated to be a constitutively fully active pyruvate kinase, with minor effects from modulators.

The gluconeogenic enzyme fructose-1,6-bisphosphatase (FBPase) is a potential drug target against leishmaniasis. Here we present biochemical and structural studies for *Lm*FBPase, by characterising its activity in a metal-dependent reaction, as well as its inhibition by AMP. The crystal structure of *Lm*FBPase is a homotetramer, composed of monomers with alternating $\alpha/\beta/\alpha/\beta/\alpha$ ‘club sandwich’ topologies. In comparison with previously revealed *Lm*FBPase structures, the AMP-complexed structure shows a rotated form of the tetramer. Comparisons of the structures reveal an ‘unlock-and-rotate’ allosteric mechanism in which AMP binding causes a series of structural changes culminating in an incomplete and non-productive active site. The structure of the effector site of *Lm*FBPase shows a different conformation from human FBPases, thereby offering a potential specific target for *Leishmania*.

Lay Summary

Many diseases correlate with abnormal glucose metabolism in cells and organisms. For instance, modulation of a glycolytic enzyme pyruvate kinase can promote cancer cell proliferation by reprogramming metabolite biosynthesis. In this study, it is discovered that amino acids are regulatory factors of pyruvate kinase. Intriguingly, some amino acids inhibit the activity of pyruvate kinase, and others activate it. By combining biophysical, biochemical and structural approaches, we revealed the mechanism of the effects of amino acids on pyruvate kinase. Amino acids trigger changes in the shape of pyruvate kinase, and thereby either activate or inhibit its activity.

Leishmania are microscopic single cell parasites that cause a spectrum of diseases, including a visceral form which is responsible for up to 40,000 deaths annually worldwide. The gluconeogenic enzyme fructose-1,6-bisphosphatase has been proposed as a potential drug target against *Leishmania*. In the current study, the mechanism of regulating the enzymic activity of fructose-1,6-bisphosphatase is revealed by generating “3D pictures” of different states of the enzyme. Further, we showed that the structure of an important site of *Leishmania* fructose-1,6-bisphosphatase shows a different conformation from that of human fructose-1,6-bisphosphatase, thereby offering a potential specific target for *Leishmania*.

Declaration

I hereby declare that the research presented in this thesis and the thesis itself have been composed and originated completely by myself at The University of Edinburgh, United Kingdom, except when otherwise stated. This thesis has not been submitted in whole or partially for any other degree.

Meng Yuan

Acknowledgments

First and foremost, I would like to thank my supervisor Professor Malcolm D. Walkinshaw. It is quite an honour to be his PhD student. He devotes his knowledge, time, encouragement and unconditional support to me. He has taught me how good science is done. As a supervisor, he has helped me more than one could ask for.

I am also deeply grateful for the endless help of Dr Linda Gilmore. From the first year of my PhD until now, she has spent hundreds of hours talking to me, listening to my naive ideas, reading and advising on all my works. She has been so patient in guiding me and inspiring me, because of nothing but her kindness.

I would like to thank all the members on the third floor of Swann Building. Dr Iain McNae taught me X-ray crystallography. Dr Martin Wear, Dr Liz Blackburn, Dr Matthew Nowicki, Dr Janice Bramham offered their help on the protein production and biophysical assays. Professor Paul Michels taught me a lot on microbiology and parasitology. Dr Wenhe Zhong, Dr Rosie Mitchell, Dr Hugh Morgan, Dr Montserrat Vasquez-Valdivieso, and Yiyuan Chen taught me the experiments practically. Not to mention Dr Li Hsuan Yen—I asked for his help for almost anything.

I also want to thank Professor Ted Hupp for his help on the immunoassays and HD-exchange experiments. Some of my important assays were carried out in his laboratory. Dr Rafael Homem from Institute of Molecular Plant Sciences taught me to do the biotin-switch assay. Joar Pinto from Vrije Universiteit Brussel taught me to make nanobodies. Additionally, I thank Professor Lenka Hernychová from Masaryk University for doing the HD-exchange experiment.

I gratefully acknowledge the Darwin Trust of Edinburgh for funding me and making my PhD work possible. I also thank the Biochemical Society and Institute of Structural and Biological Sciences for funding me to attend conferences.

I would like to give my special gratitude to my parents. Without their love throughout my life, I would never be so happy and fearless. Lastly, to my beloved fiancée, Jia Ning. She witnesses my manic laughter and agony that underpins my doctoral life span, and the life span that follows.

List of abbreviations

1,3PG	1,3-Bisphosphoglycerate
2PG	2- Phosphoglycerate
3PGA	3-Phosphoglycerate
AC ₅₀	Half-maximum activating concentration
ADP	Adenosine 5'-diphosphate
ALD	Aldolase
ALT	Alanine transaminase
AMP	Adenosine 5'-monophosphate
ATP	Adenosine 5'-triphosphate
BSA	Bovine serum albumin
CCD	Charge-coupled device
CCP4	Collaborative Computational Project Number 4
CDC	Centers for Disease Control and Prevention
CL	Cutaneous leishmaniasis
CV	Column volume
DAPk	Death-associated protein kinase
DDB2	DNA damage-binding protein 2
DHAP	Dihydroxyacetone phosphate
DLS	Dynamic light scattering
DMSO	Dimethyl sulfoxide
DND <i>i</i>	Drugs for Neglected Diseases <i>initiative</i>
EDTA	Ethylenediaminetetraacetic acid
EGFR	Epidermal growth factor receptor
ELISA	Enzyme-linked immunosorbent assay
ENO	Enolase
ERK	Extracellular signal-regulated kinase
F16BP	Fructose 1,6-bisphosphate
F26BP	Fructose 2,6-bisphosphate
F6P	Fructose 6-phosphate
FBPase	Fructose-1,6-bisphosphatase
FBPase-2	Fructose-2,6-bisphosphatase
FGFR	Fibroblast growth factor receptor

G3P	Glyceraldehyde 3-phosphate
G6P	Glucose 6-phosphate
G6Pase	Glucose-6-phosphatase
G6PDH	Glucose-6-phosphate dehydrogenase
GAPDH	Glyceraldehyde 3-phosphate dehydrogenase
GLUT1	Glucose transporter 1
GPDH	Glycerol-3-phosphate dehydrogenase
GPI, PGI	Glucose-6-phosphate isomerase, Phosphoglucoisomerase
GSH	L-glutathione
HAT	Human African trypanosomiasis
HDX	Hydrogen–deuterium exchange
HDX–MS	Hydrogen–deuterium exchange with mass spectrometry
HIF	Hypoxia-inducible factor
hnRNPs	Heterogeneous nuclear ribonucleoproteins
<i>hs</i>	<i>Homo sapiens</i>
HX	hexokinase
IC ₅₀	Half maximal inhibitory concentration
IMAC	Immobilised metal ion affinity chromatography
IPTG	Isopropyl β-D-1-thiogalactopyranoside
<i>k_{cat}</i>	Turnover number
kDa	Kilodalton
<i>K_i</i>	Inhibitor constant
<i>K_m</i>	Michaelis constant
KPSI	Kilopound per square inch
LB	lysogeny broth
LC	Liquid chromatography
LDH	L-lactate dehydrogenase
LIDAEUS	Ligand Discovery At Edinburgh UniverSity
<i>Lm</i>	<i>L. major, Leishmania major</i>
LPYK	Liver isoenzyme of pyruvate kinase
M1PYK	M1-isoenzyme of pyruvate kinase
M2PYK	M2-isoenzyme of pyruvate kinase
MLC	Myosin light chain
MMTS	S-methyl methanethiosulfonate

MRSA	Methicillin-resistant <i>Staphylococcus aureus</i>
MS	Mass spectrometry
mTOR	mechanistic target of rapamycin
mTORC	mechanistic target of rapamycin complex
NADH	β -nicotinamide adenine dinucleotide
NADP ⁺	β -nicotinamide adenine dinucleotide phosphate
NTD	Neglected tropical disease
OCT	Octamer-binding transcription factor
OD	Optical density
PAR	Poly-ADP ribose
PBS	Phosphate-buffered saline
PBS-CM	Dulbecco's phosphate-buffered saline without calcium and magnesium
PC	Pyruvate carboxylase
PCR	Polymerase chain reaction
PDB	Protein Data Bank
PEG	Poly(ethylene glycol)
PEP	Phosphoenolpyruvate
PEPCK	Phosphoenolpyruvate carboxykinase
PFK	Phosphofructokinase
PFK-2	Fructose-6-phosphate-2-kinase
PGK	Phosphoglycerate kinase
PGM	Phosphoglycerate mutase
pI	Isoelectric point
PI3K	Phosphoinositide 3-kinase
PIAS	Protein inhibitor of activated STAT
PIM2	Proviral insertion in murine lymphomas 2
PIN1	Peptidyl-prolyl <i>cis-trans</i> isomerase NIMA-interacting 1
PKB, Akt	Protein kinase B
PML	Promyelocytic leukemia
PPP	Pentose phosphate pathway
PRPP	Phosphoribosyl pyrophosphate
PTB	Polypyrimidine-tract binding
PTM	Post-translational modification
PYK	Pyruvate kinase

R5P	Ribose 5-phosphate
RMSD	Root mean square deviation
RNAi	RNA interference
rpm	Revolutions per minute
RPYK	Red blood cell isoenzyme of pyruvate kinase
SAICAR	Succinyl-5-aminoimidazole-4-carboxamide-1-ribose-5'-phosphate
sdAb	Single-domain antibody
SDS	Sodium dodecyl sulfate
SDS-PAGE	Sodium dodecyl sulfate-polyacrylamide gel electrophoresis
SEC	Size-exclusion
SOC	Super Optimal Broth
SRSF	Serine/arginine-rich splicing factor
STAT	Signal transducer and activator of transcription
SUMO	Small ubiquitin-related modifier
T3	Triiodo-L-thyronine
<i>Tb</i>	<i>T. brucei</i> , <i>Trypanosoma brucei</i>
<i>Tc</i>	<i>T. cruzi</i> , <i>Trypanosoma cruzi</i>
TCA	Tricarboxylic acid
TCEP	Tris(2-carboxyethyl)phosphine
TDA	Thermal denaturation assay, thermal shift assays
TEA	Triethanolamine
TEMED	<i>N,N,N',N'</i> -tetramethylethylenediamine
TLS	Translation libration screw
T_m	Transition temperature
TPI	Triosephosphate isomerase
Tris	Tris(hydroxymethyl)aminomethane
TY	Tryptone Yeast medium
UV	Ultraviolet
V_{HH}	Variable domain of heavy chain antibody
VL	Visceral leishmaniasis
WHO	World Health Organization

Table of Contents

Abstract	i
Lay Summary	iii
Declaration	v
Acknowledgments	vii
List of abbreviations	ix
Table of Contents	xiii
List of Figures	xix
List of Tables	xxiii
CHAPTER 1. Introduction	1
1.1 Glucose metabolic enzymes are important drug targets	2
1.1.1 Targeting glycolytic enzymes for cancer therapeutics	2
1.1.2 Targeting gluconeogenic enzymes against diabetes	5
1.1.3 Targeting glucose metabolic enzymes against diseases caused by pathogens	5
1.2 M2-type pyruvate kinase is an important target for cancer therapeutics	6
1.2.1 Pyruvate kinase is a glycolytic enzyme	6
1.2.2 Isoenzymes and alternative splicing of human PYKs	7
1.2.3 Structures of pyruvate kinases	11
1.2.4 Catalytic mechanism of pyruvate kinase	15
1.2.5 The role of M2PYK in cancer.....	17
1.2.5.1 Metabolic needs of proliferating cells	17
1.2.5.2 M2PYK promotes tumorigenesis by regulating the Warburg effect.....	18
1.2.5.3 Non-metabolic functions of M2PYK	20
1.2.5.4 Subcellular localisation of M2PYK	21
1.2.5.5 Extracellular M2PYK promotes angiogenesis	22
1.2.6 M2PYK is a cancer marker.....	22
1.2.7 Regulation of M2PYK	24

1.2.7.1 Regulation of M2PYK expression.....	26
1.2.7.2 Regulation of M2PYK activity by post-translational modifications	27
1.2.7.3 Regulation of M2PYK activity by native mutations	28
1.2.7.4 Regulation of M2PYK activity by protein-protein interactions	29
1.2.7.5 Regulation of M2PYK activity by metabolites	30
1.2.8 M2PYK as a molecular target for cancer treatment.....	31
1.3 Fructose-1,6-bisphosphatase is an important drug target.....	35
1.3.1 Neglected tropical diseases	35
1.3.2 <i>Leishmania</i> and leishmaniasis.....	37
1.3.3 FBPase is an important drug target against <i>Leishmania</i>	43
1.3.4 Sequence analysis of FBPases from <i>Leishmania</i> and other organisms	44
1.3.5 Previous studies on FBPases from other organisms	48
1.3.5.1 Previous studies on mammalian FBPases	48
1.3.5.2 Drug discovery for human FBPase.....	56
1.3.5.3 Previous studies on plant FBPases	58
1.3.5.4 Previous studies on yeast FBPases	59
1.3.5.5 Previous studies on bacterial FBPases	59
1.3.5.6 <i>Leishmania</i> FBPase as a drug target.....	61
CHAPTER 2. Materials and methods	65
2.1 Transformation, expression and cell lysis	67
2.2 Protein purification.....	69
2.2.1 Protein purification of PYKs.....	69
2.2.2 Protein purification of <i>Lm</i> FBPase.....	70
2.3 Dynamic light scattering	71
2.4 Analytical gel-filtration	71
2.5 Enzymic activity assay	71
2.5.1 Enzymic activity assay of PYKs.....	71
2.5.2 Enzymic activity assay of <i>Lm</i> FBPase	73

2.6 Thermal shift assay	75
CHAPTER 3. Protein production and characterisation of human pyruvate kinase M1 and M2.....	79
3.1 Background	79
3.2 Protein production of pyruvate kinases	80
3.2.1 Overexpression and cell lysis of human pyruvate kinases	80
3.2.2 Purification of human pyruvate kinases.....	80
3.3 Dynamic light scattering for pyruvate kinases.....	87
3.4 Kinetic properties of pyruvate kinases.....	88
3.5 M2PYK exists in an equilibrium between monomeric and tetrameric forms.....	91
3.6 Characterisation of oligomerisation states of M2PYK mutants.....	94
3.7 Thermal stability of pyruvate kinases	95
3.8 Conclusions.....	97
CHAPTER 4. Pyruvate kinase M2 is an amino acid sensor.....	101
4.1 Background.....	101
4.2 Methods.....	102
4.2.1 Enzyme-linked immunosorbent assay	102
4.2.2 Hydrogen–deuterium exchange tandem mass spectrometry assay.....	103
4.2.3 Crystallisation, data collection and processing.....	103
4.2.4 Structural analysis.....	105
4.3 Effects of amino acids on the activity of M1PYK and M2PYK.....	105
4.3.1 Enzyme assay screening	106
4.3.2 Serine retains the activity of M2PYK.....	108
4.3.3 Amino acids are uncompetitive modulators of M2PYK	109
4.4 Binding of amino acids increases the thermostability of M2PYK.....	112
4.5 Amino acids stabilise M2PYK tetramer over monomer	113
4.5.1 Effects of amino acids on the oligomerisation of M2PYK.....	113
4.5.2 Amino acids tetramerise M2PYK and bury the interface epitope.....	115
4.6 Crystal structures of M2PYK in complex with different amino acids.....	117

4.6.1 Crystallisation, data collection and structure determination	117
4.6.2 Crystal structures display an R-/T-state transition model of M2PYK modulated by amino acids	120
4.6.3 Comparison of M2PYK structures.....	125
4.7 Hydrogen/deuterium exchange mass spectrometry demonstrates the effects of amino acids on the dynamics of M2PYK.....	138
4.8 Biological significance of these studies	141
4.8.1 Nonessential amino acids are for cancer cell growth.....	141
4.8.2 The feedback regulation cycle of M2PYK/alanine/ALT may be physiologically relevant and contribute to cell proliferation	142
4.9 Conclusions and forward look.....	143
CHAPTER 5. Redox regulation of pyruvate kinase M2.....	149
5.1 Background	149
5.2 Methods.....	149
5.2.1 Enzymic activity assay.....	149
5.2.2 Analytical gel-filtration.....	149
5.2.3 Thermal shift assay	150
5.2.4 Biotin-switch assay	150
5.3 Results and discussion.....	153
5.3.1 Redox regulates the enzymic activity of M2PYK	153
5.3.2 Redox regulates the oligomerisation of M2PYK.....	154
5.3.3 Redox regulates the thermostability of M2PYK.....	155
5.3.4 Redox takes place on C326 on a tetramer interface of M2PYK.....	157
5.3.5 M2PYK tetramerising agents prevent <i>S</i> -nitrosylation	158
5.4 Conclusion.....	159
CHAPTER 6. Protein production and characterisation of <i>Leishmania</i> fructose-1,6-bisphosphatase	163
6.1 Background	163
6.2 Bioinformatic study suggests distinctive features of <i>Lm</i> FBPase	164
6.3 Protein production of <i>L. major</i> FBPase.....	168

6.3.1 Overexpression and cell lysis of <i>Lm</i> FBPase.....	168
6.3.2 The first purification step for <i>Lm</i> FBPase: IMAC	168
6.3.3 The second purification step for <i>Lm</i> FBPase: gel filtration	170
6.4 Biophysical properties of <i>Lm</i> FBPase	172
6.4.1 Determination of molecular size of <i>Lm</i> FBPase by DLS.....	172
6.4.2 Thermostability of <i>Lm</i> FBPase	173
6.5 Kinetic properties of <i>Lm</i> FBPase	174
6.5.1 <i>Lm</i> FBPase is more active under mildly alkaline conditions.....	174
6.5.2 Temperature optimisation for the enzyme assay of <i>Lm</i> FBPase.....	175
6.5.3 <i>Lm</i> FBPase exhibits relatively weak substrate-binding	176
6.5.4 F16BP exhibits homotropic allosteric regulation for <i>Lm</i> FBPase	178
6.5.5 <i>Lm</i> FBPase requires magnesium for activity	178
6.5.6 Manganese inhibits the activity of <i>Lm</i> FBPase.....	179
6.5.7 AMP is an allosteric inhibitor of <i>Lm</i> FBPase	180
6.5.8 F26BP is a competitive inhibitor of <i>Lm</i> FBPase.....	182
6.5.9 AMP and F26BP show synergistic inhibition against FBPsases	184
6.6 Conclusions	186
CHAPTER 7. Crystal structure of <i>Leishmania</i> fructose-1,6-bisphosphatase and its allosteric mechanism	189
7.1 Background	189
7.2 Methods.....	190
7.2.1 Crystallisation, data collection and processing.....	190
7.2.2 Virtual screening of small molecular inhibitors against <i>Lm</i> FBPase.....	191
7.3 Results and discussion	192
7.3.1 Crystal structure of <i>Lm</i> FBPase/AMP	192
7.3.2 Secondary structure of <i>Lm</i> FBPase.....	200
7.3.3 AMP changes the topology of the <i>Lm</i> FBPase tetramer but not the monomer	201
7.3.4 Allosteric mechanism of <i>Lm</i> FBPase.....	201

7.3.5 Different conformations of the dynamic loop.....	204
7.3.6 Conformations of FBPase active sites under different conditions.....	206
7.3.7 Asn221 may be the reason for the low substrate affinity of <i>Lm</i> FBPase.....	210
7.3.8 Structurally distinct effector site offers a drug target against <i>Lm</i> FBPase....	211
7.3.9 Structural mechanism of the AMP/F26BP synergistic inhibition of <i>Lm</i> FBPase	213
7.3.10 Virtual screening for inhibitors against the effector site of <i>Lm</i> FBPase.....	214
7.3.11 A cocktail of PFK and FBPase inhibitors could be the ‘magic bullet’ for the treatment of diseases caused by <i>Leishmania</i>	217
7.4 Conclusions	217
CHAPTER 8. Summary and forward look.....	221
8.1 Summary of thesis	221
8.1.1 Pyruvate kinase	221
8.1.2 Fructose-1,6-bisphosphatase	223
8.2 Forward look	224
8.2.1 Activator discovery against the amino-acid binding site of M2PYK	224
8.2.2 M2PYK activity and alanine biosynthesis: a rheostat-like relationship?	224
8.2.3 T-state M2PYK may promote tumorigenesis	225
8.2.4 Oxidation and dissociation of M2PYK, a chicken and egg situation	225
8.2.5 Experimental screening of <i>Lm</i> FBPase inhibitors.....	225
References	227

List of Figures

Figure 1.1 Schematic structure of the thesis.	1
Figure 1.2 Glucose metabolic pathways.	4
Figure 1.3 Primary transcription and alternative splicing of <i>PKM</i> gene.....	8
Figure 1.4 Structure models and sequence alignment of human pyruvate kinase.	10
Figure 1.5 PYK tetramers equilibrate between R-state and T-state.....	12
Figure 1.6 M1PYK forms a tighter C-C interface than M2PYK.	13
Figure 1.7 Pyruvate kinase catalysis.	16
Figure 1.8 Structure of the active site of M2PYK.	16
Figure 1.9 Cellular metabolic consequences of changes in PYK activity.	19
Figure 1.10 Life cycle of <i>Leishmania</i>	38
Figure 1.11 Status of endemicity of leishmaniases.	40
Figure 1.12 Schematic overview of glucose metabolism in <i>Leishmania</i>	42
Figure 1.13 Structure-based sequence alignment of trypanosomatid, mammalian and <i>E. coli</i> Type-I FBPases.	47
Figure 1.14 Overall structures of mammalian liver FBPase.	51
Figure 1.15 Allosteric models of human FBPases (isoforms of liver and muscle). ...	53
Figure 1.16 Comparison of the allosteric effector site of human liver FBPase in complex with AMP or the type-2 diabetes drug MB05032.	58
Figure 1.17 Allostery of FBPase from <i>E. coli</i>	60
Figure 2.1 LDH-coupled enzyme reactions for PYK activity assay.....	72
Figure 2.2 PGI/G6PDH-coupled enzyme reactions for FBPase activity assay.	74
Figure 3.1 IMAC and gel-filtration purification of wild-type M1PYK.	82
Figure 3.2 IMAC and gel-filtration purification of wild-type M2PYK.	84
Figure 3.3 IMAC and gel-filtration purification of M2PYK-C358S.	85
Figure 3.4 IMAC and gel-filtration purification of M2PYK-C326S.	86
Figure 3.5 DLS analyses of pyruvate kinases.	87
Figure 3.6 Kinetics of M1PYK and M2PYK.....	89

Figure 3.7 Comparisons of enzymic activity of M1PYK and M2PYK in the absence and presence of F16BP.	90
Figure 3.8 Gradual activity loss of M1PYK and M2PYK at 0.002 mg/ml.	91
Figure 3.9 M2PYK gradually dissociates from tetramer to monomer.	93
Figure 3.10 M1PYK remains as a tetramer after a 12-h incubation.	93
Figure 3.11 Oligomerisation states of wild-type M2PYK and mutants.	95
Figure 3.12 Thermal stability of M1PYK and M2PYK.	96
Figure 4.1 Effects of amino acids and F16BP on activity of M1PYK and M2PYK.	107
Figure 4.2 Effects of amino acids and F16BP on the gradual reduction of M2PYK activity.	108
Figure 4.3 Kinetic profiles of M2PYK in the presence or absence of different concentrations of amino acids.	110
Figure 4.4 The regulatory effects of amino acids on M2PYK activity.	111
Figure 4.5 Thermal stability of M2PYK and the effects of free amino acids.	112
Figure 4.6 Effects of amino acids on the oligomerisation state of M2PYK.	114
Figure 4.7 Determination of the specificities of anti-PYK antibodies.	115
Figure 4.8 Amino acids and F16BP minimise M2PYK dissociation.	117
Figure 4.9 Crystals of M2PYK co-crystallised with alanine, phenylalanine, tryptophan, and serine.	120
Figure 4.10 M2PYK equilibrates between R-state and T-state tetramers.	122
Figure 4.11 The bindings of amino acids on M2PYK.	123
Figure 4.12 Inhibitory amino acids push the N-terminal loop of M2PYK.	124
Figure 4.13 N-terminal conformations of M2PYK crystal structures.	127
Figure 4.14 Helices shifted by the binding of amino-acid modulators.	130
Figure 4.15 Interface bonds in the tetramer centre of M2PYK.	132
Figure 4.16 Interface bonds between Residues 399 and 418 on C-C interface.	132
Figure 4.17 T-state and R-state M2PYK structure models.	134
Figure 4.18 Interface bonds between Asp487 and Trp515 on C-C interface.	135
Figure 4.19 The effector loop curls round F16BP to stabilise the R-state.	135

Figure 4.20 Interface bonds involving Arg342 on A-A interface.....	137
Figure 4.21 Interface bonds involving Arg339 on A-A interface.....	137
Figure 4.22 Level of the closure of B-domain.	137
Figure 4.23 Deuteration rate of M2PYK in absence/presence of amino acids.	140
Figure 4.24 M2PYK monomeric structure mapped with H/D exchange rates.	140
Figure 4.25 The regulation of M2PYK by metabolites in cytosol.	145
Figure 5.1 Biotin-switch assay workflow.	152
Figure 5.2 Effects of DTT on enzymic activity of M2PYK wild type and mutants.	153
Figure 5.3 Positions of Cys326 and Cys358 of M2PYK.	154
Figure 5.4 Effects of redox environments on the oligomerisation of M2PYK.....	155
Figure 5.5 Thermal stability of M2PYK and the effects of redox environments. ...	156
Figure 5.6 S-nitrosylation degree of M2PYK wild-type and mutants.	158
Figure 5.7 S-nitrosylation M2PYK is affected by modulators.....	159
Figure 6.1 Similarity matrix of Type-I FBPase sequences among different species.	167
Figure 6.2 SDS-PAGE characterisation for the expression of <i>Lm</i> FBPase.....	168
Figure 6.3 IMAC purification of His ₆ - <i>Lm</i> FBPase.	169
Figure 6.4 Size-exclusion purification of His ₆ - <i>Lm</i> FBPase.	171
Figure 6.5 DLS analysis of <i>Lm</i> FBPase.	172
Figure 6.6 Melting temperatures (T_m) of <i>Lm</i> FBPase.	174
Figure 6.7 Enzyme activity of <i>Lm</i> FBPase at different pH values.....	175
Figure 6.8 Enzyme activity of <i>Lm</i> FBPase at different temperatures.	176
Figure 6.9 Kinetic characterisation of <i>Lm</i> FBPase.....	177
Figure 6.10 Effects of Mg ²⁺ on <i>Lm</i> FBPase enzymic activity.	178
Figure 6.11 Effects of Mn ²⁺ on <i>Lm</i> FBPase enzymic activity.	179
Figure 6.12 The inhibitory effect of AMP on <i>Lm</i> FBPase activity.....	181
Figure 6.13 Kinetic characterisation of <i>Lm</i> FBPase in the presence of different concentrations of AMP.....	181
Figure 6.14 The inhibitory effect of F26BP on <i>Lm</i> FBPase activity.	183

Figure 6.15 Kinetic characterisation of <i>Lm</i> FBPase in the presence of different concentrations of F26BP.	183
Figure 6.16 The AMP/F26BP synergistic inhibitory effect on <i>Lm</i> FBPase.....	185
Figure 7.1 Crystal and its diffraction pattern for the <i>Lm</i> FBPase/AMP complex.....	194
Figure 7.2 Overall structure and sequence of a monomer of <i>Lm</i> FBPase.....	197
Figure 7.3 Conformation of the AMP and F6P binding sites in <i>Lm</i> FBPase.....	198
Figure 7.4 Overall structures of <i>Lm</i> FBPase.....	199
Figure 7.5 Crystal structures show allosteric effects of AMP on <i>Lm</i> FBPase.....	203
Figure 7.6 Interactions between disengaged dynamic loop and the diagonal subunit of <i>Lm</i> FBPase in a rotated conformation.....	205
Figure 7.7 Comparison of active site conformations from mammalian and <i>Lm</i> FBPase structures crystallised with Mg ²⁺	208
Figure 7.8 Comparison of the active sites of mammalian and <i>L. major</i> FBPsases. ..	209
Figure 7.9 A modelled F26BP binding in the active site of <i>Lm</i> FBPase.....	211
Figure 7.10 Comparison of AMP binding sites.....	212
Figure 7.11 A series of potential inhibitors identified by LIDAEUS bound in the <i>Lm</i> FBPase effector site.....	216
Figure 8.1 Regulatory factors of M2PYK.....	222
Figure 8.2 Allosteric models of <i>Lm</i> FBPase.....	223

List of Tables

Table 1.1 PYK isoforms in humans.	7
Table 1.2 Crystal structures of human pyruvate kinases in the PDB.	14
Table 1.3 Non-metabolic functions of M2PYK.	21
Table 1.4 Summary of M2PYK as a tumour marker and elevated expression.	24
Table 1.5 Regulatory factors of M2PYK <i>in vivo</i>	25
Table 1.6 Pharmacological activators for M2PYK.	33
Table 1.7 Seventeen neglected tropical diseases targeted by WHO.	36
Table 1.8 Drugs in use and in clinical trials for leishmaniasis.	41
Table 1.9 Phylogenic tree and matrix of percent sequence identities of FBPases.	46
Table 1.10 Enzyme kinetic properties of FBPases from different organisms.	54
Table 1.11 Selected crystal structures of FBPases in PDB.	55
Table 1.12 Human liver FBPase inhibitors.	57
Table 2.1 Information of reagents used in this thesis.	65
Table 2.2 Recipes of cell culture medium used in this thesis.	66
Table 2.3 Apparatus used in this thesis.	66
Table 3.1 Amino acid sequence and chemical parameters of expressed wild-type M1PYK and M2PYK.	79
Table 3.2 Kinetic properties of M1PYK and M2PYK.	90
Table 4.1 Kinetic parameters and T_m values of M2PYK in the absence/presence of amino acid regulatorsH	110
Table 4.2 Optimal conditions for the co-crystallisation of M2PYK with amino acids.	119
Table 4.3 Data collection and refinement statistics for crystal structures of M2PYK.	119
Table 4.4 Distance between atoms on amino-acid ligands and surrounding residues.	124
Table 4.5 Comparisons of subunit rotation angles and tetramer fits among different M2PYK crystal structures.	128

Table 4.6 Distances of α -helices shifted by the binding of amino-acid ligands.	128
Table 4.7 Interface interactions of PYK in different states.....	131
Table 4.8 M2PYK modulators and their effects on cell proliferation.....	142
Table 6.1 Amino acid sequence and chemical parameters of expressed <i>Lm</i> FBPase.	163
Table 6.2 Kinetic parameters for <i>L. major</i> , mammalian and bacterial FBPases.....	177
Table 7.1 Conditions for crystallisation screening for <i>Lm</i> FBPase/AMP complex. .	193
Table 7.2 The optimal condition for <i>Lm</i> FBPase/AMP crystal growth.	194
Table 7.3 Crystallographic data collection and model refinement statistics for <i>Lm</i> FBPase/AMP complex.	195
Table 7.4 Comparisons of structures of <i>L. major</i> and mammalian FBPases.	200

CHAPTER 1

Introduction

CHAPTER 1. Introduction

This thesis concerns biophysical, biochemical, and structural studies of human pyruvate kinase (especially for the M2-isoenzyme, namely M2PYK, a cancer target) and *Leishmania* fructose-1,6-bisphosphatase (*Lm*FBPase) as a potential drug target against leishmaniases. The structure of the thesis is shown in Figure 1.1.

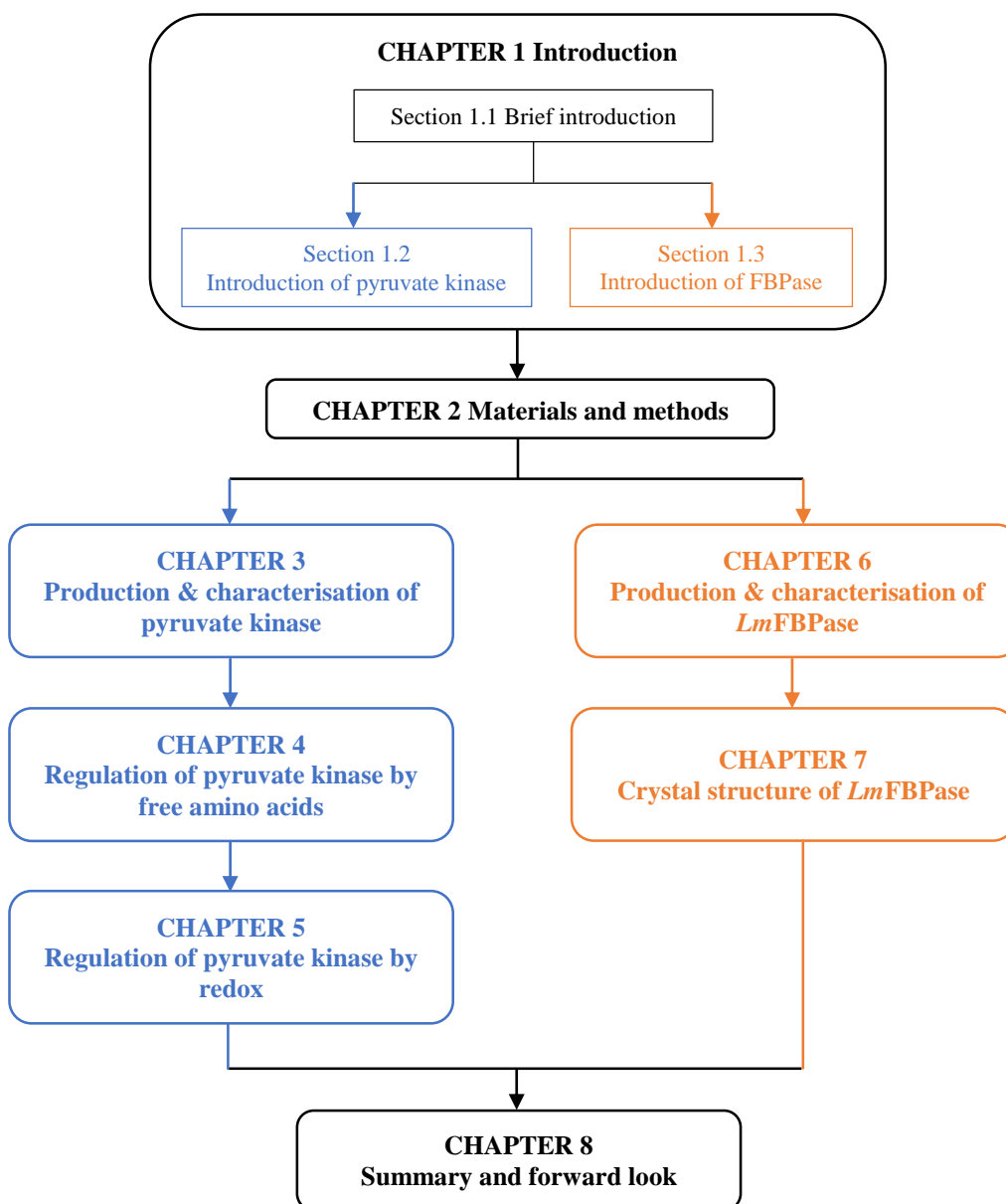


Figure 1.1 Schematic structure of the thesis.

Blue, orange, and black boxes and arrows represent different chapters/sections concerning the studies on pyruvate kinase, FBPase, and both enzymes, respectively.

1.1 Glucose metabolic enzymes are important drug targets

Glucose metabolism involves essential energy-transformation pathways in almost all known organisms. The two main glucose metabolic pathways are glycolysis and gluconeogenesis. Glycolysis is a catabolic pathway in which glucose is converted to pyruvate with release of ATP. Gluconeogenesis is an energy-storage pathway that results in the generation of glucose from certain non-carbohydrate carbon substrates, e.g. amino acids, lipids, pyruvate, etc.

Although the glucose metabolic pathways are conserved across domains, they play distinct roles in different organisms. For instance, in contrast to most organisms which adopt mitochondrial oxidative phosphorylation as a primary energy transformation pathway, glycolysis is the sole source of energy transformation in certain species of pathogenic parasites, e.g. *Plasmodium falciparum* and blood-stream form *Trypanosoma brucei* (Verlinde *et al.*, 2001, Alam *et al.*, 2014). Even in the same organism, properties of glucose metabolic pathways may vary in different tissues and according to status. For instance, the glucose metabolising properties of cancer cells are different from those of normal cells (Zhao *et al.*, 2013); hepatic gluconeogenesis is up-regulated in type-2 diabetes patients thereby contributing to hepatic glucose overproduction (Magnusson *et al.*, 1992). Due to these important roles played by glucose metabolic enzymes, which control energy transformation and cell proliferation, they are considered as promising (some are validated) drug targets against many diseases, e.g. cancer, diabetes, trypanosomiasis, etc.

1.1.1 Targeting glycolytic enzymes for cancer therapeutics

In the 1920s, Otto Warburg observed that cancer cells produce ATP mainly through the less efficient glycolytic pathway, rather than oxidative phosphorylation, even under aerobic conditions (Warburg *et al.*, 1927). This process is known as aerobic glycolysis or the ‘Warburg effect’. This metabolic reprogramming of glycolysis, although causing inefficient production of ATP, has the advantage of producing more biomass. It accumulates glycolytic intermediates which are necessary for channelling of metabolites into the biosynthesis pathways of nucleotides, amino acids and lipids.

Therefore, the metabolic reprogramming promotes tumorigenesis, and is often regarded as a hallmark of cancer cells (Vander Heiden *et al.*, 2009).

Due to its critical role in cancer cell survival, inhibition of aerobic glycolysis has become an important strategy in efforts to kill cancer cells and therapeutics (Chen *et al.*, 2007, Scatena *et al.*, 2010). Therefore, glycolysis is considered as an important target of anticancer strategies. Glucose deprivation has been found to be sufficient to induce growth inhibition and cell death in cancer cells (Aykin-Burns *et al.*, 2009, Saito *et al.*, 2009, Zhao *et al.*, 2008), which are dependent on glucose and very sensitive to glucose concentration changes (Kim & Dang, 2006). The increased glucose transport in cancer cells has been attributed primarily to the upregulation of the glucose transporter 1 (GLUT1) (Figure 1.2). A small-molecule inhibitor of GLUT1, WZB117, showed positive effects. It was shown to downregulate glycolysis, induce cell-cycle arrest, and inhibit cancer cell growth *in vitro* and *in vivo* (Liu *et al.*, 2012). Modulators of glycolytic enzymes also showed promising anti-cancer properties. For instance, hexokinase (HK) controls the conversion of glucose to glucose 6-phosphate (G6P), which serves as the starting point for glucose to enter the glycolytic pathway. The isoenzyme of hexokinase II (HKII) is a major form responsible for maintaining the high glucose catabolic rates of malignant cells (Wolf *et al.*, 2011). HKII overexpression was found in various types of cancers such as liver, breast, and lung cancers (Rempel *et al.*, 1996). HKII inhibitors 2-deoxyglucose and 3-bromopyruvate proved effective in disrupting the binding of HKII to the mitochondrion, depleting ATP, inhibiting cell cycle progression, and inducing cell death in tumours (Aft *et al.*, 2002, Dell'Antone, 2009).

The M2-isoenzyme of pyruvate kinase (M2PYK) facilitates anabolic metabolism in cancer cells, and is therefore an interesting drug target for cancer therapy. Current M2PYK activators, including TEPP-46, DASA-58, and ML-265 (Anastasiou *et al.*, 2012, Walsh *et al.*, 2010a) result in decreased cell proliferation under hypoxia and attenuated tumour growth in mice, likely due to decreased anabolic biosynthesis (Elf & Chen, 2014). This thesis mainly focuses on regulatory effects of M2PYK by natural factors, e.g. metabolites and post-translational modifications, as well as the metabolism resulting from the modulations.

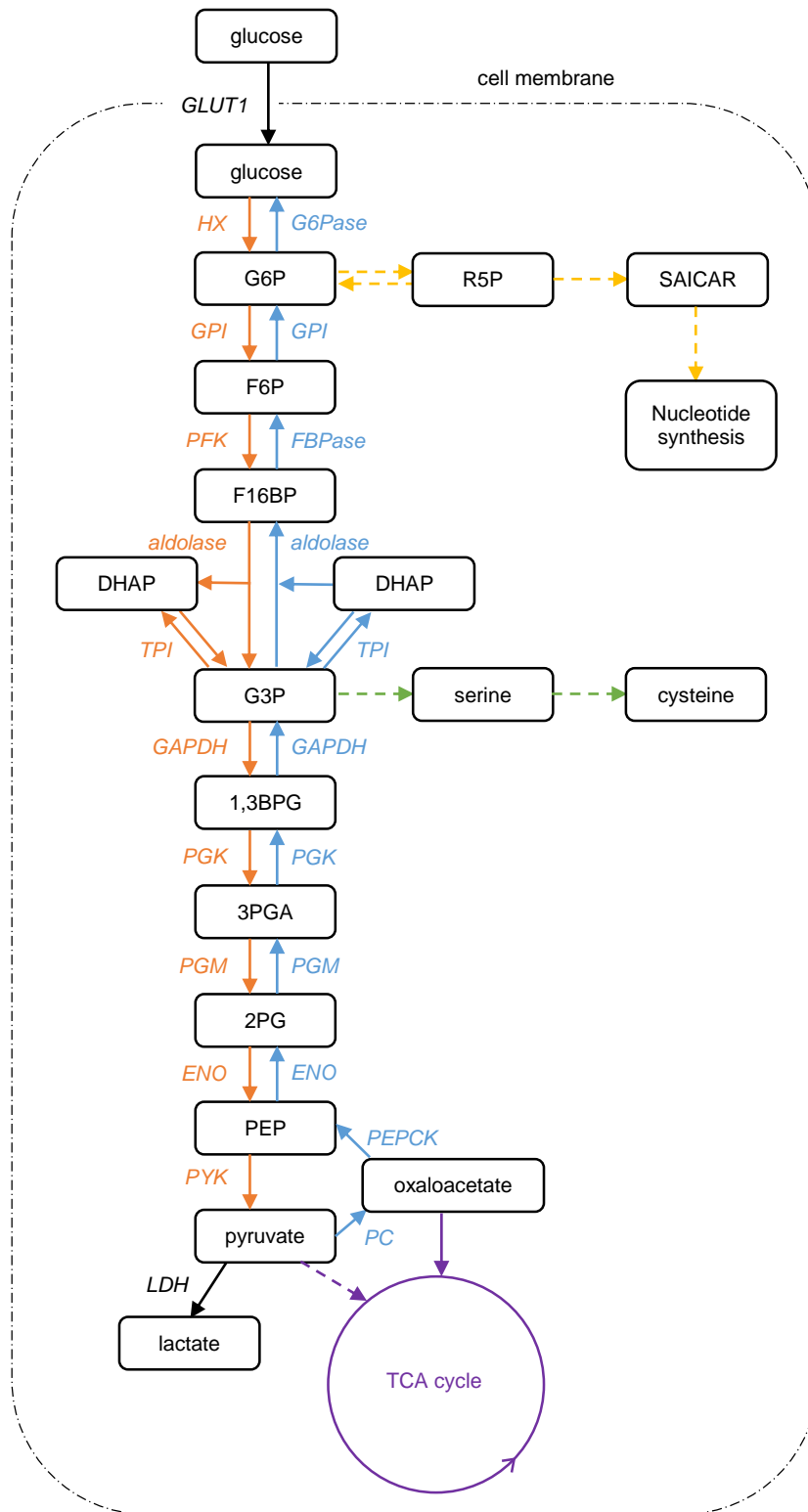


Figure 1.2 Glucose metabolic pathways.

Glycolysis, gluconeogenesis, pentose phosphate pathway, and amino acid synthesis pathway are shown in orange, blue, yellow, and green, respectively. The tricarboxylic acid (TCA) cycle is shown in purple. Solid arrows show one-step reactions, whilst dashed arrows show abbreviated multi-step catalyses. Enzymes are shown in *italics*. Full names of enzymes and metabolites correlate to abbreviations as shown in “List of abbreviations”.

1.1.2 Targeting gluconeogenic enzymes against diabetes

Type-2 diabetes is a long-term metabolic disorder that is characterised by high blood sugar, insulin resistance, and relative lack of insulin. Hepatic gluconeogenesis has been identified as a major source of hepatic glucose overproduction in type-2 diabetes patients, and therefore a promising therapeutic pathway (Magnusson *et al.*, 1992). Gluconeogenic enzymes (Figure 1.2) phosphoenolpyruvate carboxykinase (PEPCK), fructose-1,6-bisphosphatase (FBPase), and glucose-6-phosphatase (G6Pase) have been shown as promising drug targets against type-2 diabetes (van Poelje *et al.*, 2007). In particular, FBPase inhibitors have shown a reduced rate of gluconeogenesis as well as clinically meaningful reductions in fasting glucose levels in patients with type-2 diabetes (van Poelje *et al.*, 2011).

1.1.3 Targeting glucose metabolic enzymes against diseases caused by pathogens

Glucose metabolic pathways are essential for many pathogens, e.g. trypanosomatids, *Plasmodium falciparum* (van Niekerk *et al.*, 2016), *Mycobacterium tuberculosis* (de la Paz Santangelo *et al.*, 2011), methicillin-resistant *Staphylococcus aureus* (MRSA) (Zoraghi *et al.*, 2011b), etc. Glucose metabolism of trypanosomatids is dependent on the stage of its life cycle. The mitochondrion of human bloodstream-form *T. brucei* is highly repressed. In contrast the procyclic insect form of *T. brucei* possesses a well-developed mitochondrial metabolism, where glycolytic enzymes comprise only about 50% of the glycosomal protein content, which is much less than that of bloodstream-form *T. brucei* (about 90%) (Hart *et al.*, 1984, Haanstra *et al.*, 2016). Due to the essentiality of glycolysis in bloodstream-form *T. brucei*, this pathway is considered as an important target for drug discovery. In fact, each glycosomal enzyme in *T. brucei* involved in the process has been genetically validated as a target, in most cases by RNAi, occasionally by conditional knock-out studies. These experiments validated that seven glycolytic enzymes (hexokinase, phosphofructokinase, aldolase, triosephosphate isomerase, glyceraldehyde 3-phosphate dehydrogenase, phosphoglycerate mutase, and pyruvate kinase) are indeed drug targets against *T. brucei* (Albert *et al.*, 2005, Barros-Alvarez *et al.*, 2014, Fuad *et al.*, 2011). Phosphoglycerate mutase has an advantage that the enzyme in trypanosomatids is

completely different from those in humans and thus provides a promising a species-specific drug target (Fuad *et al.*, 2011). Among these glycolytic enzymes, phosphofructokinase also has a very low degree of amino-acid sequence identity between the trypanosomatid and human enzymes (21%). Comparison of the three-dimensional structures of trypanosome and human phosphofructokinase also indicated important differences with perspectives for the design of selective inhibitors (Martinez-Oyanedel *et al.*, 2007, McNae *et al.*, 2009). As a matter of fact, drug discovery against *T. brucei* phosphofructokinase is currently being carried out and nanomolar inhibitors have been identified (Brimacombe *et al.*, 2014).

It has been demonstrated that the gluconeogenic product mannogen oligosaccharide is important for *Leishmania* differentiation and survival in host macrophages (Ralton *et al.*, 2003). The gluconeogenic enzyme FBPase has been shown as a potential drug target (Naderer *et al.*, 2006). This thesis focuses on the structural basis of the allosteric regulation of *Leishmania* FBPase.

1.2 M2-type pyruvate kinase is an important target for cancer therapeutics

1.2.1 Pyruvate kinase is a glycolytic enzyme

Pyruvate kinase (PYK) is a glycolytic enzyme. It catalyses the final step of glycolysis, the transfer of a phospho group from phosphoenolpyruvate (PEP) to adenosine 5'-diphosphate (ADP), yielding one molecule of pyruvate and one molecule of adenosine 5'-triphosphate (ATP). PYK is responsible for net ATP production within the glycolytic sequence. In contrast to mitochondrial respiration, ATP regeneration by PYK is independent of oxygen supply and allows the survival of organs under hypoxic conditions (Mazurek, 2011). Moreover, PYK is a particularly important metabolic intersection because several metabolic pathways use its catalytic product pyruvate (Munoz & Ponce, 2003).

1.2.2 Isoenzymes and alternative splicing of human PYKs

M1PYK, M2PYK (both encoded by the *PKM* gene), LPYK and RPYK (both encoded by the *PKLR* gene) are the four pyruvate kinase isoforms in humans (Table 1.1) (Noguchi *et al.*, 1986b, Noguchi *et al.*, 1987). LPYK and RPYK are expressed in the liver and erythrocytes, respectively. The M1PYK isoform is found in tissues with high catabolic demand, such as muscle, heart, and the brain (Noguchi *et al.*, 1986b). M2PYK is the embryonic isoform. It is also expressed in cancer and other normal proliferating cells, such as lymphocytes and the cells of the intestinal epithelium (Imamura & Tanaka, 1972, Netzker *et al.*, 1992). Recently, it has been discovered that lack of cell proliferation does not necessarily mean lack of M2PYK expression. In fact, most adult tissues express M2PYK (Bluemlein *et al.*, 2011). Pairwise sequence identities between each two isoforms of PYK are shown in Table 1.1.

Table 1.1 PYK isoforms in humans.

Gene	Isoform	Tissue expressed in	Sequence identity (%)			
			L	R	M1	M2
<i>PKLR</i>	L	liver	100	94.3	68.0	69.2
	R	red blood cell	94.3	100	64.3	70.8
<i>PKM</i>	M1	tissues with high catabolic demand	68.0	64.3	100	95.9
	M2	most adult tissues, especially proliferating cells	69.2	70.8	95.9	100

The pairwise sequence identities are calculated with EMBOSS Needle (Rice *et al.*, 2000).

All four isoenzymes of PYK are homotetramers, with 531–574 amino acids within each subunit. The *PKM* gene is alternatively spliced to generate transcripts encoding either M1PYK or M2PYK (Figure 1.3) (Noguchi *et al.*, 1986b, Takenaka *et al.*, 1991). The human *PKM* gene has 12 exons. The ninth and tenth exons are of identical length and are isoform-specific: exon 9 is specific to M1PYK, exon 10 is specific to M2PYK, and only one of the two exons is included in the properly-spliced final transcript. In other words, the only primary-sequence difference between M1PYK and M2PYK are the 22 amino acid residues transcribed from exons 9 and 10.

The amino acid sequences of the four isoforms of human pyruvate kinase, M1PYK, M2PYK, LPYK, and RPYK are strongly conserved, and their sequence identities are higher than 64% (Table 1.1). All amino acid residues directly involved in the substrate/metal binding are identical among the four enzymes (Figure 1.4C,

highlighted with orange underlines). In particular, the sequence of LPYK is identical to RPYK, except that it lacks the N-terminal 31 amino acids (Figure 1.4C). From the primary-structure point of view, the difference between M1PYK and M2PYK is even smaller. As shown in Figure 1.4 (Panel B and C), the only different amino acid residues between M1PYK and M2PYK are located on the C-C interface of the tetramer (shown in blue), with the implication that M1PYK and M2PYK may differ in subunit interactions. Despite the otherwise strongly conserved amino acid sequences, their functions and sensitivity to regulatory factors are very different. For instance, fructose 1,6-bisphosphate (F16BP) is a strong activator of M2PYK, LPYK, and RPYK, but M1PYK is free from F16BP-binding/activation. In other words, the enzymic activity of M1PYK is as high as fully-activated M2PYK, LPYK, and RPYK (Morgan *et al.*, 2013). Moreover, M2PYK is much more susceptible to many more regulatory factors in comparison to M1PYK, i.e., modulation by metabolites, post-translational modifications, etc. (Chaneton & Gottlieb, 2012) Likewise, the enzymic activity of RPYK is more sensitive to the modulation of redox or small molecular ligands than LPYK (Yiyuan Chen, personal communication). LPYK and RPYK are both susceptible to phosphorylation and consequent inhibition on the N-terminal serine at the same position (Ser12 for LPYK and Ser43 for RPYK) (El-Maghrabi *et al.*, 1982, Riou *et al.*, 1978, Marie *et al.*, 1979, Marie *et al.*, 1980, Wang *et al.*, 2001, Prasannan *et al.*, 2012, Holyoak *et al.*, 2013).

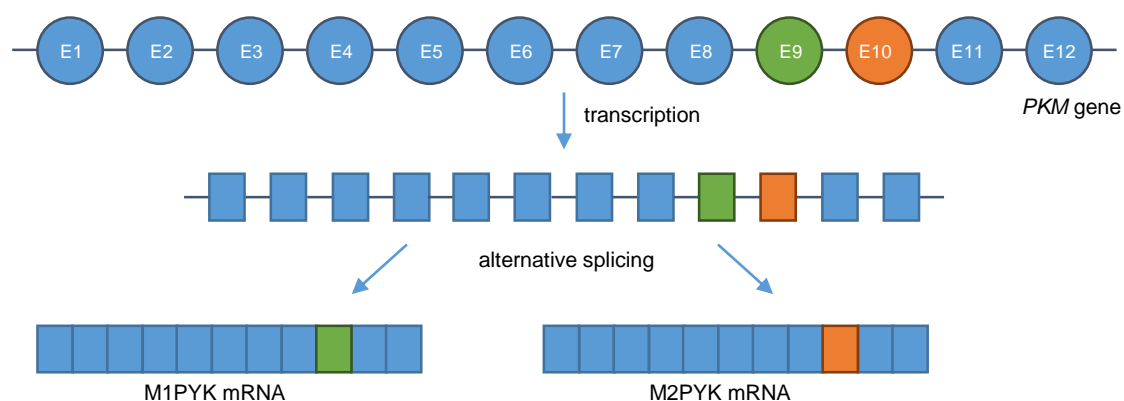


Figure 1.3 Primary transcription and alternative splicing of *PKM* gene.

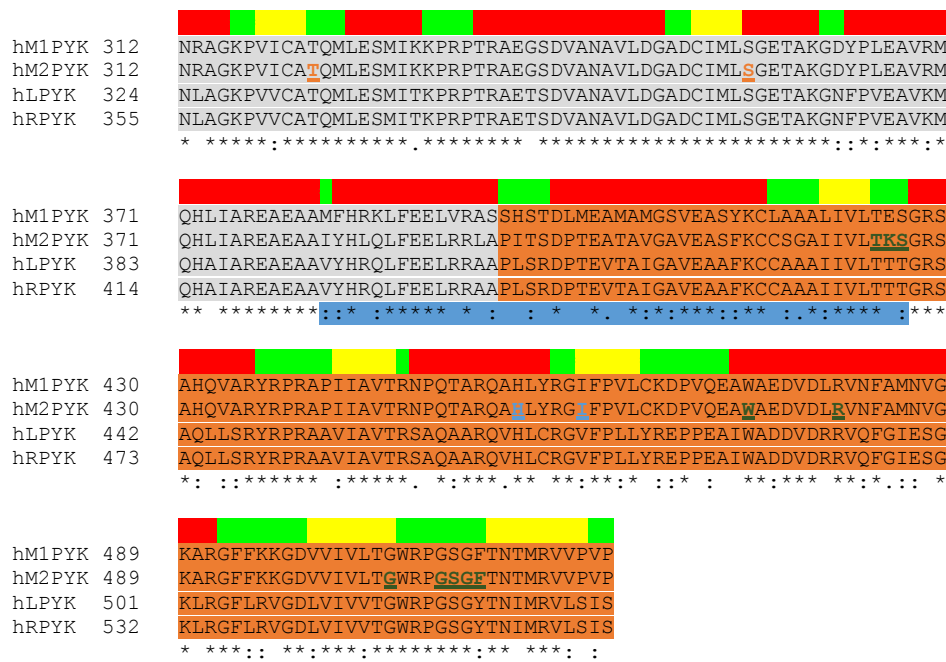


Figure 1.4 Structure models and sequence alignment of human pyruvate kinase.

(A) Architecture of human M2PYK monomer. The model is coloured to aid the identification of domains: N-terminal domain (cyan = residues 1–24); domain-A (grey = residues 25–116 and 220–402); domain-B (purple = residues 117–219); and domain-C (orange = residues 403–531). The model is built based on a previously solved crystal structure of human M2PYK (PDB ID: 4B2D) (Chaneton *et al.*, 2012). The terminal residues 1–13 as well as the N-terminal His-tag were not built into the structure model due to the lack of electron density. Positions of important sites are highlighted with arrows. Ligand compounds are shown in sticks; magnesium and potassium atoms are shown in green and purple spheres, respectively.

(B) Architecture of human M2PYK tetramer. The helices, strands, and loop regions of one subunit are shown in red, yellow, and green cartoon ribbons. The region that is different between M1PYK and M2PYK is highlighted in blue. Interfaces between subunits (A-A interface, a relatively large interface mainly formed by interactions between A-domains; and C-C interface, a relatively small interface formed by interactions between C-domains) are indicated with orange dashed lines. Same as in Panel A, this model is built based on a previously solved crystal structure of human M2PYK (PDB ID: 4B2D) (Chaneton *et al.*, 2012). The terminal residues 1–13 as well as the N-terminal His-tag were not built into the structure model due to the lack of electron density.

(C) Structure-based sequence alignment of the four isoforms of human PYKs (*PKM* Uniprot No.: P14618; *PKLR* Uniprot No.: P30613). Residues from different domains are highlighted in different colours. The colour scheme is according to Panel A, i.e., cyan=N-terminal domain, grey=A-domain, purple=B-domain, orange=C-domain. The secondary structure elements of M2PYK are shown above the alignment. The colour scheme is according to Panel B, i.e., helices=red, strands=yellow, loops=green. The fragment that is different between M1PYK and M2PYK is highlighted in blue underneath corresponding positions. Residues conserved in all aligned PYKs are labelled by an asterisk (*), whereas a colon (:), and a period (.) indicate strongly similar and weakly similar sequences, respectively. Residues involved in substrate/metal binding, F16BP-binding, and amino-acid binding are highlighted with orange, green, and blue underlines, respectively. Phosphorylation sites of LPYK and RPYK are shown in red text. The sequence alignment was performed with Clustal Omega (Sievers *et al.*, 2011). Secondary structure colours are manually added using the colour scheme of PyMOL. Methionines shown as the first amino acids in the sequences correspond to start codons ‘ATG’ in the genes, but there is no experimental evidence that these methionines are present in the mature enzymes to the author’s best knowledge.

1.2.3 Structures of pyruvate kinases

Human pyruvate kinase is generally a homotetrameric enzyme which is made up of monomers of 58–62 kDa, depending upon the isoform (Figure 1.4B). The tetramer is a dimer-of-dimers with approximate D_2 symmetry. As mentioned in the previous section, a PYK monomer consists of four domains: the N-terminal domain (residues 1–24), A-domain (residues 25–116 and 220–402), B-domain (residues 117–219); and C-domain (residues 403–531) (Figure 1.4A, residue numbers are according to the numbering of M1PYK and M2PYK). The small N-terminal domain consists of a helix-turn-helix motif that is preceded by a short stretch of residues. The A-domain is the core of the monomer and has an α_8/β_8 barrel tertiary structure motif. The intermolecular subunit contacts between the A-domains of each monomer comprise the ‘A-A interface’. A combination of β -strands and random coils make up the highly mobile B-domain that consists of a stretch of residues between Pro117 and Pro218. The active site of M2PYK lies within a cleft formed between the A- and B-domains. The C-domain consists of both α and β structural elements. The allosteric F16BP-binding pocket is located entirely within the C-domain. Another allosteric site which binds amino acids is located between the A- and C-domains. The tetramer is formed via interactions along the C-domain interfaces of each subunit, namely the ‘C-C interface’. The only fragment that is different between M1PYK and M2PYK is located on the ‘C-C interface’ (Figure 1.4).

Pyruvate kinases equilibrate between an active R-state and an inactive T-state (Morgan *et al.*, 2013). The main difference between the two states is the 11° -rigid body rotation of each subunit (Figure 1.5). Crystal structures of human pyruvate kinases in the PDB are summarised in Table 1.2. Details of the structural differences and the effectors are discussed in CHAPTER 4.

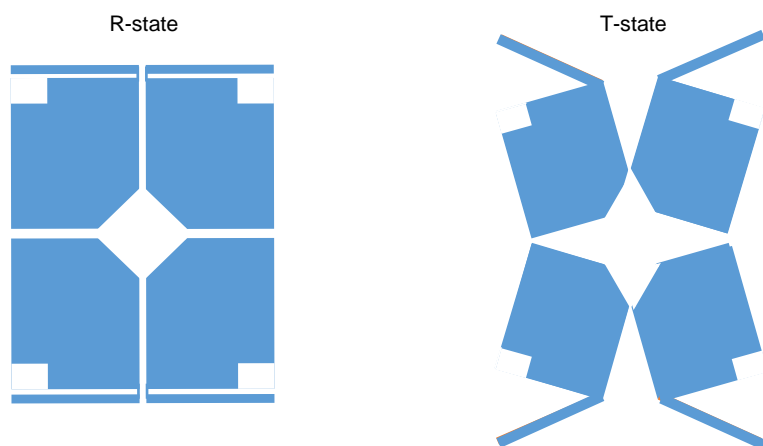


Figure 1.5 PYK tetramers equilibrate between R-state and T-state.

M1PYK is a constitutively active enzyme, and the presence of F16BP shows no activation effect on the activity of M1PYK (Morgan *et al.*, 2013). Phenylalanine has been shown to be a weak inhibitor against M1PYK (Porter & Cardenas, 1980), where the binding affinity (generally at millimolar level) depends on pH and concentrations of Mg^{2+} and PEP (Consler *et al.*, 1990, Palmer & Odedra, 1982). Alanine binds competitively with phenylalanine, but elicits little inhibitory effect (Feksa *et al.*, 2002, Williams *et al.*, 2006). In contrast, the activity of M2PYK is strongly affected by F16BP (activation) and phenylalanine (inhibition). The effects of other amino acids on M2PYK have not been well-studied apart from those of phenylalanine and serine.

The relatively slight structural differences between M1PYK and M2PYK are found on their C-C interfaces (Figure 1.4B and Figure 1.6). Gln439 is repelled by Met408 in M1PYK allowing Glu410 to form a salt bridge with Lys422. Together with Ser401, Pro404, and Tyr443, Lys422 forms a tight ‘peg-in-hole’ binding across the C-C interface of M1PYK. In contrast, in the M2PYK structure, Gln440 interacts with Glu409, and thereby disrupts the latter from forming a tight salt-bridge with Lys422 (Morgan *et al.*, 2013). This is presumably a main reason why M2PYK is more susceptible to conformational change in response to many allosteric modulators, with significantly different properties from M1PYK. For instance, M1PYK is known to occur as a homotetramer but M2PYK can equilibrate between tetramers and dimers or monomers (Eigenbrodt *et al.*, 1992, Morgan *et al.*, 2013).

The importance of Lys422 has also been confirmed by a further study carried out by Wang *et al.*, showing that M2PYK-K422R, a patient-derived mutation of M2PYK, favours a stable, inactive T-state tetramer because of strong intermolecular interactions (Wang *et al.*, 2015). They also carried out biochemical and structural characterisation of a series of human M2PYK mutants that had been proved to be of physiological importance. Analyses demonstrated that M2PYK-Y105E (phosphorylation mimic of Y105) decreases pyruvate kinase activity by inhibiting F16BP-induced R-state formation, and M2PYK-K305Q (acetylation mimic of K305) abolishes the activity by hindering tetramer formation.

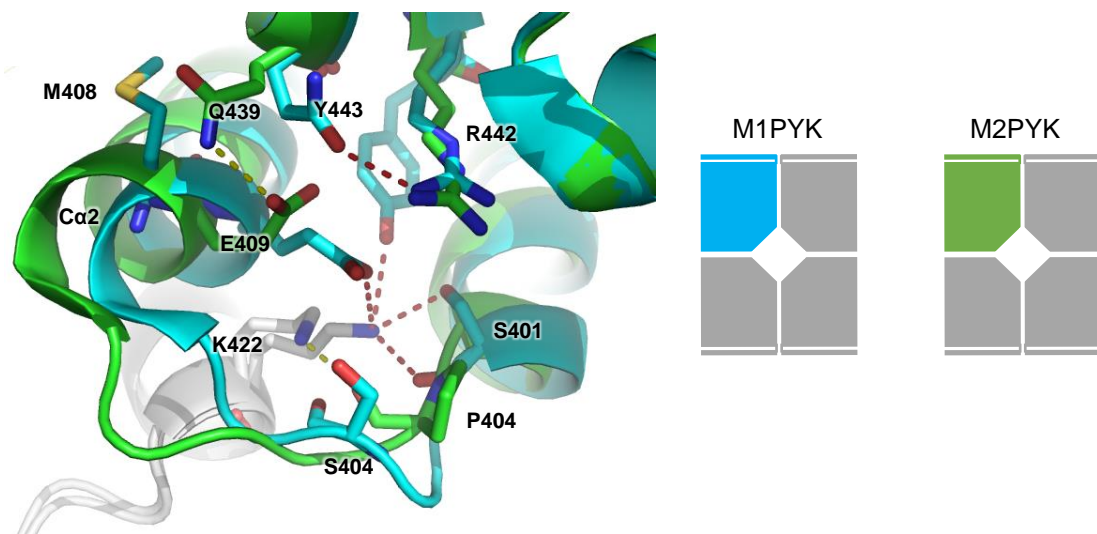


Figure 1.6 M1PYK forms a tighter C-C interface than M2PYK.

Subunits of M1PYK and M2PYK are shown in cyan and green, respectively. Adjacent subunits across the C-C interface are shown in grey. Relative positions are shown in block models. Electrostatic bonds which take place in M1PYK and M2PYK are shown in red and yellow dashed lines, respectively. In particular, Lys422 of M1PYK forms a tight ‘peg-in-hole’ interaction across the C-C interface forming four possible polar bonds. The structural models of M1PYK and M2PYK are based on previously solved crystal structures 3SRF and 4FXF, respectively (Morgan *et al.*, 2013).

Table 1.2 Crystal structures of human pyruvate kinases in the PDB.

PDB ID	Isoform	Mutation	Ligand(s)	State	Space group	Reference
3SRF	M1	wild type	PO ₄ ³⁻ , GOL ^a , PYR, K ⁺ , Mg ²⁺	R	C 2	(Morgan <i>et al.</i> , 2013)
1T5A	M2	wild type	FBP, OXA, Mg ²⁺ , K ⁺ , PO ₄ ³⁻	R	P 2 ₁ 2 ₁ 2 ₁	(Dombrauckas <i>et al.</i> , 2005)
3BJF	M2	wild type	FBP, OXA, Mg ²⁺ , K ⁺	R	P 1	(Christofk <i>et al.</i> , 2008b)
3BJT	M2	wild type	OXA, Mg ²⁺	R	P 1	(Christofk <i>et al.</i> , 2008b)
3G2G	M2	S437Y	SO ₄ ²⁻	R	P 2 ₁ 2 ₁ 2 ₁	To be published
3GQY	M2	wild type	FBP, TLA, DZG	R	P 2 ₁	To be published
3GR4	M2	wild type	FBP, TLA, DYY	R	P 2 ₁	To be published
3H6O	M2	wild type	FBP, D8G	R	P 2 ₁	To be published
3ME3	M2	wild type	FBP, 3SZ, SO ₄ ²⁻	R	P 2 ₁	To be published
3SRD	M2	wild type	FBP, OXA, Mg ²⁺ , K ⁺ , GOL	R	P 2 ₁	To be published
3SRH	M2	wild type	PO ₄ ³⁻	R	P 2 ₁	To be published
3U2Z	M2	wild type	FBP, 07T	R	P 2 ₁	To be published
4B2D	M2	wild type	FBP, Mg ²⁺ , SER	R	P 2 ₁	(Chanton <i>et al.</i> , 2012)
4FXF	M2	wild type	FBP, OXA, Mg ²⁺ , K ⁺	R	P 2 ₁	(Morgan <i>et al.</i> , 2013)
4FXJ	M2	R489A	PHE, PO ₄ ³⁻	T	P 2 ₁	(Morgan <i>et al.</i> , 2013)
4G1N	M2	wild type	OXA, Mg ²⁺ , NZT	R	C 1 2 1	(Kung <i>et al.</i> , 2012)
4JPG	M2	wild type	FBP, 1OX	R	P 2 ₁	(Guo <i>et al.</i> , 2013)
4QG6	M2	Y105E	PRO	T	P 3 ₁	(Wang <i>et al.</i> , 2015)
4QG8	M2	K305Q	MLI, GOL, K ⁺ , Mg ²⁺	R	P 2 ₁	(Wang <i>et al.</i> , 2015)
4QG9	M2	R399E	ACT, Mg ²⁺	T	P 2 ₁	(Wang <i>et al.</i> , 2015)
4QGC	M2	K422R	SO ₄ ²⁻ , GOL, K ⁺	T	P 2 ₁	(Wang <i>et al.</i> , 2015)
4RPP	M2	K422R	FBP	R	P 2 ₁	(Wang <i>et al.</i> , 2015)
4WJ8	M2	C424A	FBP, SO ₄ ²⁻ , PO ₄ ³⁻ , GOL, OXA, K ⁺ , Mg ²⁺	R	P 2 ₁	To be published
4YJ5	M2	H391Y	FBP, PYR, Mg ²⁺ , SER	R	P 2 ₁	To be published
4IMA	L	C436M	FBP, ADN, FLC, EDO, Mn ²⁺	R	P 2 ₁	(Holyoak <i>et al.</i> , 2013)
4IP7	L	S12D	FBP, ADN, 1PE, FLC, DHE, EDO, Mn ²⁺ , Na ⁺	R	P 1	(Holyoak <i>et al.</i> , 2013)
2VGB	R	wild type	FBP, PGA, Mn ²⁺ , K ⁺	R	P 2 ₁	(Valentini <i>et al.</i> , 2002)
2VGF	R	T384M	FBP, PGA, Mn ²⁺ , K ⁺	R	P 2 ₁	(Valentini <i>et al.</i> , 2002)
2VGG	R	R479H	FBP, PGA, Mn ²⁺ , K ⁺	R	P 2 ₁	(Valentini <i>et al.</i> , 2002)

^a Abbreviations used in the table: GOL: glycerol; PYR: pyruvate; OXA: oxalate; FBP: fructose 1,6-bisphosphate; TLA: L±tartaric acid; DZG: 1-(2,3-dihydro-1,4-benzodioxin-6-ylsulfonyl)-4-[(4-methoxyphenyl)sulfonyl]piperazine; DYY: 1-[(2,6-difluorophenyl)sulfonyl]-4-(2,3-dihydro-1,4-benzodioxin-6-ylsulfonyl)piperazine; D8G: 6-(2-fluorobenzyl)-2,4-dimethyl-4,6-dihydro-5H-thieno[2',3':4,5]pyrrolo[2,3-d]pyridazin-5-one; 07T: 6-(3-aminobenzyl)-4-methyl-2-methylsulfinyl-4,6-dihydro-5H-thieno[2',3':4,5]pyrrolo[2,3-d]pyridazin-5-one; SER: serine; PHE: phenylalanine; NZT: N-(4-[[4-(pyrazin-2-yl)piperazin-1-yl]carbonyl]phenyl)quinoline-8-sulfonamide; 1OX: 2-(1H-benzimidazol-1-ylmethyl)-4H-pyrido[1,2-a]pyrimidin-4-one; PRO: proline; MLI: malonate ion; ACT: acetate ion; ADN: adenosine; FLC: citrate anion; EDO: 1,2-ethanediol; 1PE: pentaethylene glycol; DHE: di(hydroxyethyl)ether.

1.2.4 Catalytic mechanism of pyruvate kinase

Pyruvate kinase catalyses the last step in glycolysis converting the substrate PEP into pyruvate, while producing one molecule of ATP from ADP per cycle. The forward reaction and generation of ATP are strongly favoured because PEP releases a significant amount of energy in comparison to ATP ($\Delta G^{\circ'}_{\text{PEP}}=58$ kJ/mol, $\Delta G^{\circ'}_{\text{ATP}}=29$ kJ/mol) (Mazurek *et al.*, 2002).

The pyruvate kinase reaction requires one monovalent cation, preferably K^+ or NH_4^+ , and two divalent cations, preferably Mg^{2+} or Mn^{2+} , for catalysis (Dombrauckas *et al.*, 2005). The pyruvate kinase reaction takes place in two steps (Figure 1.7). In the first step, a phospho group is transferred from PEP to ADP, forming an energetically less-stable enolate intermediate and ATP. The second step involves protonation of the enolate intermediate from a water molecule that is held in position by conserved active site residues (Thr328 and Ser362 in humans, Figure 1.8), thereby forming pyruvate.

The crystal structure of human M2PYK co-crystallised with catalytic products and metals revealed its catalytic mechanism (Figure 1.8). Lys270 is proposed to promote the transfer step of the phospho group by stabilising the pentavalent phosphate transition state of PEP (Bollenbach *et al.*, 1999). The K^+ cation may contribute to neutralising the developed negative charge during the phospho-group transfer reaction. The Mg^{2+} ion is coordinated to two oxygens of the oxalate (structural analogue of one of the two catalytic products, pyruvate), as well as to two additional oxygens from the carboxyl side-chain groups of Glu272 and Asp296. Arg120 belongs to the B-domain of PYK. It is also shown to be directly involved in the catalysis. This indicates that the B-domain is necessary for the formation of a complete active site. Therefore, it is reasonable to deduce that the conformation of the B-domain (its open/closed state, as well as its flexibility) is correlated to the activity of pyruvate kinase.

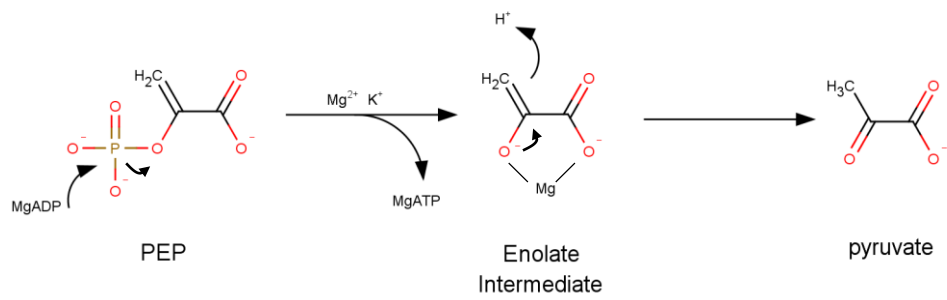


Figure 1.7 Pyruvate kinase catalysis.

This figure is adapted from (Dombrauckas *et al.*, 2005).

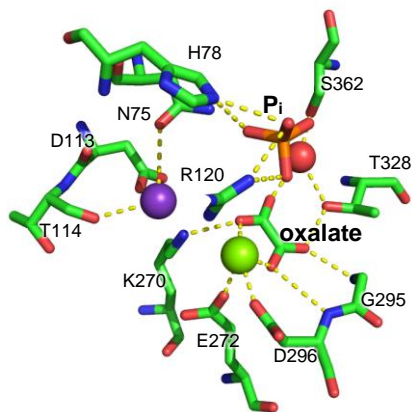


Figure 1.8 Structure of the active site of M2PYK.

Hydrogen bonds or ion strength between ligands/metals and residues are shown in yellow dashed lines. Mg²⁺ (green), K⁺ (purple), and water (red) are shown with spheres. This structural model is based on crystals structure of human M2PYK (PDB ID: 1T5A) (Dombrauckas *et al.*, 2005). Only a part of the side chain of Arg120 is shown so that the K⁺ is not obscured.

ADP is bound non-cooperatively and with high affinity by pyruvate kinases, and this binding is generally insensitive to allosteric effectors. Most regulation of pyruvate kinase activity occurs via changes in PEP binding affinity. In the absence of allosteric activators, the PYK tetramers have low affinity for PEP and exhibit positive cooperativity of PEP binding. The affinity of PEP can be increased by binding of allosteric activators (e.g. F16BP), which also abolishes the positive cooperativity of PEP binding (Dombrauckas *et al.*, 2005, Morgan *et al.*, 2013).

In addition to using ADP as a substrate, PYK has been shown to accept other nucleotide substrates *in vitro*, including GDP, IDP, UDP, dADP, and CDP (in order of decreasing affinity, all weaker than ADP) (Plowman & Krall, 1965). Moreover, oxaloacetate has also been shown as a PYK substrate that can be converted to pyruvate, i.e., a decarboxylase reaction (Zhong *et al.*, 2014).

1.2.5 The role of M2PYK in cancer

M2PYK has been demonstrated to play a central role in reprogramming cell metabolism in cancer cells (Yang & Lu, 2015). M2PYK has been found to be inactivated by post-translational modification, protein-protein interaction, and modulation by binding of metabolites (Eigenbrodt & Glossmann, 1980, Wong *et al.*, 2015, Warner *et al.*, 2014). Further, it has been shown that inhibition of pyruvate kinase is necessary for channelling of metabolites into anabolic pathways, e.g. the pentose phosphate pathway, to support the biosynthesis required by a rapidly dividing cell (Eigenbrodt *et al.*, 1992). The connection of M2PYK to both cancer signalling and cancer metabolism makes it a particularly important therapeutic target.

1.2.5.1 Metabolic needs of proliferating cells

Biomass includes lipids, carbohydrates, nucleotides and amino acids that are required for cell replication and proliferation. Lipids are required for the formation of new membranes, nucleotide precursors to support DNA replication and provide RNA for new ribosomes. Generating and assembling these building blocks requires not only ATP, but also carbon and nitrogen precursors and the reducing equivalents necessary to process them (Cairns *et al.*, 2011, Vander Heiden *et al.*, 2009). Anabolic metabolism

typically requires shunting of glucose carbon from glycolysis to biosynthetic pathways, e.g. the pentose phosphate pathway (PPP). The PPP produces ribose 5-phosphate and phosphoribosyl pyrophosphate (PRPP), which is required for nucleotide biosynthesis. The oxidative PPP also generates reducing equivalents in the form of NADPH. Glucose carbon is also shunted from glycolysis for serine and glycine biosynthesis. Dihydroxyacetone phosphate is used for generation of lipids. In brief, glycolytic intermediates are required for generating cellular building blocks, and thereby promoting cell proliferation.

1.2.5.2 M2PYK promotes tumorigenesis by regulating the Warburg effect

PYK controls the final step of glycolysis. The modulation of PYK activity contributes to integrating intracellular signalling inputs with the metabolic state of the cell. The reduction of PYK activity is thought to allow the accumulation of phosphorylated glycolytic intermediates, channelled into biosynthetic pathways for generating cellular building blocks, and thereby promoting rapid replication (Eigenbrodt *et al.*, 1992). When PYK is active, the glycolytic rate is high, respiration is partially suppressed, and most pyruvate is rapidly converted to lactate (Figure 1.9). This normally occurs under glucose-rich conditions when the level of F16BP, the major activator of M2PYK (Kato *et al.*, 1989), is high. By contrast, a reduction in PYK activity leads to a decrease in lactate production, which is associated with the accumulation of PEP and other upstream glycolytic intermediates such as 3PGA, GA3P and G6P. Consequently, there is an increase in the synthetic pathways branching from these metabolites. Many allosteric regulators and post-translational modifications of M2PYK keep the enzyme under control and are required to support tumour growth. This theory of PYK activity-dependent cell metabolism is also supported by an observation that a single switch from M1PYK (fully active) to M2PYK (less active) is necessary for the shift in cellular metabolism to aerobic glycolysis and that this promotes tumorigenesis (Christofk *et al.*, 2008a). M2PYK activators applied in cancer cell culture, xenograft models, or *in vivo* experiments also showed significant reduction of cancer cell proliferation and/or tumour growth (Kung *et al.*, 2012, Anastasiou *et al.*, 2012, Parnell *et al.*, 2013, Chen *et al.*, 2014, Zhang *et al.*, 2015, Morgan *et al.*, 2013). Collectively, evidence supports a threshold level of PYK glycolytic activity being critical to aerobic glycolysis.

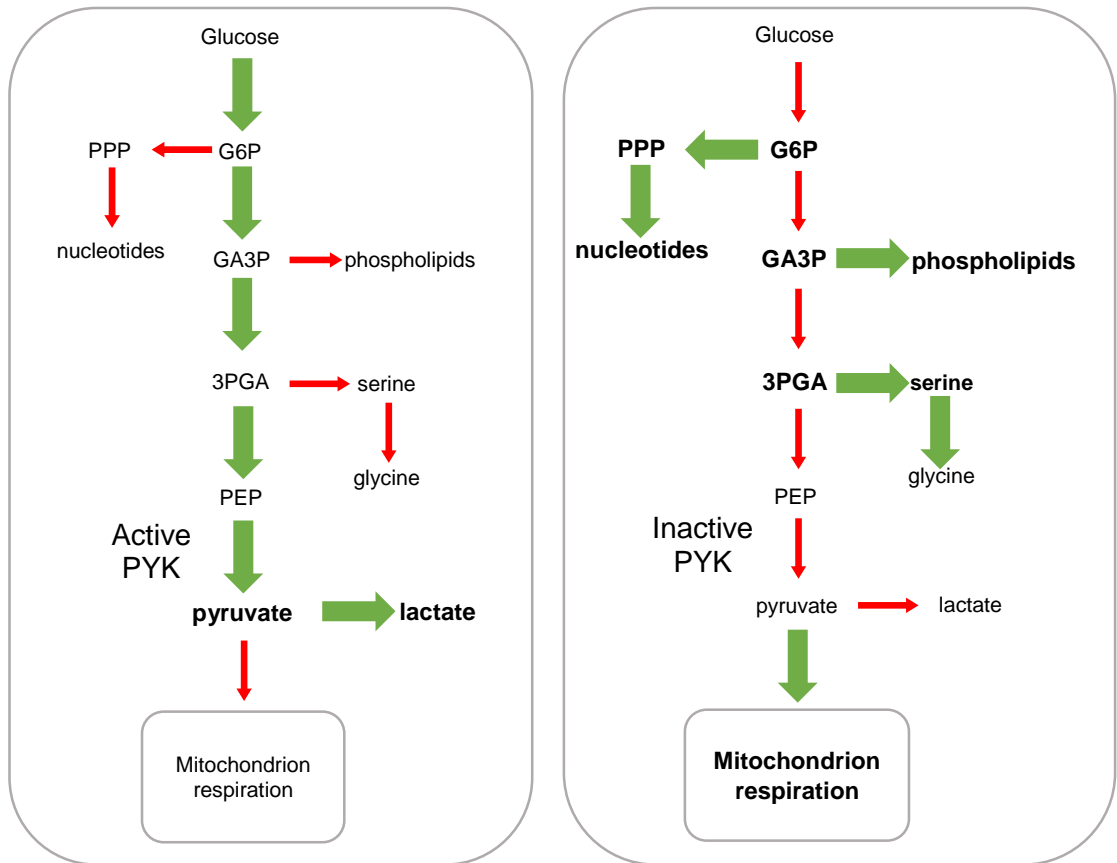


Figure 1.9 Cellular metabolic consequences of changes in PYK activity.

Reaction steps under high activity are shown with green arrows; low-activity reactions are shown with red arrows. Bold fonts show upregulated products/pathways. This figure is adapted from Figure 2 in (Chaneton & Gottlieb, 2012).

1.2.5.3 Non-metabolic functions of M2PYK

Recent work has reported non-metabolic functions for M2PYK (Table 1.3). For instance, M2PYK has been reported to act not only as a pyruvate kinase, but also a protein kinase, and thus regulate gene expression or the cell cycle. Moreover, protein-protein interactions involving M2PYK have also been reported to play important roles in cancer cell signalling.

It has been reported that M2PYK, acting as a protein kinase, is able to phosphorylate histone H3 (Yang *et al.*, 2012a), signal transducer and activator of transcription 3 (STAT3) (Gao *et al.*, 2012), BUB3 (Jiang *et al.*, 2014a), myosin light chain 2 (MLC2) (Jiang *et al.*, 2014b), extracellular signal-regulated kinase 1 (ERK1) (Keller *et al.*, 2014), and AKT1 substrate 1 (AKT1S1) (He *et al.*, 2016) (Table 1.3). The phosphorylation of these protein substrates was likely to have taken place at the active site of M2PYK, where the phospho group was transferred from the phospho-donor PEP, because the protein kinase activity of M2PYK is completely inhibited by ADP (Keller *et al.*, 2014, Yang *et al.*, 2012a). Moreover, using protein microarray experiments, it has been revealed that 149 human proteins, mostly protein kinases, are phosphorylated by M2PYK (Keller *et al.*, 2014).

Studies showed that only dissociated M2PYK (i.e., dimers or monomers) has protein kinase activity (Lv *et al.*, 2013, Gao *et al.*, 2012, Gao *et al.*, 2013a). This observation explains why M1PYK, which has not been observed to dissociate into a dimer/monomer, lacks protein kinase activity (Gao *et al.*, 2012, Yang *et al.*, 2012a, Jiang *et al.*, 2014b, Gao *et al.*, 2013a). However, the ability of succinyl-5-aminoimidazole-4-carboxamide-1-ribose-5'-phosphate (SAICAR) that can activate both the pyruvate kinase activity (that implies its ability to promote the tetramerisation of M2PYK) and the protein kinase activity of M2PYK, contradicts this report (Keller *et al.*, 2012, Keller *et al.*, 2014). Clearly, the structural basis of the protein kinase activity of M2PYK requires further investigation.

M2PYK, but not M1PYK, has also been reported to activate gene expression by binding to and thereby activating the hypoxia-inducible factor 1- α (HIF1 α) transcription factor in cancer cells (Luo *et al.*, 2011) and activated macrophages

(Palsson-McDermott *et al.*, 2015). M2PYK has also been reported to interact with many other proteins (Mazurek, 2011), including octamer-binding transcription factor 4 (OCT4) (Lee *et al.*, 2008), and glyceraldehyde 3-phosphate dehydrogenase (GAPDH) (Das *et al.*, 2016), and thereby regulate cell proliferation.

Table 1.3 Non-metabolic functions of M2PYK.

Target	Effect of target	Functional location of M2PYK	Subsequent effects	Reference
histone H3	phosphorylation of Thr11	active site	promotes gene transcription and tumorigenesis	(Yang <i>et al.</i> , 2012a)
STAT3	phosphorylation of Tyr705	active site	promotes gene transcription and tumorigenesis	(Gao <i>et al.</i> , 2012)
BUB3	phosphorylation of Tyr207	active site	regulates chromosome segregation and mitosis progression of tumour cells	(Jiang <i>et al.</i> , 2014a)
MLC2	phosphorylation of Tyr118	active site	promotes cytokinesis and cell proliferation	(Jiang <i>et al.</i> , 2014b)
ERK1	phosphorylation of Thr202	active site	promote mitogen-induced cell proliferation	(Keller <i>et al.</i> , 2014)
AKT1S1	phosphorylation of Ser202/203	active site	activates mTORC1 signalling and autophagy inhibition in cancer cells	(He <i>et al.</i> , 2016)
Oct-4	protein-protein interaction	C-domain	promotes gene transcription	(Lee <i>et al.</i> , 2008)
DDB2	phosphorylation	Not specified	reduces cell survival upon UV irradiation	(Xie <i>et al.</i> , 2015)
HIF1 α	protein-protein interaction	Not specified	activates HIF1 α , modulates IL-1 β production and Warburg effect in LPS-activated macrophages	(Palsson-McDermott <i>et al.</i> , 2015)
GAPDH	protein-protein interaction	Not specified	regulates GAPDH enzyme activity	(Das <i>et al.</i> , 2016)

1.2.5.4 Subcellular localisation of M2PYK

As a glycolytic enzyme, M2PYK predominantly localises in the cytosol. However, M2PYK but not M1PYK has also been found to translocate into the cell nucleus in epidermal growth factor receptor (EGFR)-driven cancer cells (Yang *et al.*, 2011). Upon EGFR activation, activated ERK1/2 binds to the C-C interface of M2PYK, resulting in phosphorylation of Ser37 of the latter. Phosphorylated M2PYK recruits peptidyl-prolyl *cis-trans* isomerase NIMA-interacting 1 (PIN1) for isomerisation of M2PYK, which promotes its monomerisation (Yang *et al.*, 2012b, Yang & Lu, 2013). Therefore, M2PYK that exposes its ‘nuclear localisation sequence’ binds to importin α 5 and translocates to the nucleus (Yang *et al.*, 2012b). In addition, sumoylation of M2PYK mediated by the small ubiquitin-related modifier (SUMO)-E3 ligase protein inhibitor of activated STAT 3 (PIAS3), and acetylation of M2PYK at Lys433 mediated by the p300 acetyltransferase prevent the binding of F16BP to M2PYK, thereby enhancing its nuclear translocation, too (Lv *et al.*, 2013, Spoden *et al.*, 2009).

In the cell nucleus, M2PYK is reported to play a role in cell cycle progression via β -catenin transactivation (Yang *et al.*, 2011) and direct phosphorylation of histone H3, upregulating the expression of c-Myc and cyclin D1, thereby promoting the Warburg effect (Yang *et al.*, 2012a, Yang & Lu, 2013). Nuclear M2PYK has also been reported to promote mitotic progression and chromosome segregation via direct phosphorylation of the spindle checkpoint BUB3 (Jiang *et al.*, 2014a), and cytokinesis via direct phosphorylation of MLC2 (Jiang *et al.*, 2014b). On the contrary, nuclear M2PYK binds directly to poly-ADP ribose (PAR), and this PAR-binding capability is critical for its nuclear localisation. Inhibition of poly(ADP-ribose) polymerase prevents nuclear retention of M2PYK and therefore suppresses cell proliferation and tumour growth (Li *et al.*, 2016).

1.2.5.5 Extracellular M2PYK promotes angiogenesis

It has long been known that M2PYK can be secreted into extracellular environments, and is released into the circulation of cancer patients. However, it was not known how M2PYK is released into the blood, and whether the circulating M2PYK has any physiological function(s) in tumour progression. In 2015, Li *et al.* demonstrated that M2PYK in the blood facilitates tumour growth by promoting tumour angiogenesis (Li *et al.*, 2014b). It was shown that M2PYK promoted tumour angiogenesis by increasing endothelial cell proliferation, migration, and cell-ECM (extracellular matrix) adhesion. Only the dissociated M2PYK possessed the activity in promoting tumour angiogenesis, which is consistent with the observations that M2PYK in circulation of cancer patients is a dimer form (Hugo *et al.*, 1999). Further, it was reported that secreted M2PYK, especially its dimeric form, induces EGFR phosphorylation and activates the EGFR downstream signalling in triple-negative breast cancer cells (Hsu *et al.*, 2016). Thus, it has been revealed that extracellular M2PYK can promote cancer cell proliferation through EGFR activation.

1.2.6 M2PYK is a cancer marker

In the 1980s, Eigenbrodt *et al.* discovered that M2PYK can dissociate from active tetramers into nearly inactive dimers, in which its C-C interface is exposed (Eigenbrodt

& Glossmann, 1980). Immunohistochemical experiments and enzyme-linked immunosorbent assays (ELISAs) for colon cancers and lung cancers were carried out with specific anti-M2PYK antibodies (Mazurek *et al.*, 1993). The results showed that diagnosed cancers correlated well with the amount of dissociated dimeric M2PYK, namely 'Tumor M2-PK', and thereby indicated a promising cancer marker (Eigenbrodt *et al.*, 1992, Mazurek *et al.*, 1993). A company called Schebo was then launched with the ELISA kits and immunochromatographic strips for cancer diagnosis with the anti-Tumor M2-PK antibodies.

'Tumor M2-PK' is released from tumours into the blood and/or stool of the tumour patients, and thus can be quantified by this immunoassay. It has been confirmed that the 'Tumor M2-PK' cancer marker can be used for the diagnosis for patients with several different types of cancers, including renal cell carcinoma, melanoma, lung, breast, cervical, ovarian, pancreatic, gastric and colorectal cancers, as well as in pleural fluid of patients with chest malignancies which correlates with tumour stages (Elia *et al.*, 2008) (summarised in Table 1.4). This means that Tumor M2-PK is an organ-nonspecific biomarker which reflects the metabolic activity and proliferation capacity of tumours from different entities.

However, some tests targeting Tumor M2-PK showed low sensitivity and/or specificity, indicating this diagnosis might not be a suitable single marker for renal cell carcinoma (Varga *et al.*, 2002, Roigas *et al.*, 2003, Weinberger *et al.*, 2007) or colorectal cancers (Shastri & Stein, 2007, Haug *et al.*, 2008, Shastri *et al.*, 2008, Shastri & Stein, 2008). Systematic reviews and meta-analyses clarified that this assay is generally sensitive and specific for the screening of colorectal cancer (Tonus *et al.*, 2012, Uppara *et al.*, 2015, Liu *et al.*, 2015), but not for pancreatic cancer (Kumar *et al.*, 2007a). The reason for these controversial results may be due to the variety of disease stages, as well as different sample-processing methods. Moreover, the epitope of these antibodies used for the diagnosis is not clear. As a result, further structural investigation on the M2PYK-antibody interaction is required to show the binding mode and position.

Table 1.4 Summary of M2PYK as a tumour marker and elevated expression.

Type of cancer	Evidences of M2PYK as a tumour marker	Evidences of elevated M2PYK expression
breast cancer	(Lüftner <i>et al.</i> , 1999)	(Lüftner <i>et al.</i> , 1999)
bladder carcinoma	Not shown	(Bluemlein <i>et al.</i> , 2011, Li <i>et al.</i> , 2014a)
cervical	(Kaura <i>et al.</i> , 2004)	Not shown
colon cancer	(Hardt <i>et al.</i> , 2000, Hardt <i>et al.</i> , 2003, Schulze, 1999, Schneider & Schulze, 2003, Zhang <i>et al.</i> , 2004, Hardt <i>et al.</i> , 2004, Schneider <i>et al.</i> , 2005, Shastri <i>et al.</i> , 2006, Haug <i>et al.</i> , 2007, Haug <i>et al.</i> , 2006, Hathurusinghe & Goonetilleke, 2007, Kumar <i>et al.</i> , 2007b, Mulder <i>et al.</i> , 2007, Koss <i>et al.</i> , 2008, Hardt & Ewald, 2008, Majumdar <i>et al.</i> , 2010, Fatela-Cantillo <i>et al.</i> , 2012, Sithambaram <i>et al.</i> , 2015)	(Christofk <i>et al.</i> , 2008a, Bluemlein <i>et al.</i> , 2011)
esophageal squamous cell cancer	Not shown	(Zhan <i>et al.</i> , 2013)
glinoma	Not shown	(van Veelen <i>et al.</i> , 1977, Desai <i>et al.</i> , 2014)
head and neck cancer	Not shown	(Desai <i>et al.</i> , 2014)
liver cancer	Not shown	(Imamura & Tanaka, 1972, Bluemlein <i>et al.</i> , 2011)
lung carcinoma	(Schneider <i>et al.</i> , 1999, Schneider <i>et al.</i> , 2000, Schneider <i>et al.</i> , 2003b, Schneider <i>et al.</i> , 2003a, Papadaki <i>et al.</i> , 2011, Liu <i>et al.</i> , 2015)	(Schneider <i>et al.</i> , 2002, Bluemlein <i>et al.</i> , 2011, Karachaliou <i>et al.</i> , 2013)
melanoma	(Ugurel <i>et al.</i> , 2005)	Not shown
meningioma	Not shown	(van Veelen <i>et al.</i> , 1977, Desai <i>et al.</i> , 2014)
ovarian cancer	(Landt <i>et al.</i> , 2010)	Not shown
pancreatic cancer	(Ventrucci <i>et al.</i> , 2004, Siriwardana <i>et al.</i> , 2006)	Not shown
renal cell carcinoma	(Oremek <i>et al.</i> , 1998, Oremek <i>et al.</i> , 1999, Wechsel <i>et al.</i> , 1999)	(Brinck <i>et al.</i> , 1994, Wechsel <i>et al.</i> , 1999, Bluemlein <i>et al.</i> , 2011)
thyroid cancer	Not shown	(Bluemlein <i>et al.</i> , 2011, Feng <i>et al.</i> , 2013)

1.2.7 Regulation of M2PYK

The activity of pyruvate kinase plays a central role in reprogramming cancer cell metabolism (discussed in detail in Section 1.2.5). Therefore, the regulation of the expression of different PYK isoenzymes, together with the enzyme activity of PYKs, modulates cancer cell proliferation. Moreover, M2PYK can act as a protein kinase under certain conditions, which also contributes to regulating cell proliferation. A series of regulatory effects on M2PYK are described below and summarised in Table 1.5.

Table 1.5 Regulatory factors of M2PYK *in vivo*.

Effector	Classification	Effect	Effect mechanism	Effect position	Reference
hnRNPs	splicing factor	activation of M2PYK expression	switch expression of M1PYK to M2PYK	exon 9 of PKM gene	(Clower <i>et al.</i> , 2010)
PTB	splicing factor	activation of M2PYK expression	switch expression of M1PYK to M2PYK	exon 9 of PKM gene	(Clower <i>et al.</i> , 2010)
SRSF3	splicing factor	activation of M2PYK expression	switch expression of M1PYK to M2PYK	exon 10 of PKM gene	(Wang <i>et al.</i> , 2012)
miR-122	microRNA	inhibition of M2PYK expression	reduce both the mRNA and protein levels of M2PYK	M2PYK mRNA	(Liu <i>et al.</i> , 2014)
miR-133a	microRNA	inhibition of M2PYK expression	regulate transcript of M2PYK	PKM transcript	(Wong <i>et al.</i> , 2008)
miR-133b	microRNA	inhibition of M2PYK expression	regulate transcript of M2PYK	PKM transcript	(Wong <i>et al.</i> , 2008)
miR-326	microRNA	inhibition of M2PYK expression	reduce protein levels of M2PYK	M2PYK mRNA	(Kefas <i>et al.</i> , 2010)
high glucose	acetylation	inhibition of enzyme activity	reduce F16BP binding and promote dissociation of M2PYK	Lys305	(Lv <i>et al.</i> , 2011)
p300	acetylation	inhibition of enzyme activity	reduce F16BP binding and promote dissociation of M2PYK	Lys433	(Lv <i>et al.</i> , 2013)
ROS	oxidation	inhibition of enzyme activity	promote dissociation of M2PYK	Cys358	(Anastasiou <i>et al.</i> , 2011)
ERK2	phosphorylation	inhibition of enzyme activity	recruit isomerisation by PIN1 and thus dissociate	Ser37	(Yang <i>et al.</i> , 2012b)
FGFR1	phosphorylation	inhibition of enzyme activity	reduce F16BP binding and promote dissociation of M2PYK	Tyr105	(Hitosugi <i>et al.</i> , 2009)
PIM2	phosphorylation	inhibition of enzyme activity	not shown	Thr454	(Yu <i>et al.</i> , 2013)
Bloom syndrome	native mutation	activation of enzyme activity	less allosteric, more like M1PYK	H391Y	(Anitha <i>et al.</i> , 2004)
Bloom syndrome	native mutation	inhibition of enzyme activity	promote association of M2PYK, stabilise T-state	K422R	(Anitha <i>et al.</i> , 2004)
DAPk	protein-protein interaction	activation of enzyme activity	stabilise tetramer	not shown	(Mor <i>et al.</i> , 2012)
MUC1-C	protein-protein interaction	activation of enzyme activity	stabilise tetramer	C474	(Kosugi <i>et al.</i> , 2011)
JMJD5	protein-protein interaction	inhibition of enzyme activity	promote dissociation of M2PYK	tetramer interface	(Wang <i>et al.</i> , 2014)
phosphotyrosine	protein-protein interaction	inhibition of enzyme activity	reduce F16BP binding	near FBP-binding site	(Christofk <i>et al.</i> , 2008b)
PML	protein-protein interaction	inhibition of enzyme activity	promote dissociation of M2PYK	not shown	(Shimada <i>et al.</i> , 2008)
F16BP	metabolite	activation of enzyme activity	promote association of M2PYK, stabilise R-state	FBP site	(Dombrauckas <i>et al.</i> , 2005)
SAICAR	metabolite	activation of enzyme activity	not shown	not FBP site	(Keller <i>et al.</i> , 2012)
serine	metabolite	activation of enzyme activity	promote association of M2PYK, stabilise R-state	amino acid binding site	(Chaneton <i>et al.</i> , 2012)
cysteine	metabolite	inhibition of enzyme activity	promote dissociation of M2PYK	not shown	(Nakatsu <i>et al.</i> , 2015)
phenylalanine	metabolite	inhibition of enzyme activity	promote association of M2PYK, stabilise T-state	amino acid binding site	(Morgan <i>et al.</i> , 2013)
T3	metabolite	inhibition of enzyme activity	promote dissociation of M2PYK	not shown	(Morgan <i>et al.</i> , 2013)

Effects of expression, post-translational modification, native mutation, protein-protein interaction, and binding of metabolites on M2PYK are highlighted in blue, red, green, yellow, and grey, respectively.

1.2.7.1 Regulation of M2PYK expression

The constitutively fully active isoenzyme of pyruvate kinase M1PYK is highly expressed in most normal tissues. An alternatively spliced isoform, M2PYK, is found primarily in tumour and embryonic cells and is susceptible to modulation of its enzymic activity. Inhibiting pyruvate kinase activity may reprogram cell metabolism and thereby promote cell proliferation.

M1PYK and M2PYK are both transcribed from the *PKM* gene (Figure 1.3). The alternative splicing of the pre-mRNA by heterogeneous nuclear ribonucleoproteins (hnRNPs) A1 and A2, polypyrimidine-tract binding (PTB) protein splicing factors, and the serine/arginine-rich splicing factor 3 (SRSF3) results in the generation of M2PYK by the inclusion of exon 10 and the exclusion of exon 9, which is specific to M1PYK (Noguchi *et al.*, 1986a, David *et al.*, 2010, Wang *et al.*, 2012) (Table 1.5). Complementary to this mechanism, it has also been demonstrated that the PI3K/Akt/mTOR network leads to the upregulation of M2PYK expression by transcriptional activation through the combination of HIF-1 α and c-Myc (Sun *et al.*, 2011).

The binding of miRNAs, noncoding RNAs to specific target mRNAs has also been found to promote their degradation and/or hinder the translation of M2PYK. It was reported that miRNA 133a, 133b, 122, 326 target the *PKM* transcript or M2PYK mRNA, and thereby regulate the expression of M2PYK (Wong *et al.*, 2008, Kefas *et al.*, 2010, Liu *et al.*, 2014).

Analyses of 16 tumour types using the cancer genome atlas RNASeq and exon array datasets revealed that an isoform switch from M1PYK to M2PYK occurs in glioblastomas (Desai *et al.*, 2014). It has also been reported that replacement of M2PYK with M1PYK inhibits aerobic glycolysis and tumour growth (Christofk *et al.*, 2008a). Despite lack of the isoform switch in other tumour types, expression of M2PYK has been found to be increased in all cancer types examined (Bluemlein *et al.*, 2011, Desai *et al.*, 2014). For instance, elevated M2PYK expression has been demonstrated in breast cancer, bladder carcinoma, colon cancer, esophageal squamous

cell cancer, glioma, head and neck cancer, liver cancer, lung carcinoma, meningioma, renal cell carcinoma, thyroid cancer, etc. (summarised in Table 1.4) These findings point to a crucial role for expression of M2PYK in tumour growth.

1.2.7.2 Regulation of M2PYK activity by post-translational modifications

Post-translational modifications including phosphorylation, oxidation, hydroxylation and acetylation also regulate M2PYK activity to promote cancer proliferation (Table 1.5).

It has been reported that oncogenic forms of fibroblast growth factor receptor type 1 (FGFR1) inhibit M2PYK activity by direct phosphorylation on Tyr105, which was found to be common in human cancers (Hitosugi *et al.*, 2009). It inhibits the formation of active, tetrameric M2PYK by disrupting the binding of F16BP, and thereby inducing M2PYK dissociation and promoting tumour growth. In contrast, SH2-containing protein tyrosine phosphatase 1 has been shown to dephosphorylate p-M2PYK^{Y105}, and inhibit nuclear function of M2PYK (Tai *et al.*, 2016). ERK2 has been demonstrated to phosphorylate M2PYK at Ser37. Phosphorylated M2PYK Ser37 recruits PIN1 for *cis-trans* isomerisation of M2PYK, and thereby enables the latter to dissociate and translocate into cell nucleus (Yang *et al.*, 2012b). Thr454 of M2PYK has also been found to be phosphorylated by a protein serine/threonine kinase proviral insertion in murine lymphomas 2 (PIM2), resulting in multiple changes to M2PYK function, such as inhibiting its enzymic activity and promoting a cancer cell's dependence on glycolysis (Yu *et al.*, 2013).

High glucose concentration can stimulate the acetylation of Lys305 of M2PYK, and inhibits its pyruvate kinase activity *in vitro* (Lv *et al.*, 2011). It then promotes its lysosomal-dependent degradation via chaperone-mediated autophagy. An acetylation mimic M2PYK-K305Q abolishes the activity by hindering tetramer formation, even in the presence of F16BP (Wang *et al.*, 2015). Ectopic expression of the K305Q mutant accumulates glycolytic intermediates and promotes cell proliferation and tumour growth (Lv *et al.*, 2011). M2PYK can also be acetylated by p300 acetyltransferase at Lys433, which is unique to M2PYK and directly interacts with F16BP (Lv *et al.*, 2013). Acetylation prevents M2PYK activation by interfering with F16BP binding and

promotes the nuclear accumulation and protein kinase activity of M2PYK. The acetylation mimetic M2PYK-K433R mutant promotes cell proliferation and tumorigenesis. In contrast, the deacetylation of Lys433 of M2PYK by sirtuin6 can abolish M2PYK nuclear protein kinase and transcriptional coactivator functions, and thereby suppress M2PYK-dependent cell proliferation and tumorigenesis (Bhardwaj & Das, 2016, Park *et al.*, 2016).

Redox potential has been shown to play an important role on the modulation of M2PYK function. A study carried out in A549 human lung cancer cells found that an increase in the concentrations of intracellular reactive oxygen species (ROS) led to decreased M2PYK activity (Anastasiou *et al.*, 2011). The oxidation-promoted dissociation of M2PYK decreased its protein kinase activity that caused accumulation of glycolytic intermediates, and thereby promoted cell proliferation and tumorigenesis. This inhibition was reversed after treatment of cell lysates with the reducing agent dithiothreitol (DTT). It was proposed that Cys358 is mainly responsible for its regulation by oxidation. Both mutating Cys358 to Ser and the addition of M2PYK-activator DASA-10 (which stabilises M2PYK as a tetramer) protected M2PYK from oxidation. Both protection showed the capabilities of preventing M2PYK from dissociation, as well as consequent tumorigenesis.

It has also been shown that sumoylation of M2PYK mediated by the small ubiquitin-related modifier (SUMO)-E3 ligase protein inhibitor of activated STAT 3 (PIAS3) is consistent with nuclear localisation of M2PYK (Spoden *et al.*, 2009).

1.2.7.3 Regulation of M2PYK activity by native mutations

In 2004, two missense mutations H391Y and K422R of M2PYK were found in cells from Bloom syndrome patients, who are prone to develop cancer (Anitha *et al.*, 2004). Later studies showed unique properties of these two M2PYKs including loss of activity by 75% and 20% of the K422R and H391Y mutants, respectively (Akhtar *et al.*, 2009, Gupta *et al.*, 2010, Iqbal *et al.*, 2014b, Wang *et al.*, 2015). Interestingly, the H391Y mutant of M2PYK acquired M1PYK-like properties. For instance, it showed a 6-fold increase in affinity for PEP and behaved like an allosteric protein with compromised cooperative binding. The H391Y mutant showed a reduced effect of the allosteric

modulators phenylalanine and F16BP. In contrast, affinity for PEP was decreased significantly by the K422R mutant. A recent structural study showed that the K422R mutant was unable to dissociate into dimers/monomers (Wang *et al.*, 2015). It suggested that the reason why the enzymic activity of K422R is lower than the wild-type M2PYK in the absence of F16BP is because it tends not to form the R-state conformation under such conditions. It was also reported that cells co-expressing M2PYK and mutant (K422R or H391Y) showed significantly aggressive cancer metabolism as compared with cells expressing either wild-type or mutant M2PYK independently (Iqbal *et al.*, 2014b).

1.2.7.4 Regulation of M2PYK activity by protein-protein interactions

M2PYK-driven glycolytic activity is also modulated through protein-protein interactions (Table 1.5). In 2008, Christofk *et al.* revealed that M2PYK binds directly and selectively to tyrosine-phosphorylated proteins (Christofk *et al.*, 2008b). The binding of phosphotyrosine-containing proteins to M2PYK results in the release of F16BP, leading to inhibition of M2PYK enzymic activity. It was further revealed that this regulation of M2PYK by phosphotyrosine signalling diverts glucose metabolites from ATP production to anabolic processes.

JMJD5 is a Jumonji C domain-containing dioxygenase. It directly interacts with M2PYK at an inter-subunit interface region, which hinders M2PYK tetramerisation and blocks pyruvate kinase activity, and thus modulates metabolic flux in cancer cells. This interaction also influences translocation of M2PYK into the nucleus (Wang *et al.*, 2014).

The Mucin 1-C (MUC1-C) oncoprotein promotes tumorigenesis in part via inhibiting M2PYK activity (Kosugi *et al.*, 2011). Interaction of MUC1-C with M2PYK Cys474 within its C-domain, results in M2PYK activation, suggesting stabilisation of the tetrameric state. However, EGFR phosphorylates MUC1-C on Tyr46, which causes MUC1-C to interact with M2PYK at Lys433 instead, leading to inhibition of M2PYK activity and upregulation of aerobic glycolysis.

The death-associated protein kinase (DAPk) tumour suppressor binds M2PYK, and activates M2PYK via tetramer stabilisation (Mor *et al.*, 2012). It has also been reported that the cytosolic promyelocytic leukemia (PML) protein specifically associates with M2PYK, inhibits its activity, and increases lactate production (Shimada *et al.*, 2008).

1.2.7.5 Regulation of M2PYK activity by metabolites

Many small metabolites (e.g. amino acids, nucleotides, glycolytic intermediates, hormones, etc.) have been reported to modulate M2PYK enzymic activity via direct binding, and thereby regulate cell proliferation (Table 1.5). In other words, M2PYK is both controlling and controlled by metabolic flux, and thus may play a central role in cell metabolism.

F16BP is an upstream glycolytic intermediate of pyruvate kinase. It is converted from/to fructose 6-phosphate by phosphofructokinase and fructose-1,6-bisphosphatase in glycolysis and gluconeogenesis, respectively (Figure 1.2). It is a major allosteric activator of M2PYK (Mazurek *et al.*, 2005). Each chain of M2PYK contains a F16BP binding site, close to the C-C interface of the C-domain (Figure 1.4A). Despite being distant from the active site, F16BP increases enzymic activity and the binding affinity of PEP, promotes tetramerisation, and stabilises the active state of M2PYK. Six micromolar F16BP can activate M2PYK by 50% (Morgan *et al.*, 2013). In contrast, M1PYK is a constitutively fully active pyruvate kinase. It does not bind F16BP due to structural differences at the F16BP binding pocket. M1PYK and F16BP-activated M2PYK have almost identical kinetic parameters, and both are locked into the same three-dimensional conformation (Morgan *et al.*, 2013).

The free amino acid L-phenylalanine has been reported to allosterically inhibit both M1PYK and M2PYK enzymic activity (Porter & Cardenas, 1980, Williams *et al.*, 2006, Morgan *et al.*, 2013). The phenylalanine binding site is distinct from both the active site and the F16BP binding site (Figure 1.4A), stabilises the T-state conformation of the tetramer (Figure 1.5), and thereby inhibits the enzymic activity. Likewise, L-cysteine also specifically inhibited the activity of M2PYK (Nakatsu *et al.*, 2015).

L-serine binds in the same pocket as L-phenylalanine, but acts as an allosteric activator (Eigenbrodt *et al.*, 1983, Chaneton *et al.*, 2012). As a result, the activity of this glycolytic enzyme, which may control flux, is highly dependent on the *de novo* biosynthesis of serine (Chaneton *et al.*, 2012). In contrast, serine-starved, M2PYK-expressing cells reduce glycolytic flux (presumably through M2PYK inactivation) and accumulate glycolytic intermediates such as 3-phosphoglycerate, a precursor of serine biosynthesis. In other words, there is a ‘rheostat-like’ mechanistic relationship between M2PYK activity and serine biosynthesis. The allosteric mechanism of serine is unknown despite a solved serine-bound M2PYK crystal structure (PDB code: 4B2D), because this structure contains another activator, F16BP.

The thyroid hormone triiodo-L-thyronine (T3) has also been shown to inhibit the enzymic activity of M2PYK. It promotes the dissociation of M2PYK, and stabilises the enzyme in an inactive monomeric state (Ashizawa *et al.*, 1991, Morgan *et al.*, 2013). The binding of T3 on M2PYK has also been shown to promote cell proliferation (Morgan *et al.*, 2013).

M2PYK is also activated by an intermediate metabolite in the *de novo* purine synthesis pathway, SAICAR, at physiologically relevant concentrations, presumably binding at an allosteric site separate from that of FBP (Keller *et al.*, 2012, Keller *et al.*, 2014). Knockdown of adenylysuccinate lyase, the enzyme involved in SAICAR metabolism in cells, prevents SAICAR degradation and promotes the survival of cells in glucose limiting conditions.

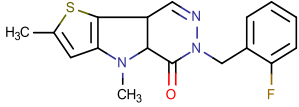
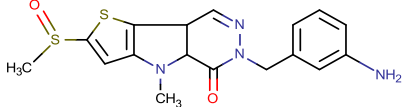
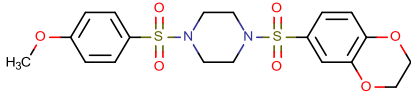
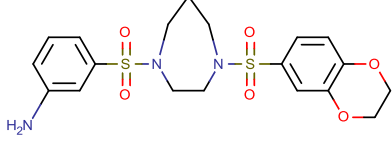
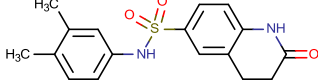
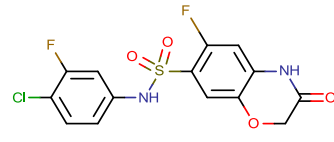
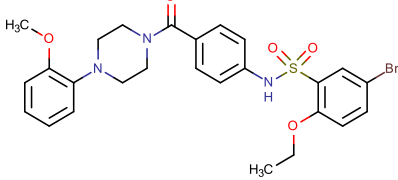
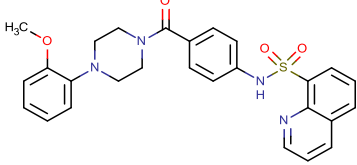
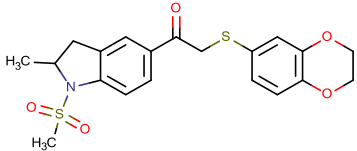
1.2.8 M2PYK as a molecular target for cancer treatment

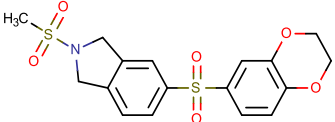
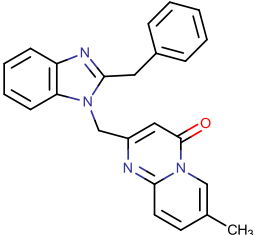
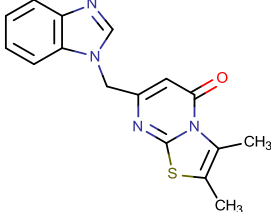
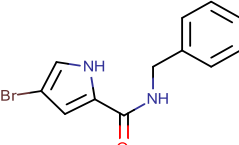
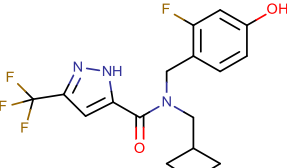
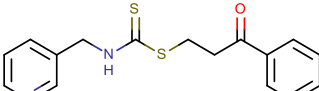
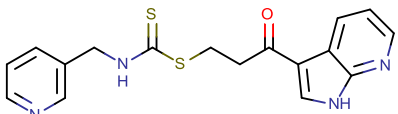
M2PYK plays a central role in reprogramming cancer cell metabolism. Extensive studies have demonstrated that the activation of M2PYK enzymic activity by stabilising it as an active tetramer may cause cancer cells to revert to a metabolic state like that of normal cells (Christofk *et al.*, 2008a, Guo *et al.*, 2013). Therefore, it has been hypothesised that pharmacological activators of M2PYK activity can inhibit tumorigenesis. Indeed, some efforts of design and discovery of small-molecule

M2PYK activators (summarised below and in Table 1.6) produced successful results in the inhibition of cancer cell proliferation and/or tumorigenesis.

A large-scale high-throughput screening (with approximately 300,000 compounds) was carried out for the screening of M2PYK activators (Boxer *et al.*, 2010, Walsh *et al.*, 2011, Anastasiou *et al.*, 2012). Two groups of compounds (thieno[3,2-b]pyrrole[3,2-d]pyridazinones and *N,N'*-sulfonamides) were identified which activate the enzymic activity of M2PYK. After optimisation, specific activators at nanomolar-levels, TEPP-46 and DASA-58, were identified from both groups. Both bind to an allosteric site on the A-A interface of M2PYK. Moreover, the property of tumorigenesis inhibition was observed when tested on H1299 xenograft models. Some other compounds designed for the activation of M2PYK are also summarised in Table 1.6. Intriguingly, the correlation between M2PYK activation and cancer cell proliferation is not consistent among all studies. The effect of M2PYK activators on cell proliferation can be cell medium-dependent (especially for non-essential amino acids in the cell medium) (Kung *et al.*, 2012), reviewed in (Warner *et al.*, 2014). The reason may be related to the amino acid-regulatory effect of M2PYK. This thesis focuses on the effects of amino acids on M2PYK. Biophysical, biochemical and structural analyses show the effects of free amino acid ligands on the thermostability, flexibility, enzymic activity, oligomerisation state, and conformation of M2PYK.

Table 1.6 Pharmacological activators for M2PYK.

Scaffold	Structure	AC ₅₀ (nM)	Effect on cell proliferation	Reference
Screening hit		63	inhibition	(Jiang <i>et al.</i> , 2010) (Anastasiou <i>et al.</i> , 2012)
Reported lead (TEPP-46)		92		
Screening hit		111	inhibition	(Boxer <i>et al.</i> , 2010) (Anastasiou <i>et al.</i> , 2012)
Reported lead (DASA-58)		38		
Screening hit		790	not reported	(Walsh <i>et al.</i> , 2011)
Reported lead		90		
Screening hit		676	inhibition	(Kung <i>et al.</i> , 2012)
Reported lead		14		
Screening hit		550	not reported	(Yacovan <i>et al.</i> , 2012)

Reported lead		17		
Screening hit		3500		
Reported lead		86		
Screening hit		36000		
Reported lead		11	inhibition	(Xu <i>et al.</i> , 2014)
Screening hit		7640		
Reported lead		1000	inhibition	(Zhang <i>et al.</i> , 2015)

1.3 Fructose-1,6-bisphosphatase is an important drug target

Fructose-1,6-bisphosphatase (D-fructose-1,6-bisphosphate 1-phosphohydrolase; EC 3.1.3; FBPase) is a gluconeogenic enzyme that catalyses the breakdown of fructose 1,6-bisphosphate (F16BP) into fructose 6-phosphate (F6P) and phosphate (P_i). FBPase has been shown to be a potential drug target against *Leishmania* (Naderer *et al.*, 2006), a pathogenic parasite that causes deaths ranging from 20,000 to 40,000 people annually in tropical countries (Alvar *et al.*, 2012). In this thesis biochemical and structural characterisations of *L. major* FBPase are shown, thereby demonstrating the molecular basis of the allosteric inhibition of this enzyme.

1.3.1 Neglected tropical diseases

Neglected tropical diseases (NTDs) are infectious diseases that predominate in the tropical belt and principally impact the world's poorest people (Feasey *et al.*, 2010). They are chronic and disabling conditions leading to acute illness, long-term disability and early death. Yet they have been neglected for decades, initially as part of a general disregard for the developing world, and more recently due to the intensity of focus on HIV/AIDS, tuberculosis and malaria (Hotez *et al.*, 2007). NTDs are endemic in 149 countries and affect an estimated 1.4 billion people (Hotez *et al.*, 2014, Karl *et al.*, 2015). It has been widely believed that it is not economically feasible to develop drugs, diagnostic methods, and vaccines specifically for the NTDs, owing to the lack of commercial markets or conventional business models (Yamey & Hotez, 2007). An estimated 100 million people in the Latin American and Caribbean region live on extreme poverty. Almost all of the "bottom 100 million" people suffer from at least one NTD, including one-half of the poorest people in the region infected with hookworms, 10% with Chagas disease, and up to 1-2% with dengue, schistosomiasis, and/or leishmaniasis (Hotez *et al.*, 2013). NTDs therefore also constitute a very significant burden on the already strained healthcare systems and the economies of many developing countries.

The 17 NTDs which were indicated in the World Health Organization (WHO) report “First WHO report on neglected tropical diseases” and in a subsequent fact sheet, are summarised in Table 1.7 (WHO, 2010, 2015a). The responsible pathogens can be separated into different biological groups, including (1) bacteria (ocular serovars of *Chlamydia trachomatis*); (2) vector-borne protists (such as *Trypanosoma cruzi*); (3) filarial worms (such as *Onchocerca volvulus*); (4) soil-transmitted helminths; and (5) the two species of non-tuberculosis mycobacteria that produce leprosy and Buruli ulcers (Feasey *et al.*, 2010). Among the 17 NTDs, only six can be controlled or eliminated through mass administration of safe and effective medicines or by other, effective interventions (CDC, 2011).

Table 1.7 Seventeen neglected tropical diseases targeted by WHO.

Disease	Pathogen
Trachoma	<i>Chlamydia trachomatis</i>
Buruli ulcer	<i>Mycobacterium ulcerans</i>
Chagas disease (American trypanosomiasis)	<i>Trypanosoma cruzi</i>
Chikungunya	Chikungunya virus
Dengue and severe dengue	Dengue virus
Dracunculiasis (guinea-worm disease)	<i>Dracunculus medinensis</i>
Echinococcosis	<i>Echinococcus</i>
Foodborne trematodiasis	trematode worms (most common species affecting humans are <i>Clonorchis</i> , <i>Opisthorchis</i> , <i>Fasciola</i> and <i>Paragonimu</i>)
Trypanosomiasis, human African (sleeping sickness)	<i>Trypanosoma brucei</i>
Leishmaniasis	<i>Leishmania</i>
Leprosy	<i>Mycobacterium leprae</i>
Lymphatic filariasis	Filariodidea
Onchocerciasis	<i>Onchocerca volvulus</i>
Rabies	rabies virus
Schistosomiasis	<i>Schistosoma</i>
Soil-transmitted helminth infections	<i>Ascaris lumbricoides</i> , <i>Trichuris trichiura</i> , <i>Necator americanus</i> , and <i>Ancylostoma duodenale</i>
Taeniasis/cysticercosis	<i>Taenia solium</i> and <i>T. saginata</i>
Yaws	<i>Treponema pallidum</i> subspecies <i>pertenue</i>

The WHO has set goals to control or eliminate eleven NTDs by 2020 (highlighted in grey in Table 1.7) and launched a roadmap in January 2012 to guide this global plan (WHO, 2012). Basic research on NTD-causing parasites and drug/vaccine

developments against NTDs have proliferated despite the lack of commercial profits, thanks to the efforts of pharmaceutical companies, scientists, governments, global health organisations, and philanthropic foundations (e.g. Bill & Melinda Gates Foundation). For instance, there are no fewer than six vaccines for NTDs currently in clinical trials, with three for schistosomiasis, one for hookworm disease (i.e., soil-transmitted helminth infections), one for visceral leishmaniasis, and one for dengue fever (Hotez *et al.*, 2016).

For drug development, there has been a movement toward returning to phenotypic-based whole-organism screening assays (Kotz, 2012). In the area of Human African trypanosomiasis (HAT), two compounds have recently progressed into clinical trials by the Drugs for Neglected Diseases *initiative* (DNDi): the nitroimidazole, fexinidazole (Torreale *et al.*, 2010), and the oxaborole, SCYX-7158 (Jacobs *et al.*, 2011). Both of these drugs were discovered through phenotypic screening. On the other hand, molecular target-based approaches have also been adopted for the development of NTD drugs. For instance, low-nanomolar inhibitors of *Trypanosoma brucei* (*T. brucei*) protein kinase GSK3 have been developed and demonstrated to be potent *in vitro* inhibitors of *T. brucei* proliferation (Gilbert, 2013). In addition, a novel nanomolar inhibitor, ML251, has also been discovered using a structure-based compound screening approach, against *T. brucei* phosphofructokinase (PFK), a recently validated drug target (Albert *et al.*, 2005, McNae *et al.*, 2009, Walsh *et al.*, 2010b, Brimacombe *et al.*, 2014).

1.3.2 *Leishmania* and leishmaniasis

Most trypanosomatids have a complicated life-cycle. These organisms are transmitted between their mammalian hosts by insects. For example, *Leishmania* is transmitted by the bites of infected female phlebotomine sandflies (Figure 1.10). *Leishmania* exist in two main morphologically distinct forms: motile flagellated promastigotes which occur in the sand-fly vector, and non-flagellated amastigotes which infect and replicate in the phagolysosome of human macrophages. In detail, the sandflies inject the infective stage (i.e., promastigotes) from their proboscis during blood meals ①. Promastigotes that reach the puncture wound are phagocytosed by macrophages ②.

and other types of mononuclear phagocytic cells. Promastigotes transform in these cells into the human tissue stage of the parasite (i.e., amastigotes) (3), which multiply by simple division and proceed to infect other mononuclear phagocytic cells (4). Parasite, host, and other factors affect whether the infection becomes symptomatic and whether cutaneous or visceral leishmaniasis results. Sandflies become infected by ingesting infected cells during blood meals (5, 6). In sandflies, amastigotes transform into promastigotes, develop in the gut (7), and migrate to the proboscis (8).

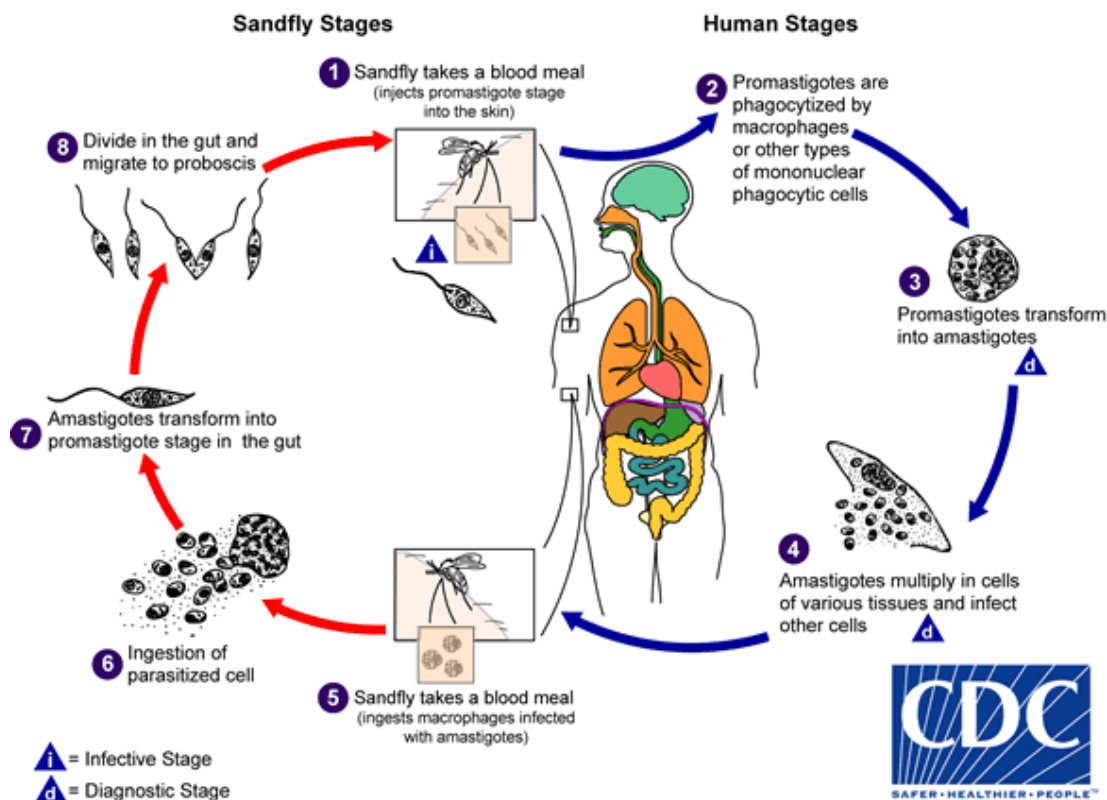


Figure 1.10 Life cycle of *Leishmania*.

This figure is from www.cdc.gov.

Trypanosomatids of the genera *Trypanosoma* (which includes *T. cruzi* that causes Chagas disease, and a species *T. brucei* that causes HAT) and *Leishmania* are parasitic protists which cause a spectrum of diseases in humans and many animals. In particular, *Leishmania* species are responsible for cutaneous and visceral diseases such as ulcers, destructive lesions and an infection of the liver and spleen that is usually fatal if untreated. The WHO estimates that approximately 1.3 million new cases of leishmaniases occur annually and are observed in 98 countries in Asia, Africa, South

and Central America (Figure 1.11) (WHO, 2015b). Of these cases, 300,000 are the visceral form also known as kala-azar, and estimates of deaths from this disease range from 20,000–40,000 people annually (Alvar *et al.*, 2012). Some species tend to cause visceral leishmaniasis (e.g. *L. infantum* and *L. donovani*), whereas the other major manifestation — cutaneous leishmaniasis, is a skin infection mainly caused by *L. major* and *L. tropica* (Barrett & Croft, 2012). Additionally, rarer forms including mucocutaneous leishmaniasis, diffuse cutaneous leishmaniasis, and post-kala-azar dermal leishmaniasis (Alvar *et al.*, 2006). Anti-leishmanial vaccines are not currently available, and treatments rely on chemotherapy, but are characterised by low efficacy, high toxicity, or widespread resistance (Table 1.8).

Glycosomes are cell organelles related to peroxisomes, which are found only in protists of the groups Kinetoplastea and Diplonemida, such as the genera *Leishmania* and *Trypanosoma*. Glycosomes primarily contain glucose metabolic enzymes, including the first six or seven glycolytic enzymes, and some gluconeogenic enzymes (Figure 1.12) (Opperdoes & Borst, 1977, Michels *et al.*, 2006, Szöör *et al.*, 2014, Haanstra *et al.*, 2016). Cells of the cultured promastigote form of *Leishmania* spp. contain about 20–50 glycosomes, whereas about ten glycosomes are found in the much smaller intracellular amastigote (Szöör *et al.*, 2014, Cull *et al.*, 2014).

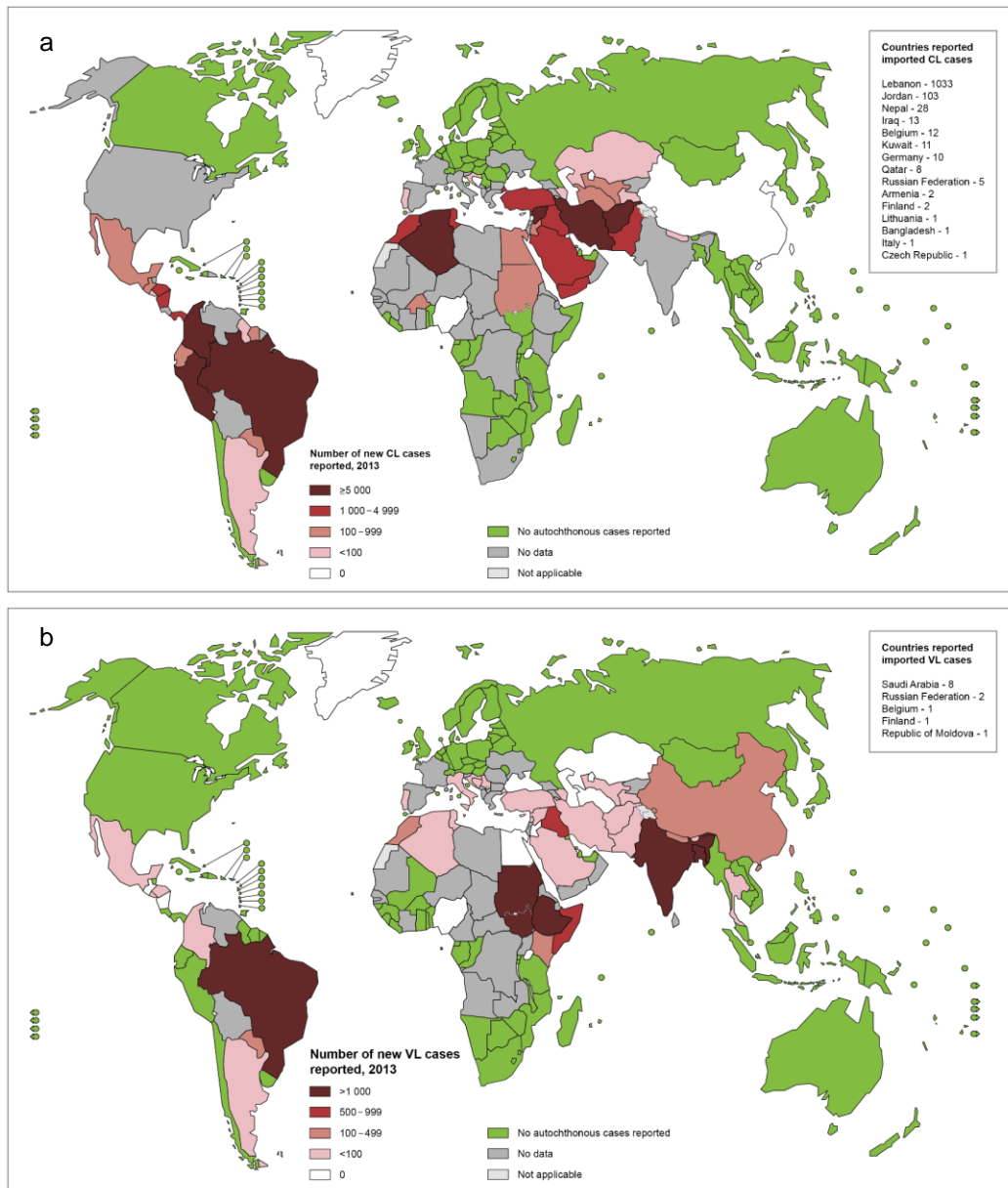


Figure 1.11 Status of endemicity of leishmaniases.
 (a) Cutaneous leishmaniasis. (b) Visceral leishmaniasis. Figures are from www.who.int

Table 1.8 Drugs in use and in clinical trials for leishmaniasis.

	Drug	Comments
visceral leishmaniasis		
First-line drugs	Pentavalent antimonials: sodium stibogluconate (pentostam); Meglumine antimoniate (Glucantime)	Parenteral administration; reported toxicities in pregnant women; resistance in Bihar, India Slow i.v. infusion; known toxicities, used in India where there is resistance to antimonials
	Amphotericin B (Fungizone)	Further clinical studies on single-dose infusion in India
	Liposomal amphotericin B (AmBisome)	First oral drug; concerns over teratogenicity, compliance
	Miltefosine	Intramuscular administration; registered in India; less effective in Sudan
	Paromomycin	
Clinical trials	Amphotericin B lipid formulations Co-administrations: AmBisome + miltefosine, AmBisome + paromomycin, miltefosine + paromomycin	Other formulations shown effective in clinical studies Highly effective, short course treatment in phase III trials in India; in further clinical studies
cutaneous leishmaniasis		
First-line drugs	Pentavalent antimonials: sodium stibogluconate (Pentostam); Meglumine antimoniate (Glucantime)	Standard treatments; variable efficacy between types and species of <i>Leishmania</i>
	Amphotericin B (Fungizone)	For specific types in South America
	Pentamidine	For specific types in South America
	Paromomycin (topical formulation)	Marketed formulation
Clinical trials	Paromomycin (topical formulation, Phase III)	Well-tolerated formulation, also containing 0.5% gentamicin
	Miltefosine (oral, Phase III)	
	Imiquimod	Topical immunomodulator, adjunct therapy to antimonials in Phase II

This table is adapted from (Barrett & Croft, 2012).

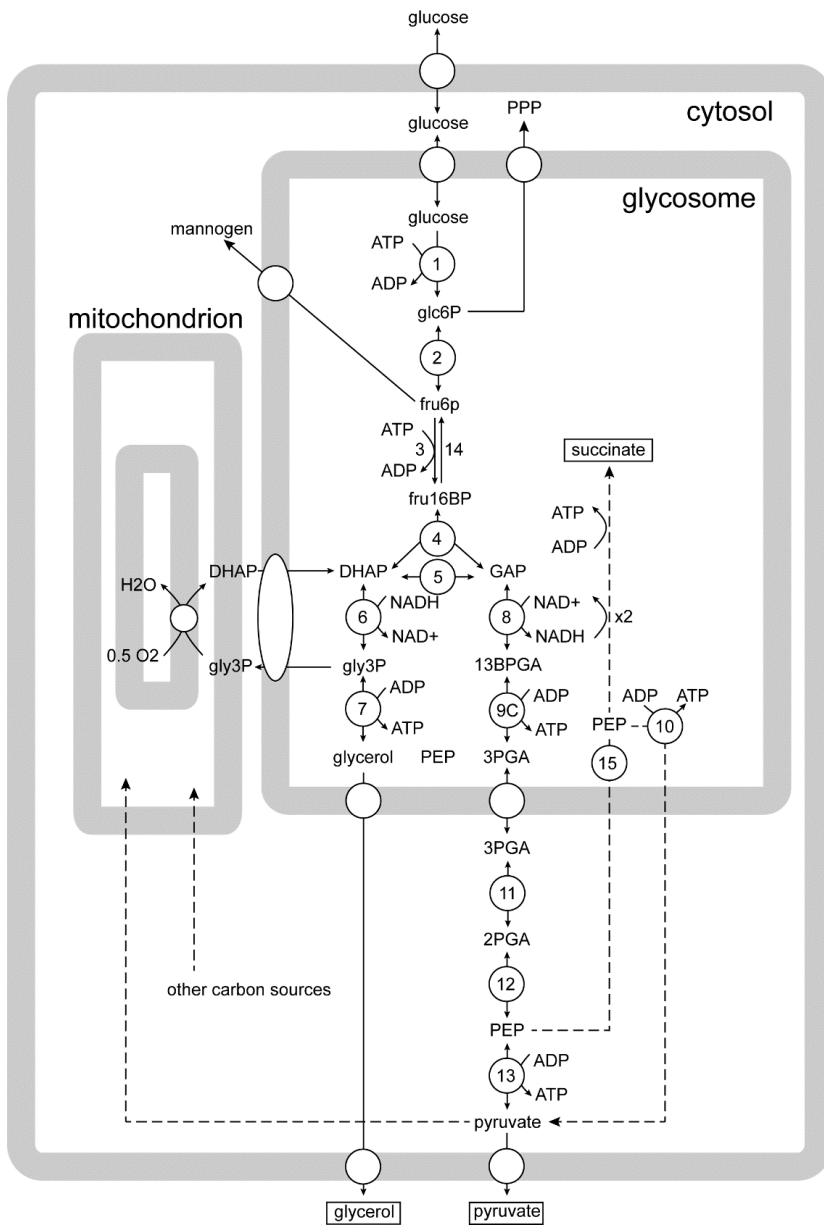


Figure 1.12 Schematic overview of glucose metabolism in *Leishmania*.

Solid lines represent the major glycolytic routes that are expressed in most developmental stages of all trypanosomatids parasites, dashed lines show environment-dependent pathways. Enzymes are shown with numbers. 1. hexokinase; 2. phosphoglucosomerase; 3. phosphofruktokinase; 4. aldolase; 5. triosephosphate isomerase; 6. glycerol-3-phosphate dehydrogenase; 7. glycerol kinase; 8. glyceraldehyde-3-phosphate dehydrogenase; 9. phosphoglycerate kinase c; 10. pyruvate phosphate dikinase; 11. phosphoglycerate mutase; 12. enolase; 13. pyruvate kinase; 14. fructose-1,6-bisphosphatase; 15. phosphoenolpyruvate carboxykinase. The pathways shown here are proposed by Szöör *et al.* (Szöör *et al.*, 2014) and integrated with a putative gluconeogenesis pathway in *Leishmania* (Rodriguez-Contreras & Hamilton, 2014).

1.3.3 FBPase is an important drug target against *Leishmania*

Leishmania spp. develop into extracellular flagellated promastigotes within the alimentary tract of primarily phytophagous sandflies, and are thus in a sugar-rich environment. But when transformed into amastigotes in the human body their major residence is in the phagolysosomes of macrophages, which have low levels of carbohydrates but are rich in amino acids and fatty acids. By contrast, blood-stream form *T. brucei* relies on the catabolism of sugars and has glycosomes which are wholly devoted to glycolysis (Sanchez-Moreno *et al.*, 1992). *Leishmania* spp. may rely more on other metabolic processes for their free energy (e.g. via gluconeogenesis which channels metabolites into the synthesis of mannogen). The glycolytic enzyme content of their glycosomes is considerably lower than *T. brucei* (Gualdrón-López *et al.*, 2012, Barros-Alvarez *et al.*, 2014). In the form of amastigotes, *Leishmania* actively carry out gluconeogenesis even in the presence of external sugar (Rodriguez-Contreras & Landfear, 2006). In contrast, the specific activities of the glycolytic enzymes hexokinase, phosphofructokinase, glucose-6-phosphate dehydrogenase and pyruvate kinase are considerably reduced (Burchmore & Hart, 1995, Opperdoes & Michels, 2001, 2008). Due to the importance of gluconeogenesis for *Leishmania* spp., it is considered as an important target for drug discovery.

It has been demonstrated that the gluconeogenic product mannogen oligosaccharide is important for *Leishmania* differentiation and survival in host macrophages (Ralton *et al.*, 2003). FBPase is a gluconeogenic enzyme that catalyses the breakdown of F16BP into fructose 6-phosphate (F6P) and phosphate. To show the growth and other properties of *Leishmania* without the gluconeogenic pathway, *L. major* FBPase-null amastigotes were developed. The result showed that *L. major* was able to survive the FBPase deletion, although it was unable to grow in the absence of hexose, and suspension in glycerol-containing medium resulted in rapid depletion of internal carbohydrate reserves. Further, *L. major* FBPase-null promastigotes were internalised by macrophages and able to differentiate into amastigotes but were unable to replicate in the macrophage phagolysosome. Similarly, the mutant persisted in mice but failed to generate normal lesions (Naderer *et al.*, 2006). The identification that *Lm*FBPase is important for proliferation of the human pathogenic form of the parasite and formation

of lesions, renders it a potential drug target and thus gives impetus to the requirement for further detailed biochemical and structural characterisation of this enzyme.

1.3.4 Sequence analysis of FBPases from *Leishmania* and other organisms

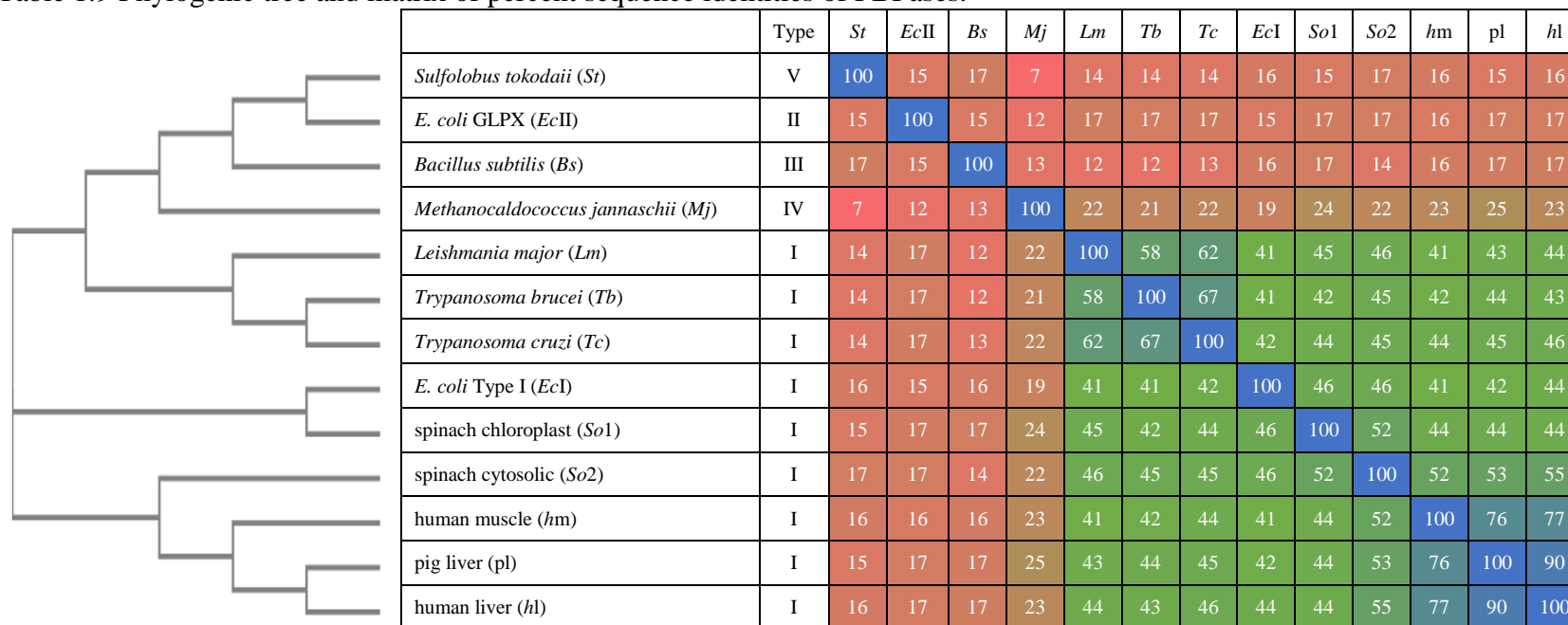
Most characterised FBPases belong to the superfamily of lithium-sensitive metal-dependent phosphatases that also includes three families of inositol phosphatases (clan CL0171, Pfam data base) (York *et al.*, 1995). FBPases are classified into five types according to their sequence similarity (Donahue *et al.*, 2000, Stec *et al.*, 2000, Nishimasu *et al.*, 2004). Type I FBPase is the form in eukaryotes, as well as homologs in other organisms. Type I–III FBPases are found in bacteria. Type IV FBPase from archaea carries out both FBPase activity and inositol monophosphatase activity. Type V FBPase that is widely found in thermophilic prokaryotes is significantly different from the other four types of FBPases in both sequence and structural aspects (Nishimasu *et al.*, 2004). Type I FBPase has been extensively studied, but types II–V FBPases remain largely uncharacterised. Sequence alignment and phylogenetic studies of FBPases from different organisms shows that the different types of FBPase are highly distinct (Table 1.9). All comparative identity values are higher than a comparative random sequence identity value of 6% (Chung & Subbiah, 1996).

The amino acid sequence of *Lm*FBPase, classified as a Type-I FBPase, is compared with other representative FBPases in Table 1.9 and Figure 1.13. Sequences of FBPases from *Leishmania*, *T. brucei*, and *T. cruzi* share 58–67% identity, which is less conserved than many trypanosomatid glycolytic enzymes. For instance, the sequence identity of trypanosomatid pyruvate kinases is about 75%. Trypanosomatid phosphofructokinases also share sequence identity greater than 70%. This observation correlates with the variety of gluconeogenic pathways (discussed in the previous Section 1.3.3) among different species of trypanosomatids, implying that diversity of this gluconeogenic enzyme might contribute to different sugar requirements of these species.

*Lm*FBPase has 44% and 41% overall sequence identity with human liver FBPase (*hl*FBPase) and human muscle FBPase (*hm*FBPase), respectively. The active sites

from *LmFBPase* and mammalian FBPsases are very well conserved, with 13 of 14 residues being identical, except for the replacement of Tyr221 by Asn in *LmFBPase* (Figure 1.13), which may diminish its binding to substrate. The dynamic loop which has been shown to be catalytically important in mammalian FBPsases is in a similar position in *LmFBPase*, but shows functionally important sequence differences (Figure 1.13 and highlighted in Figure 1.14). AMP is an inhibitor of mammalian FBPsases (McGrane *et al.*, 1983). The AMP sites from *LmFBPase* and mammalian FBPsases are relatively poorly conserved. Intriguingly, the basic residue Lys112, which was predicted to be one of three conserved residues required for the inhibitory effect of AMP (Gao *et al.*, 2014), is replaced by an acidic residue Asp112 in *LmFBPase* (Figure 1.13). The poor conservation of the effector site may offer the potential for drug discovery. However, the lack of biochemical and structural evidence for the inhibitory allosteric effects of AMP on *LmFBPase* challenges the robustness of its potential as a therapeutic target. For this reason, work reported in this thesis included enzymic and structural experiments on *LmFBPase*, and thereby revealed its enzyme kinetic properties and allosteric mechanism.

Table 1.9 Phylogenetic tree and matrix of percent sequence identities of FBPases.



Sequence alignment and generation of the phylogenetic tree of *Lm*FBPase (Uniprot No.: O97193), *Tb*FBPase (Q95PL6), *Tc*FBPase (Q4DE31), human liver isoenzyme (P09467), human muscle isoenzyme (O00757), pig liver isoenzyme (P00636), *E. coli* Type-I isoenzyme (P0A993), *E. coli* GLPX isoenzyme (P0A9C9), *Sulfolobus tokodaii* (F9VMT6), *Bacillus subtilis* (Q45597), *Methanocaldococcus jannaschii* (Q57573), spinach chloroplast isoenzyme (P14766), and spinach cytosolic isoenzyme (P22418) were performed with Clustal Omega (Sievers *et al.*, 2011) and Clustal W2 (Larkin *et al.*, 2007). Classification of each FBPase is shown in this table. Sequence identities among FBPases from different organisms are shown as percentages. The level of conservation represented by different colours, where blue represents high conservation, green represents modest and red represents poor conservation. All identity values are higher than a random sequence identity value of 6% (Chung & Subbiah, 1996). The colours are plotted with Microsoft Excel.

```

LmFBPase 1 MDVVRTPTPT--TTLTQYII-KSQP-PHSRGDFTLLMMAIQTSVKVIEKN
TbFBPase 1 -MPDYS---RVPSTLMQFLMHNQPK--GSRGAFLLMMAIQTSVKVIEMN
TcFBPase 1 -MEPRA---NIPATLVQFLMHSQPR--SSRGEFTLLMTAIQTAVKVIKHX
hlFBPase 1 -MADQAPFDTDVNTLTRFVMEGRK-ARGTGELTQLLNSLCTAVKAISSA
hmFBPase 1 -MTDRSPFETDMLTLTRYVMEGRQ-ARGTGELTQLLNSMLTAIKAISSA
plFBPase 1 -MTDQAAPFDTNIVTLTRFVMEGRK-ARGTGEMTQLLNSLCTAVKAISTA
ecFBPase 1 -----MKTLEGFIVKQHEFSHATGELTALLSAIKLGAKIHRD
          ** .: : . . : . * : * * : : . * *

LmFBPase 46 IRRAGMKGMLGYIAGQSANATCDHQAKLDVVISNIAFKAYLLSSTVVCVLG
TbFBPase 46 IRSAGAQLFGHINDGRANATCDAQAKLDVVANNAFKAYLMSASVSVFMG
TcFBPase 46 IRSAGMQGLFGYLSHDSSNATCDTQARLDVIANNAFKAYLISSSVSVFLG
hlFBPase 49 VRKAGIAHLYG-IAG-STNVTCDQVKKLDVLSNDLVMMMLKSSSFATCVLV
hmFBPase 49 VRKAGLAHLYG-IAG-SVNVTCDEVKLDVLSNLSLVINMVQSSYSTCVLV
plFBPase 49 VRKAGIAHLYG-IAG-STNVTCDQVKKLDVLSNDLVINVLKSSSFATCVLV
ecFBPase 40 INKAGLVLDILG-ASG-AENVQCEVQKLDLDFANEKKAALKARDIVAGIA
          : : * * : * : * * : * * : * * : * * : * *

LmFBPase 96 SEEEQMIIAESGRRGDYLIFFDPLDGSNIDANVSVGSIWGVWRLPKDT
TbFBPase 96 SEEDSIVVSSGQQGDYVVFDPDLDGSNIDANISIGSVWGIWCLPKGT
TcFBPase 96 SEEEESLVLVEGERQGHYVVFDPDLDGSNIDANISVGSIWGIWRISDEK
hlFBPase 97 SEEDKHAIIVEPEKRGKYVVCDFDLDGSNIDCLVSVGTIFGIYRK-KST
hmFBPase 97 SEENKDAIITAKEKRGKYVVCDFDLDGSNIDCLASIGTIFAIYRK-TSE
plFBPase 97 SEEDKNAIIVEPEKRGKYVVCDFDLDGSNIDCLVSVGTIFGIYRK-NST
ecFBPase 88 SEEDEIIVFEGCEHAKYVVLMDPLDGSNIDVNVSVGTIFSIYRRVTPV
          *** : . : : . . : * : * * * * * * * * * * * * * * *

LmFBPase 146 TIN-SVEDANAVIRMLKGTDMVSAGYAVYGSATNLVLTSGHGVDFGLDP
TbFBPase 146 KVR-TTKDALVKLPRLSGRYLVSSGYAMYGTATNLVITGSGVNGFTLDT
TcFBPase 146 KIT-TMEEANEVLKRLSGKCLVSAGYAMYGTATNLVLTFGHGVDFGLDP
hlFBPase 146 DEP-SEKDA-----LQPGRNVAAGYALYGSATMLVLMDCGVNCFMLDP
hmFBPase 146 DEP-SEKDA-----LQCGRNVAAGYALYGSATMLVALSTGQGVDFMLDP
plFBPase 146 DEP-SEKDA-----LQPGRNVAAGYALYGSATMLVLMVNGVNCVCFMLDP
ecFBPase 138 GTPVTEEDF-----LQPGNKQVAAGYVYGSSTMLVYTTGCGVHAFTYDP
          . : * . * : * * * : * * * : . : * * * * *

LmFBPase 195 NIGEFILTHPHISIPKRSIYSVNEGNYGKWPWFKEYIDYLYK--NKTT
TbFBPase 195 TVGEFIHTHPNITLQSRPIYSVNEGNLRHWDWAFKQYLHHIKN--EGEK
TcFBPase 195 PIGEFIHHTPHITLPAIRAISVNEGNFNCWPEWPKYMNHVK---AGSK
hlFBPase 190 AIGEFILVDKDKVKKKGIYSLNEGYARDFPAVTEYIQRKKFPDNSA
hmFBPase 190 ALGEFVLVEKDKVKKKGIYSLNEGYAKYFDAATEVYVQKKKFPEDGSA
plFBPase 190 AIGEFILVDRDKVKKKGIYSINEGYAKEFPAITEYIQRKKFPDNSA
ecFBPase 183 SLGVFCLCQERMRFPKGTYSINEGNYIKFPNGVKKYIKFCQEDKSTN
          : * * * . : : : * * * * * : : * * * : : .

LmFBPase 243 -RYSARYIGSMVGD IHR TLL YGGIFCYPK DANQVEGKLRLLYE AAPMAMI
TbFBPase 243 -AYTARYIGSMVAD IHR TLL YGGIFCYPGDKKPGGKLRLLYEA EAFMFL
TcFBPase 242 -LYTARYIGSMVADVHR TLL YGGIFCYPDLKRPEGKIRLLYE AAPLAML
hlFBPase 240 -PYGARYVGSMDVHR TLV YGGIFLYPANKKSPNGKLRLLYECNPMAYV
hmFBPase 240 -PYGARYVGSMDVHR TLV YGGIFLYPANQKSPKGLRLLYECNPMAYI
plFBPase 240 -PYGARYVGSMDVHR TLV YGGIFMYPANKKSPKGLRLLYECNPMAYV
ecFBPase 233 RPYTSRYIGSLVAD FHRNLLKGGIYLYPSTASHPDGKLRLLYECNPMAF
          * : * * * * * * * * * * * * * * * * * * * * * * *

LmFBPase 292 VEQAGGKAVGSNGRILEQSITRLHQRTPVYFGSRQEVLDLMAFRDRNVKT
TbFBPase 293 IEQAGGLALTGDGRLLDVVPKEIHQRAPVFMGSRREVELCMSFKQKYNDR
TcFBPase 292 VEQAGGKASTGKGRVLDVMPKPHQRVAVYMGSRREVNCLSFQKSEQKQ
hlFBPase 289 MEKAGGMATTGKEAVLDIVPTDIHQRAPVILGSPDDVLEFLKVYEKH---
hmFBPase 289 IEQAGGLATTGTQPVLDVKPEAIHQRPVILGSPEDVQEYLTVCVQKN---
plFBPase 289 MEKAGGLATTGKEAVLDIVPTDIHQRAPVILGSPEDVTELEIYQKH---
ecFBPase 283 AEQAGGKASDGKERILDIIPETLHQRRSFFVGNHMHVEDVERFIREF---
          * : * * * * * . : * : * * * . * . . *

LmFBPase 342 EALAPTSKSL
TbFBPase 340 GGVQRERSKSL
TcFBPase 339 STSK----L
hlFBPase 336 -----SAQ
hmFBPase 336 -----QAGS
plFBPase 336 -----AAK
ecFBPase 330 -----PDA

```

Figure 1.13 Structure-based sequence alignment of trypanosomatid, mammalian and *E. coli* Type-I FBPsases.

*Lm*FBPase (O97193), *Tb*FBPase (Q95PL6), *Tc*FBPase (Q4DE31, putative), human liver isoenzyme (*hl*FBPase, P09467), human muscle isoenzyme (*hm*FBPase, O00757), pig liver isoenzyme (*pl*FBPase, P00636) and *E. coli* Type-I isoenzyme (*ec*FBPase, P0A993). The secondary structure elements of *Lm*FBPase are shown above the alignment. Helices are shown by red, β -strands are shown by yellow, and loop regions are shown by green. The ‘dynamic loops’ (residues 50–71, all residue numbers are according to *Lm*FBPase) are labelled in purple. Residues identical in all aligned FBPsases are labelled by an asterisk (*), whereas a colon (:), and a period (.) indicate strongly similar and weakly similar sequences, respectively. Residues at the active sites are highlighted in cyan. Residues which interact with AMP are highlighted in orange. Residues involved in the tetramer central interactions are highlighted in grey. The sequence alignment was performed with Clustal Omega (Sievers *et al.*, 2011). Secondary structure colours are manually added using the colour scheme of PyMOL. Methionines shown as the first amino acids in the sequences correspond to start codons ‘ATG’ in the genes, but there is no experimental evidence that these methionines are present in the mature enzymes to the author’s best knowledge.

1.3.5 Previous studies on FBPsases from other organisms

1.3.5.1 Previous studies on mammalian FBPsases

(1) Mammalian FBPsases are homotetramers

Mammalian FBPsase is a homotetramer with a molecular mass of 37 kDa for each monomer (Figure 1.14, important crystal structures of FBPsases are summarised in Table 1.11 and Appendix Table 1). There are two main isoforms of FBPsases for mammals — the ‘liver’ isoenzyme and the ‘muscle’ isoenzyme [FBPsase extracted from kidney is identical to the liver isoform according to the cDNA sequences (Burton *et al.*, 1993)]. The Michaelis constant K_m (the substrate concentration at which the reaction rate is half of the maximal velocity) of the mammalian liver isoenzyme is about 1.5 μ M for the substrate F16BP. The active site that embraces the substrate F16BP (or catalytic products F6P and phosphate) and three divalent metals is located near the large interface (Figure 1.14) (Ke *et al.*, 1989b). It has been shown that the three divalent metal ions (Mg^{2+} , Mn^{2+} , or Zn^{2+}) which coordinate the 1-phospho group, are required for its hydrolysis (Benkovic & deMaine, 1982, Tejwani, 1983).

(2) Allosteric mechanism of the liver isoform of FBPsase

AMP is a non-competitive allosteric inhibitor for the liver isoform of FBPsase with an inhibitor constant (K_i) in the range of 1.6–16 μ M, depending on different species. The AMP binding site is located about 30 Å away from the active site (Figure 1.14). The binding of AMP transforms the ‘planar tetramer’ (the R-state) to a ‘rotated tetramer’

(the T-state) by inducing a 15°-pairwise rotation of subunits C1 and C2 relative to subunits C3 and C4 (Figure 1.14). The key catalytic residue Asp68 is located in the middle of the ‘dynamic loop’ (residues 50–72) (Choe *et al.*, 2000). In this inactive state, the dynamic loop is stabilised in a ‘disengaged conformation’ by the diagonal subunit. The ‘dynamic loop’ also changes its secondary structure upon the R-/T-state switch (Figure 1.14). The region ‘⁵²GIAHLY⁵⁷’ only adopts a loop conformation in T-state, but in R-state it adopts a 3_{10} -helix conformation. Likewise, the regions ‘⁵⁹IAGST⁶³’ and ‘⁶⁹QVK⁷¹’ only adopt conformations as β -strands in the R-state, but as loops in the T-state.

Fructose 2,6-bisphosphate (F26BP) is a competitive inhibitor which binds to the active site of FBPase (Pilkis *et al.*, 1981, Van Schaftingen & Hers, 1981). In 2007, Hines *et al.* successfully obtained a pig liver FBPase crystal co-crystallised with F26BP. FBPase complexed with F26BP exhibits an 11° rotation between the two dimers, which is similar to the T-state induced by AMP (McGrane *et al.*, 1983, Hines *et al.*, 2007a). Moreover, it has been shown that AMP inhibition can be enhanced up to 10 fold in the presence of F26BP, namely ‘AMP/F26BP synergism’ (Pilkis *et al.*, 1981, Van Schaftingen & Hers, 1981). Thus, even though the AMP concentration is relatively constant *in vivo*, the fluctuation of F26BP levels can dynamically alter FBPase activity (Okar & Lange, 1999).

Intermediate transition-state structures have also been identified in X-ray structures of mutant FBPases. The FBPase A54L adopts an I_R-state (intermediate-state structure that adopts a conformation closer to R-state) while I10D adopts an I_T-state (closer to T-state) (Iancu *et al.*, 2005, Gao *et al.*, 2013b). The A54L enzyme retains wild-type levels of activity, but the IC₅₀ of AMP increases 50-fold. It grows in two crystal forms in the presence of saturating AMP. In one form, the AMP-bound tetramer is in a R-like conformation, whereas in the other form, the AMP-bound tetramer is in a T-like conformation (namely I_T-state), where Ile10 was displaced from the central hydrophobic pocket. This I_R-state structure suggests that the mutation of Ala54→Leu destabilises the T-state of FBPase (Iancu *et al.*, 2005). The AMP binding triggers a 15° subunit-pair rotation of wild-type pig liver FBPase. By contrast, the I10D mutant only responded with a 12° rotation upon AMP binding, and thereby forms an I_T-state (Iancu

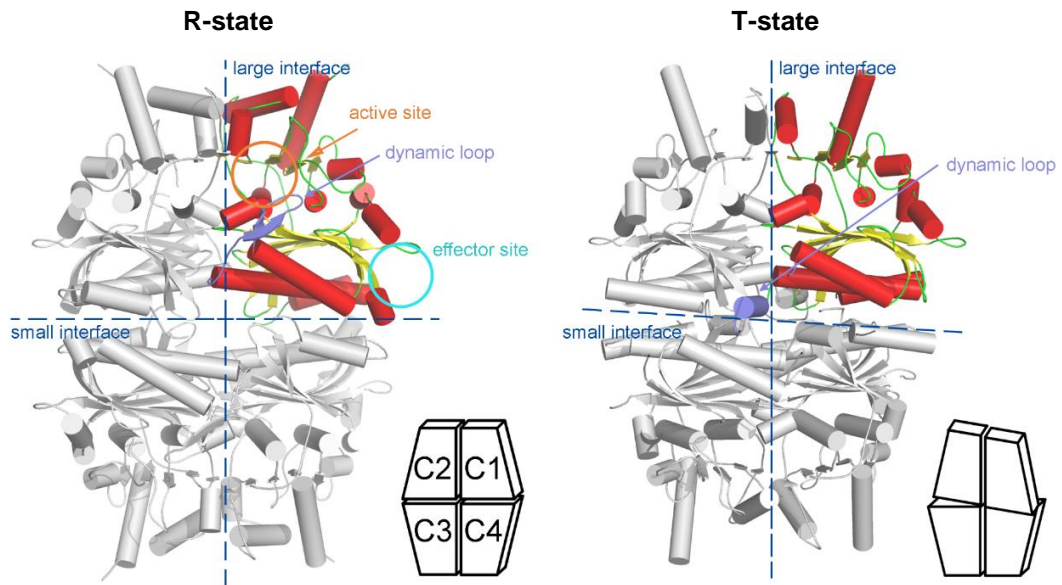
et al., 2005). These transition-state structures revealed the allosteric mechanism of pig liver FBPase, as well as the structural importance of residues located in the dynamic loop and the N-terminal loop, respectively.

(3) Allosteric mechanism of the muscle isoform of FBPase

In mammals, in addition to the liver isoform discussed as above, a second isoform of FBPase (the ‘muscle form’) is also capable of the hydrolysis of F16BP. In 1998, Tillmann *et al.* isolated cDNA encoding human muscle FBPase (Tillmann & Eschrich, 1998). In comparison with the liver isoform of FBPase, the muscle isoform shares ~75% sequence identity and strong structural conservation. In 2003, Rakus *et al.* carried out a careful comparison between human liver and muscle FBPases (Rakus *et al.*, 2003) (summarised in Table 1.10). The catalytic properties of both isoforms (K_m , K_{cat} , and $K_a[Mg^{2+}]$) are similar. Moreover, it has been shown that F26BP was able to inhibit the activity of both isoforms with a similar inhibitor constant. However, there is a 44-fold difference for the AMP inhibitory constant (K_i values for liver and for muscle FBPase are 4.8 μM and 0.14 μM , respectively), despite the identical amino acids that are directly involved in AMP binding (Rakus *et al.*, 2005).

In 2016, Barciszewski *et al.* presented the first R-state crystal structure of human muscle FBPase (Barciszewski *et al.*, 2016). It showed, in contrast to the well-studied R-state of the liver enzyme, which is flat the R-state of the muscle enzyme is strikingly different, with a perpendicular orientation of the upper and lower dimers (Figure 1.15). The crystal structure of the muscle isozyme R form shows that in this arrangement of the tetramer completely new protein surfaces are exposed that are most likely targets for the interactions with various cellular and enzymic partners.

(A)



(B)

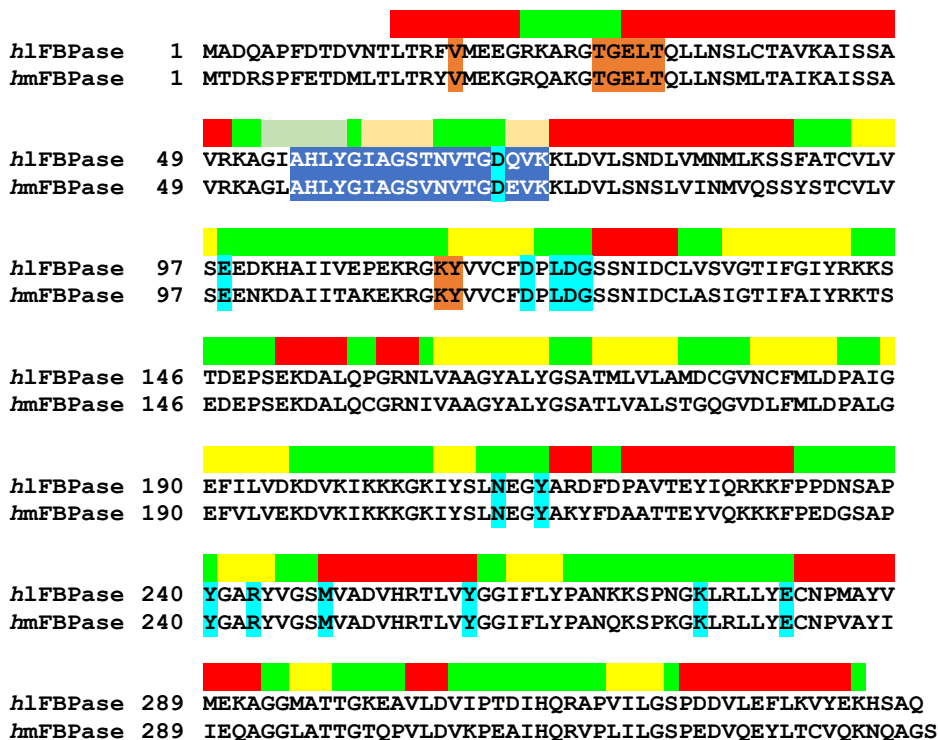


Figure 1.14 Overall structures of mammalian liver FBPase.

(A) The large interface [between the Chain 1/Chain 4 (C1C4) dimer and the C2C3 dimer] and the small interface (between the C1C2 dimer and the C3C4 dimer) are shown in dashed lines in each homotetramer. Secondary structures are shown in different colours in Chain 1 (helices, β -strands and loop regions in red, yellow and green, respectively) and on top of the amino acid sequence in Panel B. The position of the active site is shown with an orange circle in the structure,

whereas its residue codes are highlighted by orange background in the alignment in Panel B. Similarly, the effector site is shown in cyan. The dynamic loop (residues 50–72) is indicated in blue. Schematic models [adapted from diagrams in (Gidh-Jain *et al.*, 1994)] are shown in the bottom right. Structure of mammalian liver FBPAse (PDB code: 1EYI and 1EYJ for R-state and T-state, respectively) (Choe *et al.*, 2000) is used to show the structural model.

(B) Sequence alignment of human liver and muscle FBPAses. Secondary structures are shown in different colours (helices, β -strands and loop regions in red, yellow and green, respectively) on top of the sequences. In particular, the region ⁵²GIAHLY⁵⁷ is shown in light green, because it only adopts a loop conformation in T-state, but in R-state it adopts a 3_{10} -helix conformation. Likewise, the regions ⁵⁹IAGST⁶³ and ⁶⁹QVK⁷¹ are highlighted in light yellow, because they only adopt conformations as β -strands in R-state, but as loops in T-state. Residues corresponding to active site and effector site are highlighted in orange and cyan, respectively.

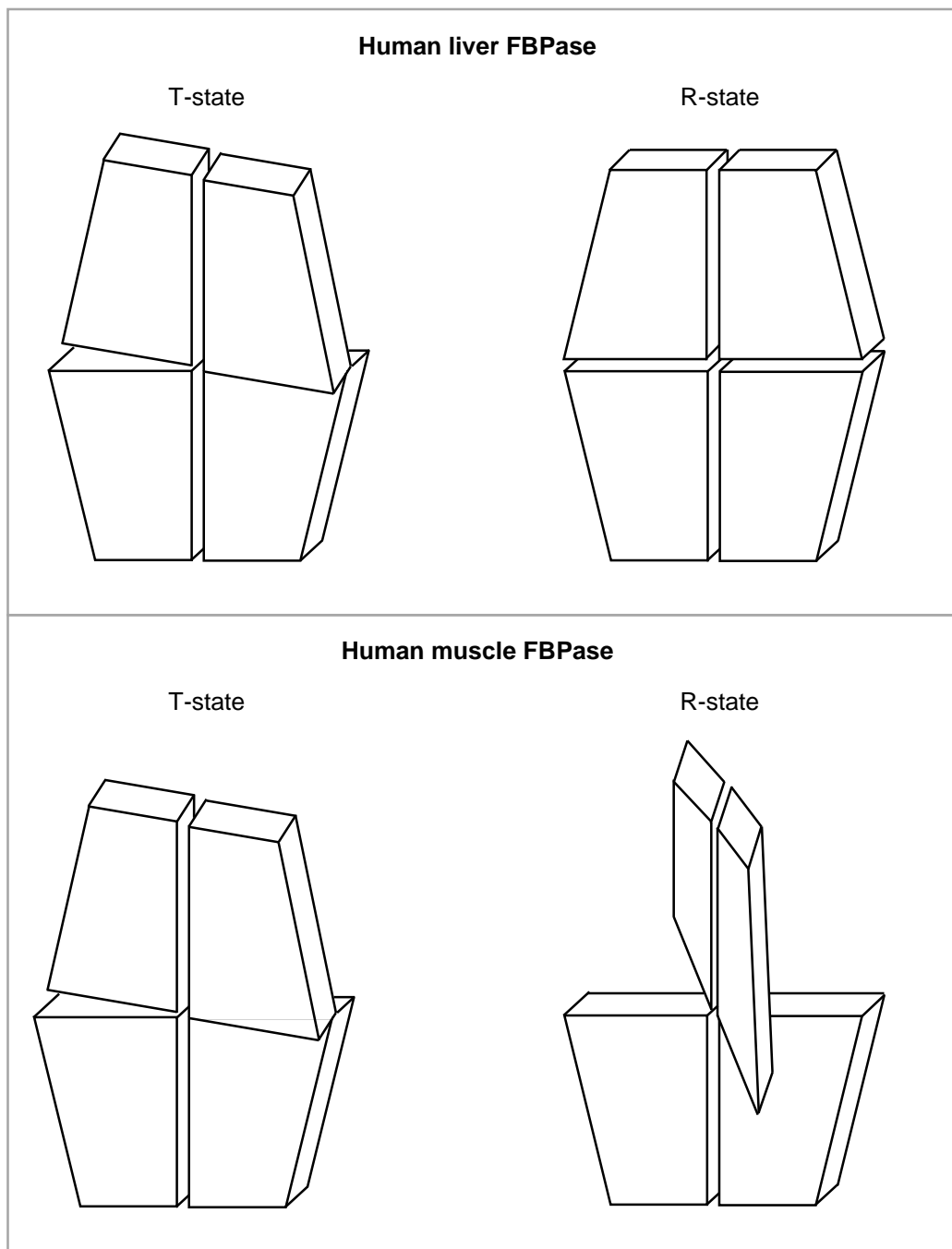


Figure 1.15 Allosteric models of human FBPases (isoforms of liver and muscle).

Schematic models are based on structures shown in (Gidh-Jain *et al.*, 1994) and (Barciszewski *et al.*, 2016).

Table 1.10 Enzyme kinetic properties of FBPases from different organisms.

Organism	Isoform	Type	K_m [F16BP] (μM)	K_{cat} (s^{-1})	K_a [Mg^{2+}] (μM)	K_i [AMP] (μM)	K_i [F26BP] (μM)	Temperature	pH	Reference
<i>Bacillus methanolicus</i>	glpX C	II	14	1.2	NS	NS	NS	55	7.7	(Stolzenberger <i>et al.</i> , 2013)
<i>Bacillus methanolicus</i>	glpX P	II	440	3.9	NS	NS	NS	55	7.7	(Stolzenberger <i>et al.</i> , 2013)
Bovine	liver	I	1.6	NS ^a	390	16	NS	37	7.5	(Rakus <i>et al.</i> , 2000)
Bovine	lung	I	4.4	14.8	310	14	0.21	37	7.5	(Rakus <i>et al.</i> , 2000)
<i>Clonorchis sinensis</i>	N/A	I	41.9	NS	650	250	NS	37	7.2	(Liang <i>et al.</i> , 2013)
<i>Corynebacterium glutamicum</i>	N/A	II	14	3.3	NS	90	NS	30	7.7	(Rittmann <i>et al.</i> , 2003)
<i>Cyprinus carpio</i> (fish)	liver	I	3	NS	567	8.4	NS	25	7.5	(Gizak <i>et al.</i> , 2012)
<i>Cyprinus carpio</i> (fish)	muscle	I	5.3	NS	426	0.71	NS	25	7.1	(Gizak <i>et al.</i> , 2012)
<i>Escherichia coli</i>	cytosolic	I	1.7	24	1	18.1	NS	22	7.5	(Hines <i>et al.</i> , 2007b)
<i>Escherichia coli</i>	glpX	II	35	NS	NS	no effect	NS	NS	7.7	(Donahue <i>et al.</i> , 2000)
human	liver	I	2.2	22	190	4.8	0.17	37	7.5	(Rakus <i>et al.</i> , 2003)
human	muscle	I	1.4	18.9	180	0.14	0.09	37	7.5	(Rakus <i>et al.</i> , 2003)
<i>Leptospira interrogans</i>	N/A	I	1	NS	1300	0.58	0.05	22	7.5	(Gao, 2013)
<i>Mycobacterium tuberculosis</i>	glpX II	II	44	1	250	NS	NS	30	7.7	(Gutka <i>et al.</i> , 2011b)
<i>Pelophylax esculentus</i> (frog)	muscle	I	1.68	NS	263	0.2	NS	25	7.5	(Dziewulska-Szwajkowska & Dżugaj, 2010)
Pig	liver	I	1.75	22	670	1.61	0.26	NS	7.5	(Choe <i>et al.</i> , 2000)
Pig	lung	I	4.1	16	300	7	NS	37	7.5	(Rakus <i>et al.</i> , 2000)
Rabbit	liver	I	1.3	NS	0.3	0.9	1.3	25	9.5	(Liu & Fromm, 1990)
<i>Saccharomyces cerevisiae</i>	YK23	new ^b	200	4.9	NS	10000	NS	30	NS	(Kuznetsova <i>et al.</i> , 2010)
Spinach	cytosolic	I	2–4	NS	260	120	0.07	NS	7.5–8.2	(Daie, 1993)
Spinach	chloroplast	I	33	NS	2000	no effect	no effect	NS	8.8 (oxidised) 7.5–8.2 (reduced)	(Daie, 1993)
<i>Sulfolobus tokodaii</i>	N/A	V	27	2.5	500	NS	NS	100	8.0	(Nishimasu <i>et al.</i> , 2004)

^a NS: data not shown in the paper.

^b The paper on *S. cerevisiae* FBPase suggested a new metal-independent eukaryotic FBPase type that cannot be classified into the canonical Type I–V.

Table 1.11 Selected crystal structures of FBPases in PDB.

PDB ID	Source	Type	Mutation	Ligand(s)	State	Space Group	Resolution	Reference
1LBV	<i>Archaeoglobus fulgidus</i>	IV	wild type	none	N/A	$P 1 2_1 1$	1.80	(Stieglitz <i>et al.</i> , 2002)
1NI9	<i>Escherichia coli</i>	II (<i>glpX</i>)	wild type	SO ₄ ²⁻	N/A	$P 4_1 2_1 2$	2.00	(Brown <i>et al.</i> , 2009)
2OX3	<i>Escherichia coli</i>	I	wild type	F6P ^a , PEP	R	$I 2 2 2$	2.18	(Hines <i>et al.</i> , 2007b)
2Q8M	<i>Escherichia coli</i>	I	wild type	AMP, BG6, Cl ⁻ , BFP, Mg ²⁺	T	$P 4_1 2 2$	2.05	(Hines <i>et al.</i> , 2007c)
1FTA	<i>Homo sapiens</i>	I (liver)	wild type	AMP	T	$P 2_1 2_1 2_1$	2.30	(Gidh-Jain <i>et al.</i> , 1994)
2FHY	<i>Homo sapiens</i>	I (liver)	wild type	A37, Mg ²⁺	T	$P 2_1 2_1 2_1$	2.95	(von Geldern <i>et al.</i> , 2006)
3IFA	<i>Homo sapiens</i>	I (muscle)	E69Q, V85L	AMP, GOL, SO ₄ ²⁻	T	$C 2 2 2$	1.93	(Zarzycki <i>et al.</i> , 2011)
4HE2	<i>Homo sapiens</i>	I (muscle)	Q32R	AMP, Cl ⁻ , Mg ²⁺ , PO ₄ ³⁻ , Zn ²⁺	R	$P 4_2 2_1 2$	1.60	(Shi <i>et al.</i> , 2013)
5ET5	<i>Homo sapiens</i>	I (muscle)	wild type	none	R	$I 4_1 2 2$	1.67	(Barciszewski <i>et al.</i> , 2016)
5ET6	<i>Homo sapiens</i>	I (muscle)	wild type	AMP	T	$C 2 2 2$	1.85	(Barciszewski <i>et al.</i> , 2016)
1DK4	<i>Methanocaldococcus jannaschii</i>	IV	wild type	Phosphate, Zn ²⁺	N/A	$P 2_1 2_1 2_1$	2.60	(Stec <i>et al.</i> , 2000)
1BK4	<i>Oryctolagus cuniculus</i>	I (liver)	wild type	Mg ²⁺ , SO ₄ ²⁻	R	$I 2 2 2$	2.30	(Weeks <i>et al.</i> , 1999)
1D9Q	<i>Pisum sativum</i>	I (chloroplast)	wild type (oxidised)	none	N/A	$P 1 2_1 1$	2.40	(Chiadmi <i>et al.</i> , 1999)
3F3K	<i>Saccharomyces cerevisiae</i>	YK23	wild type	GOL	N/A	$P 2_1 2_1 2_1$	1.75	(Kuznetsova <i>et al.</i> , 2010)
1SPI	<i>Spinacia oleracea</i>	I (chloroplast)	wild type	none	N/A	$P 1 2_1 1$	2.80	(Villaret <i>et al.</i> , 1995)
1UMG	<i>Sulfolobus tokodaii</i>	V	wild type	2FP, Mg ²⁺ , MPD	N/A	$I 4 2 2$	1.80	(Nishimasu <i>et al.</i> , 2004)
1CNQ	<i>Sus scrofa</i>	I (liver)	wild type	F6P, Phosphate, Zn ²⁺	R	$I 2 2 2$	2.27	(Choe <i>et al.</i> , 1998)
1EYI	<i>Sus scrofa</i>	I (liver)	wild type	F6P, Mg ²⁺ , Phosphate	R	$I 2 2 2$	2.32	(Choe <i>et al.</i> , 2000)
1EYJ	<i>Sus scrofa</i>	I (liver)	wild type	AMP, F6P, Mg ²⁺ , Phosphate	T	$P 2_1 2_1 2$	2.28	(Choe <i>et al.</i> , 2000)
1FJ6	<i>Sus scrofa</i>	I (liver)	Y57W	F6P, Phosphate, Zn ²⁺	R	$I 2 2 2$	2.50	(Nelson <i>et al.</i> , 2000)
1FJ9	<i>Sus scrofa</i>	I (liver)	Y57W	AMP, F6P, Phosphate, Zn ²⁺	T	$P 2_1 2_1 2$	2.50	(Nelson <i>et al.</i> , 2000)
1FSA	<i>Sus scrofa</i>	I (liver ^d)	K42A	AMP, F6P, Mg ²⁺	T	$P 2_1 2_1 2$	2.30	(Lu <i>et al.</i> , 1996)
1Q9D	<i>Sus scrofa</i>	I (liver)	wild type	F6P, Mg ²⁺ , OII, Phosphate	I ^b	$P 2_1 2_1 2$	2.35	(Choe <i>et al.</i> , 2003)
1YYZ	<i>Sus scrofa</i>	I (liver)	A54L	AMP, F6P, Mg ²⁺ , Phosphate	I _R ^c	$I 2 2 2$	1.85	(Iancu <i>et al.</i> , 2005)
2F3D	<i>Sus scrofa</i>	I (liver)	I10D	AMP, F6P, Phosphate, Zn ²⁺	I _T ^c	$I 2 2 2$	1.83	(Gao <i>et al.</i> , 2013b)
5FBP	<i>Sus scrofa</i>	I (liver ^d)	wild type	F6P	R	$P 3_2 2 1$	2.10	(Ke <i>et al.</i> , 1991b)
3ROJ	<i>Synechocystis</i>	II	wild type	AMP, Cl ⁻ , GOL, Mg ²⁺ , SO ₄ ²⁻	N/A	$P 6_5$	2.30	To be published
5A5L	<i>Thermosynechococcus elongatus</i>	II	wild type	Mg ²⁺ , Phosphate	N/A	$I 4_1 2 2$	2.34	(Cotton <i>et al.</i> , 2015)

Full table of all published crystal structures is shown in Appendix Table 1 (<https://1drv.ms/w/s!An9gBV9AQR6hgY53N5VdYtI6xpK0hA>).

^a Abbreviations are shown in Appendix Table 1.

^b I-state: The FBPase-OC252 complex rotates 14° on the small interface, falling some 3° short of the canonical T-state, namely 'I-state'.

^c I_R or I_T state: R-like or T-like state of the AMP-product complex of A54L FBPase.

^d FBPase extracted from kidney is identical to the liver isoform according to the cDNA sequences (Burton *et al.*, 1993).

1.3.5.2 Drug discovery for human FBPase

Hepatic gluconeogenesis has been identified as a major source of hepatic glucose overproduction in type-2 diabetes patients (Magnusson *et al.*, 1992). The majority of type-2 diabetes patients fail to reach desired glucose levels, despite the availability of several therapies, none of which produce glucose-lowering effects via inhibition of the gluconeogenic pathway (Dang *et al.*, 2012). FBPase has been shown as a drug target for type-2 diabetes as gluconeogenic enzyme that controls the incorporation of all three-carbon substrates into glucose without risking hypoglycaemia (Steinmann & Santer, 2012).

Drugs targeting human FBPase have been extensively studied and designed for the treatment of type-2 diabetes (summarised in Table 1.12). Three classes of inhibitors have been reported: those interacting with the active site (competitive inhibitors), a site at the tetramer centre (uncompetitive), and the AMP site (non-competitive). Attempts to discover potent and selective inhibitors at the active site showed a lack of progress (Pilkis *et al.*, 1986). Uncompetitive inhibitors [e.g. anilinoquinazolines (Wright *et al.*, 2002) and benzoxazole benzenesulfonamides (Lai *et al.*, 2006)] bound to the hydrophobic pocket of the tetramer centre, with modestly potent inhibitions. Inhibitors bound to the AMP site have gained particular success for reducing the activity of human liver FBPase. Among the compounds studied *in silico*, *in vitro* and *in vivo*, phosphonic acid-containing thiazoles (Erion *et al.*, 2005, Dang *et al.*, 2012) and tricyclic compounds (Tsukada *et al.*, 2009) have been demonstrated to bind to the effector site of human liver FBPases at the nanomolar level. In particular, the compounds in the CS-917 family discovered by Dang *et al.* from Metabasis Therapeutics, Inc. have advanced into phase 2b human clinical trials, and have been shown to lower blood glucose levels in patients with type-2 diabetes (Dang *et al.*, 2012). These phosphonic acid-containing thiazoles mimic AMP binding, which binds with Val17, Thr27, Gly28, Glu29, Leu30, Lys112, and Tyr113 of human FBPase (Figure 1.16). As discussed earlier in Section 1.3.4, the basic Lys112 is replaced by an acidic and shorter aspartic acid in *Lm*FBPase. In this case, a chemical modification on the phospho group of the phosphonic acid-containing thiazoles might be a strategy for the development of anti-*Leishmania* FBPase drugs. In addition, high-throughput

screening assays have identified aromatic sulfonylureas as FBPase inhibitors mimicking AMP (Hebeisen *et al.*, 2008). By bridging two adjacent allosteric binding sites using two aromatic sulfonylureas as anchor units and covalently linking them, it was shown to be possible to obtain dual binding AMP site inhibitors that exhibit a strong inhibitory effect. These observations may also provide extensive insights into the design of drugs against *Lm*FBPase.

Table 1.12 Human liver FBPase inhibitors.

Name	Binding site	Best IC ₅₀ (nM)	PDB code	Reference
Anilinoquinazoline	Tetramer centre	830	1KZ8	(Wright <i>et al.</i> , 2002)
3-(2-carboxy-ethyl)-4,6-dichloro-1 <i>H</i> -indole-2-carboxylic acid	AMP site	2500	1LEV	(Wright <i>et al.</i> , 2003)
Phosphonic acid-containing thiazoles (CS-917)	AMP site	16	not provided ^a	(Erion <i>et al.</i> , 2005, Dang <i>et al.</i> , 2007, Dang <i>et al.</i> , 2009, Dang <i>et al.</i> , 2010, Dang <i>et al.</i> , 2011a, Dang <i>et al.</i> , 2011b, Dang <i>et al.</i> , 2012)
Benzoxazole benzenesulfonamides	Tetramer centre	570	not provided	(Lai <i>et al.</i> , 2006)
Dimerised sulfonylureas	AMP site	3	2JJK, 2VT5	(Hebeisen <i>et al.</i> , 2008)
Heteroaromatic organofluorine	AMP site	3090	not determined ^b	(Rudnitskaya <i>et al.</i> , 2009)
Tricyclic compounds	AMP site	1	3A29, 3KC1, 3KC0, 3KBZ	(Tsukada <i>et al.</i> , 2009, Tsukada <i>et al.</i> , 2010a, Tsukada <i>et al.</i> , 2010b, Tsukada <i>et al.</i> , 2010c)
Sulfonylureido thiazoles	AMP site	40	not provided	(Kitas <i>et al.</i> , 2010)
N-substituted indoles, pyrroles, and triarylpyrazoles	AMP site	32	not determined	(Rudnitskaya <i>et al.</i> , 2010)
Aminopyridines	AMP site	80	2Y5L, 2Y5K	(Hebeisen <i>et al.</i> , 2011)
7-nitro-1 <i>H</i> -indole-2-carboxylic acid derivatives	AMP site	990	not determined	(Bie <i>et al.</i> , 2014)
2,5-Diphenyl-1,3,4-oxadiazoles	AMP site	2300	not determined	(Liao <i>et al.</i> , 2014)

^a Crystal structure for the protein-inhibitor complex is available, but PDB code is not provided.

^b Crystal structure not determined.

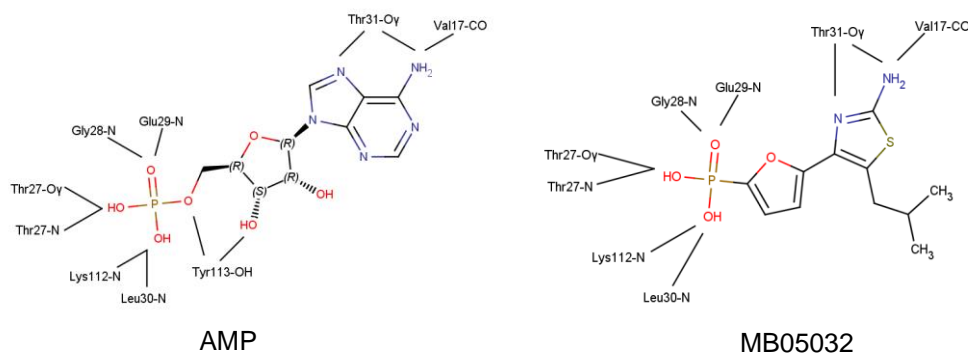


Figure 1.16 Comparison of the allosteric effector site of human liver FBPase in complex with AMP or the type-2 diabetes drug MB05032.

MB05032 is a compound in the CS-917 family (van Poelje *et al.*, 2011).

1.3.5.3 Previous studies on plant FBPases

There are two main isoforms of Type-I FBPases in plants, the cytosolic isoenzyme and the chloroplast isoenzyme (Table 1.10). The cytosolic isoenzyme is a non-photosynthetic isoform. Kinetic and allosteric properties of the cytosolic isoenzyme are remarkably similar to the mammalian FBPases (Zimmermann *et al.*, 1978, Kelly *et al.*, 1982, Daie, 1993). In the absence of effector molecules, the K_m of the cytosolic FBPase is about 4–6 μM . The enzyme requires Mg^{2+} and is subject to inhibition by AMP (non-competitive inhibition; $K_i=120 \mu\text{M}$) and strong inhibition by F26BP (competitive inhibition, $K_i=0.07 \mu\text{M}$) (Stitt & Heldt, 1985, Stitt, 1990). F26BP increases the enzyme's sensitivity to AMP inhibition and dramatically decreases the substrate affinity (100-fold), resulting in sigmoidal saturation curves (Herzog *et al.*, 1984).

The chloroplast isoenzyme mainly exists in photosynthetic cells, working as a part of the Calvin cycle in carbon fixation. It is a homolog of the cytosolic isoenzyme. It shows different properties in sequence, kinetic and structural aspects in comparison with the cytosolic isoenzyme. Unlike the AMP- and F26BP-sensitive cytosolic isoenzyme, the chloroplast isoenzyme is redox-regulated by light (i.e., redox-signalling). It was shown that light turns off the enzyme activity by inducing formation of a disulfide bond in an important regulatory loop (Chiadmi *et al.*, 1999). Mutation of any of the cysteines into serine results in constitutively active FBPases, with reduced or no sensitivity to reducing agent (Jacquot *et al.*, 1995, Jacquot *et al.*, 1997, Rodriguez-Suarez *et al.*,

1997). In 1995, Villeret *et al.* reported the first crystal structure of chloroplast FBPase. It showed a 'super-T' form homotetramer, which demonstrates an increased three-degree pairwise rotation in comparison with the T-state pig kidney FBPase (Villeret *et al.*, 1995). In another crystal structure in an oxidised state reported later (Chiadmi *et al.*, 1999), it was shown that the disulfide bond formation promotes a shift in strands $\beta 1$ and $\beta 2$ and pushes a valine sidechain into cation binding sites, which is a conflict with the engaged conformation of the catalytically important dynamic loop, thereby disrupting the catalysis.

1.3.5.4 Previous studies on yeast FBPases

In *Saccharomyces cerevisiae*, the Type-I FBPase is allosterically controlled by AMP and F26BP like mammalian FBPases (Donahue *et al.*, 2000, Entian *et al.*, 1988). In 2010, Kuznetsova *et al.* discovered a novel FBPase, namely YK23 (Kuznetsova *et al.*, 2010). It was found that the FBPase activity of YK23 was not sensitive to AMP (up to 10 mM), whereas F26BP inhibited YK23 activity competitively. YK23 represents the first metal-independent FBPase and a second FBPase family in eukaryotes.

1.3.5.5 Previous studies on bacterial FBPases

E. coli Type-I FBPase (*ec*FBPase-I) is required for growth on gluconeogenic substrates and probably represents the main gluconeogenic FBPase (Fraenkel & Horecker, 1965). It shares 43.6% and 40.4% sequence identity with human liver and *Leishmania* FBPases, respectively. Like other conventional Type-I FBPases, it can be inhibited by AMP ($K_i=18 \mu\text{M}$, less effective than mammalian FBPases) and F26BP, despite the absence of F26BP in *E. coli* (Kelley-Loughnane *et al.*, 2002, Hines *et al.*, 2007a). Dilution of *ec*FBPase-I leads to slow loss of activity, indicating that the dimeric form of *ec*FBPase-I is less active than the tetrameric. Anion activators, such as PEP or citrate, bind to an allosteric site at the small interface and promote the formation of tetramers, which adopt a similar conformation to the R-state mammalian FBPase (Hines *et al.*, 2007b). Unlike mammalian FBPases, *ec*FBPase-I stays in the R-state in the presence of F26BP (Kelley-Loughnane *et al.*, 2002). Binding to the large interface, glucose 6-phosphate (G6P) has been shown as an inhibitor of *ec*FBPase-I, which was further characterised as a synergistic inhibitor with AMP (Hines *et al.*, 2007c). *ec*FBPase-I

also shows a 9°-pairwise rotation along the small interface upon AMP binding, like mammalian FBPases. The structure not only shows the rotation of the C1-C2 dimer relative to the C3-C4 dimer, but an additional 3°-rotation of C1 relative to C2, and C3 relative to C4, causing significant disruption to the active site (Figure 1.17). Moreover, the dynamic loops in both active and inactive forms of *ec*FBPase-I structures are disordered (Hines *et al.*, 2006, 2007b, Hines *et al.*, 2007c).

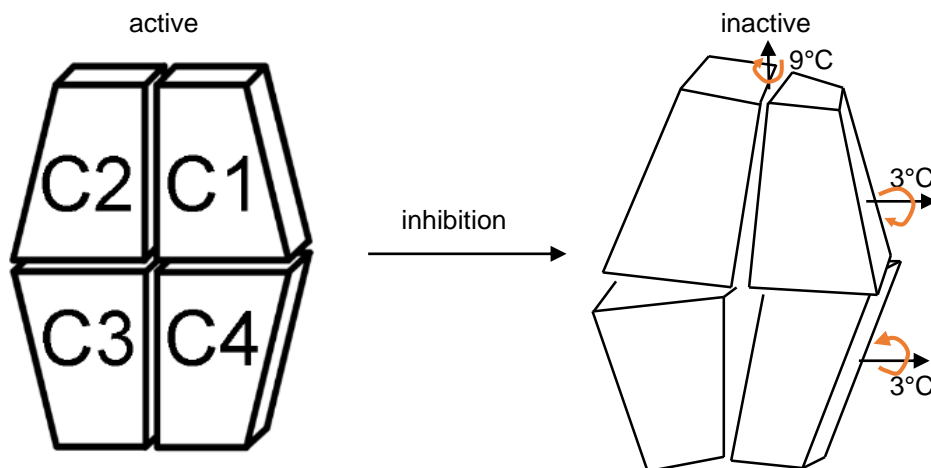


Figure 1.17 Allostery of FBPase from *E. coli*.

Schematic models are based on structures shown in (Hines *et al.*, 2006, 2007b, Hines *et al.*, 2007c).

In 2009, Brown *et al.* demonstrated Type-II FBPase in *E. coli* (i.e., the *glpX* isoform) (Brown *et al.*, 2009). It was shown to be a metal-dependent elongated dimer (molecular mass 118 kDa) with a low affinity for F16BP (Table 1.10). The *glpX* (Type-II FBPase) has long been considered as the only FBPase in *Mycobacterium tuberculosis*, and thus a promising gluconeogenic target for drug discovery (Gutka *et al.*, 2011b, Gutka *et al.*, 2011a, Gutka *et al.*, 2015). However, FBPase activity was unexpectedly detected in a Δ GLPX *Mycobacterium tuberculosis* mutant grown on gluconeogenic carbon sources (Ganapathy *et al.*, 2015). A further study indicated that the genome encodes an alternative FBPase (GPM2, Rv3214) that can maintain gluconeogenesis in the absence of GLPX. Consequently, deletion of both GLPX and GPM2 would be required for disruption of gluconeogenesis.

1.3.5.6 *Leishmania* FBPase as a drug target

Located in glycosomes, trypanosomatid FBPases are classified as Type-I FBPases (Naderer *et al.*, 2006). Despite a potential drug target against *Leishmania*, *Lm*FBPase and other trypanosomatid FBPases are poorly studied. This thesis reports enzyme kinetic and structural studies on *Lm*FBPase, thereby demonstrating its allosteric mechanism and potential for drug design.

CHAPTER 2

Materials and methods

CHAPTER 2. Materials and methods

This chapter shows the reagents (Table 2.1), cell culture medium (Table 2.2), and apparatus (Table 2.3) used in this thesis. Moreover, general methods including protein production, dynamic light scattering, analytical gel-filtration, enzyme assays, and thermal shift assays are also described in this chapter.

Table 2.1 Information of reagents used in this thesis.

Reagent name	Abbreviation	Product No.	Supplier
adenosine 5'-diphosphate	ADP	A4386	Sigma-Aldrich
adenosine 5'-monophosphate	AMP	1930	Sigma-Aldrich
adenosine 5'-triphosphate	ATP	A7699	Sigma-Aldrich
bovine serum albumin	BSA	A2153	Sigma-Aldrich
calcium chloride	N/A	C8106	Sigma-Aldrich
cobalt(II) chloride	N/A	255599	Sigma-Aldrich
D-fructose 1,6-bisphosphate	F16BP	F6803	Sigma-Aldrich
D-fructose 6-phosphate	F6P	F3627	Sigma-Aldrich
Dulbecco's phosphate-buffered saline without calcium and magnesium	PBS-CM	D5652	Sigma-Aldrich
glucose-6-phosphate dehydrogenase	G6PDH	G6378	Sigma-Aldrich
L-alanine	N/A	A7627	Sigma-Aldrich
L-arginine hydrochloride	N/A	A5131	Sigma-Aldrich
L-asparagine	N/A	A0884	Sigma-Aldrich
L-aspartic acid	N/A	A9256	Sigma-Aldrich
L-cysteine	N/A	C1276	Sigma-Aldrich
L-cystine	N/A	C8755	Sigma-Aldrich
L-glutamic acid	N/A	G1251	Sigma-Aldrich
L-glutamine	N/A	G3126	Sigma-Aldrich
glycine	N/A	G7126	Sigma-Aldrich
L-histidine	N/A	H8125	Sigma-Aldrich
L-isoleucine	N/A	I2752	Sigma-Aldrich
L-leucine	N/A	L8000	Sigma-Aldrich
L-lysine	N/A	L5626	Sigma-Aldrich
L-methionine	N/A	M9625	Sigma-Aldrich
L-phenylalanine	N/A	P2126	Sigma-Aldrich
L-proline	N/A	P0380	Sigma-Aldrich
L-serine	N/A	S4500	Sigma-Aldrich
L-threonine	N/A	T8625	Sigma-Aldrich
L-tryptophan	N/A	T0254	Sigma-Aldrich
L-tyrosine	N/A	T3754	Sigma-Aldrich
L-valine	N/A	V0500	Sigma-Aldrich
L-ascorbic acid	N/A	A5960	Sigma-Aldrich
L-lactate dehydrogenase	LDH	L1254	Sigma-Aldrich
L-glutathione	GSH	G4251	Sigma-Aldrich
manganese(II) chloride	N/A	M3634	Sigma-Aldrich
N,N,N',N'-tetramethylethylenediamine	TEMED	T9281	Sigma-Aldrich
oxalate	N/A	247537	Sigma-Aldrich
oxaloacetate	N/A	O4126	Sigma-Aldrich
phospho(enol)pyruvic acid	PEP	P7002	Sigma-Aldrich
phosphoglucose isomerase	PGI	P5381	Sigma-Aldrich

poly(ethylene glycol) 3,350	PEG3,350	88276	Sigma-Aldrich
poly(ethylene glycol) 8,000	PEG8,000	81268	Sigma-Aldrich
S-methyl methanethiosulfonate	MMTS	64306	Sigma-Aldrich
sodium dodecyl sulfate	SDS	L6026	Sigma-Aldrich
sodium molybdate	N/A	331058	Sigma-Aldrich
sodium phosphate monobasic	N/A	71505	Sigma-Aldrich
streptavidin resin	N/A	85881	Sigma-Aldrich
triethanolamine hydrochloride	TEA	T1502	Sigma-Aldrich
tris(2-carboxyethyl)phosphine	TCEP	C4706	Sigma-Aldrich
tris(hydroxymethyl)aminomethane	Tris	252859	Sigma-Aldrich
β -nicotinamide adenine dinucleotide	NADH	N8129	Sigma-Aldrich
β -nicotinamide adenine dinucleotide phosphate	NADP+	N0505	Sigma-Aldrich
Dithiothreitol	DTT	MB1015	Melford
isopropyl β -D-1-thiogalactopyranoside	IPTG	MB1008	Melford
kanamycin	N/A	K0126	Melford
Ethylenediaminetetraacetic acid	EDTA	10355410	Fisher Scientific
imidazole	N/A	10284730	Fisher Scientific
SYPRO® Orange	N/A	S-6650	Thermo Fisher Scientific
Zeba spin desalting columns 7K MWCO 0.5 ml	N/A	89882	Thermo Fisher Scientific
Oxoid™ yeast extract	N/A	LP0021	Thermo Fisher Scientific
plasmid Miniprep Kit	N/A	27104	QIAGEN
yeast extract	N/A	YEA02	Formedium
agar	N/A	AGA02	Formedium
tryptone	N/A	TRP01	Formedium
Bacto™ Tryptone	N/A	211705	BD

Recipe of PBS-CM: a mixed powder containing 0.2 g/L KCl, 0.2 g/L KH₂PO₄, 8.0 g/L NaCl, and 1.15 g/L anhydrous Na₂HPO₄.

General salts were purchased from Fisher Scientific. Restriction enzymes and other enzymes used for cloning were purchased from New England BioLabs. Vector and *E. coli* competent cells were purchased from Novagen. Fructose 2,6-bisphosphate is a gift from Dr David A. Okar at the Veterans Administration Medical Center, United States.

Table 2.2 Recipes of cell culture medium used in this thesis.

Cell culture medium	Recipe (for 1 L medium)
Lysogeny broth	10 g Tryptone, 5 g yeast extract, and 10 g NaCl, pH 7.2
Lysogeny broth agar	10 g Tryptone, 5 g yeast extract, 10 g NaCl, and 15 g agar, pH 7.2
2× Tryptone yeast	16 g Tryptone, 10 g yeast extract, and 5 g NaCl, pH 7.4
Super optimal broth	20 g Bacto™ Tryptone, 5 g Oxoid™ yeast extract, 0.58 g NaCl, 0.188 g KCl, 2.47 g MgSO ₄ , 2.03 g MgCl ₂ , and 3.60 g glucose

Table 2.3 Apparatus used in this thesis.

Name of apparatus	Manufacturer
multi-mode microplate reader SpectraMax® M5	Molecular Devices Corporation
iQ5 real-time PCR detection system	Bio-Rad
Zetasizer APS for DLS	Malvern
Avanti® J-26 XPI centrifuge	Beckman Coulter
HiTrap IMAC Sepharose FF columns	GE Healthcare Life Sciences
HiLoad® 16/60 Superdex® 200 pg column	GE Healthcare Life Sciences
HiPrep 16/60 Sephacryl® S-200 HR column	GE Healthcare Life Sciences
Superdex® 200 PC 3.2/30 column	GE Healthcare Life Sciences
Constant Systems TS cell disruptor	Constant Systems Limited
Nanodrop® 2000 UV-Vis Spectrophotometer	Thermo Scientific
Vivaspin® tubes	Sartorius

2.1 Transformation, expression and cell lysis

All five proteins (wild-type M1PYK, wild-type M2PYK, M2PYK C326S, M2PYK C358S, and *LmFBPase*) described in this thesis were expressed in *E. coli* with plasmids prepared previously in our lab (Morgan *et al.*, 2013, Vasquez-Valdivieso, 2013, Mitchell, 2014). The PYKs are N-terminally His₆-tagged with a thrombin-cleavage site (MGSSHHHHHSSGLVPRGSH), whereas the *LmFBPase* contains a C-terminal His₆ tag (AAALEHHHHHH). The pET24a plasmid encoding *LmFBPase* was a gift from Professor Paul A. M. Michels.

For all PYKs except for M2PYK C326S, pET28a plasmids that encode each protein was transformed into chemically competent BL21(DE3) *E. coli* cells. Briefly, approximately 100 ng of each plasmid was added into 25 µl *E. coli* cells. The samples were incubated on ice for 30 min, followed by 42 °C-heat shock for 45 s. The samples were then incubated on ice for 2 min. Afterwards, 250 µl of 37 °C Super Optimal Broth (SOC) was mixed into each sample and incubated for 1 h at 37 °C with shaking at 250 rpm. The bacteria were then streaked onto lysogeny broth (LB) agar plates with 50 µg/ml kanamycin for the selection of cells containing the expression plasmid at 37 °C overnight.

Single colonies were used to inoculate 50 ml LB medium containing 50 µg/ml kanamycin and incubated at 37 °C overnight with shaking at 250 rpm. Twenty microlitres of the overnight culture was used to inoculate 1 L of 2× Tryptone Yeast (TY) medium containing 50 µg/ml kanamycin in 2-L Erlenmeyer flasks. The cells were incubated at 37 °C at 250 rpm until the optical density at 600 nm (OD₆₀₀) reached 0.8 to 1.0. The cell culture was cold-shocked for 1 h at 4 °C, followed by induction with IPTG (final concentration 1 mM) for 18 h at 18 °C with shaking at 250 rpm. Cells were harvested in a JLA-8.1000 rotor at 15,900×g for 20 min at 10 °C. Cell pellets from 1 L cultures were then flash-frozen with liquid nitrogen and stored at -80 °C.

The trial of expression of M2PYK C326S using the protocol described above, failed to produce detectable amounts of soluble PYK protein. Optimisations were carried out using a series of different *E. coli* cells, media, and induction methods. The successful strategy is shown below. After pET28a plasmids that encode the expression of

M2PYK C326S were transformed into BL21 star *E. coli* cells, a 50-ml culture was grown as described above. Ten microlitres of the overnight culture was used to inoculate 1 L of LB media in 2-L Erlenmeyer flasks. The cells were incubated at 37 °C at 250 rpm until the OD₆₀₀ reached 0.6 to 0.8. IPTG was added to a final concentration of 1 mM to induce expression and the culture was incubated at 18 °C for 3 h with shaking at 250 rpm. Cell harvest and storage were carried out the same as described above.

The plasmid pET24a encoded *L. major* FBPase had been amplified by PCR using *L. major* (MHOM/SU/73/5-ASKH) genomic DNA. This overexpression plasmid was transformed into *E. coli* BL21(DE3) as described above. Single colonies were picked from LB kanamycin (50 µg/ml) agar plates and inoculated into 50 ml of LB medium (containing 50 µg/ml kanamycin). Cultures were grown overnight at 37 °C and 250 rpm. Ten millilitres of the overnight culture were inoculated into 500 ml of LB medium (containing 50 µg/ml kanamycin) in 2-L Erlenmeyer flasks. The cell culture was grown at 37 °C and 250 rpm to an OD₆₀₀ of 1.0, at which time transcription was induced by the addition of IPTG (final concentration 1 mM). The culture was maintained (at 30 °C and 120 rpm) for an additional 24 h. The cells were then harvested and stored in the same way as described above.

The cell lysis methods used for all five samples (wild-type M1PYK, wild-type M2PYK, M2PYK C326S, M2PYK C358S, and *Lm*FBPase) were almost identical, except for differences in lysis buffers. Briefly, cell pellets stored at -80 °C were thawed on ice, followed by a thorough mixture with cold lysis buffer (30 ml lysis buffer for each cell pellet from a 1-L culture). The cells were then disrupted with a constant cell disruption system at 25 kilopound per square inch (KPSI, 1 KPSI = 6.9 MPa) at 4 °C, followed by a 30-ml lysis buffer rinse at the same condition (also collected as lysate). The lysate was then centrifuged at 6 °C for 45 min at 60,000×g with a JA-25.50 rotor, and the supernatant was filtered through a 0.2-µm syringe filter and loaded onto an ÄKTA Protein Purification Systems for purification.

The lysis buffer for all PYKs consists of: 50 mM NaH₂PO₄, 300 mM NaCl, 20 mM imidazole, and EDTA-free protease inhibitors (one tablet per 100 ml lysis buffer, same

as below), pH 8.0. The lysis buffer for *Lm*FBPase consists of: 50 mM TEA, 300 mM NaCl, 20 mM imidazole, and 1 tablet EDTA-free protease inhibitors, pH 8.0.

2.2 Protein purification

2.2.1 Protein purification of PYKs

Purifications for all proteins followed a two-step strategy, with an IMAC crude purification followed by a size-exclusion polishing step. For the purification of all PYKs except for M2PYK C326S, filtered cell lysate was loaded onto a 5-ml HiTrap IMAC Sepharose Fast Flow column (pre-charged with cobalt) at 2 ml/min. The flow rate was maintained at 2 ml/min during all IMAC purification steps. The column was washed with 12 column volumes (CVs) of buffer A (50 mM NaH₂PO₄, 300 mM NaCl, 20 mM imidazole, pH 8.0) followed by an additional wash step with 15 CVs of 20% buffer B (50 mM NaH₂PO₄, 300 mM NaCl, 250 mM imidazole, pH 8.0) to remove contaminants. The His-tagged PYKs were eluted with five CVs of undiluted buffer B. Eluted samples were concentrated with Vivaspin[®] tubes (cut-off molecular mass 30 kDa, centrifuge at 4,000×g at 4 °C) to a final volume of approximately 2 ml. The samples were then subjected to the second purification step using a HiLoad[®] 16/600 Superdex[®] 200 column (pre-equilibrated with PBS-CM, a commercial PBS buffer free from magnesium and calcium, pH 7.4) for size-exclusion at the flow rate of 1 ml/min. Purified fractions were collected and concentrated to about 20 mg/ml with Vivaspin[®] tubes using the same method described above. The concentration of proteins [diluted to the dynamic range of the spectrophotometer (absorbance reading 0.1–1.0)] were measured with the absorbance at the wavelength of 280 nm using a Nanodrop[®] 2000 spectrophotometer. The theoretical extinction coefficient is calculated as $\epsilon_{280\text{nm}}=29,910 \text{ M}^{-1} \text{ cm}^{-1}$ using the ExPASy Server (Gasteiger *et al.*, 2005). Absorption values were measured in triplicate to ensure consistency and a mean value calculated. The concentration of each measurement was calculated according to the Beer-Lambert law: $A = \epsilon \times c \times l$, where A is the absorbance at a particular wavelength, ϵ is the absorption coefficient, and l is the path length of the cuvette (or cell) which holds the solution of concentration c . The concentration measurements were checked by SDS-

PAGE. Concentrated samples in PBS-CM were flash frozen with liquid nitrogen and stored at -80 °C.

The purification of M2PYK C326S was almost identical to that of other PYK proteins as described above. The only difference was that the buffer used for the size-exclusion and protein storage was PBS-CM containing 10% glycerol, instead of PBS-CM only, for the protection of M2PYK C326S from freeze-thaw damage.

2.2.2 Protein purification of *Lm*FBPase

*Lm*FBPase was also purified with an IMAC step followed by size-exclusion chromatography. Filtered cell lysate was loaded onto a 5-ml HiTrap IMAC Sepharose Fast Flow column (pre-charged with cobalt) at 3 ml/min. The flow rate was maintained at 3 ml/min during all IMAC purification steps. The column was washed with ten CVs of buffer A (50 mM TEA, 300 mM NaCl, 20 mM imidazole, pH 8.0) followed by gradient elution (from 0% to 100% of buffer B during 18 CVs, buffer B contained 50 mM TEA, 300 mM NaCl, 500 mM imidazole, pH 8.0). Eluted samples were concentrated with Vivaspin tubes (cut-off molecular mass 30 kDa, centrifuge at 4,000×g at 4 °C) to a final volume of approximately 2 ml. The samples were then subjected to the second purification step using a HiPrep 16/60 Sephacryl® S-200 HR column (pre-equilibrated with SEC buffer containing 20 mM TEA, 5 mM MgCl₂, 50 mM KCl, and 10% glycerol, pH 7.2) for size-exclusion chromatography at a flow rate of 0.5 ml/min. Purified fractions were collected and concentrated to about 4 mg/ml with Vivaspin tubes using the method described above. The concentrations of proteins (theoretical extinction coefficient 45,840 M⁻¹ cm⁻¹) were measured with the absorbance same as described above. Concentrations were measured in triplicate to ensure consistency, and a mean value calculated. The concentration measurements were checked by SDS-PAGE. Concentrated samples in SEC buffer were flash frozen with liquid nitrogen and stored at -80 °C.

2.3 Dynamic light scattering

Dynamic light scattering (DLS) was used to measure the particle size in solution, in order to obtain information on molecular size and protein aggregation. In this study, DLS analyses were performed using a Zetasizer Auto Plate Sampler instrument. Each protein sample was diluted to 1 mg/ml with its corresponding storage buffer (i.e., PBS-CM for PYK samples except M2PYK C326S, PBS-CM containing 10% glycerol for M2PYK C326S, and TEA buffer containing 10% glycerol for *LmFBPase*). Fifty microlitres of the 1 mg/ml protein sample was added into each well of a 384-well microtitre plate. The corresponding storage buffers were used as a reference. Samples were tested in triplicate.

2.4 Analytical gel-filtration

Analytical gel-filtration was carried out to characterise the oligomerisation/dissociation of PYK under different conditions. The assays were carried out on a Superdex[®] 200 PC 3.2/30 gel-filtration column (PBS-CM was used for pre-equilibration and sample elution). Four hundred microlitres of 0.1 mg/ml purified PYK was incubated with or without modulators in PBS-CM at room temperature at pH 7.4 for 12 h. After the incubation, samples were loaded independently onto the analytical gel-filtration column. Twenty-five microlitres of samples were injected, and the column flow rate was maintained at 0.1 ml/min. Protein peaks were monitored using absorbance at both 280 nm and 214 nm.

2.5 Enzymic activity assay

2.5.1 Enzymic activity assay of PYKs

The enzymic activity assays were performed based on a LDH-coupled enzyme system at 37°C by monitoring the decrease of NADH absorbance at 340 nm. The mechanism of the assay is shown in Figure 2.1. In the presence of ADP, PYKs catalyse the dephosphorylation reaction from PEP to pyruvate, which is then transformed to lactate

by LDH in the presence of NADH. During the reaction, NADH, which absorbs light at 340 nm, is transformed to NAD⁺. As a result, the activity of PYK can be identified by measuring the decreasing absorbance at 340 nm, in the presence of PEP, ADP, NADH, and LDH (Morgan *et al.*, 2012, Chen *et al.*, 2011, Vander Heiden *et al.*, 2010, Zoraghi *et al.*, 2011a, Zhong, 2013).

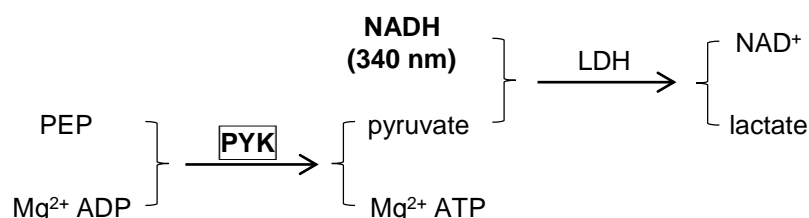


Figure 2.1 LDH-coupled enzyme reactions for PYK activity assay.

For the determination of kinetics of PYKs in the absence/presence of modulators, enzymic activity assays were performed as follows. Fifty microlitres of 0.002 mg/ml of PYK in PBS-CM was incubated with or without modulators in PBS-CM supplemented with 1 mM DTT (or other redox reagents if stated) in each well of a 96-well microtitre plate at 37 °C at pH 7.4 for 10 min. Then the same volume of assay buffer [PBS-CM supplemented with 10 mM MgCl₂, 100 mM KCl, 1 mM NADH, 40 U/ml LDH, as well as saturating ADP (4 mM) and titrated substrate PEP (0–10 mM) (or saturating concentration of PEP and different concentrations of ADP)] was added to each well to start the reaction. The decrease in absorbance at 340 nm (the absorbance of NADH) was measured for 5 min at 37 °C using a plate reader. The kinetic parameters (V_{max} , $K_{0.5}$, and n_H) were determined by fitting curves with the equation below (allosteric equation) to the data. V is the enzyme velocity, V_{max} is the maximum enzyme velocity in the same units as V , $K_{0.5}$ is the concentration of substrate that produces a half-maximal enzyme velocity, n_H is the Hill coefficient.

$$V = \frac{V_{max} \times [substrate]^{n_H}}{K_{0.5}^{n_H} + [substrate]^{n_H}}$$

The determination of time-dependent activity change was carried out using a similar method as shown above, with two modifications. The first modification was that the concentrations of substrates were saturating (i.e., final concentration 5 mM PEP and 2

mM ADP). The second was that the PYKs were incubated for different lengths of time after dilution from 20 mg/ml to 0.002 mg/ml.

The identification of PYK activity modulators was performed by enzymic activity assays as follows. One point nine microlitres of 20 mg/ml PYK in PBS-CM were added individually into 5 ml of different compounds in PBS-CM at pH 7.4 followed by an incubation at 37 °C for 30 min. Then the same volume of assay buffer [PBS-CM supplemented with 10 mM MgCl₂, 100 mM KCl, 1 mM NADH, 40 U/ml LDH, as well as sub-saturating substrates PEP (1 mM) and ADP (0.8 mM)] was added into the protein solution and mixed (so the concentrations of all reagents were halved). The decrease in absorbance at 340 nm (the absorbance of NADH) was measured for 5 min at 37 °C using a plate reader.

A concentration range of different modulators (0–1 mM for phenylalanine, 0–3 mM for alanine, 0–4 mM for tryptophan, and 0–30 mM for serine) were used for the detection of binding affinities against M2PYK. Briefly, the different concentrations of modulators were incubated with 0.002 mg/ml M2PYK in the presence of 1 mM DTT at 37 °C for 10 min. Assay buffer (containing metals and LDH, as above) supplemented with sub-saturating concentration of PEP and ADP were added to start the reaction. The catalysis was monitored as above.

2.5.2 Enzymic activity assay of *Lm*FBPase

Phosphoglucose isomerase (PGI) and glucose-6-phosphate dehydrogenase (G6PDH) were used as coupled enzymes in assays for *Lm*FBPase. The mechanism of the PGI/G6PDH-coupled enzyme assay is shown in Figure 2.2. Briefly, F16BP was hydrolysed into phosphate and F6P, which was isomerised to G6P by PGI in the presence of NADP⁺. The latter was further catalysed by G6PDH into NADPH, which has apparent absorption at the wavelength of 340 nm. This series of reactions was used to monitor the catalysis of *Lm*FBPase.

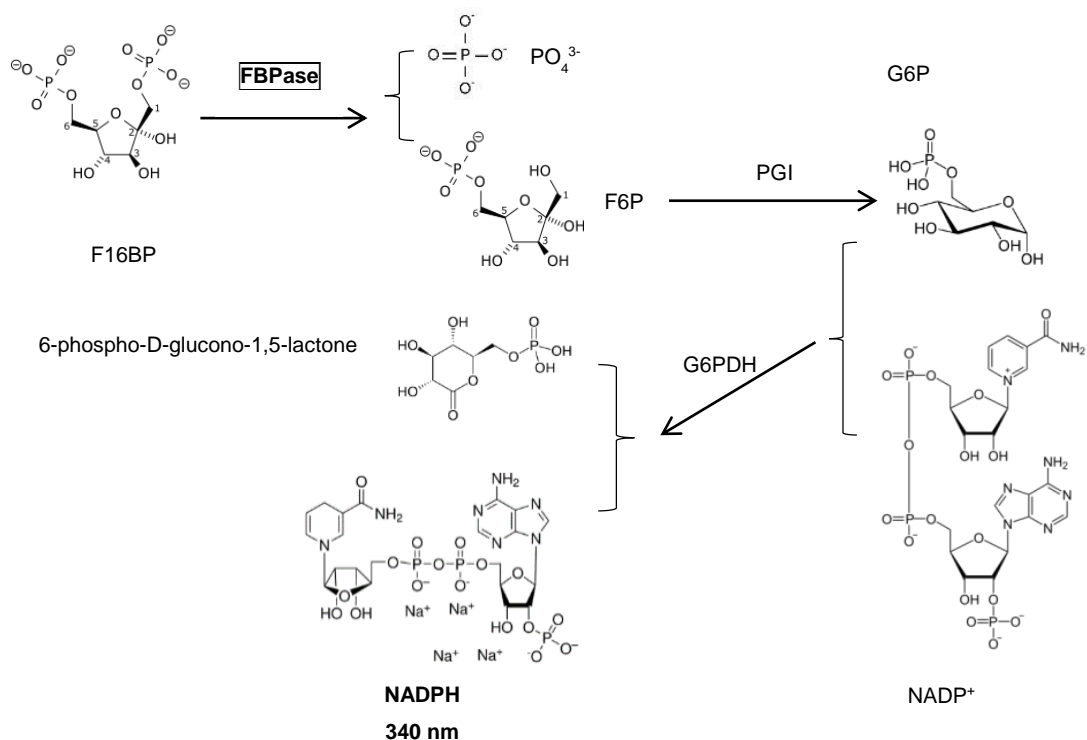


Figure 2.2 PGI/G6PDH-coupled enzyme reactions for FBPase activity assay.

For the determination of kinetic parameters of *Lm*FBPase, enzyme activity assays were performed as follows. Fifty microliters of different concentrations of F16BP (from 0 μ M to 500 μ M) in assay buffer [50 mM TEA, 100 mM KCl, 10 mM $MgCl_2$, 5% glycerol, pH 8.0] were added into each well in a 96-well microtitre plate. Fifty microliters of solution containing 4.6 μ g/ml of *Lm*FBPase, 1.4 U/ml of PGI, 0.8 U/ml of G6PDH, and 0.5 mM of $NADP^+$ in the same assay buffer were added to each well to start the catalytic reaction. The increase in absorbance at 340 nm (the absorbance of NADH) was measured for 5 min at 37 $^{\circ}C$ using a plate reader. Modifications of the assay buffer were made for investigation of different effects (pH, metal concentration, etc.) on *Lm*FBPase activity. The same calculation method as described above was used for the catalytic properties of *Lm*FBPase.

For the determination of the effects of AMP and manganese on *Lm*FBPase activity, 50 μ l of different concentrations of AMP or $MnCl_2$ (from 0 mM to 2 mM) in assay buffer in the presence of a sub-saturating concentration of F16BP (40 μ M) were added to each well. After 50 μ l of a mixed solution containing 4.6 μ g/ml of *Lm*FBPase, 1.4 U/ml

of PGI, 0.8 U/ml of G6PDH, and 0.5 mM of NADP⁺ in the same assay buffer was added to each well to start the reaction, the enzyme activities were assayed at 37 °C.

2.6 Thermal shift assay

Thermal shift assays (namely thermal denaturation assays, TDAs) were performed to characterise the thermal stability of proteins as well as modulator effects by monitoring changes in the fluorescence signal of SYPRO[®] Orange dye as it interacts with a protein undergoing thermal unfolding. For the investigation of PYKs, 120 µl of 0.5 mg/ml PYK was incubated with or without modulator in PBS-CM at room temperature at pH 7.4 for 1 h. Afterwards, the sample solutions were mixed with Sypro Orange in a 96-well PCR plate (50 µl/well). The plates were sealed with optical quality sealing tape (Bio-Rad) and heated in an i-Cycler iQ5 real-time PCR detection system (Bio-Rad) from 20 to 80 °C in increments of 0.5 °C. Fluorescence changes in the wells of the plate were monitored simultaneously with a charge-coupled device (CCD). The wavelengths for excitation and emission were 485 and 575 nm, respectively. The temperature midpoint for the protein unfolding transition, T_m , was calculated using the Bio-Rad iQ5 software.

CHAPTER 3

Protein production and characterisation of human pyruvate kinase M1 and M2

CHAPTER 3. Protein production and characterisation of human pyruvate kinase M1 and M2

3.1 Background

Four pyruvate kinases (wild-type M1PYK, wild-type M2PYK, M2PYK-C326S, and M2PYK-C358S) have been purified and characterised in this study. The plasmids were made in our laboratory (Morgan *et al.*, 2013, Mitchell, 2014). Briefly, cDNA encoding human M1PYK and M2PYK with N-terminal His tags and a thrombin-cleavage site (MGSSHHHHHHSSGLVPRGSH) were codon-optimised for *E. coli* expression and inserted into pET28a vectors. The amino acid sequence as well as the theoretical parameters of the bacterially expressed pyruvate kinases are shown in Table 3.1.

Table 3.1 Amino acid sequence and chemical parameters of expressed wild-type M1PYK and M2PYK.

Sequence of His ₆ -M1PYK ^a									
1	<u>MGSSHHHHHH</u>	<u>SSGLVPRGSH</u>	MSKPHSEAGT	AFIQTQQLHA	AMADTFLEH	MCRLDIDSPP	ITARNTGIIC	TIGPASRSVET	
81	LKEMIKSGMN	VARLNFSHGT	HEYHAETIKN	VRTATESFAS	DPILYRPVA	VALDTKGPEI	RTGLIKSGGT	AVELKKGATL	
161	KITLDNAYME	KCDENILWLD	YKNICKVVEV	GSKIYVDDGL	ISLQVKQKG	ADFLVTEVEN	GGSLGSKKGV	NLPGAAVDLPA	
241	VSEKDIQDLK	FGVEQDVMV	FASFIRKASD	VHEVRKVLGE	KGKNIKIIS	KIENHEGVRR	FDEILEASDG	IMVARGDLGIE	
321	IPAELVFLAQ	KMMIGRCNRA	GKPVICATQM	LESMIKKPRP	TRAEGSDVA	NAVLDGADCI	MLSGETAKGD	YPLEAVRMQHL	
401	IAREAEAAMF	HRKLFEELVR	ASSHSTDLM	AMAMGSVEAS	YKCLAAALI	VLTESGRSAH	QVARYRPRAP	IIAVTRNPQTA	
481	RQAHLYRGIF	PVLCKDPVQE	AWAEDVDLRV	NFAMNVGKAR	GFFKKGDVV	IVLTGWRPGS	GFTNTMRVVP	VP	
Sequence of His ₆ -M2PYK									
1	<u>MGSSHHHHHH</u>	<u>SSGLVPRGSH</u>	MSKPHSEAGT	AFIQTQQLHA	AMADTFLEH	MCRLDIDSPP	ITARNTGIIC	TIGPASRSVET	
81	LKEMIKSGMN	VARLNFSHGT	HEYHAETIKN	VRTATESFAS	DPILYRPVA	VALDTKGPEI	RTGLIKSGGT	AVELKKGATL	
161	KITLDNAYME	KCDENILWLD	YKNICKVVEV	GSKIYVDDGL	ISLQVKQKG	ADFLVTEVEN	GGSLGSKKGV	NLPGAAVDLPA	
241	VSEKDIQDLK	FGVEQDVMV	FASFIRKASD	VHEVRKVLGE	KGKNIKIIS	KIENHEGVRR	FDEILEASDG	IMVARGDLGIE	
321	IPAELVFLAQ	KMMIGRCNRA	GKPVICATQM	LESMIKKPRP	TRAEGSDVA	NAVLDGADCI	MLSGETAKGD	YPLEAVRMQHL	
401	IAREAEAAYI	HLQLFEELRR	LAPITSDPTE	ATAVGAVEAS	FKCCSGAII	VLTESGRSAH	QVARYRPRAP	IIAVTRNPQTA	
481	RQAHLYRGIF	PVLCKDPVQE	AWAEDVDLRV	NFAMNVGKAR	GFFKKGDVV	IVLTGWRPGS	GFTNTMRVVP	VP	
Isoform	Number of residues	Theoretical molecular mass	Theoretical pI ^b	Theoretical extinction coefficient					
M1PYK	551	60,225 Dalton	8.01	29,910 M ⁻¹ cm ⁻¹					
M2PYK	551	60,077 Dalton	8.22	29,910 M ⁻¹ cm ⁻¹					

^a Amino acid sequences corresponding to N-terminal His-tags and thrombin-cleavage sites are underlined. The differences between M1PYK and M2PYK are highlighted in light blue. Mutagenesis sites C326 and C358 are highlighted in red and green, respectively.

^b Theoretical isoelectric point (pI), molecular mass and extinction coefficient were obtained from ExPASy Server (Gasteiger *et al.*, 2005). The mass of the start codon Met is included and it is assumed to be translated as Met in the mature protein (same for all proteins described in this study), but there is no experimental evidence that it is present in the mature enzyme.

The methods of protein production and characterisation of human pyruvate kinases are briefly described in CHAPTER 2.

3.2 Protein production of pyruvate kinases

Four human pyruvate kinases are produced for this study, including wild-type M1PYK, wild-type M2PYK, M2PYK-C326S, and M2PYK-C358S. All proteins are expressed by *E. coli*, and purified with cobalt-based immobilised metal affinity columns followed by a second step purification with size exclusion chromatography.

3.2.1 Overexpression and cell lysis of human pyruvate kinases

Human pyruvate kinases (wild-type M1PYK, wild-type M2PYK, and M2PYK-C358S) were overexpressed in *E. coli* BL21(DE3) in 2× TY medium with an 18-h IPTG-induction at 18 °C. However, this method failed to produce soluble M2PYK-C326S. A systematic optimisation of bacteria strain, cell medium, and induction condition indicated a successful expression in *E. coli* BL21 star in LB medium with a 3-h IPTG induction at 18 °C.

The harvested cells were lysed at 4 °C at 25 KPSI with a constant cell disruptor. The lysate was centrifuged to remove insoluble portion. The expression of pyruvate kinases was characterised by SDS-PAGE.

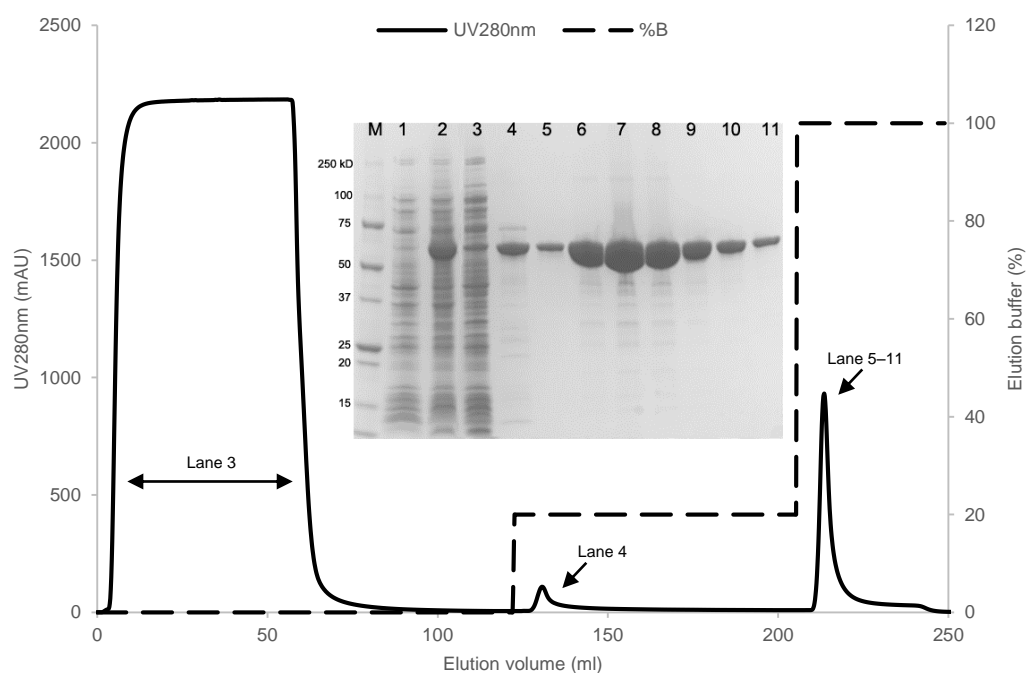
3.2.2 Purification of human pyruvate kinases

The cell lysate was then loaded onto a 5-ml cobalt-based IMAC column for metal-affinity purification. Unbound proteins were washed away in the flow-through fractions. Twenty millimolar imidazole was maintained in the initial loading buffer to remove weakly-bound proteins. An additional wash step of 20% buffer B (i.e., 76 mM of imidazole) was also included to minimise contaminating proteins. The His₆MPYK protein was eluted over a five column volume step gradient using 300 mM of imidazole, which competed with the chelation of the His₆-tag on the cobalt column, and thereby eluted the target protein.

For the purification of wild-type M1PYK, two peaks were eluted from the IMAC column at different concentrations of Buffer B (Figure 3.1A). The first peak came off at 20% Buffer B (corresponding to 76 mM imidazole), and showed contaminants along with M1PYK as shown in the SDS-PAGE gel (Lane 4). A larger, second peak was eluted at 100% Buffer B. These proteins analysed by SDS-PAGE showed M1PYK with a few other protein bands indicating the presence of small amounts of contaminants. A second gel-filtration polishing step was required for the improvement of the protein purity.

The purified sample of wild-type M1PYK from the IMAC step of purification was loaded onto a size-exclusion column HiLoad 16/600 Superdex 200 that was pre-equilibrated with the size-exclusion buffer (PBS-CM, a commercial PBS free from magnesium and calcium, pH 7.4) for a second-step polishing purification. The sample was purified at a constant flow rate of 1 ml/min, where M1PYK eluted as a smaller peak followed by a large peak at the retention volume of about 60 ml (Figure 3.1B). Protein from each fraction of the peak was characterised by SDS-PAGE (Figure 3.1B), which shows a purity higher than 95% corresponding to M1PYK in both peaks. Purified proteins from each peak were tested for enzyme activity. The specific activity of enzyme from the first (smaller) peak was only 70% of that from the second (larger) peak. The observation of the first peak is probably due to precipitation of M1PYK. M1PYK corresponding to the second peak that displayed 100% activity was collected and concentrated to 5.5 mg/ml with a Vivaspin tube. The final yield was about 7 mg from 1 L of cell culture. The product in the size-exclusion buffer (PBS-CM) was flash frozen with liquid nitrogen and stored at -80 °C.

(a) IMAC for wild-type M1PYK



(b) gel-filtration for wild-type M1PYK

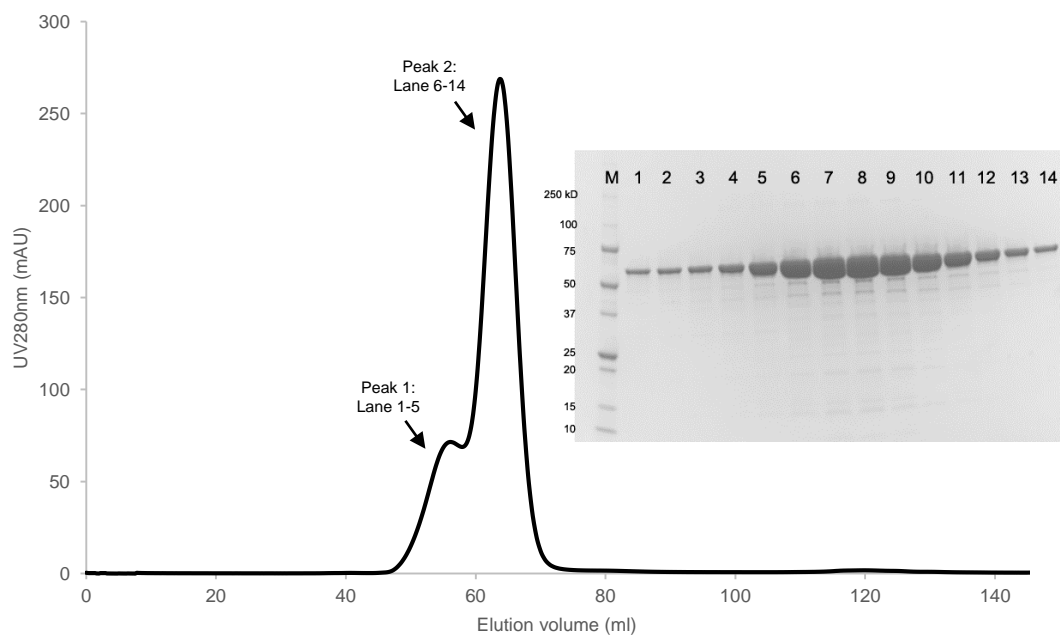


Figure 3.1 IMAC and gel-filtration purification of wild-type M1PYK.

The elution of proteins was monitored by a UV spectrometer at 280 nm (represented by the solid line). Dashed line shows the percentage of Buffer B used for the IMAC purification. Peaks corresponding to each lane characterised by SDS-PAGE are indicated in arrows. 'M' represents marker. For the SDS-PAGE characterisation of IMAC purification samples, Lane 1 and 2 correspond to pre- and post-induction *E. coli* cells, respectively.

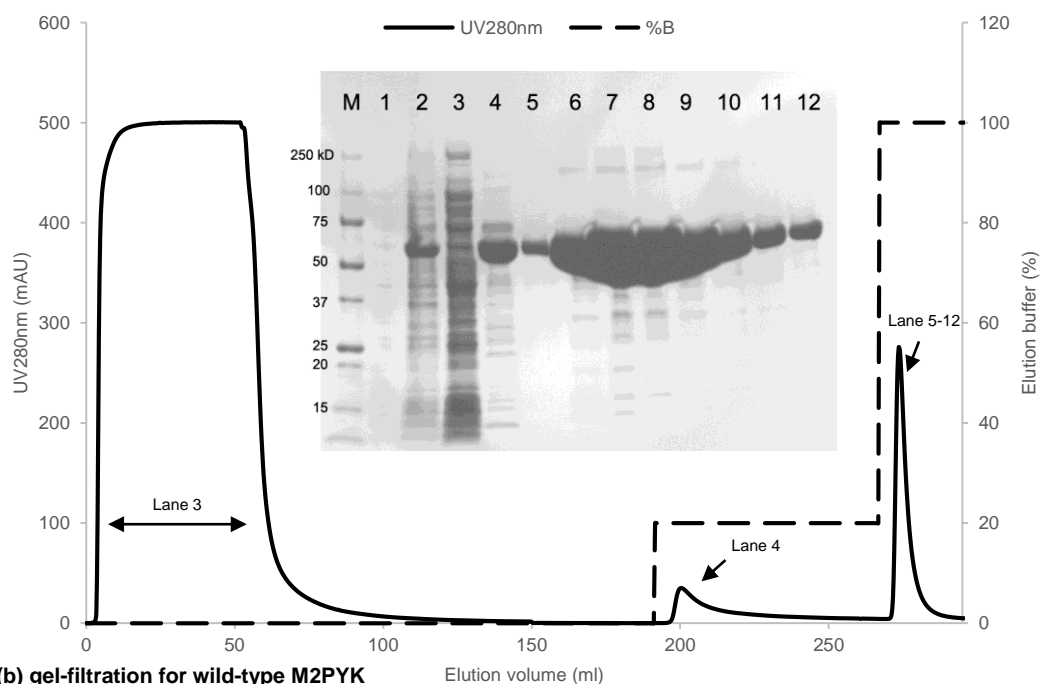
The purification steps of wild-type M2PYK, M2PYK-C358S, and M2PYK-C326S are identical to that for wild-type M1PYK as described above, except that 10% glycerol was added to the gel-filtration buffer of M2PYK-C326S to protect it from freeze-thaw damage. The purification of wild-type M2PYK, M2PYK-C358S, and M2PYK-C326S with IMAC columns also included a 20% Buffer B washing step to reduce contamination (Figure 3.1a, Figure 3.2a, Figure 3.3a, and Figure 3.4a). Larger, second peaks were eluted at 100% Buffer B.

In the polishing step of gel-filtration, the wild-type M2PYK and M2PYK-C358S were both eluted at a retention volume of approximately 61 ml (Figure 3.2b, Figure 3.3b), which is similar to that of wild-type M1PYK (Figure 3.1b). Unlike the latter, wild-type M2PYK and M2PYK-C358S showed almost single peaks, indicating purified non-precipitated enzymes. Small peaks at the retention volume of approximately 75 ml imply dissociated pyruvate kinases. Only fractions corresponding to the large peaks were pooled together. Both wild-type M2PYK and M2PYK-C358S were concentrated to approximately 20 mg/ml with a Vivaspin tube. The final yield was about 15 mg and 20 mg from 1 L of cell culture, respectively. The products in the size-exclusion buffer (PBS-CM) were flash frozen with liquid nitrogen and stored at -80 °C.

Surprisingly, M2PYK-C326S showed three peaks in the gel-filtration step (Figure 3.4b), with only the second one corresponding to the retention volume (approximately 61 ml) of a tetrameric pyruvate kinase. The first peak at the retention volume of 46 ml indicates protein precipitation¹. SDS-PAGE characterisation (Figure 3.4b) showed that proteins from both Peak 2 and Peak 3 correspond to the molecular mass of pyruvate kinase (60 kDa), indicating a trend of dissociation from PYK tetramer (240 kDa, corresponding to Peak 2 at the retention volume of 61 ml) to monomer (60 kDa, corresponding to Peak 3 at the retention volume of 75 ml). Further experiments using analytical gel-filtration (Section 3.6) confirmed this hypothesis. Peak 2 and Peak 3 were separately concentrated to 1–2 mg/ml with Vivaspin tube. The final yield was only 2 mg from 1 L of cell culture, which is much lower than that of other PYK isoform or mutants. The products from both peaks in the size-exclusion buffer (10% glycerol in PBS-CM) were flash frozen with liquid nitrogen and stored separately at -80 °C.

¹ GE Healthcare: Size Exclusion Chromatography – Principles and Methods.

(a) IMAC for wild-type M2PYK



(b) gel-filtration for wild-type M2PYK

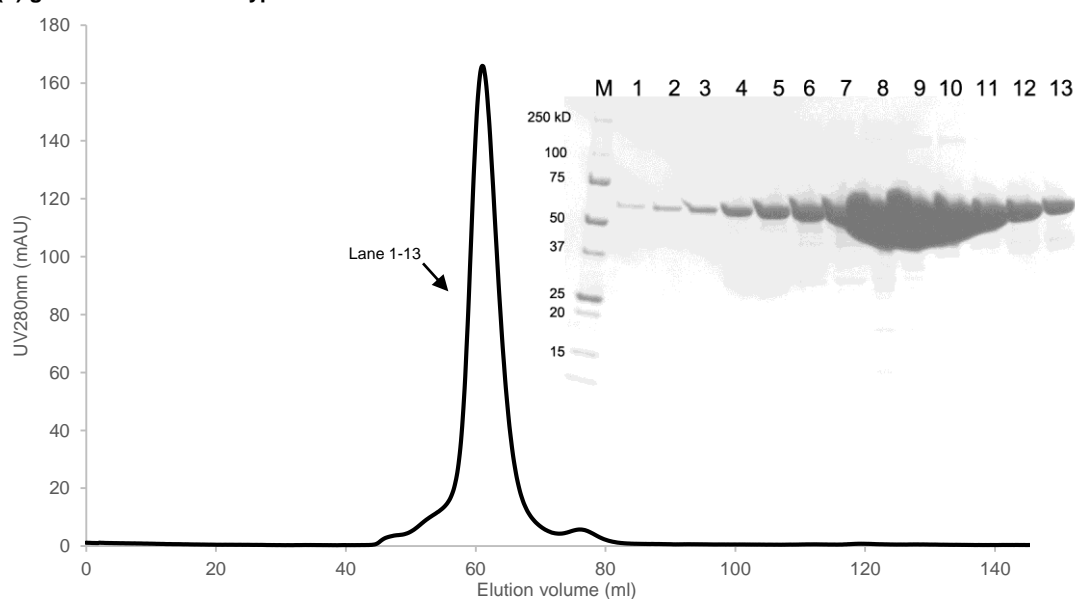
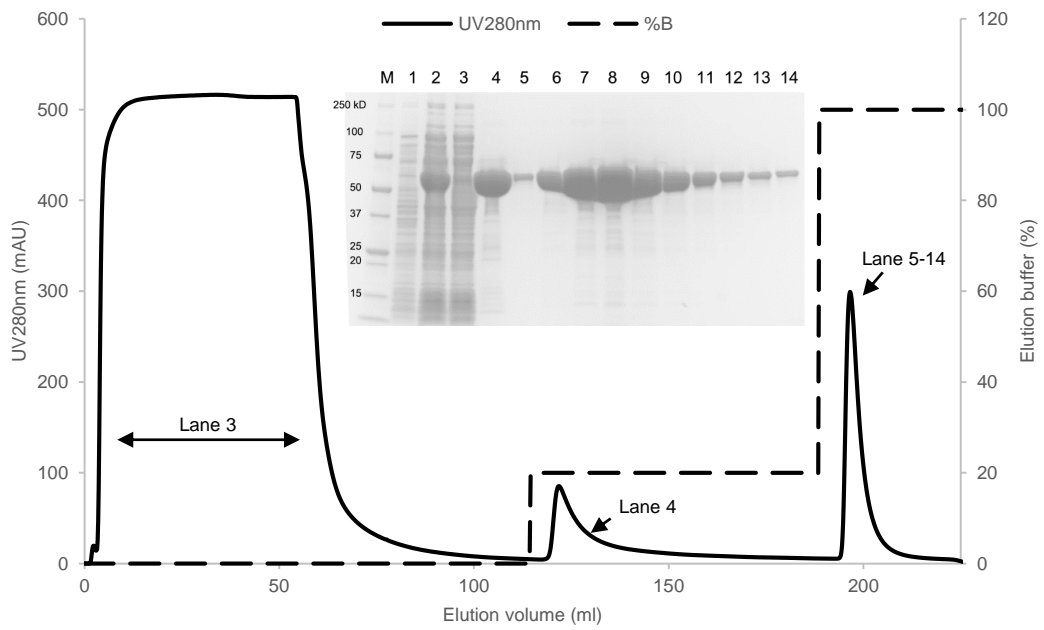


Figure 3.2 IMAC and gel-filtration purification of wild-type M2PYK.

The elution of proteins was monitored by a UV spectrometer at 280 nm (represented by the solid line). Dashed line shows the percentage of Buffer B used for the IMAC purification. Peaks corresponding to each lane characterised by SDS-PAGE are indicated in arrows. 'M' represents marker. For the SDS-PAGE characterisation of IMAC purification samples, Lane 1 and 2 correspond to pre- and post-induction *E. coli* cells, respectively.

(a) IMAC for M2PYK-C358S



(b) gel-filtration for M2PYK-C358S

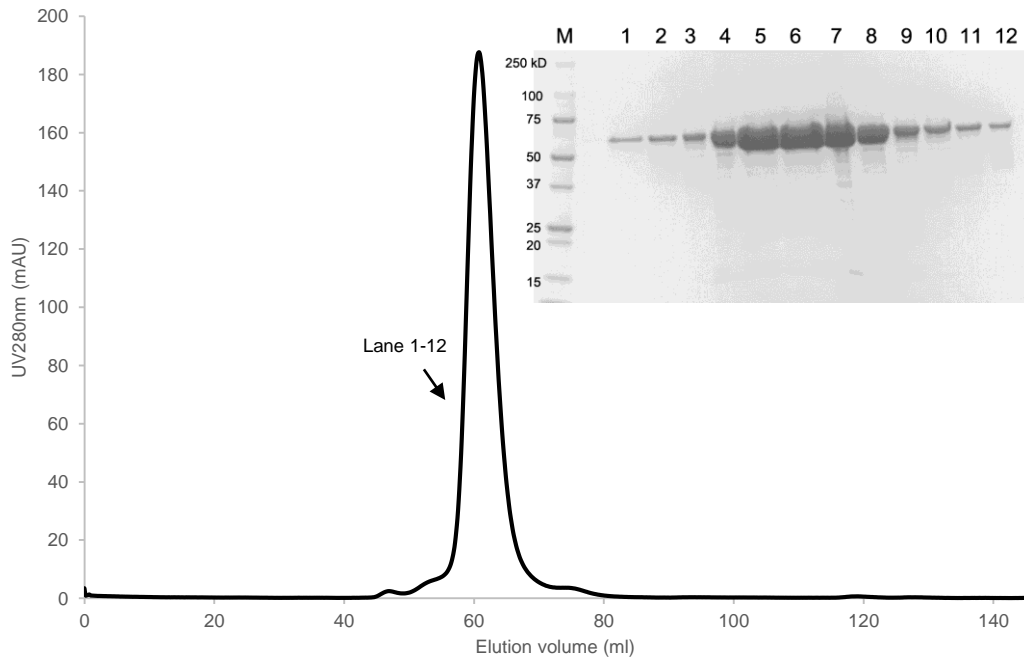
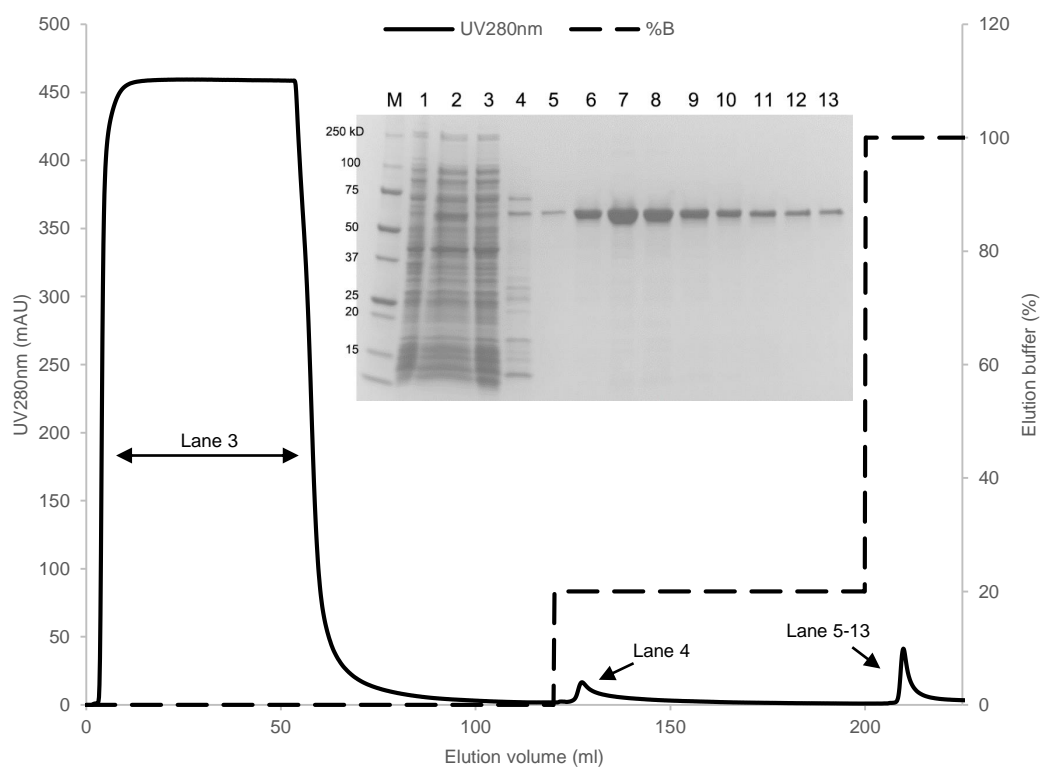


Figure 3.3 IMAC and gel-filtration purification of M2PYK-C358S.

The elution of proteins was monitored by a UV spectrometer at 280 nm (represented by the solid line). Dashed line shows the percentage of Buffer B used for the IMAC purification. Peaks corresponding to each lane characterised by SDS-PAGE are indicated in arrows. 'M' represents marker. For the SDS-PAGE characterisation of IMAC purification samples, Lane 1 and 2 correspond to pre- and post-induction *E. coli* cells, respectively.

(a) IMAC for M2PYK-C326S



(b) gel-filtration for M2PYK-C326S

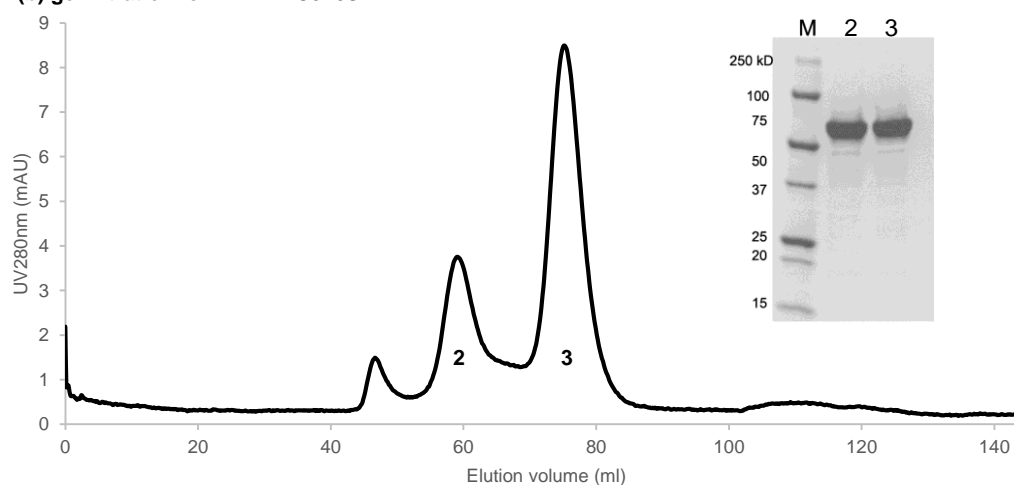


Figure 3.4 IMAC and gel-filtration purification of M2PYK-C326S.

The elution of proteins was monitored by a UV spectrometer at 280 nm (represented by the solid line). Dashed line shows the percentage of Buffer B used for the IMAC purification. Peaks corresponding to each lane characterised by SDS-PAGE are indicated in arrows. 'M' represents marker. For the SDS-PAGE characterisation of IMAC purification samples, Lane 1 and 2 correspond to pre- and post-induction *E. coli* cells, respectively. For the SDS-PAGE characterisation of gel-filtration purification samples, Lane 2 and 3 correspond to Peak 2 and Peak 3 in the purification curve, respectively.

3.3 Dynamic light scattering for pyruvate kinases

Dynamic light scattering (DLS) assays were carried out for the determination of the molecular size and aggregation of purified pyruvate kinases (wild-type M1PYK, wild-type M2PYK, M2PYK-C358S, and M2PYK-C326S). Briefly, pyruvate kinases stored at -80 °C were thawed on ice and diluted to 1 mg/ml with the gel-filtration buffer.

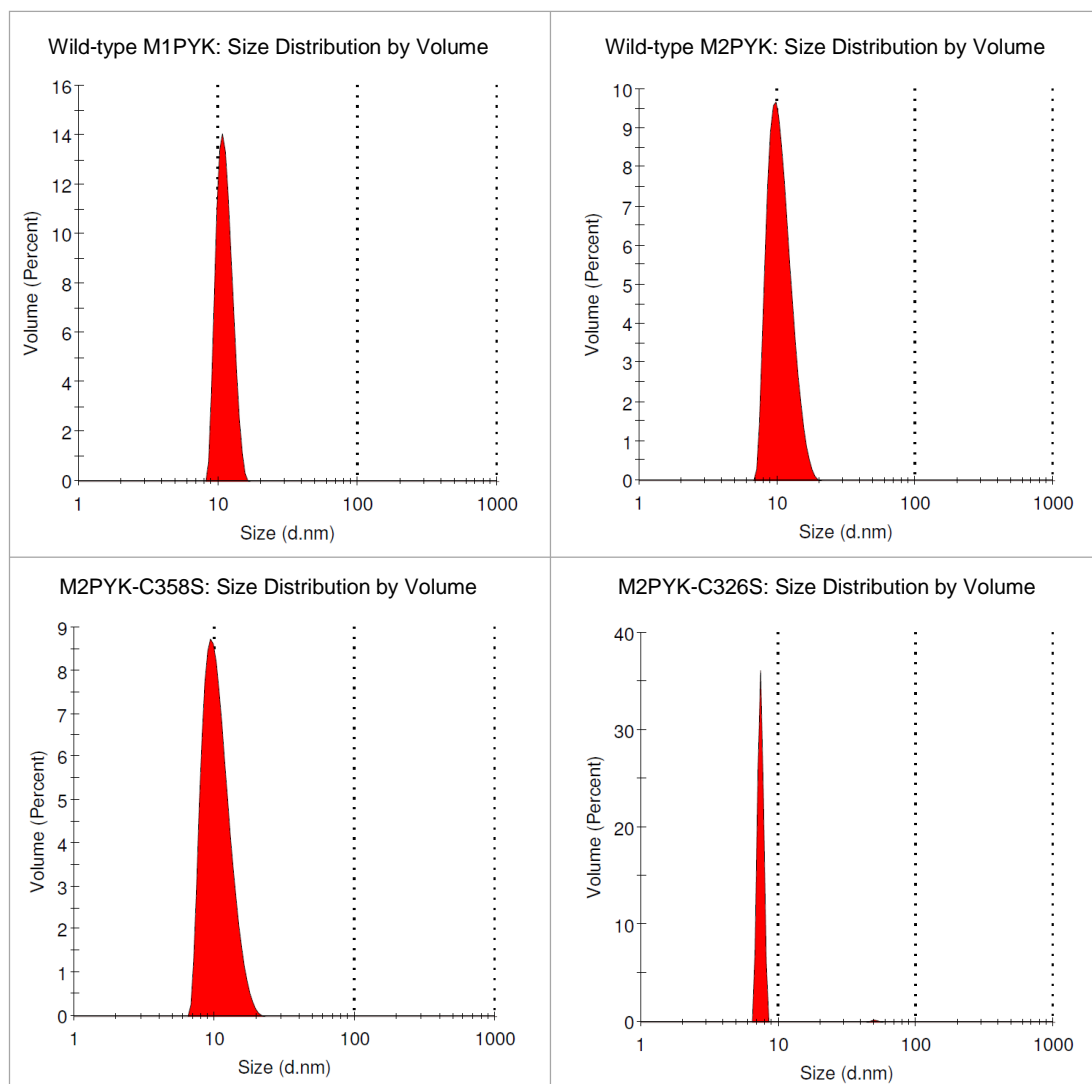


Figure 3.5 DLS analyses of pyruvate kinases.

The DLS results of pyruvate kinases are presented as size distribution by volume with Size (d.nm) shown at X-axis and Volume (percentage) at Y-axis. All the pyruvate kinases exhibit as monodisperse proteins.

The results showed that all purified pyruvate kinases exist as monodisperse proteins (Figure 3.5). For wild-type M1PYK, wild-type M2PYK and M2PYK-C358S, the mean hydrodynamic radius and molecular mass are all approximately 12 nm and 240 kDa, respectively, suggesting their tetrameric form. For M2PYK-C326S taken from the tetrameric peak (Figure 3.4, Peak 2), the result suggested a hydrodynamic radius of 7.4 nm, with its molecular mass of 72 kDa. It implies that M2PYK-C326S is predominantly monomeric. Further analytical gel-filtration experiment (Section 3.6) confirmed this observation.

3.4 Kinetic properties of pyruvate kinases

Enzymic activity assays for pyruvate kinases were carried out based on an LDH-coupled system at 37°C by monitoring the decrease of NADH absorbance at 340 nm. In the presence of ADP, PYKs catalyse the dephosphorylation reaction from PEP to pyruvate, which is then transformed to lactate by LDH in the presence of NADH. During the reaction, NADH, which absorbs light at 340 nm, is also transformed to NAD⁺.

Both M1PYK and M2PYK catalyse the transformation of PEP and ADP (Figure 3.6). The kinetic comparisons are summarised in Table 3.2 and Figure 3.7.

M1PYK shows the highest activity ($V_{\max} = 139.7 \pm 4.6 \mu\text{mol}/\text{min}/\text{mg}$) and lowest affinity for PEP ($K_m = 0.13 \pm 0.02 \text{ mM}$), regardless of the presence of F16BP. This correlates with previously published results, that M1PYK is a constitutively active enzyme, where the addition of F16BP made essentially no difference to the kinetics (Morgan *et al.*, 2013).

By contrast, wild-type M2PYK showed the lower activity in comparison with M1PYK in the absence of F16BP. The specific activity was only $100.4 \pm 2.5 \mu\text{mol}/\text{min}/\text{mg}$, with a relatively weak binding of PEP ($K_m = 0.54 \pm 0.05 \text{ mM}$). Addition of effector F16BP to M2PYK resulted in significant activation, with near-M1PYK activity. It increased both its apparent activity ($V_{\max} = 129.1 \pm 5.7 \mu\text{mol}/\text{min}/\text{mg}$) and the binding affinity of PEP ($K_m = 0.14 \pm 0.03 \text{ mM}$). The addition of F16BP did not significantly

change the binding affinity of the other substrate ADP (K_m from 0.37 ± 0.03 mM to 0.29 ± 0.03 mM).

The mutant M2PYK-C358S showed similar properties as the wild type. But the other mutant, M2PYK-C326S, displayed distinctive properties (Figure 3.7). First, the apparent activity of M2PYK-C326S is much lower than that of the other isoform and mutants. It correlates with the fact that M2PYK-C326S is a monomeric form of pyruvate kinase, which has a very low activity (Morgan *et al.*, 2013, Iqbal *et al.*, 2014a). The effector F16BP activated M2PYK-C326S, but only to approximately 30% of the maximum activity of pyruvate kinase. Further evidence using analytical gel-filtration indicating M2PYK-C326S tends to form monomers as shown in Section 3.6.

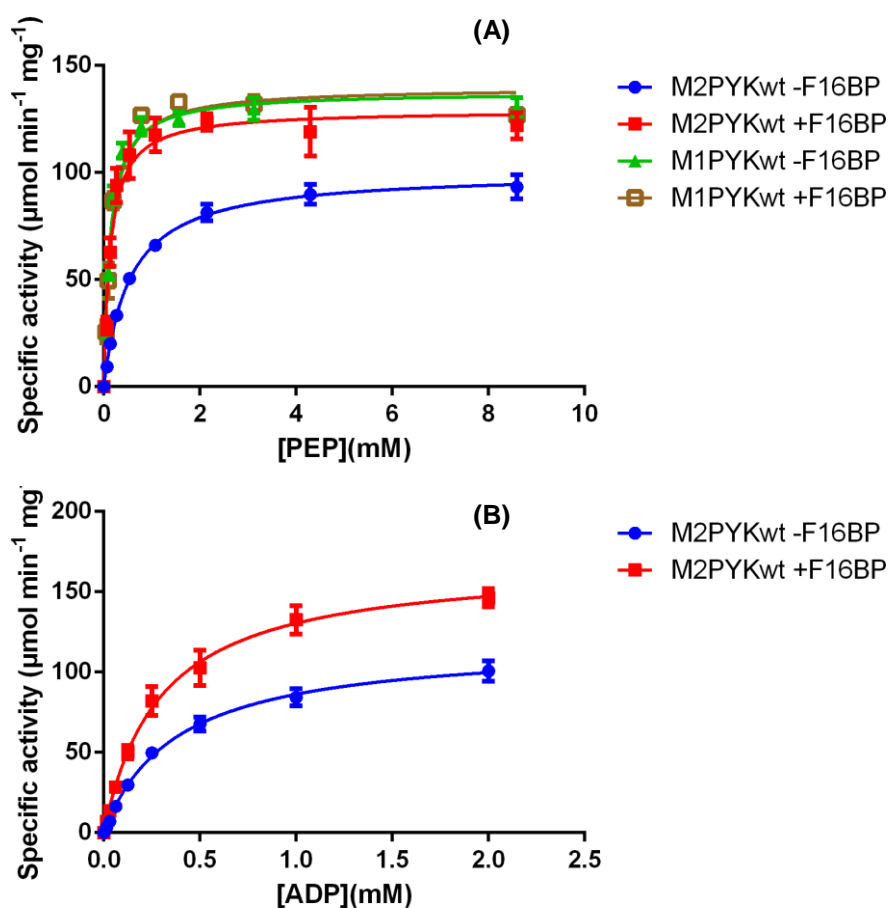


Figure 3.6 Kinetics of M1PYK and M2PYK.

(A) The kinetic characterisations of the catalysis of PEP at saturating concentration of ADP in the absence and presence of $100 \mu\text{M}$ of F16BP.

(B) The kinetic characterisations of the catalysis of ADP at saturating concentration of PEP in the absence and presence of $100 \mu\text{M}$ of F16BP.

Table 3.2 Kinetic properties of M1PYK and M2PYK.

	M1PYK		M2PYK	
	-F16BP	+F16BP	-F16BP	+F16BP
V_{\max} ($\mu\text{mol}/\text{min}/\text{mg}$)	137.6 ± 4.6^a	139.7 ± 5.3	100.4 ± 2.5	129.1 ± 5.7
$K_m[\text{PEP}]$ (mM)	0.13 ± 0.02	0.15 ± 0.02	0.54 ± 0.05	0.14 ± 0.03
$K_m[\text{ADP}]$ (mM)	ND ^b	ND	0.37 ± 0.03	0.29 ± 0.03

^a Data represent the mean \pm SD of three experiments.

^b not detected.

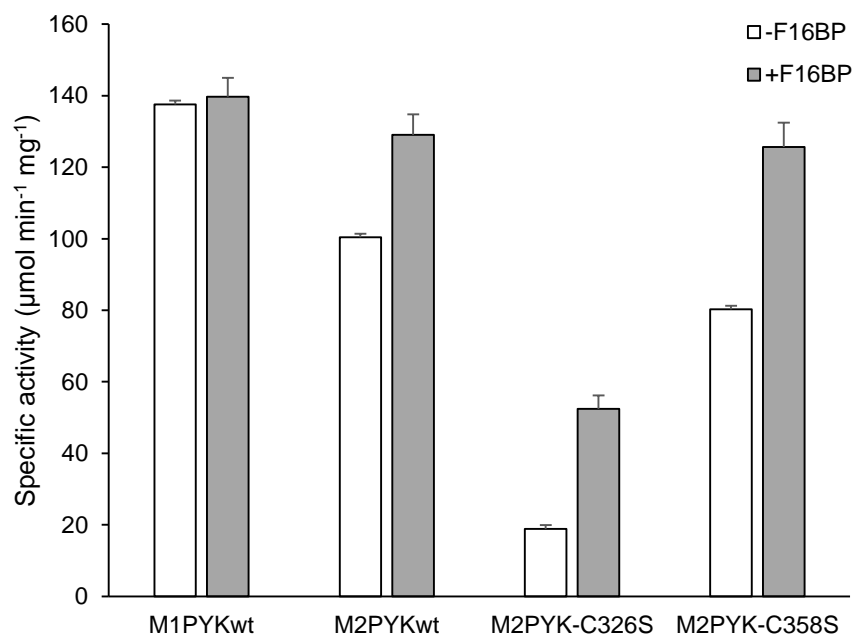


Figure 3.7 Comparisons of enzymic activity of M1PYK and M2PYK in the absence and presence of F16BP.

Data represent the mean \pm SD of three experiments.

3.5 M2PYK exists in an equilibrium between monomeric and tetrameric forms

It is well-established that regulatory factors like metabolites (e.g. triiodothyronine) and post-translational modifications (e.g. acetylation, phosphorylation) may promote the dissociation of M2PYK from tetramer to inactive dimer/monomer (Section 1.2.7 and Table 1.5) (Wong *et al.*, 2015).

Here it is shown that the dissociation of M2PYK is concentration-dependent. Both M1PYK and M2PYK were stored at high concentrations (higher than 5 mg/ml). It was observed that the enzymic activity of M2PYK gradually reduced after the enzyme was diluted to and incubated at 0.002 mg/ml in PBS-CM at room temperature (Figure 3.8). By contrast, the loss of M1PYK activity is much less. This observation implied that M2PYK gradually transforms from an active form to an inactive one.

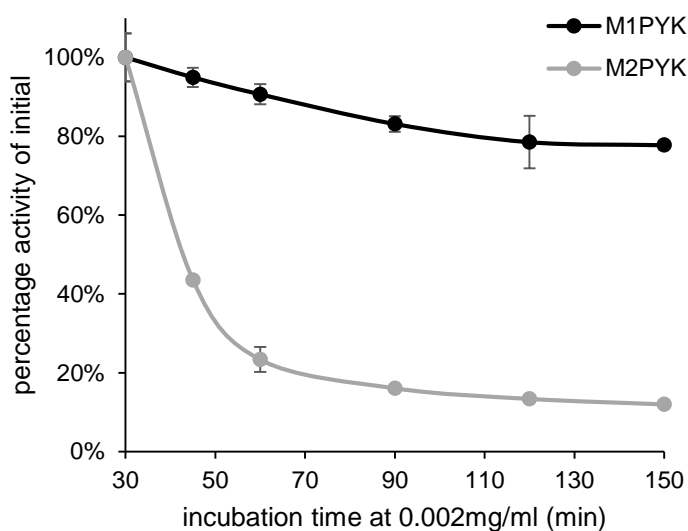


Figure 3.8 Gradual activity loss of M1PYK and M2PYK at 0.002 mg/ml.

Data represent the mean \pm SD of three experiments.

A further assay using analytical gel-filtration shows that M2PYK can gradually dissociate into monomers at low concentration. Briefly, the analytical gel-filtration was performed by monitoring the UV absorbance at 214 nm for 25 μ l samples of 0.1 mg/ml M2PYK which had been incubated in PBS-CM (pH 7.4) for 0 h, 1 h, 2 h, 5.5 h, 8 h, and 12 h at room temperature (Figure 3.9). The results indicate that M2PYK dissociated slowly from tetramer to monomer. The tetramer:monomer ratio reached an

equilibrium of about 1:4 (1:1 if consider a tetramer as one) after 8 h. In contrast, M1PYK retained its tetrameric form without dissociation (Figure 3.10, under the same experimental condition as M2PYK). It correlates with the observation that the gradual activity-loss after being diluted to a low concentration of M1PYK is far less marked than that of M2PYK.

Previous reports showed that unlike tetrameric M2PYK, the monomer/dimer forms of M2PYK have little pyruvate kinase activity (Wong *et al.*, 2015, Eigenbrodt *et al.*, 1992, Mazurek *et al.*, 1993). It is probably because a complete active site requires the stabilisation of an adjacent subunit (Morgan *et al.*, 2013). Metabolites like L-cysteine and T3, as well as post-translational modifications, have been shown to promote the dissociation of M2PYK, and thereby reduce its enzymic activity. Here by integration of analytical gel-filtration and enzyme assay, it is shown that the dissociation of M2PYK and the consequent activity loss at low concentration, are natural effects. By contrast, M1PYK retains the tetrameric form and its enzymic activity.

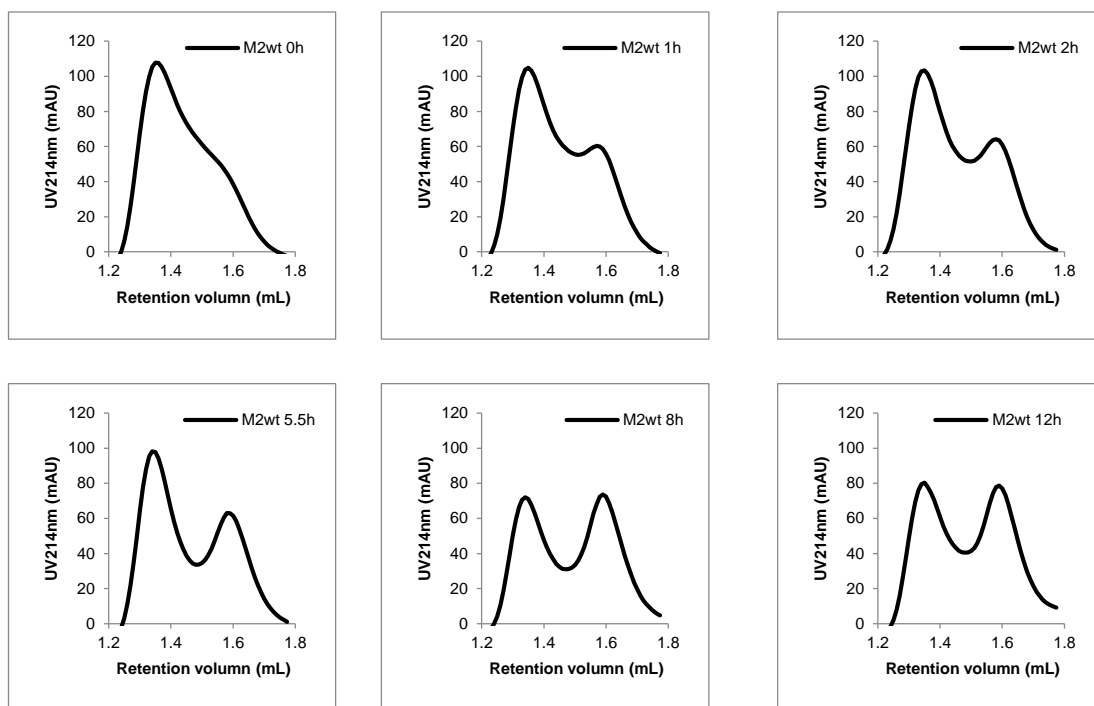


Figure 3.9 M2PYK gradually dissociates from tetramer to monomer.

M2PYK was incubated at 0.1 mg/ml in PBS-CM at room temperature for different time-lengths. Analytical gel-filtration for M2PYK was carried out to determine the tetramer (left peaks) : monomer (right peaks) ratio with a Superdex® 200 PC 3.2/30 gel-filtration column. Twenty-five microlitres of sample was subjected to the assay each time.

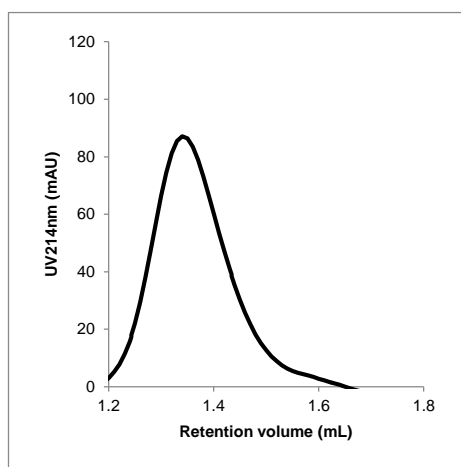


Figure 3.10 M1PYK remains as a tetramer after a 12-h incubation.

M1PYK was incubated at 0.1 mg/ml in PBS-CM at room temperature for 12 h. Analytical gel-filtration for M1PYK was carried out to determine the oligomerisation state with a Superdex® 200 PC 3.2/30 gel-filtration column. Twenty-five microlitres of sample was subjected to the assay.

3.6 Characterisation of oligomerisation states of M2PYK mutants

Wild-type M2PYK gradually dissociates from tetramer to monomer at low concentrations. At room temperature, 0.1 mg/ml wild-type M2PYK reached the equilibrium of its oligomerisation state after incubation for 12 h (Figure 3.9).

In 2011, Anastasiou *et al.* discovered that the enzymic activity and oligomerisation state of M2PYK depends on its redox state (Anastasiou *et al.*, 2011). They suggested that Cys358 was the main residue that was affected by oxidation (or nitrosylation) and further showed that the activity of the mutant M2PYK-C358S is free from effects of reducing agents or oxidants. However, the assumption that the mutant C358S can retain all properties of M2PYK except for the protection from oxidation, had not been proved. In other words, the free-from-oxidation feature of M2PYK-C358S might have been an artefact due to a direct effect of the mutagenesis.

In this study, it is shown that the oligomerisation state of M2PYK-C358S is different from that of the wild type. The proportion of the tetramer at 0.1 mg/ml is much higher than that of the wild type (Figure 3.11). An alternative explanation for the effect of the C358S mutation is that it protects some other cysteines, located in subunit interfaces (e.g. Cys326, Cys424, etc.), from exposure to environmental oxidative factors and thus being oxidised and/or nitrosylated. As a result, the free-from-oxidation feature of M2PYK-C358S discovered by Anastasiou *et al.* might be due to an indirect mechanism, i.e., M2PYK-C358S increases the stability of the tetramer, and thereby protects the enzyme from interfacial oxidation.

In 2014, Mitchell indicated that Cys326 might be another main redox-sensitive residue in M2PYK (Mitchell, 2014). For further confirmation, a mutant M2PYK-C326S was produced and characterised in this study. Analytical gel-filtration result showed that M2PYK-C326S is entirely monomeric at 0.1 mg/ml (Figure 3.11). This correlates with our previous results by the purification of size-exclusion chromatography (Figure 3.4B), DLS (Figure 3.5), and enzymic activity assay (Figure 3.7), which suggested an enzyme with smaller size and low enzymic activity. More detailed results and descriptions of the redox-regulation of M2PYK are shown in CHAPTER 5.

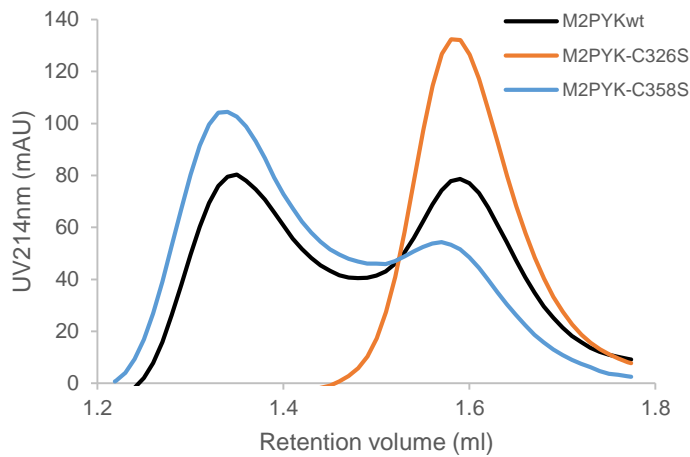


Figure 3.11 Oligomerisation states of wild-type M2PYK and mutants.

Proteins were incubated at 0.1 mg/ml in PBS-CM at room temperature for 12 h. Analytical gel-filtration was carried out to determine the tetramer (left peaks) : monomer (right peaks) ratio with a Superdex® 200 PC 3.2/30 gel-filtration column. Twenty-five microlitres of sample was subjected to the assay each time.

3.7 Thermal stability of pyruvate kinases

The unfolding rates of human pyruvate kinases as a function of increasing temperature were determined with a thermal shift assay (a.k.a., thermal denaturation assay, TDA). An increase in melting temperature [T_m , defined as the temperature midpoint for the protein unfolding transition (Morgan *et al.*, 2010)] reflects ligand binding and reduced conformational flexibility. The results showed that the T_m of M2PYK is 47.5 °C. The addition of the allosteric activator F16BP to M2PYK *apo*enzyme shows a dramatic increase in the T_m , from 47.5 °C to 54.5 °C (Figure 3.12). M1PYK also shows a T_m at 47.5 °C, which is identical to that of M2PYK in the absence of F16BP. Intriguingly, M1PYK displays a second melting temperature at 62 °C. This result correlates with previous observations, which indicate M1PYK is a more stable enzyme than M2PYK.

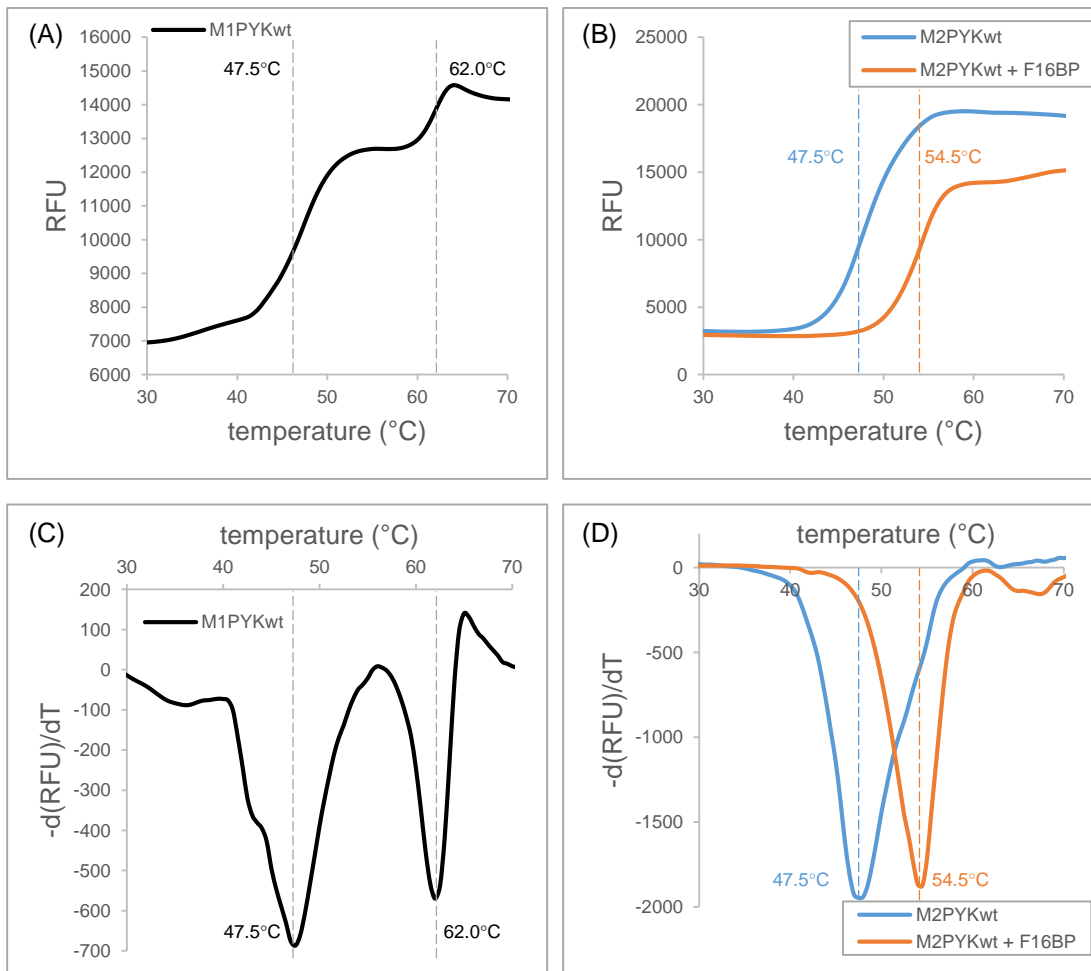


Figure 3.12 Thermal stability of M1PYK and M2PYK.

Thermal shift assay results for 0.5 mg/ml M1PYK (Panel A, black line) and M2PYK (Panel B) in the absence (blue line) and the presence (orange line) of F16BP. Panel C and D show derivative plots of the fluorescence readings. The unfolding of M1PYK in PBS buffer gives T_m values of 47.5 °C and 62 °C. Binding of F16BP shifts the T_m of M2PYK from 47.5 °C to 54.5 °C.

3.8 Conclusions

Four human pyruvate kinases (wild-type M1PYK, wild-type M2PYK, M2PYK-C326S, M2PYK-C358S) were produced in *E. coli* for this study. After the first purification step with IMAC, all the crude samples were subjected to a polishing step using size exclusion chromatography. A further DLS assay confirmed all the proteins as monodisperse, and showing no aggregation in the protein solutions. It also indicated that the size of M2PYK-C326S is much smaller than that of the other three samples, implying its propensity for forming monomers.

Enzyme kinetic assays also demonstrated that F16BP activated M2PYK to near-M1PYK values, by increasing its apparent activity and the binding affinity of the substrate PEP. By contrast, the enzymic activity of M1PYK was not affected by F16BP. Further, by integration of analytical gel-filtration and enzyme assay, it is also shown that tetrameric M2PYK can gradually dissociate into monomers at low concentration. Consequently, the enzymic activity of M2PYK is reduced. By contrast, M1PYK retains the tetrameric form and its enzymic activity. These observations were also confirmed by the thermal denaturation assay, showing the thermal stabilisation effect of F16BP on M2PYK.

Assays using analytical gel-filtration also showed that M2PYK-C358S had a higher tetramer ratio. On the other hand, M2PYK-C326S is entirely monomeric, which has a much lower activity than that of the other isoform/mutants.

CHAPTER 4

Pyruvate kinase M2 is an amino acid sensor

CHAPTER 4. Pyruvate kinase M2 is an amino acid sensor

4.1 Background

L-phenylalanine was shown to be an inhibitor of both M1PYK and M2PYK (Porter & Cardenas, 1980, Williams *et al.*, 2006, Morgan *et al.*, 2013). In contrast, L-serine was shown to bind to the same site, but displayed an activation effect on M2PYK (Chaneton *et al.*, 2012). For M1PYK, it was also reported that some other amino acids (e.g. L-alanine, L-cysteine, L-proline, etc.) may also bind to the same pocket, although no significant activity effect was observed. Residues of the amino acid-binding pocket are identical between M1PYK and M2PYK. As a result, these amino acids may also bind to M2PYK. As shown in CHAPTER 3, the M2PYK tetramer is much less stable than M1PYK. Hence, the enzymic activity and conformation of M2PYK might be more sensitive to these free amino acids.

In this study, the effects of all amino acids on M1PYK and M2PYK are systematically investigated, and the allosteric amino-acid binding pocket was shown to be important for the regulation of PYK conformation and activity. Intriguingly, M2PYK but not M1PYK was shown to be regulated in opposing ways (i.e. underwent both activation and inhibition) by different amino acids. Binding to the same effector site, serine acted as an activator by stabilising M2PYK in the active R-state tetramer, whereas some hydrophobic amino acids, such as phenylalanine, alanine and tryptophan allosterically inhibited the activity of M2PYK by trapping the inactive T-state tetramer. The activity of M1PYK was affected only by phenylalanine that inhibited modestly. Enzymic, biophysical and structural studies provide insights into the mechanism of the allosteric regulation of M2PYK by different amino acids that show contrasting activating or inhibitory effects.

4.2 Methods

4.2.1 Enzyme-linked immunosorbent assay

Enzyme-linked immunosorbent assays (ELISAs) based on isoform-specific antibodies were developed for the determination of M1PYK and M2PYK. Because the specific epitopes are located on the C-C interface, which is buried in its tetrameric state, this assay was also used for the characterisation of the oligomerisation states of M2PYK.

The specific antibodies were produced in Professor Ted Hupp's laboratory. Briefly, specific peptide immunogens from M1PYK and M2PYK were covalently conjugated with the carrier protein BSA, and injected into Balb/c female mice (6–7 weeks) at two week intervals. The mice showing best selectivity were chosen as a spleen donor. After the production of hybridoma, cell lines secreting specific monoclonal antibodies were screened and expanded. The specific monoclonal antibodies against M1PYK and M2PYK were identified, purified and conjugated with horseradish peroxidase (HRP) for further ELISAs.

For the determination of antibody specificity, 100 μl /well of 0–10 $\mu\text{g}/\text{ml}$ M1PYK or M2PYK was coated onto a 96-well plate for 1 h at room temperature with carbonate buffer (pH 9.6). The wells were then blocked with 100 μl /well of PBS/Tween 20/3% BSA for 1 h at room temperature. One hundred microlitres of HRP-labelled anti-M1PYK mouse antibody and HRP-labelled anti-M2PYK mouse antibody (1 $\mu\text{g}/\text{ml}$ in PBS) were added to each well for an incubation of 1 h at room temperature. Electrochemiluminescence (ECL) solutions were added at 50 μl /well to develop the luminescence, and were read immediately with a plate reader. Three washes with PBS/Tween 20/3% BSA were performed between each step.

For the study of the effects of ligands (F16BP and amino acids) on the oligomerisation state of M2PYK, anti-His-tag antibody (stock solution of unknown concentration) diluted 1000-fold with carbonate buffer pH 9.6 was coated onto wells at 50 μl /well at 4 °C overnight. The wells were then blocked with 100 μl /well of PBS/Tween 20/3% BSA for 1 h at room temperature. Titrated M2PYK (0–2.5 $\mu\text{g}/\text{ml}$) was incubated with or without ligands (10 mM for all amino acids and 1 mM for F16BP) in PBS/Tween

20/3% BSA at room temperature for 1 h. Then 100 μ l of the solution was added to each prepared well for an incubation of 1 h. Afterwards, 100 μ l of PBS/Tween 20/3% BSA containing 4 μ g/ml HRP-conjugated M2PYK antibody was added to each well to incubate for 1 h at room temperature. Electrochemiluminescence (ECL) solutions were added at 50 μ l/well to develop the luminescence, and were read immediately with a plate reader. Three washes with PBS/Tween 20/3% BSA were performed between each step.

4.2.2 Hydrogen–deuterium exchange tandem mass spectrometry assay

Hydrogen–deuterium exchange tandem mass spectrometry assay (HD exchange) was used to investigate the dynamics of M1PYK and M2PYK, as well as effects of activity regulators (F16BP, amino acids, T3, etc.).

First, 1 mg/ml of M1PYK and M2PYK were incubated with or without 5 mM F16BP, 50 mM of amino acids, 10 μ M T3, or 25 mM DTT in PBS for 1 h at room temperature. Afterwards, 95 μ l of heavy water D₂O (or H₂O as control) was added to each 5 μ l of incubated sample. The hydrogen–deuterium exchange was allowed to proceed for 10 min. Finally, 1 μ l of 1 M glycine.HCl was added to each sample to quench the exchange reaction. Samples were then flash-frozen with liquid nitrogen and subjected to further mass spectrometry analyses in the laboratory of Prof. Ing. Lenka Hernychová in Masaryk University.

4.2.3 Crystallisation, data collection and processing

M2PYK was co-crystallised with L-phenylalanine, L-alanine, L-tryptophan and L-serine. Single crystals of M2PYK were obtained at 17 °C by vapour diffusion using the hanging drop technique. The drops were formed by mixing 1.5 μ l of wild-type M2PYK (20 mg/ml) solution containing ligands with 1.5 μ l reservoir solution (composed of 11–16% PEG 3,350, 100 mM sodium cacodylate, 50 mM MgCl₂, and 100 mM KCl). In addition, final concentration of 20 mM L-alanine was added for the co-crystallisation of M2PYK/Ala crystals; 50 mM L-phenylalanine was added for M2PYK/Phe crystals; 100 mM L-serine, 1 mM oxalate, and 1 mM ATP were added

for M2PYK/Ser crystals; 30 mM L-tryptophan was added for M2PYK/Trp crystals. The pH for obtaining optimal crystals was 7.2–7.8. Before data collection, crystals were dipped in a freezing solution consisting of reservoir solution supplemented with same amount of ligands as in the original solution, as well as up to 35% PEG 3,350, which eliminated the appearance of ice rings.

The X-ray diffraction datasets were collected on Beamline I03 (for the M2PYK/Ala structure), I04-1 (for the M2PYK/Phe and the M2PYK/Trp structures), I-24 (for the M2PYK/Ser structure) at the Diamond synchrotron radiation facility in Oxfordshire, United Kingdom. Each dataset was obtained from a single crystal flash-frozen in liquid nitrogen. Data were then processed with iMOSFLM (Battye *et al.*, 2011) and scaled with SCALA (Evans, 2006), or processed automatically with xia2 (Winter, 2009).

All four M2PYK structures were solved by molecular replacement using the program PHASER (McCoy *et al.*, 2007). A monomer (Chain A) from the previously determined tetrameric structure of M2PYK (in the R-state, PDB ID: 4B2D) served as the search model for the M2PYK/Ser structure. Chain A of a different M2PYK structure (in the T-state, PDB ID: 4FXJ) was used as the search model for the M2PYK/Phe, M2PYK/Ala and M2PYK/Trp structures. There were clear molecular replacement solutions for all structures. The resulting models were then subjected to 10 cycles of rigid body refinement using the program REFMAC (Murshudov *et al.*, 1997). Afterwards, manual changes were made to models to adjust side chain conformations and to add additional residues to the N-terminus using COOT (Emsley & Cowtan, 2004). The models were then subjected to several rounds of translation libration screw (TLS) refinement and restrained refinement, and ligand molecules were added where clear unbiased F_o-F_c electron density was observed. No NCS restraint was defined due to the small differences among subunits. Water molecules were added to the model using COOT, and after several rounds of restrained refinement, R/R_{free} values converged. Detailed data collection and refinement statistics for PYK structures are summarised in

Table 4.3.

4.2.4 Structural analysis

Crystal structures of M2PYK in complex with different amino-acid ligands solved in this study (M2PYK/Phe, M2PYK/Ala, M2PYK/Trp, M2PYK/Ser), together with previously solved structures, were systematically compared and analysed for understanding the molecular mechanism of the allosteric regulation of M2PYK.

Distances between atoms on amino-acid ligands and surrounding residues were measured with PDBsum (Laskowski *et al.*, 1997). Interface bonds of the tetrameric structures were measured with PDBePISA (Krissinel & Henrick, 2005).

Comparisons of subunit rotation angles and tetramer fits among different M2PYK crystal structures were performed with a software ‘Superpose’ in the CCP4 package (Winn *et al.*, 2011, Krissinel & Henrick, 2004). The rotation matrices generated by superposing each pair of structures with ‘Superpose’ were adopted to calculate the subunit rotation angle following the equation shown as below:

$$\theta = \cos^{-1} \frac{X_{11} + Y_{22} + Z_{33} - 1}{2}$$

where θ is the subunit rotation angle, X_{11} , Y_{22} , and Z_{33} represent the X_{11} , Y_{22} , and Z_{33} values in the rotation matrix calculated for the superposition.

Coordinates of C α atoms in superposed structures were extracted from each PDB file. Distances between C α atoms of each pair of structures were calculated with the equation:

$$A = \sqrt{(X_1 - X_2)^2 + (Y_1 - Y_2)^2 + (Z_1 - Z_2)^2}$$

where A is the distance between C α atoms, X_1 , Y_1 , Z_1 represent the three-dimensional coordinate of the first C α atom, and X_2 , Y_2 , Z_2 represent that of the second C α atom.

4.3 Effects of amino acids on the activity of M1PYK and M2PYK

Regulatory effects of amino acids on the constitutively active M1PYK have been extensively studied (Carminatti *et al.*, 1971, Consler *et al.*, 1992, Cheng *et al.*, 1996,

Lonhienne & Winzor, 2002, Williams *et al.*, 2006, Herman & Lee, 2009, Fenton *et al.*, 2010, Prasanna *et al.*, 2013, Urness *et al.*, 2013). The results showed that only L-phenylalanine regulates M1PYK, by a mild non-competitive inhibition of its enzymatic activity (Carminatti *et al.*, 1971, Williams *et al.*, 2006). All the other amino acids had little direct regulatory effects on M1PYK. By contrast, M2PYK is known to respond to a wider range of effector molecules. Previously effects of L-phenylalanine and L-serine on M2PYK were reported (Morgan *et al.*, 2013, Chaneton *et al.*, 2012). In this study, effects of all amino acids on M1PYK and M2PYK are systematically screened by enzymic activity assay, and the regulatory mechanism investigated by different biophysical and structural approaches.

4.3.1 Enzyme assay screening

An enzyme assay was carried out for the screening of PYK activity modulators. M1PYK and M2PYK were incubated with 2.5 mM amino acids including alanine, arginine, asparagine, aspartic acid, cysteine, glutamic acid, glutamine, glycine, histidine, isoleucine, leucine, lysine, methionine, phenylalanine, proline, serine, threonine, tryptophan, tyrosine and valine (all L-isomers) or with no amino acid (as the ‘no ligand’ control) for 30 min. F16BP was used as a positive control. The reaction was performed in PBS at pH 7.4 at 37 °C. The experiment were independently repeated for three times.

Many amino acids showed strong effects on M2PYK activity (indicated by grey bars in Figure 4.1). Phenylalanine and alanine were the most powerful inhibitors (nearly 100% inhibition) among all tested amino acids. Methionine, proline, tryptophan valine and were also strong inhibitors (65–90% inhibition), whereas the inhibition by isoleucine, threonine, and cysteine was more modest (20–50% inhibition). Histidine and serine were identified as strong activators (about 30% activation) for M2PYK. As an extensively studied natural activator of M2PYK, F16BP showed the strongest activation among all tested ligands (about 40% activation). The other ligands did not show significant effects on M2PYK activity. In contrast, M1PYK (shown in white bars) was only very slightly inhibited (about 10% inhibition) by phenylalanine, as well as by arginine, glycine and lysine. But all the other ligands, including F16BP, were not

identified as strong regulators for M1PYK. The results for M1PYK correlate well with previous reports (Carminatti *et al.*, 1971, Williams *et al.*, 2006).

It is interesting that nearly all M2PYK inhibitors (except cysteine) have hydrophobic side chains. On the contrary, both amino acid activators (histidine and serine) are hydrophilic. These observations imply that the hydrophobicity of the amino acid side chain might trigger conformational changes of M2PYK, thereby inhibiting/activating its enzymic activity. Intriguingly, cysteine has a similar structure to the strong M2PYK activator serine, but inhibited its activity. It has been suggested that cysteine functions by dissociating the M2PYK tetramers (Nakatsu *et al.*, 2015).

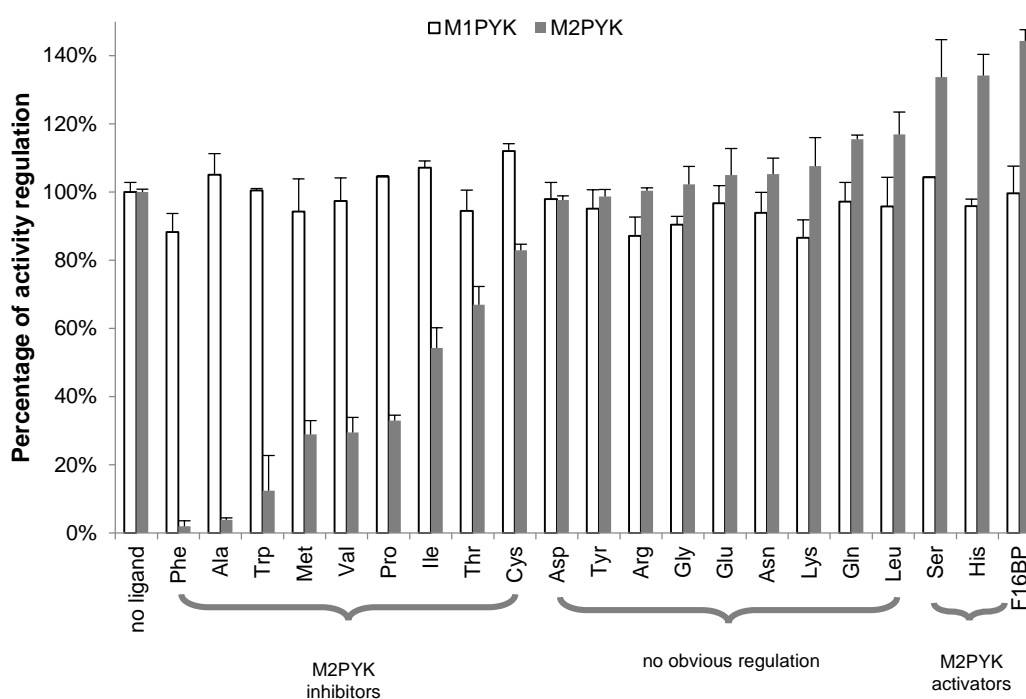


Figure 4.1 Effects of amino acids and F16BP on activity of M1PYK and M2PYK.

Data represent the mean \pm SD of three experiments.

4.3.2 Serine retains the activity of M2PYK

In this study, it was shown that M2PYK gradually dissociates from active tetramer to inactive monomers, and thereby reduces its enzymic activity (Section 3.5). Here the mechanism of regulatory factors was investigated using an enzyme assay in a time-dependent manner (Figure 4.2). M2PYK was diluted from high concentration (20 mg/ml) to low concentration (0.002 mg/ml) into solutions with or without modulators for incubation for different lengths of time. This shows that the activity reduction rate of M2PYK in the presence of activators F16BP or L-serine is lower than that of M2PYK alone. F16BP showed its activation effect at the beginning of the incubation, probably due to its fast rate of binding and then locking M2PYK in an active R-state conformation (Morgan *et al.*, 2013). Intriguingly, unlike F16BP, serine did not show significant activation at the beginning of the incubation. Instead, it displays its activation by decreasing the gradual activity reduction of M2PYK. As shown in Figure 3.9, M2PYK gradually dissociates from active tetramer to inactive monomers. Hence, serine may contribute to the tetramer-stabilisation to act as an “apparent activator” of M2PYK. By contrast, the inhibitors L-phenylalanine, L-alanine, and L-tryptophan inhibited the activity of M2PYK to lower than 20% from the beginning of the incubation.

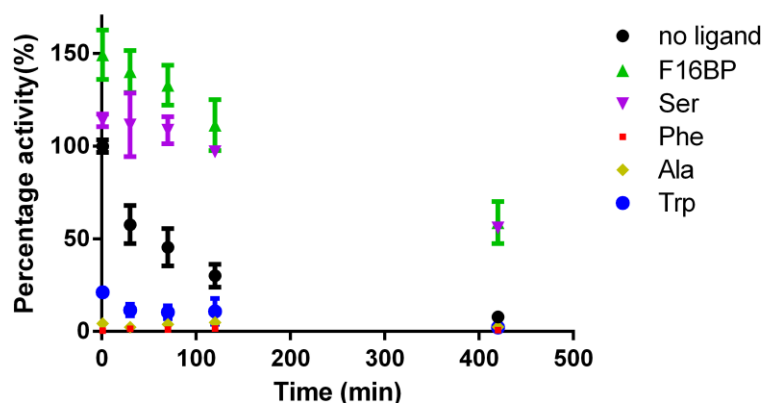


Figure 4.2 Effects of amino acids and F16BP on the gradual reduction of M2PYK activity.

Five millimolar F16BP or amino acid was incubated M2PYK at low concentration (0.002 mg/mL) for 1, 30, 70, 120, and 420 min at room temperature. 100% activity is defined by the highest activity of M2PYK in the absence of ligand. The activity of M2PYK decreased until equilibrium in the absence of any ligand (black dots). Data represent the mean \pm SD of three experiments.

4.3.3 Amino acids are uncompetitive modulators of M2PYK

For the investigation of enzymic effects of the amino acid regulators on M2PYK, enzyme kinetic assays for PEP were carried out in the presence or absence of three inhibitors (alanine, phenylalanine and tryptophan) and an activator (serine). The kinetic curves are shown in Figure 4.3. Binding affinities of the amino acids are also determined with the enzyme assay at a sub-saturating concentration of PEP (Figure 4.4 and summarised in Table 4.1).

It was shown that using PEP as a substrate (saturated ADP, without effector), M2PYK has an apparent V_{\max} value of approximately 100 $\mu\text{mol}/\text{min}/\text{mg}$ and a $K_{0.5}[\text{PEP}]$ of about 0.4 mM. As shown in Figure 4.3 and Figure 4.4, addition of either of the three inhibitors significantly decreased V_{\max} and increased $K_{0.5}[\text{PEP}]$, with a concomitant promotion of cooperativity (Hill coefficient from 1.0 to more than 2.0). Although all the three tested inhibitors show a similar inhibitory pattern on M2PYK, they had different binding affinities. Alanine has the highest binding affinity (K_i 22.0 μM), with phenylalanine and tryptophan binding affinities of 68.5 μM and 471 μM , respectively. By contrast, serine activated M2PYK by increasing both V_{\max} and the PEP affinity. The results show that all the four amino acid regulators are allosteric uncompetitive modulators of M2PYK. Further, it was demonstrated that these amino acids effect M2PYK in physiological ranges (Zhao *et al.*, 2014). In particular, high concentrations (millimolar-level) of alanine and serine in cancer tissues are both higher than their binding affinities to M2PYK, implying that cancer glycolysis is under the control of amino acid flux. More detailed discussion of the physiological relevant of the amino-acid-mediated regulation is in Section 4.8.

It was reported previously that phenylalanine inhibition of M1PYK alters the apparent affinity of PEP without altering V_{\max} and is, therefore, a K-type allosteric system (Williams *et al.*, 2006). However, here we show V-type regulatory effects of amino acids on M2PYK (Traut, 2008). The enzyme may alter its conformation, thereby both its activity and the binding affinity of substrate, in response to the binding of its effectors.

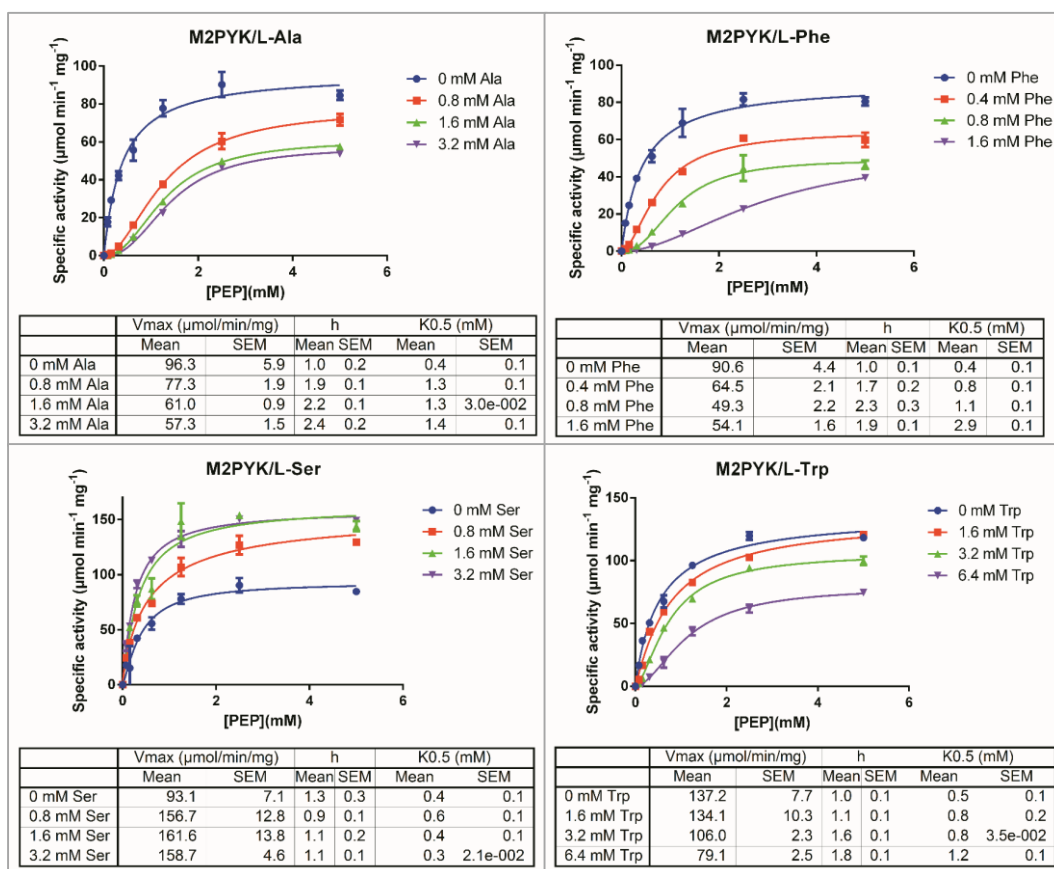


Figure 4.3 Kinetic profiles of M2PYK in the presence or absence of different concentrations of amino acids.

Data represent the mean \pm standard error of two experiments.

Table 4.1 Kinetic parameters and T_m values of M2PYK in the absence/presence of amino acid regulators

	$K_{0.5}$ PEP (mM)	hill coefficient	K_i/K_d (μ M)	T_m ($^{\circ}$ C)
M2PYK	0.4 ± 0.1	1.0 ± 0.2	N/A	47.5
M2PYK+Phe	2.9 ± 0.1	2.3 ± 0.3	68.5	55.0
M2PYK+Ala	1.4 ± 0.1	2.4 ± 0.2	22.0	53.5
M2PYK+Trp	1.2 ± 0.1	1.8 ± 0.1	471	51.5
M2PYK+Ser	0.3 ± 0.1	1.1 ± 0.1	2130	51.0
M2PYK+F16BP	0.1 ± 0.1	1.0 ± 0.0	AC_{50} 6.5	54.5

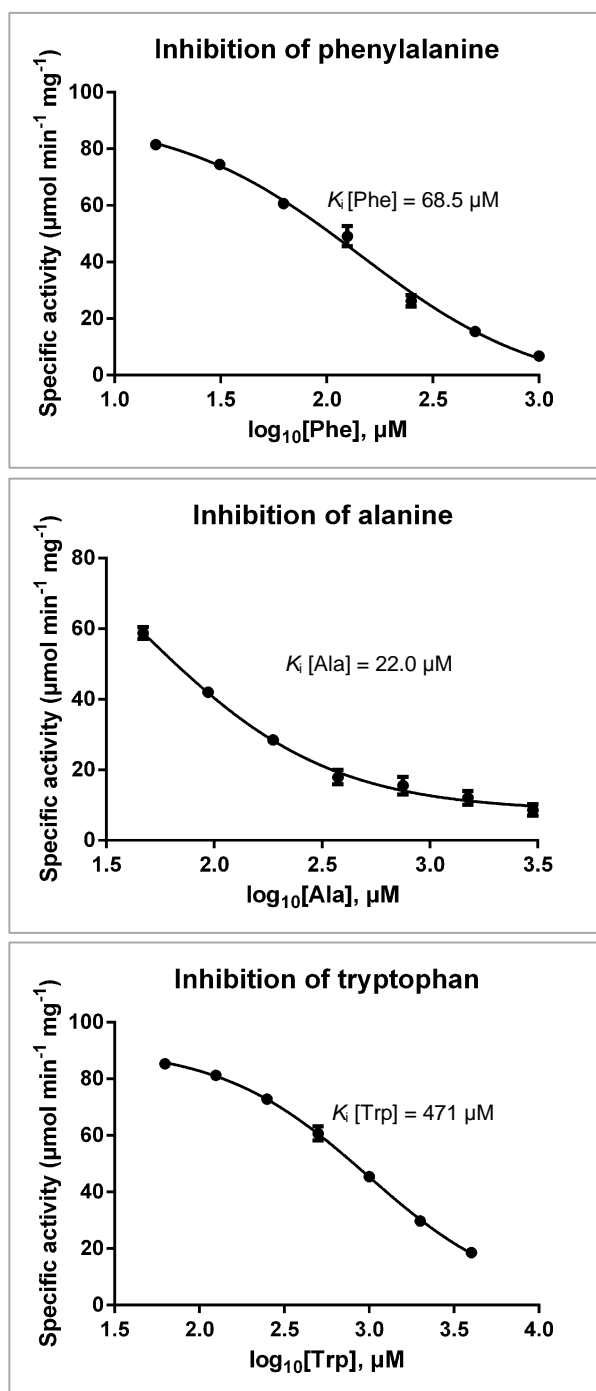


Figure 4.4 The regulatory effects of amino acids on M2PYK activity.

Data represent the mean \pm SD of three experiments.

4.4 Binding of amino acids increases the thermostability of M2PYK

The thermal stability of M2PYK has been reported to be affected by conformational changes and ligand binding (Morgan *et al.*, 2013, Wang *et al.*, 2015). Using a thermal shift assay for the determination of protein unfolding temperature, it is shown that M2PYK is stabilised not only by the well-studied activator F16BP (Figure 3.12), but also the amino acid regulators. As shown in Figure 4.5 (summarised in Table 4.1), all amino acid regulators increased the melting temperature (T_m). Among these amino acids, the inhibitors alanine, phenylalanine and tryptophan increased the T_m of M2PYK from 47.5 °C to 55.0 °C, 53.5 °C, and 51.5 °C, respectively. The activator serine also induced a 3.5 °C up-shift for the T_m of M2PYK. Intriguingly, unlike the smooth melting curves shown for the other ligands, alanine and serine triggered melting curves which consisted of two peaks.

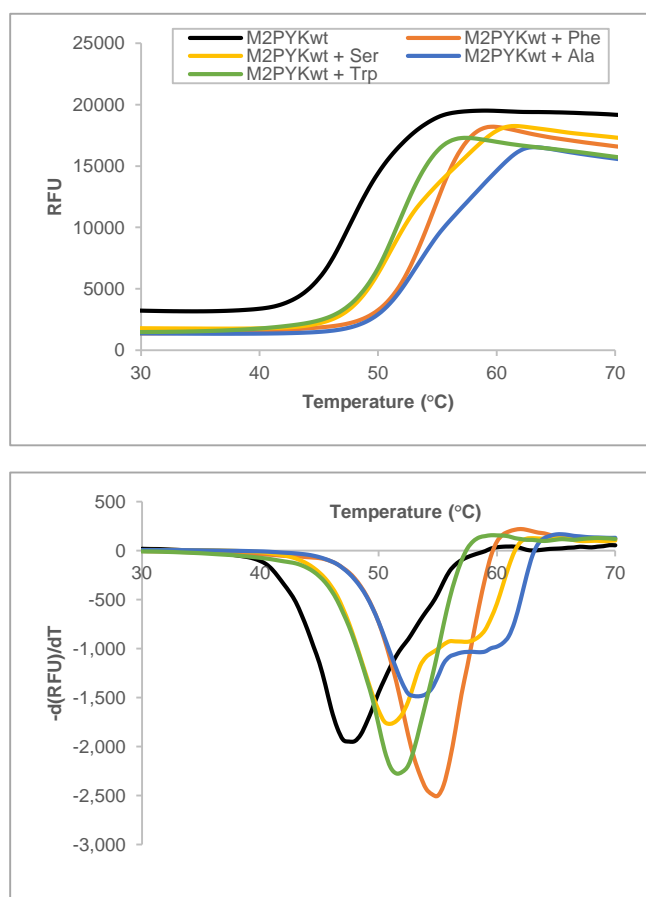


Figure 4.5 Thermal stability of M2PYK and the effects of free amino acids.

Thermal shift assay results for 0.5 mg/ml M2PYK in the absence or presence of 10 mM free amino acids. The bottom panel shows derivative calculations of the fluorescence readings.

4.5 Amino acids stabilise M2PYK tetramer over monomer

In Section 3.5, it was shown that tetrameric M2PYK can gradually dissociate into inactive monomers at low concentration, and therefore the enzymic activity of M2PYK is reduced. In contrast to serine which retains the activity of M2PYK, some hydrophobic amino acids (e.g. phenylalanine, alanine, tryptophan, etc.) inhibit the enzymic activity of M2PYK. Analytical gel-filtration and ELISA were used to validate the hypothesis, that serine stabilises M2PYK as an active tetramer, whereas amino-acid inhibitors stabilise M2PYK in an inactive conformation.

4.5.1 Effects of amino acids on the oligomerisation of M2PYK

Previous results indicate that M2PYK dissociated slowly from tetramer to monomer. The tetramer:monomer ratio reached an equilibrium of about 1:4 (or 1:1 if consider tetramer as one molecule) after 8 h (Figure 3.9). M1PYK however, retained its tetrameric form without dissociating (Figure 3.10).

For the investigation of the effects of amino acids on the oligomerisation of M2PYK, analytical gel-filtration tests were carried out for M2PYK in the presence of four different inhibiting or activating amino acids (Figure 4.6). Briefly, 0.4 ml samples of 0.1 mg/ml of M2PYK were incubated in the absence/presence of 10 mM alanine, phenylalanine, serine or tryptophan in PBS-CM at pH 7.4 at room temperature for 12 h to reach equilibrium. The results show that not only the activator serine, but also all the inhibitory amino acids, stabilised tetramers over monomers. It is likely that alanine and tryptophan function by stabilising the T-state inactive tetramer in the same manner as that previously reported for phenylalanine (Morgan *et al.*, 2013), whereas serine induces the formation of an R-state tetramer.

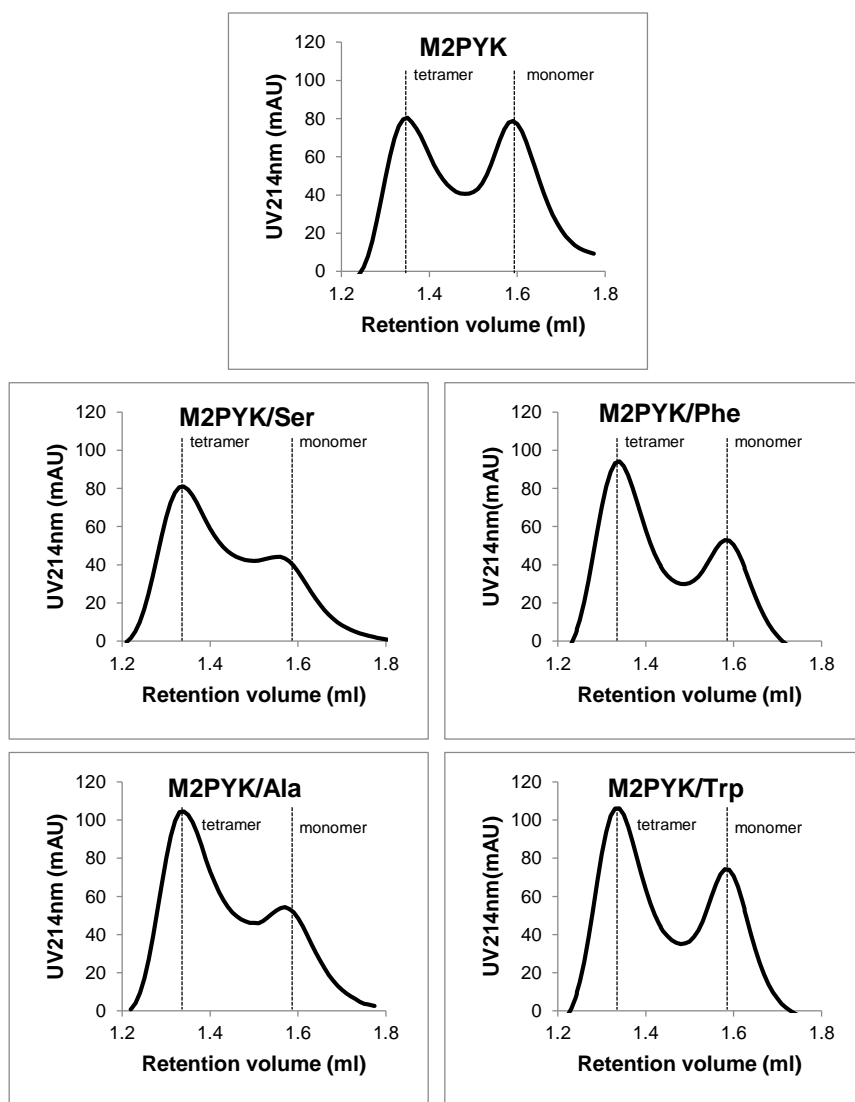


Figure 4.6 Effects of amino acids on the oligomerisation state of M2PYK.

Analytical gel-filtration for 0.1 mg/ml M2PYK incubated in PBS-CM (pH 7.4) in the absence/presence of 10 mM serine, phenylalanine, alanine, or tryptophan for 12 h at room temperature (monitored at 214 nm). The tetramer (left peaks) : monomer (right peaks) ratio was determined with a Superdex® 200 PC 3.2/30 gel-filtration column. Twenty-five microlitres of sample was subjected to the assay each time.

4.5.2 Amino acids tetramerise M2PYK and bury the interface epitope

The detection limit of the analytical gel-filtration technique limited the experiment from demonstrating the association effects of amino acids at lower concentrations of M2PYK. As a result, a highly selective antibody¹ that only binds to the C-C interface of M2PYK by immunising with an epitope specific for this region (Figure 1.4) was adopted for the investigation of oligomerisation effects of free amino acids on M2PYK.

First, the selectivity of two monoclonal antibodies was confirmed by isoform-specific ELISAs. Purified M1PYK and M2PYK were coated on a 96-well microtitre plate separately. Two antibodies (namely 'RAS' and 'RLA') generated from mice immunised with M1PYK-specific epitope and M2PYK-specific epitope were added to each well (Figure 4.7). The ELISA carried out with antibody 'RAS' displayed high signal against M1PYK, but little signal against M2PYK. This was termed 'anti-M1PYK antibody'. The antibody 'RLA' showed its binding to M2PYK but not to M1PYK, and is termed 'anti-M2PYK antibody'. This indicates that both antibodies are highly specific against their respective PYK isoforms. Moreover, the hyperbolic curve of the RLA-M2PYK interaction implies a tighter binding than that of the RAS-M1PYK interaction which adopts a linear curve at the same PYK concentration range.

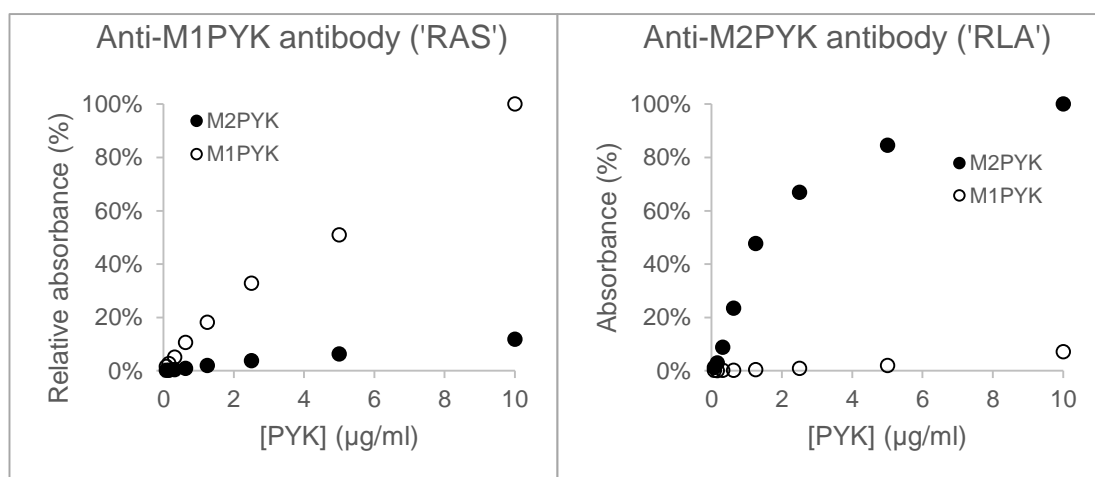


Figure 4.7 Determination of the specificities of anti-PYK antibodies.

M1PYK-specific epitope and M2PYK-specific epitope were immunised in mice to generate specific monoclonal antibodies 'RAS' and 'RLA', respectively. Titrated M1PYK and M2PYK were coated onto a 96-well microtitre plate. Antibodies were incubated against each PYK.

¹ This antibody is a gift from Prof. Ted Hupp, Edinburgh Cancer Research Centre.

The binding of the anti-M2PYK antibody on the C-C interface of M2PYK (hidden when tetrameric) reflects the amount of monomer/dimer but not tetramer, thereby measuring the association effects of amino acids. ELISA tests were performed to characterise these effects. Low concentrations of His₆-M1/2PYK (0–2.5 µg/ml) were incubated with no ligand, 10 mM of each amino acid, or 1 mM F16BP as a positive control for 1 h in PBS-CM at pH 7.4 at room temperature. The incubated solutions were added to 96-well plates pre-coated with anti-His-tag antibodies. HRP-conjugated anti-M2PYK antibodies were then incubated, followed by luminescence reading. The results (Figure 4.8) showed that the reading for M2PYK in the absence of stabilising ligands was significantly higher than M1PYK or than M2PYK with F16BP, alanine, phenylalanine, serine and tryptophan. It indicates that (1) the antibody is specific against M2PYK, with little cross-reactivity with M1PYK; and (2) low concentrations of M2PYK were able to dissociate thereby exposing the epitope on the C-C interface, to which the antibody was bound. But the same concentrations of M2PYK were maintained significantly as tetramers by F16BP, alanine, phenylalanine, serine and tryptophan. As a result, the epitope was hidden and incapable of being bound by the antibody. The results demonstrated that F16BP and amino acids were able to minimise the dissociation of M2PYK at low concentrations.

It has been widely accepted that the M2PYK tetramer has higher activity relative to its monomeric/dimeric forms (Ashizawa *et al.*, 1991, Eigenbrodt *et al.*, 1992, Mazurek *et al.*, 2005, Chaneton & Gottlieb, 2012, Li *et al.*, 2014c). However, we show that the activity is not necessarily correlated with its oligomerisation – apart from the active R-state tetramer, M2PYK can also be stabilised as an alternative T-state tetramer which is inactive (Morgan *et al.*, 2013). It has also been shown that M2PYK can be stabilised in T-state by post-translational modifications and mutations (Wang *et al.*, 2015). It seems likely that the amino acid inhibitors, alanine, phenylalanine and tryptophan, are also T-state tetramer stabilisers thereby inhibiting the M2PYK activity. Meanwhile, serine might activate M2PYK by favouring the R-state tetramer.

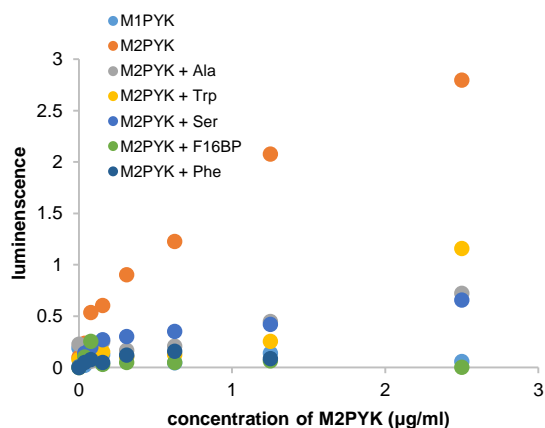


Figure 4.8 Amino acids and F16BP minimise M2PYK dissociation.

The anti-M2PYK antibody is specifically binding to the C-C interface of M2PYK. A high signal of M2PYK only in the ELISA result shows a stronger binding of the antibody on the C-C interface. Lower signals of in the presence of ligands correspond to the previous observation by analytical gel-filtration, which showed that these ligands prevent the dissociation of M2PYK, and thereby bury the C-C interface.

4.6 Crystal structures of M2PYK in complex with different amino acids

The role of the natural effector F16BP which binds 40 Å away from the active site (Figure 1.4) of M2PYK has been extensively studied as a promoter of the R-state tetrameric form with concomitant activation (Dombrauckas *et al.*, 2005, Morgan *et al.*, 2013, Ashizawa *et al.*, 1991, Sparmann *et al.*, 1973). Other reports have shown that M2PYK can transit into an inactive T-state tetramer (Morgan *et al.*, 2013, Wang *et al.*, 2015). Here with the solution of wild-type M2PYK crystal structures co-crystallised with alanine, phenylalanine, serine and tryptophan, it is demonstrated that different amino acids control the activity of M2PYK by stabilising the M2PYK tetramer in either a T or R state.

4.6.1 Crystallisation, data collection and structure determination

Wild-type M2PYK was co-crystallised with different amino acids in similar conditions. The concentration for PEG 3,350 was optimised in the range of 9%–18%. The pH was optimised from 6.7 to 8.2. Near-solubility concentrations were used for each amino acid, which all gave diffracting crystals except alanine. After the alanine concentration trial (from 10–100 mM), a lower concentration of 20 mM alanine was chosen. This

may be because alanine is a structural analogue of PEP, which might be able to bind into the active site at high concentration and interfere with crystal growth.

The optimal condition for each crystal growth is listed in Table 4.2. The crystal of M2PYK with the activator serine grew as plates. Crystals grown with all the three inhibitors, alanine, phenylalanine, and tryptophan, are all rod-shaped (Figure 4.9). The crystal growth process and crystal parameters (e.g. unit cells, space groups, etc., shown in

Table 4.3) of M2PYK/Phe and M2PYK/Trp are almost identical. However, although alanine inhibits M2PYK in an enzymatically similar way to phenylalanine or tryptophan, the crystal of M2PYK/Ala was rather different. First, M2PYK/Ala crystals were favoured by higher pH (pH 7.8–8.0). Second, molecules packed in different ways. For the M2PYK/Ala crystal structure, three asymmetric tetramers (i.e., twelve chains) were found in one unit cell (space group: $P 2_1 2_1 2_1$). In contrast, only one tetramer (i.e., four chains) was found in one unit cell (space group: $P 1 2_1 1$) in M2PYK/Phe or M2PYK/Trp crystal structures.

Table 4.2 Optimal conditions for the co-crystallisation of M2PYK with amino acids.

	M2PYK/Ala	M2PYK/Phe	M2PYK/Trp	M2PYK/Ser
Crystallisation method	Hanging drop	Hanging drop	Hanging drop	Hanging drop
Temperature (K)	290.15	290.15	290.15	290.15
Drop size	3 μ l	3 μ l	3 μ l	3 μ l
Duration of crystal growth	7 days	42 days	42 days	65 days
M2PYK (mg/ml)	10	10	10	10
amino acid (mM)	20	50	30	100
PEG 3,350	11%	16%	15%	14%
sodium cacodylate (mM)	50	50	50	50
TEA (mM)	20	20	20	20
PO ₄ ³⁻ (mM)	5	5	5	5
Na ⁺ (mM)	70	120	120	120
K ⁺ (mM)	50	50	50	50
Mg ²⁺ (mM)	25	25	25	25
ATP (mM)	0	0	0	1
oxalate (mM)	0	0	0	1
pH	7.8	7.4	7.4	7.2

Table 4.3 Data collection and refinement statistics for crystal structures of M2PYK.

	M2PYK/Ala	M2PYK/Phe	M2PYK/Trp	M2PYK/Ser
Data collection				
Space group	P 2 ₁ 2 ₁ 2 ₁	P 1 2 ₁ 1	P 1 2 ₁ 1	P 1
Cell dimensions				
<i>a</i> , <i>b</i> , <i>c</i> (Å)	160.72, 199.36, 243.23	97.37, 70.34, 168.64	96.88, 70.58, 168.50	93.35, 108.94, 124.34
α , β , γ (°)	90.00, 90.00, 90.00	90.00, 106.06, 90.00	90.00, 106.02, 90.00	89.72, 71.13, 66.94
Wavelength (Å)	0.9763	0.91741	0.91741	0.97625
Resolution (Å)	199.33 – 3.72 (18.97 – 3.72)	71.88 – 2.46 (11.00 – 2.46)	72.54 – 3.20 (3.314 – 3.20)	13.24 – 2.96 (116.50 – 2.96)
<i>R</i> _{merge}	0.125 (0.039 – 0.832)	0.077 (0.027 – 0.605)	0.196 (0.024 – 0.845)	0.074 (0.035 – 0.544)
<i>I</i> / σ <i>I</i>	7.5 (25.0 – 1.8)	14.2 (44.7 – 2.5)	7.5 (33.7 – 1.4)	8.4 (18.4 – 1.8)
Completeness (%)	95.3 (92.6 – 96.3)	98.8 (99.4 – 99.6)	98.2 (97.7 – 99.4)	98.6 (95.9 – 98.0)
Multiplicity	4.2 (3.8 – 4.3)	5.8 (5.5 – 5.7)	2.9 (3.0 – 3.0)	2.7 (2.7 – 2.7)
Refinement				
<i>R</i> _{work} / <i>R</i> _{free}	0.239/0.280	0.198/0.224	0.224/0.259	0.226/0.254
No. atoms	46156	14661	14943	31857
Protein	46065	14512	14809	31776
Ligand/ion	60	44	35	56
Water	31	105	99	25
<i>B</i> -factors (Å ²)	135.10	50.60	59.70	74.40
Protein	135.20	50.70	59.80	74.40
Ligand/ion	80.80	51.60	84.10	73.90
Water	114.70	37.00	32.70	40.80
R.m.s. deviations				
Bond lengths (Å)	0.007	0.014	0.012	0.015
Bond angles (°)	0.94	1.59	1.52	1.72
Ramachandran plot (%)				
Favoured regions	95	98	97	95
Allowed regions	4.66	2	3	4.39
Disallowed regions	0.34	0	0	0.61
Conformation	T-state	T-state	T-state	R-state

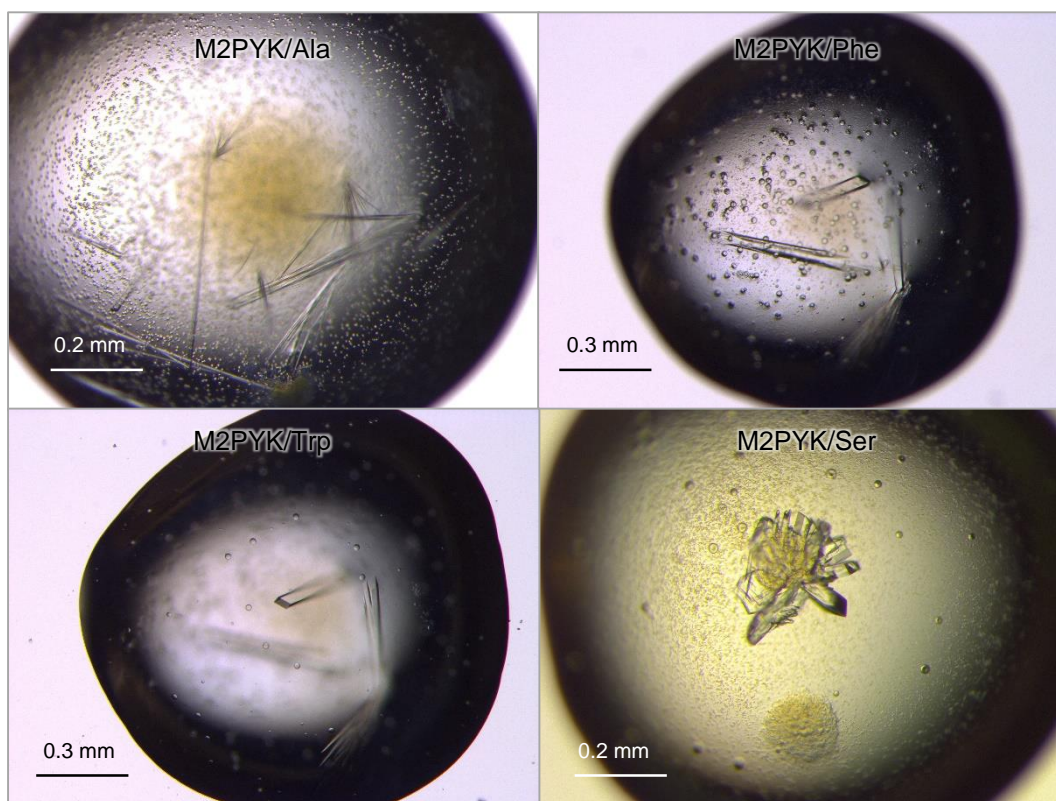


Figure 4.9 Crystals of M2PYK co-crystallised with alanine, phenylalanine, tryptophan, and serine.

4.6.2 Crystal structures display an R-/T-state transition model of M2PYK modulated by amino acids

Chaneton *et al.* have shown an R-state M2PYK structure in complex with serine by soaking M2PYK/F16BP crystal into serine (Chaneton *et al.*, 2012). In this structure it was not possible to clarify whether F16BP alone was responsible for locking M2PYK in a standard R-state conformation. Here we show the M2PYK crystal structure co-crystallised with serine, in the absence of F16BP density in the effector sites. We thus show that serine (on its own) was able to stabilise M2PYK in the R-state, thereby increasing its enzymic activity. Moreover, a T-state structure of a mutated form of M2PYK (R489A) co-crystallised with phenylalanine has been reported previously (Morgan *et al.*, 2013). Here T-state structures of wild-type M2PYK with bound amino acids are shown, further confirming that the R-/T-state transition was not caused by the mutation but by amino acid regulators.

M2PYK was co-crystallised with three inhibitory amino acids (phenylalanine, alanine, and tryptophan) and an activative amino acid (serine). Four crystal structures were solved and compared. First, it was shown that M2PYK equilibrates between an active R-state tetramer and an inactive T-state tetramer in the presence of different amino acids. The conformation transformation is facilitated by a rigid-body rotation of 11° of each subunit (Figure 4.10). Bound to the same pocket, hydrophobic amino acids alanine, phenylalanine, and tryptophan stabilise M2PYK as T-state, whereas hydrophilic amino acid serine stabilises R-state. It is clear that amino-acid modulators regulate the activity of M2PYK by triggering different (active and inactive) conformations.

By co-crystallising M2PYK with inhibitory amino acids (alanine, phenylalanine, tryptophan) or activating amino acid (serine), the amino-acid ligands were found to bind to the same allosteric pocket located between the A-domain and C-domain (Figure 4.11) of each subunit. The carboxyl groups of these amino acid ligands are bound to the side chains of Asn70 and Arg106, and their amino groups to the side chain of His464 and the main-chain oxygen on Ile469. The distances between atoms on amino-acid ligands and surrounding residues are summarised in Table 4.4. It suggests that the binding mode of all amino-acid ligands are similar, except for the binding to Arg43 (Table 4.4, Figure 4.11 and Figure 4.12).

It is shown that the side-chain hydroxyl group of the ligand serine form a hydrogen bond with the main-chain oxygen of Arg43 located on the N-terminus (Figure 4.12). By contrast, inhibitory amino acids push the N-terminal loop away by approximately 6 \AA , due to their hydrophobic side-chains, and thereby trigger the R-/T-state rigid body rotation.

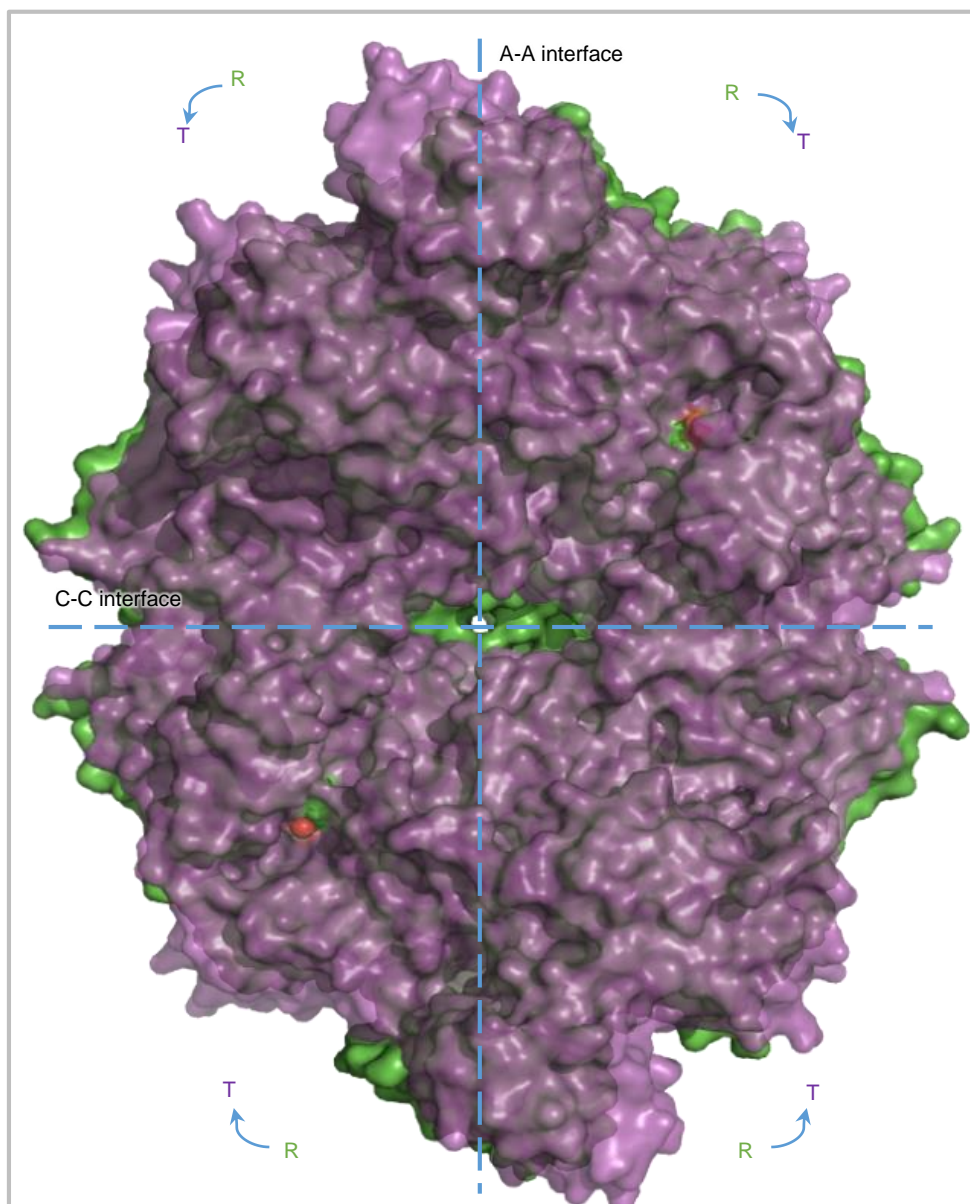


Figure 4.10 M2PYK equilibrates between R-state and T-state tetramers.

M2PYK equilibrates between an active R-state tetramer (green) and an inactive T-state tetramer (purple). The conformation transformation is facilitated by the rotation of each subunit. Bound to a same site, hydrophobic amino acids alanine, phenylalanine, and tryptophan stabilise M2PYK as T-state, whereas hydrophilic amino acid serine stabilises R-state.

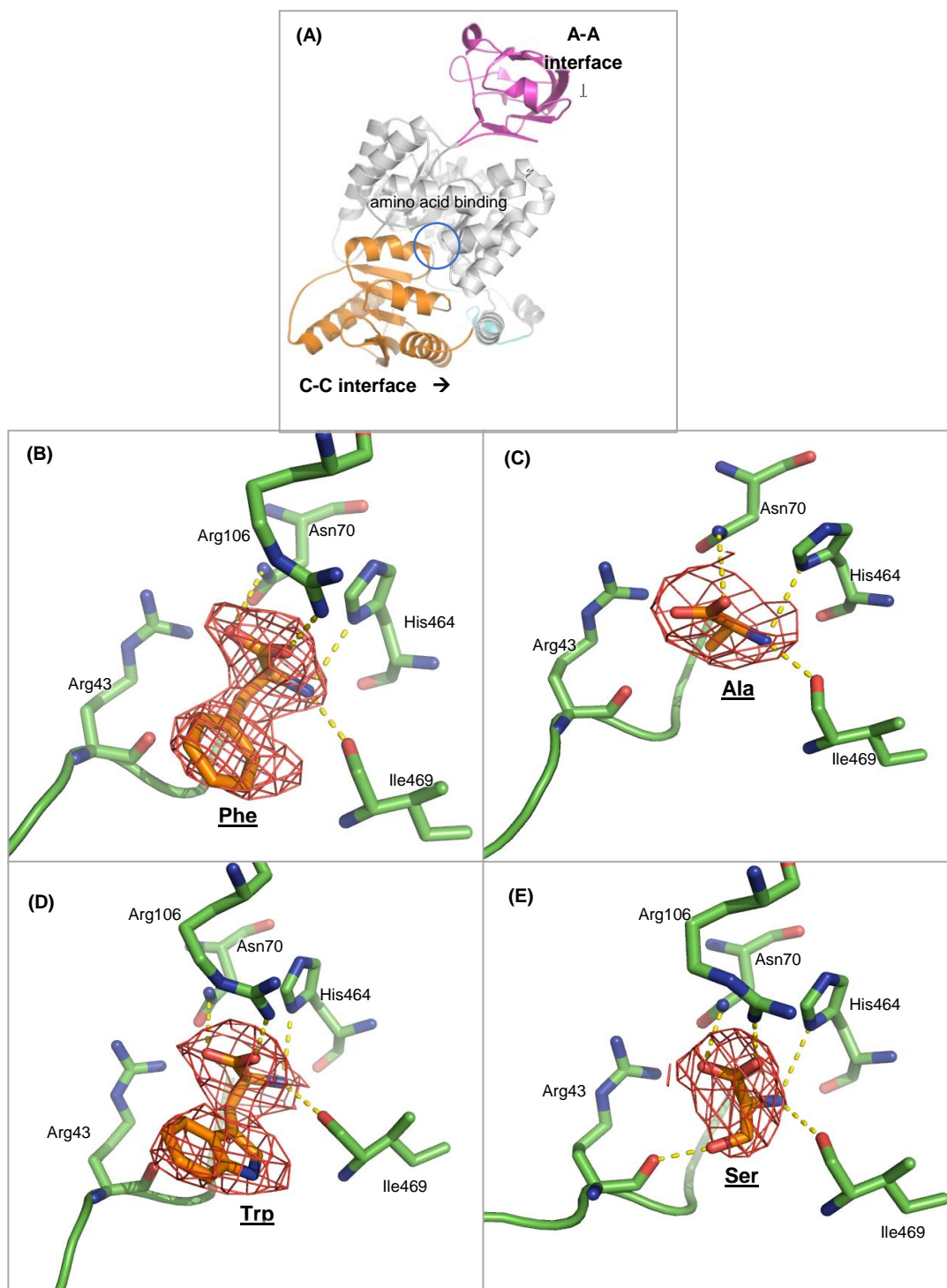


Figure 4.11 The bindings of amino acids on M2PYK.

(A) Architecture of M2PYK monomer. N-terminus (cyan = residues 1–24); domain-A (grey = residues 25–116 and 220–402); domain-B (purple = residues 117–219); and domain-C (orange = residues 403–531). Location of the amino acid binding site is highlighted.

(B–E) Structures of the amino acid binding site bound with Phe, Ala, Trp, and Ser, respectively. Hydrogen bonds and ion strength are shown in yellow dashed lines. The electron density of amino acid ligand in panel B, C, D, and E (coloured in orange) is from F_o-F_c maps contoured at the 3.0σ , 1.8σ , 2.4σ , and 2.0σ level, respectively.

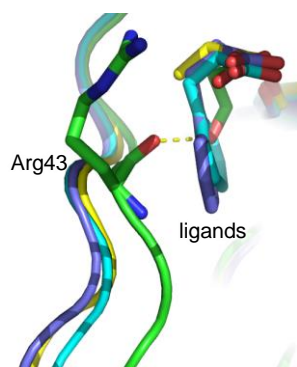


Figure 4.12 Inhibitory amino acids push the N-terminal loop of M2PYK.

Green: serine; purple: phenylalanine; cyan: tryptophan, yellow: alanine. Hydrogen bond is shown in yellow dashed lines.

Table 4.4 Distance between atoms on amino-acid ligands and surrounding residues.

atom on ligand	receptor	distance between atoms (Å)			
		M2PYK/Phe	M2PYK/Trp	M2PYK/Ala	M2PYK/Ser
CA	R43/CA	7.4	7.7	7.1	6.2
O	N70/ND2	3.3	3.3	3.1	3.4
O	R43/NH1	4.3	3.9	4.1	3.9
OXT	N70/ND2	4.3	4.0	4.1	3.3
OXT	R106/NH2	2.9	2.7	8.0 ^a	3.2
OXT	H464/ND1	3.5	3.3	3.5	3.1
N	I469/O	2.7	2.6	2.9	3.2
N	H464/ND1	3.1	3.2	3.5	3.6
NE1	N44/OD1	N/A ^b	3.4	N/A	N/A
NE2	G468/O	N/A	3.6	N/A	N/A
OG	R43/O	N/A	N/A	N/A	2.6

^a The density of the side chain of Arg106 is ambiguous.

^b not applicable, because the atom is not available in this amino-acid ligand.

4.6.3 Comparison of M2PYK structures

Here the four M2PYK crystal structures solved in this study are systematically compared, including three T-state structures co-crystallised with three inhibitor amino-acid ligands (phenylalanine, alanine, and tryptophan), and an R-state structure co-crystallised with the activator serine.

(1) The amino acid binding pocket

As shown in Figure 4.12, a direct conformational effect of amino-acids ligand binding is on the amino acid binding site. All the three inhibitory amino acids pushed the N-terminal loop of M2PYK by approximately 6 Å in comparison with an R-state M2PYK crystal structure without amino-acid ligand, whilst the activator serine stabilised the loop by forming a hydrogen bond with the main-chain oxygen of Arg43 and the hydroxyl group of its side chain.

(2) Structural differences in the N-terminal sequence

In the R-state crystal structure co-crystallised with serine, the N-terminal residues (1–12) were disordered and could not be fitted into electron density. In T-state structures with phenylalanine or tryptophan, the disordered sequence was even longer (residues 1–22). Surprisingly, although the M2PYK/Ala structure is also in T-state, the N-terminal loop was more stable, and thus was solved in the crystal structure (start from residue Pro5). This is the longest N-terminal loop solved in all published M2PYK structures up to now. The comparison of the N-terminal loops from these structures in different conformations is shown in Figure 4.13.

In the R-state structure stabilised with serine (green), an ‘engaged region’ was formed with electrostatics between Gln16-Gln17 and Asp34-Ser37-Pro38. As a result, the Gln16-Gln17 region was stabilised and thus ordered. Binding with the inhibitors, the hydrophobic side chains of phenylalanine (purple) and tryptophan (yellow) push the N-terminal loop, thereby flipping Ile40 which blocks the engaged region. In consequence, the Gln16-Gln17 fragment is disordered. This is further confirmed by the M2PYK/alanine structure (blue), in which the ‘engaged region’ is disrupted so that it adopts another conformation. This region is further stabilised by the salt-bridge

formed with His6 and Glu282 on the adjacent tetramer. This probably provides an interpretation of why (a) the N-terminal loop in the M2PYK/Ala structure is more ordered than other structures; (b) M2PYK/Ala unit cells pack with three tetramers in the asymmetric unit; (c) M2PYK/Ala structure favoured high pH.

(3) T and R state conformations stabilised by amino acid ligands

Inhibitors alanine, phenylalanine, and tryptophan stabilise M2PYK as T-state, whereas the activator serine stabilises R-state. The conformational transformation is facilitated by a rigid-body rotation of 9° – 11° of each subunit (Figure 4.10).

Systematic comparisons of subunit rotation angles (pink) and tetramer fits (blue) among different M2PYK crystal structures are shown in Table 4.5. This shows that the T-state structures of M2PYK/Phe and M2PYK/Trp are very similar, with only 0.47° subunit-rotation and an RMS of 0.26 \AA (only C α atoms were compared, as below). These two structures are also very similar to a previously solved T-state crystal structure of M2PYK-R489A co-crystallised with phenylalanine (PDB code: 4FXJ). The other extreme conformation (R-state) shows in the M2PYK/Ser structure, which displays an about 11° subunit-rotation and RMS values as high as approximately 4.7 \AA in comparison with the T-state structures. This M2PYK/Ser crystal structure is similar to previously solved R-state structures of M2PYK (4B2D, M2PYK/F16BP soaked with serine; 4FXF, M2PYK/F16BP) and M1PYK (3SRF), confirming that serine alone stabilises the R-state of M2PYK. The crystal structure of M2PYK/Ala is in an intermediate conformation between the extreme T-state (e.g. M2PYK/Phe, M2PYK/Trp) and the extreme R-state (e.g. M2PYK/Ser). It shows an approximately 3.5° subunit-rotation in comparison to the extreme T-state structures, and about 9.1° to R-state structures. In a comparison by RMS-fit, it is 1.5 \AA away from the extreme T-state structures, and about 3.7 \AA from R-state structures. The parameters of the intermediate conformation of M2PYK/Ala suggest that it is more similar to the extreme T-state conformation. The intermediate conformation of the M2PYK/Ala may also provide explanations to its unique crystallisation process and crystallographic parameters (Table 4.2 and Table 4.3).

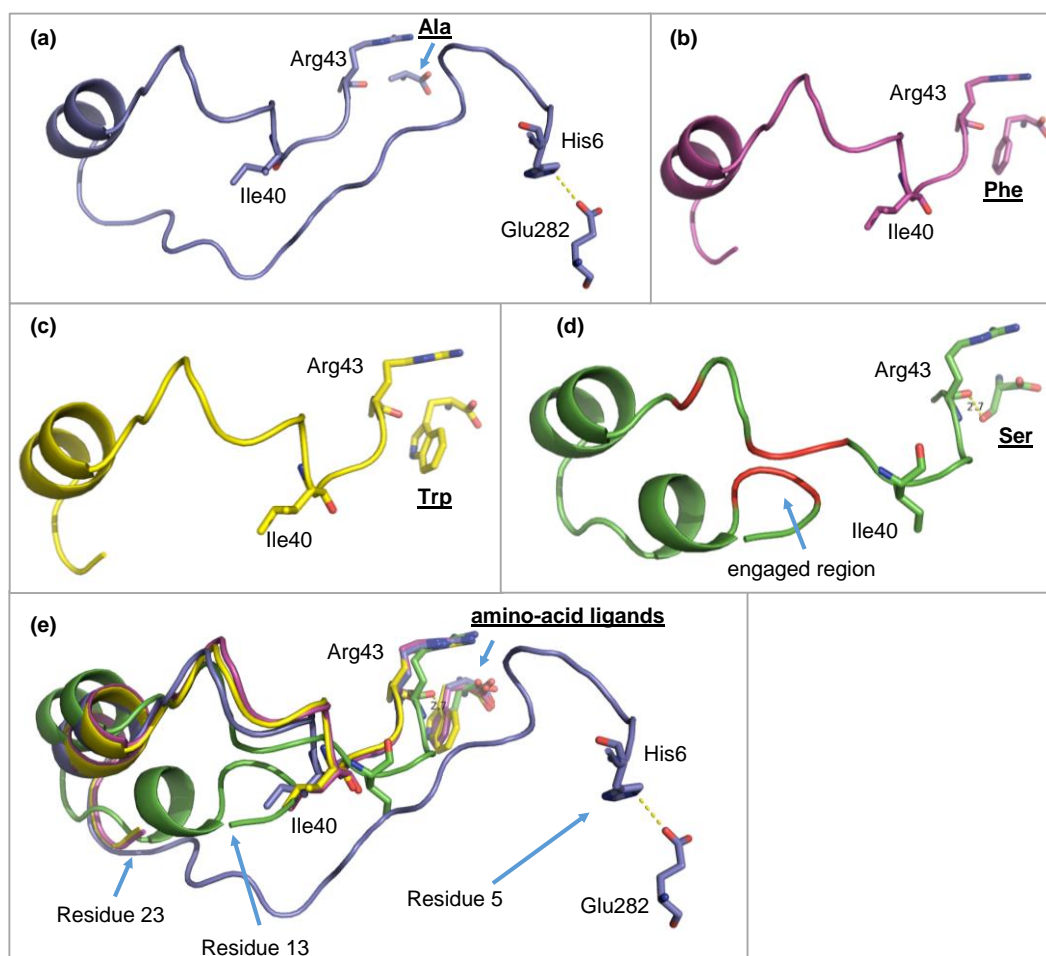


Figure 4.13 N-terminal conformations of M2PYK crystal structures.

(a-d) N-terminal conformations of M2PYK/Ala structure (blue), M2PYK/Phe structure (purple), M2PYK/Trp structure (yellow), and M2PYK/Ser structure (green). Particularly, in figure (d), the 'engaged region' formed with electrostatics between Gln16-Gln17 and Asp34-Ser37-Pro38 are highlighted in red. (e) Aligned N-terminal conformations. N-terminal fragments are too disordered to be modelled. The 'solvable' ends are indicated in the figure (Residue 5, 23, 23, and 13 for alanine, phenylalanine, tryptophan, and serine, respectively).

Table 4.5 Comparisons of subunit rotation angles and tetramer fits among different M2PYK crystal structures.

	Ala	Phe	Trp	Ser	4FXJ	4B2D	4FXF	3SRF
Ala		3.23	3.66	9.1	3.56	9.25	9.19	9.29
Phe	1.45		0.47	11.28	0.38	11.23	11.12	11.76
Trp	1.58	0.26		11.52	0.59	11.53	11.37	12.05
Ser	3.65	4.68	4.76		11.50	0.65	1.08	1.66
4FXJ	1.49	0.38	0.60	4.68		11.40	11.25	11.99
4B2D	3.70	4.69	4.79	0.42	4.68		0.97	1.99
4FXF	3.33	4.23	4.33	0.93	4.24	0.93		2.71
3SRF	3.88	5.00	5.10	0.95	5.01	1.06	1.55	

Blue: RMS fit (Å) (tetramer-tetramer best fit, calculated with C α atoms). Red: subunit rotation angles (°) (calculated based on the tetramer-tetramer RMS best fit).

4FXJ: A published crystal structure with M2PYK-R489A and ligand phenylalanine (Morgan *et al.*, 2013).

4B2D: A published crystal structure with M2PYK/F16BP/Ser (Chaneton *et al.*, 2012).

4FXF: A published crystal structure with M2PYK/F16BP (Morgan *et al.*, 2013).

3SRF: A published crystal structure with M1PYK (Morgan *et al.*, 2013).

Table 4.6 Distances of α -helices shifted by the binding of amino-acid ligands.

Helices	Residue number	Ser/Phe	Ala/Phe	Trp/Phe	M1PYK
H1	Residues 26–31	2.69	0.82	0.22	3.07
H2	Residues 58–67	0.34	0.33	0.14	0.30
H3	Residues 81–96	0.43	0.26	0.14	0.43
H4	Residues 223–234	0.45	0.35	0.20	0.35
H5	Residues 248–258	0.29	0.43	0.22	0.30
H6	Residues 274–278	0.41	0.22	0.26	0.30
H7	Residues 280–286	0.20	0.37	0.18	0.36
H8	Residues 294–300	1.75	0.59	0.19	1.32
H9	Residues 306–320	0.65	0.29	0.17	0.55
H10	Residues 332–335	0.94	0.52	0.10	1.21
H11	Residues 342–354	0.78	0.21	0.13	0.80
H12	Residues 363–366	0.50	0.44	0.14	0.52
H13	Residues 371–387	1.33	0.38	0.11	1.39
H14	Residues 391–401	1.21	0.40	0.14	1.12
H15	Residues 408–422	0.78	0.28	0.17	1.25
H16	Residues 436–442	0.53	0.25	0.18	0.68
H17	Residues 457–462	0.41	0.27	0.14	0.40
H18	Residues 463–465	0.36	0.33	0.10	0.26
H19	Residues 482–499	0.47	0.43	0.24	0.78

Values shown in the table are averaged C α -distances of α -helices in different M2PYK structures (Å). Numbers of α -helices are labelled in Figure 4.14. Significant shifts are highlighted with different colours, and the colour coding is also shown in Figure 4.14.

(4) Conformational changes of the TIM barrel and interface bonds of M2PYK upon amino-acid binding

The position shifts of each α -helix of the M2PYK structure, caused by amino-acid binding, were investigated by calculating the $C\alpha$ distances in different structures, in order to study the effects of different amino-acid binding on the intra-subunit conformation of M2PYK. The comparisons were carried out between the structures of M2PYK/Ser and M2PYK/Phe, M2PYK/Ala and M2PYK/Phe, M2PYK/Trp and M2PYK/Phe, M1PYK and M2PYK/Phe. Averaged $C\alpha$ -distances of α -helices in different M2PYK structures are shown in Table 4.6. Significant position-shifts are highlighted in different colours and mapped into an M2PYK structure (Figure 4.14). Moreover, interface bonds between subunits in different states are shown in Table 4.7.

It is shown that the M2PYK/Phe structure and the M2PYK/Trp structure are almost identical in all the α -helices. The binding of alanine caused moderate conformational changes in α -helix 1 (H1), H8, and H10 in comparison with that of the phenylalanine-bound structure. More significantly, binding of phenylalanine caused significant changes in comparison with the R-state structures (e.g. M2PYK/Ser, M1PYK, etc.). The highest shift takes place on the N-terminal α -helix H1, which is linked to N-terminal loop that can be directly shifted by amino-acid binding. This fragment (Residues 24–31) is also responsible for switching the interface bond from locking the A-A interface (in T-state, Asp24-Arg400 salt-bridge across the A-A interface) to locking the C-C interface (in R-state, Asp24-Arg400 salt-bridge across the C-C interface) (Figure 4.15). The important Arg400 also locates in an α -helix H14, which is significantly shifted by the binding of different amino acids. This observation suggests that the amino-acid triggered rigid-body rotation may initiate from the N-domain shift, causing the Asp24/Arg400 salt bridge to switch from locking the A-A to locking the C-C interfaces. Meanwhile, another salt bridge Arg400/E396 across the C-C interface is also formed upon the conformational change (Figure 4.15).

The binding of different amino acids also shifted the positions of H8, H9, H10, H11, H13, and H15. Most of the shifted α -helices are involved in the A-A interface interactions. For instance, H13 directly interacts with the H9 in the adjacent subunit. On the other side of the helix, H13 also interacts with the N-terminal loop (Figure

4.14). Hence, the shift of H13 may be caused by the conformational change of the N-terminal loop, which is amino-acid-dependent. Another shifted α -helix H15 (Residues 408–422) is involved in the C-C interface interaction. In an R-state structure, Lys422 forms a hydrogen-bond with the main-chain oxygen of Pro403 across the C-C interface (Figure 4.15). In T-state, this interface interaction is pulled out and thus unlocked.

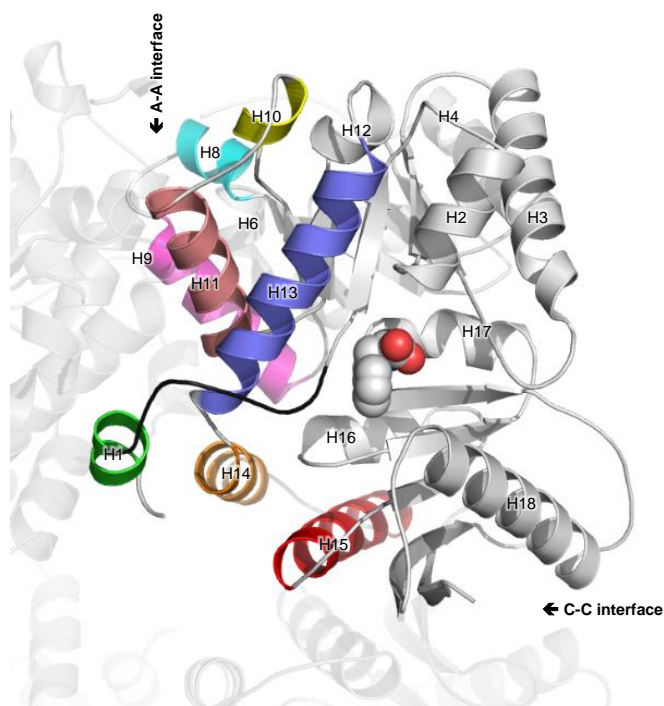


Figure 4.14 Helices shifted by the binding of amino-acid modulators.

Significant distance shifts are highlighted in different colours. B-domains are not shown in this figure. Different colours corresponding to each α -helix are shown in Table 4.6. The amino-acid binding site is shown in spheres. The N-terminal loop is shown in black. Adjacent subunits are shown in transparent models. Positions of the A-A interface and the C-C interface are labelled by arrows.

Table 4.7 Interface interactions of PYK in different states.

<u>M2PYK/Phe A-Ainterface</u>		<u>M2PYK/Ser A-Ainterface</u>		<u>M1PYK A-Ainterface</u>		<u>M2PYK/Phe C-Cinterface</u>		<u>M2PYK/Ser C-Cinterface</u>		<u>M1PYK C-Cinterface</u>	
<u>Chain A</u>	<u>Chain B</u>	<u>Chain A</u>	<u>Chain B</u>	<u>Chain A</u>	<u>Chain B</u>	<u>Chain A</u>	<u>Chain D</u>	<u>Chain A</u>	<u>Chain D</u>	<u>Chain A</u>	<u>Chain D</u>
C31	R316	C31	R316	C31	R316	D487	W515				
D24	R400					D487	R516				
D347	R342					E484	R516				
D347	S346	D347	S346	D347	S346			D24	R400	D24	R400
D36	H274	D36	R278	D36	H274					M22	R400
E28	R319	E28	R319	E28	R319			E396	R400		
E304	R339							E418	R399		
E384	K305	E384	K305	E384	K305			K422	P403		
E397	L27	E397	L27	E397	L27					S402	K422
E397	F26	E397	F26	E397	F26					S405	K422
		G179	R339	G179	R339	M525	M525	M525	M525	M525	M525
		G295	R342	G295	R342	N523	V527	N523	V527	N523	V527
		G298	R339	G298	R339						
H274	D36	H274	D36	H274	D36						
I35	K305	I35	K305	I35	K305						
K305	E384	K305	E384	K305	E384						
K311	N350	K311	N350	K311	N350						
L27	E397	L27	E397	L27	E397						
Q329	R342	Q329	R342	Q329	R342						
Q393	Q393	Q393	Q393	Q393K							
R278	D36	R278	D36								
		R294	R342	R294	R342						

Interface bonds that are rearranged upon R/T state conformational change are highlighted in yellow. The Q393 in M2PYK that is replaced by K393 is highlighted in green.

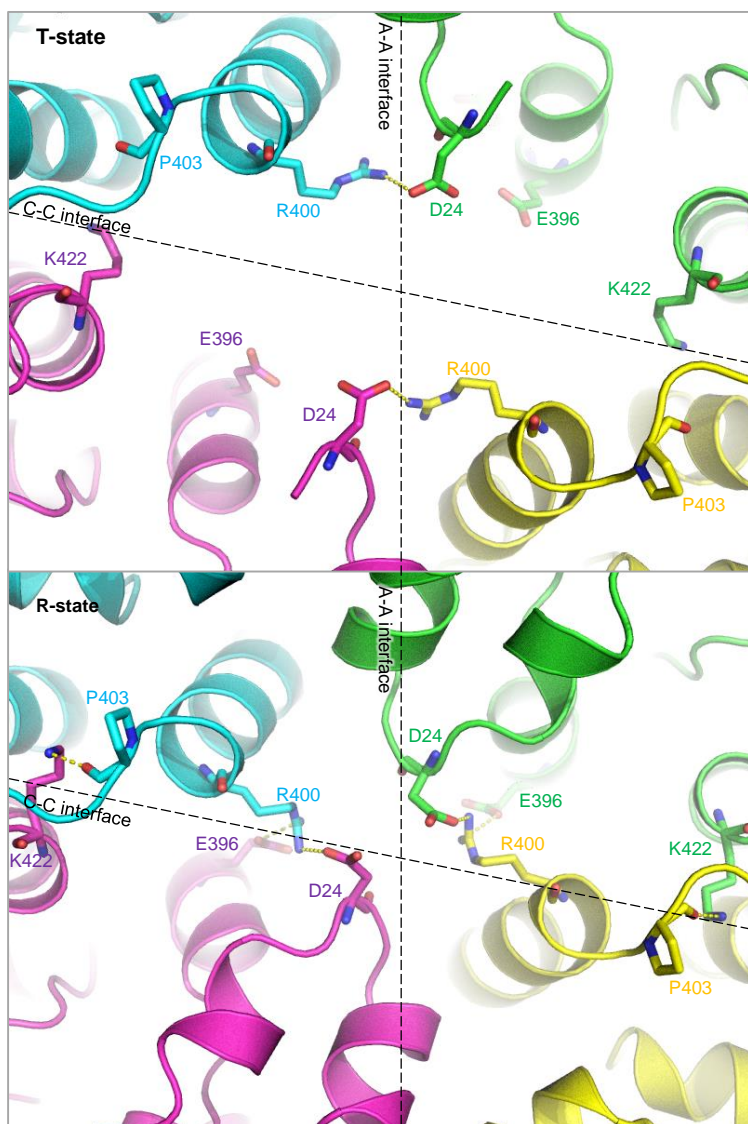


Figure 4.15 Interface bonds in the tetramer centre of M2PYK.

The four subunits of M2PYK tetramer are shown in different colours.

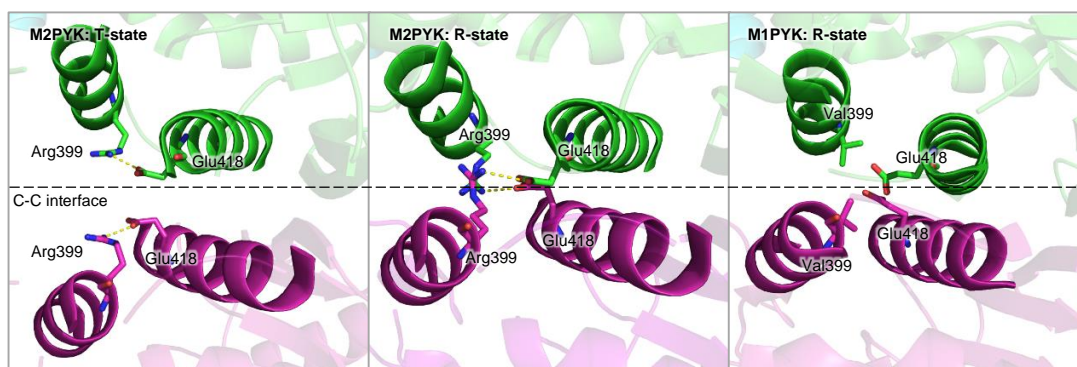


Figure 4.16 Interface bonds between Residues 399 and 418 on C-C interface.

Green and purple colours represent two different subunits.

The rigid-body rotations, triggered by binding of different amino-acid ligands, re-organise the interactions within the C-C interface. In the T-state structure of M2PYK, Arg399 forms a salt-bridge with Glu418 on the same subunit (Figure 4.16). However, the rigid-body rotation from T-state to R-state conformation pulls the adjacent subunit across the C-C interface closer, and consequently, the Arg399 turns to interact with Glu418 on the adjacent subunit, instead of interacting with that on the same subunit. It is also interesting that the interacting Arg399 is replaced by Val399 in M1PYK, and thus loses the ability to form this salt-bridge.

The allosteric mechanism of M2PYK is simplified and summarised in Figure 4.17. Beyond the re-organisation of the Asp24-Arg400 and Arg399-Glu418 salt-bridges, some other important changes also take place upon binding of different amino-acid modulators.

The rigid-body rotation from the R-state conformation to T-state disrupts the C-C interface interactions near the tetramer centre. However, other strong hydrogen bonds are formed at the other end of the C-C interface. For instance, Asp487-Trp515 bonds across the C-C interface are formed in T-state conformations (Figure 4.18). Trp515 is located on the effector loop of M2PYK (Figure 4.19), and rotating the tetramer toward R-state disrupts this interface bond. F16BP activates the enzymic activity of M2PYK by pulling out the effector loop and breaking the Asp487-Trp515 hydrogen bond with stabilises the T-state conformation (Figure 4.19) (Morgan *et al.*, 2013).

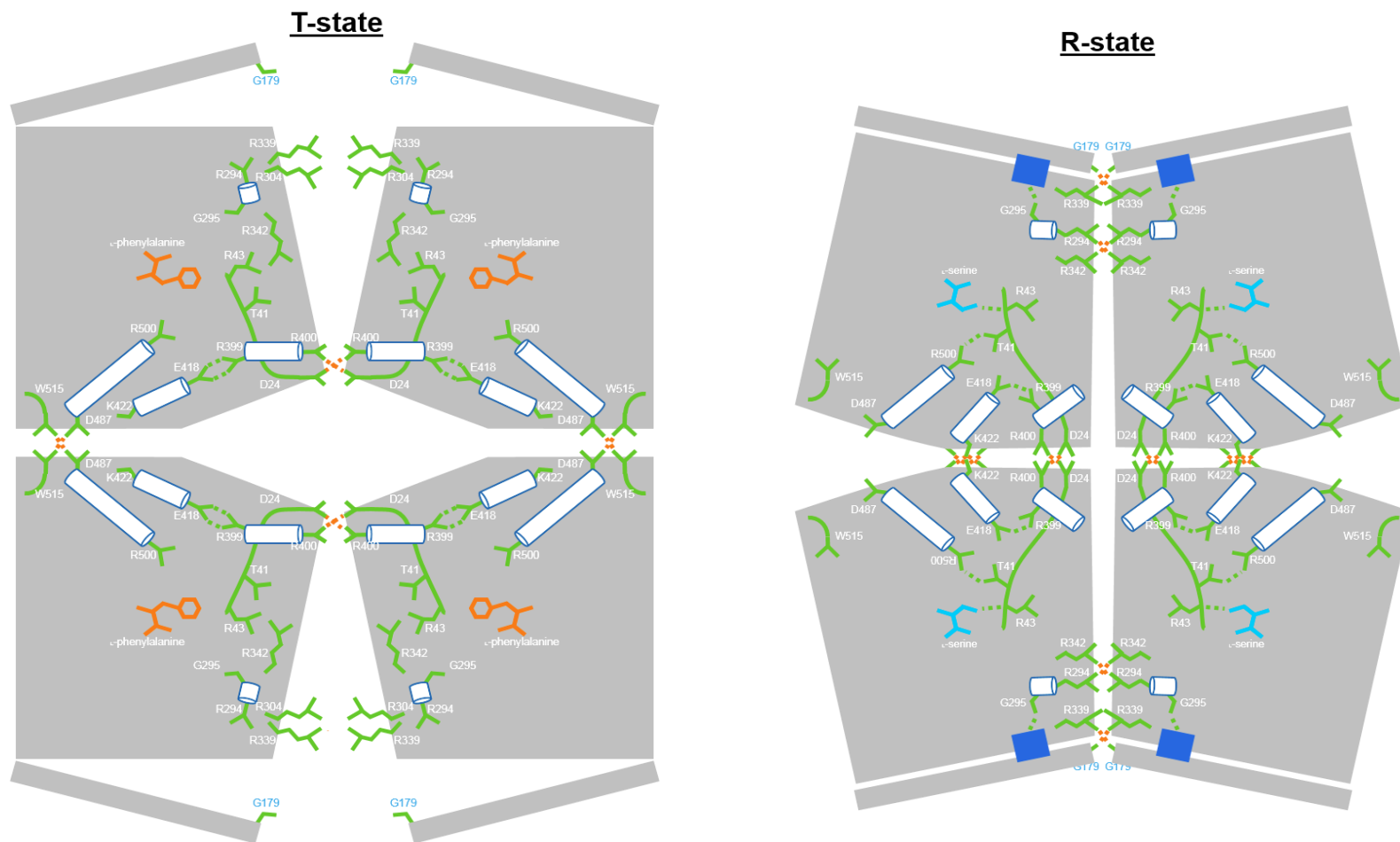


Figure 4.17 T-state and R-state M2PYK structure models.

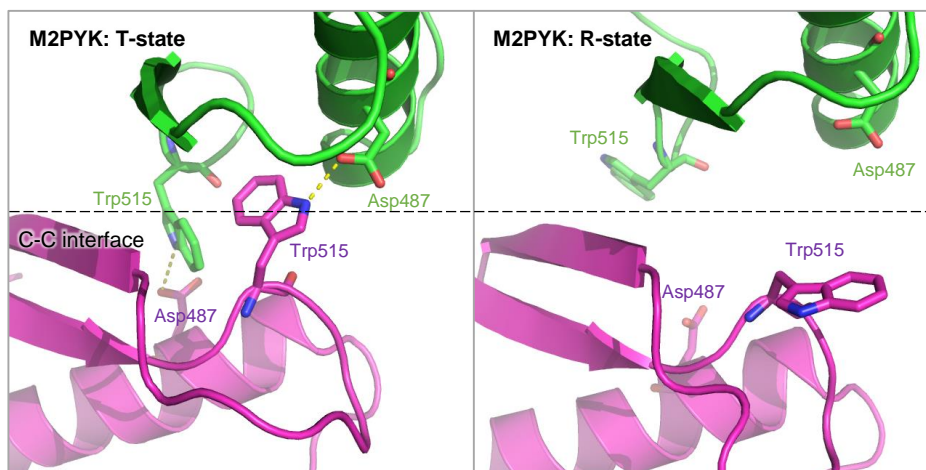


Figure 4.18 Interface bonds between Asp487 and Trp515 on C-C interface.

Green and purple colours represent two different subunits.

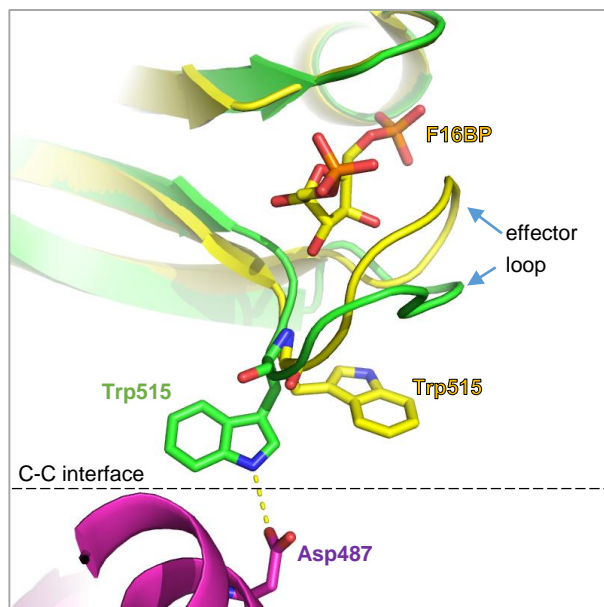


Figure 4.19 The effector loop curls round F16BP to stabilise the R-state.

Green and yellow colours represent T-/R-states of M2PYK. The purple model represents the adjacent subunit across the C-C interface. The M2PYK/Phe structure solved in this study was used to build the T-state model. Previously solved M2PYK/F16BP structure (PDB code: 4FXF) was used to build the R-state model.

The closure of the B-domain of PYK is responsible for the formation of a complete active site, and thereby facilitates the catalysis of PYK. Therefore, the activity of PYK is dependent on the state and stability of the B-domain (Dombrauckas *et al.*, 2005).

Upon the rigid-body rotations, interface hydrogen-bonds on the A-A interface are also re-organised. The R-to-T rigid-body “rock” of M2PYK places Arg342 in position to prime the active site by stabilising the short glycine-rich H8 helix (²⁹⁵Gly-Asp-Leu-Gly-Ile-Glu-Pro³⁰¹) of an adjacent subunit (Figure 4.20). Moreover, Arg339 binds to Gly179 (a residue on the B-domain) on the adjacent subunit across the A-A interface in an R-state conformation, and thus stabilises the closure of the B-domain, thereby forming a complete active site. By contrast, a T-state structure has a larger gap at the A-A interface, so that the B-domain is not able to be stabilised by Arg339 from the adjacent subunit, and thus the complete active site cannot be stabilised (Figure 4.20).

Levels of the closure of B-domains are investigated by measuring the distances between Pro53 (on A-domain) and Thr129 (on B-domain) (Dombrauckas *et al.*, 2005). The results show that the level of the closure of B-domain correlate well with the conformational state of the structure (Figure 4.22). All structures that adopt an inactive T-state conformation have relatively open B-domains (i.e., distances greater than 18 Å). In contrast, all R-state structures display relatively closed B-domains (i.e., distances lower than 18 Å). The results confirmed that the catalytic activity of M2PYK requires a stabilised closed B-domain.

The involvement of adjacent subunits in shaping the active site provides a clear explanation for the inactivity of monomeric PYK and also therefore an explanation of the inhibitory effect of T3, which stabilises monomeric M2PYK.

In summary, the activity of M2PYK is dependent on the stabilisation/closure of its B-domain, which is required for the formation of a complete active site, and the state of the B-domain, requires stabilisation from an adjacent subunit across the A-A interface. Any conformational change that interferes (e.g. rotation to a T-state tetramer that introduces a gap at the A-A interface, or dissociation into monomer which completely disrupts this stabilisation effect), can eliminate the enzymic activity of pyruvate kinase.

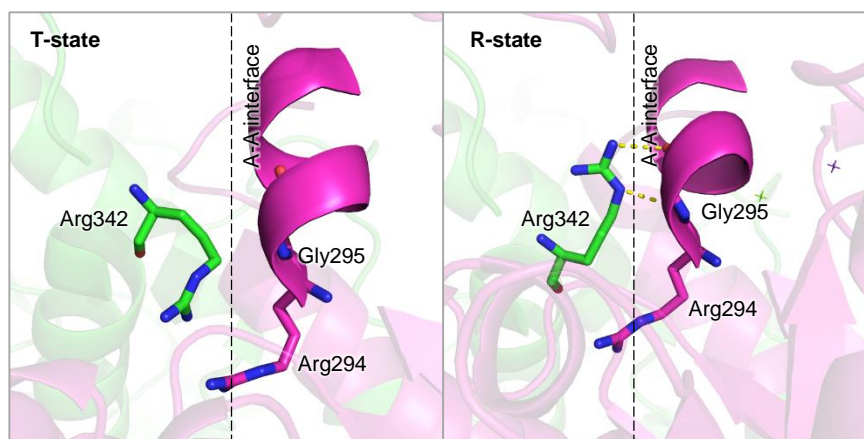


Figure 4.20 Interface bonds involving Arg342 on A-A interface.

Green and purple colours represent two different subunits.

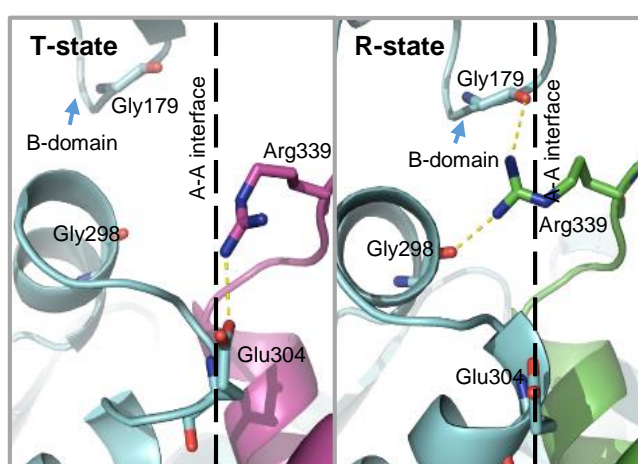


Figure 4.21 Interface bonds involving Arg339 on A-A interface.

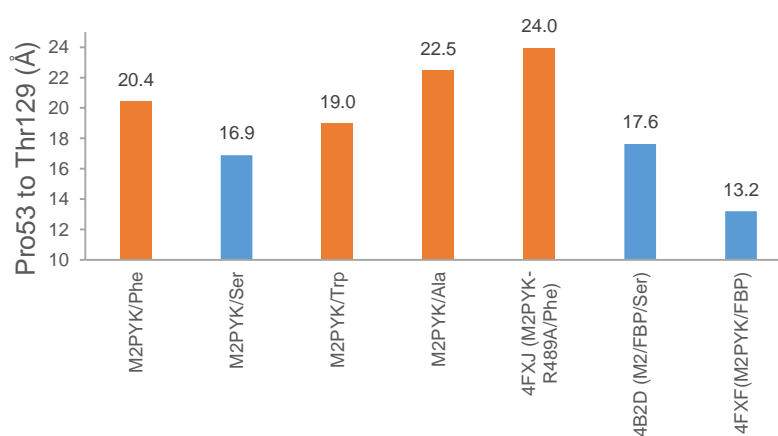


Figure 4.22 Level of the closure of B-domain.

The level of the closure of B-domain is represented by the distance between Pro53 (A-domain) and Thr129 (B-domain). Structures in T-state conformation are shown in orange, while the ones in R-state conformation are in blue.

4.7 Hydrogen/deuterium exchange mass spectrometry demonstrates the effects of amino acids on the dynamics of M2PYK

Crystal structures of M2PYK co-crystallised with inhibitory amino acids phenylalanine, alanine, and tryptophan display T-state conformations. By contrast, M2PYK co-crystallised with the activator serine shows an R-state conformation. The end-state structures provide useful information about the allosteric mechanism of M2PYK. Hydrogen/deuterium exchange mass spectrometry was carried out to complement these static models and to provide a dynamic picture of M2PYK, and insight into the inhibitory mechanism of these amino-acid modulators.

Amide hydrogen/deuterium exchange of proteins monitored by mass spectrometry is an established powerful method for probing protein conformational dynamics and protein interactions (Yan & Maier, 2009). The method uses isotope labelling to probe the rate at which protein backbone amide hydrogens undergo exchange. Exchange rates reflect the conformational mobility, hydrogen bonding strength, and solvent accessibility in the protein structure. Mass spectrometry is used to monitor the exchange level as mass changes through the incorporation of deuterium into the protein.

M2PYK was incubated with or without 50 mM amino acids (phenylalanine, alanine, tryptophan, and serine) in PBS. Afterwards, heavy water D₂O (or H₂O as control) was added to allow the hydrogen–deuterium exchange reaction. Samples were then flash-frozen with liquid nitrogen and subjected to further mass spectrometry analyses in the laboratory of Prof. Ing. Lenka Hernychová in Masaryk University.

The results are shown in Figure 4.23 and Figure 4.24. The percentage deuteration rates of M2PYK without ligand, and with alanine, phenylalanine, or serine, are displayed with solid lines in Figure 4.23, and mapped onto the M2PYK monomeric structures (Figure 4.24). The deuteration rate is shown with colour coding in Figure 4.24, where blue, white and red represent low, moderate and high deuteration rate, respectively. Effects of amino-acid modulators on the deuteration rate (i.e., percentage deuteration rate of M2PYK with amino acid subtracted by that of M2PYK without ligand) are also shown with dashed lines in Figure 4.23.

First, the N-terminal fragments of M2PYK, especially for the N-terminal loop involved in amino-acid ligand binding, display a high deuteration rate (labelled as ‘①’ in Figure 4.23 and Figure 4.24, same as below). It suggests that the N-terminal loop is highly flexible in all the proteins.

Second, the deuteration rate of α -helix H19 (labelled as ‘②’ in Figure 4.23 and Figure 4.24) which locates on the C-C interface of M2PYK is strongly suppressed by all amino-acid modulators. This correlates with the results that all amino-acid ligands prevent the dissociation of M2PYK (Section 4.5), and thereby prevent the amino acids on the C-C interface from being exposed and thus deuterium-exchanged.

It is also shown that the deuteration rate of the α -helices H2, H5 (coded according to Table 4.6, labelled as ‘③’ and ‘④’ in Figure 4.23 and Figure 4.24) are suppressed by the binding of the inhibitory amino acids phenylalanine and alanine, but not by the activator serine. The deuteration rate of the α -helix H17 (labelled as ‘⑤’ in Figure 4.23 and Figure 4.24) is suppressed by inhibitor phenylalanine, but increased by the activator serine. However, the other inhibitor, alanine, did not display significant change on the deuteration rate of H17.

It is also clear that amino-acid ligands have significant effects on the deuteration rate of α -helix H13 (labelled as ‘⑥’ in Figure 4.23 and Figure 4.24). H13 directly interacts with the H9 in the adjacent subunit. On the other side of the helix, H13 also interacts with the N-terminal loop. It is not clear why inhibitor alanine and activator serine can both suppress the deuteration rate of H13, but the other inhibitor phenylalanine did not show significant effects.

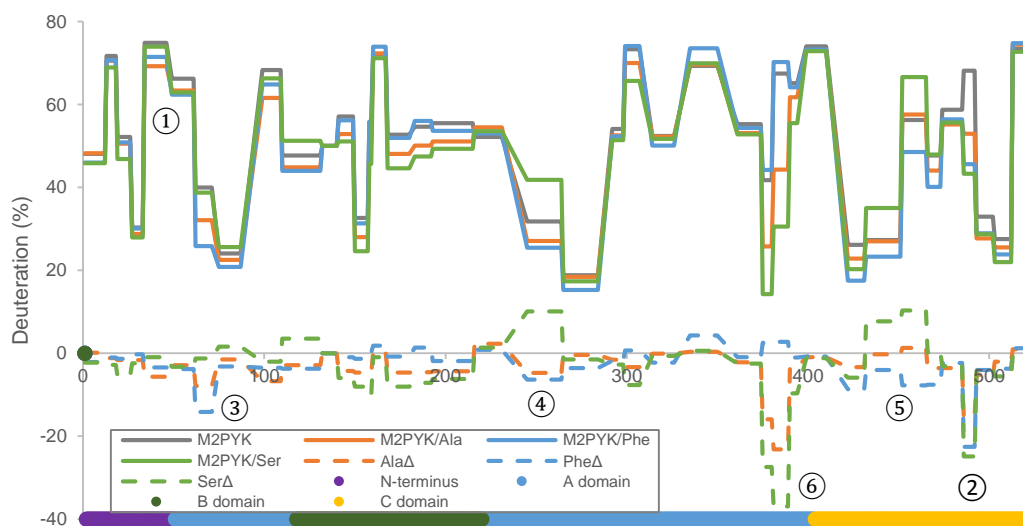


Figure 4.23 Deuteration rate of M2PYK in absence/presence of amino acids.

Percentage deuteration rates of M2PYK with and without ligand are displayed with solid lines. Effects of amino-acid modulators on the deuteration rate (i.e., deuteration rate of M2PYK with amino acid subtracted by that without ligand) are shown in dashed lines. Residue numbers are shown in the X-axis. Corresponding positions are shown with different colours at the bottom of the figure (N-terminus: purple; A-domain: blue; B-domain: green; C-domain: yellow). Particular positions described in the main text are labelled with numbers.

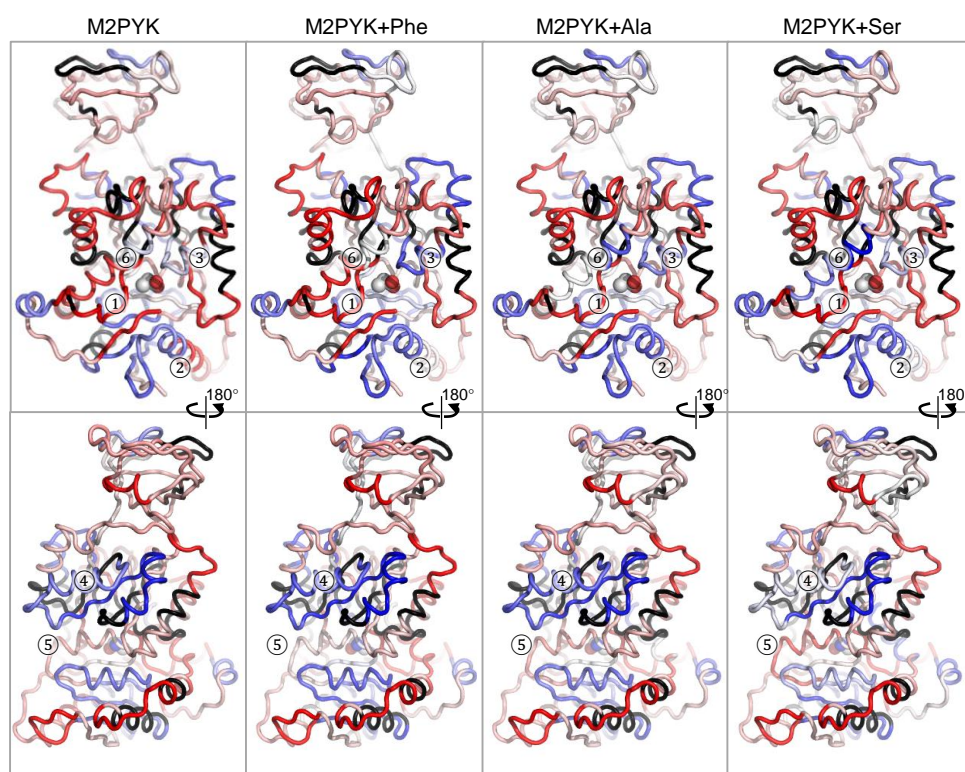


Figure 4.24 M2PYK monomeric structure mapped with H/D exchange rates.

Blue, white and red represent low, moderate and high deuteration rate, respectively. Particular positions described in the main text are labelled with numbers.

4.8 Biological significance of these studies

4.8.1 Nonessential amino acids are for cancer cell growth

Many natural products were found as direct M2PYK modulators. To target this promising cancer target, extensive *in silico* and experimental methods have been performed to discover other M2PYK activators. One hypothesis is suggested that M2PYK activators could reduce cancer cell proliferation by activating the glycolytic pathway thereby reducing metabolites required for cell growth. In line with the idea it was shown that M2PYK inhibitors could stimulate cancer cell proliferation as expected (e.g. T3, demonstrated as a M2PYK-dissociation promoter) (Morgan *et al.*, 2013). Intriguingly, investigations of the effects of M2PYK modulators on cancer cell proliferation provided controversial results. In experiments of cancer cell growth, not all M2PYK activators are able to reduce the cell proliferation. Similarly, not all M2PYK inhibitors stimulated the cell growth, either. A list of M2PYK activity modulators and their effects on cell proliferation is summarised in Table 4.8.

It was found that some M2PYK activators have limited effects on cell viability in cell culture using standard conditions (Kung *et al.*, 2012). However, these compounds have demonstrated profound activity in models where nonessential amino acids (NEAAs), such as serine, have been depleted. In this study, it is shown that free amino acid ligands are able to prevent M2PYK from dissociation. This phenomenon provides insights into the mechanism of the NEAA-depletion effect on cancer cell proliferation. In the normal cell medium (containing NEAAs), redundant serine would be able to tetramerise M2PYK regardless of the presence of M2PYK activators (which also promote tetramerisation). In this case, the effect of the activators is minimal. However, the effect of M2PYK activators on reducing cell proliferation can be much more significant because the M2PYK dissociation can take place due to the depletion of the NEAAs. This assumption requires further confirmation with cell proliferation assays in cell medium supplemented with different amino acids.

Table 4.8 M2PYK modulators and their effects on cell proliferation.

Compound	Effect on M2PYK activity	Effect on cell proliferation <i>in vitro</i>	Effect on tumour growth	Cell medium	Reference
pyridazinones	activation	ND ^a	ND	ND	(Jiang <i>et al.</i> , 2010)
hydroxybenzoic acid	inhibition	inhibition	ND	normal	(Vander Heiden <i>et al.</i> , 2010)
sulfonamides	activation	ND	ND	ND	(Walsh <i>et al.</i> , 2011)
Shikonin	inhibition	inhibition	ND	normal	(Chen <i>et al.</i> , 2011)
arylsulfonylindolines	activation	ND	ND	ND	(Yacovan <i>et al.</i> , 2012)
sulfonamides	activation	inhibition	inhibition	NEAA-depleted	(Kung <i>et al.</i> , 2012)
sulphonamides and pyridazinones	activation	inhibition	inhibition	unknown	(Anastasiou <i>et al.</i> , 2012)
Vitamin K3 and K5	inhibition	ND	ND	normal	(Chen <i>et al.</i> , 2012)
pyridazinones	activation	not significant	ND	unknown	(Guo <i>et al.</i> , 2013)
phenylalanine	inhibition	activation	ND	normal	(Morgan <i>et al.</i> , 2013)
T3	inhibition	activation	ND	normal	
F16BP	activation	inhibition	ND	normal	
pyrazole-carboxamide	activation	inhibition	inhibition	NEAA-depleted	(Parnell <i>et al.</i> , 2013)
tetrahydro-quinoline	activation	inhibition	inhibition	normal	(Chen <i>et al.</i> , 2014)
sulfonamides	activation	inhibition	ND	NEAA-depleted	(Kim <i>et al.</i> , 2015)
carbamodithioic esters	activation	inhibition	ND	normal	(Zhang <i>et al.</i> , 2015)

^a ND: not detected.

4.8.2 The feedback regulation cycle of M2PYK/alanine/ALT may be physiologically relevant and contribute to cell proliferation

Despite regulation by the dietary essential amino acids, e.g. phenylalanine and tryptophan, which may act as nutrient sensors to terminate the glycolytic pathway by inhibiting M2PYK activity, M2PYK has also been shown to play an important role in tuning the production of amino acids, which have feedback regulatory effects on M2PYK. For instance, serine was shown to act as a ‘rheostat’ between M2PYK activity and serine biosynthesis (Chaneton *et al.*, 2012). Here we propose that alanine may also have a feedback regulatory effect on M2PYK. In the physiological range, alanine is a strong specific inhibitor of M2PYK (Shingyoji *et al.*, 2013). In theory, the elevation of alanine can inhibit M2PYK activity thereby stimulating cancer cell proliferation. As evidence, alanine transaminase (ALT), a metabolic enzyme that catalyses pyruvate to alanine in the presence of L-glutamate (and reverse), was found to be elevated in patients with malignant tumours (Chougule *et al.*, 2008). As a result, the inhibition of ALT activity is expected to reduce the production of alanine, which would lead to an elevated activity of M2PYK. And this expectation was demonstrated

in fish, by stimulating the PYK activity by dietary ALT inhibitors (Gonzalez *et al.*, 2012). The feedback regulation cycle of M2PYK/alanine/ALT seems physiologically realistic and contributive to cell proliferation. Further cellular studies may reveal its therapeutic importance.

4.9 Conclusions and forward look

M2PYK catalyses the conversion of PEP to pyruvate as the final step of glycolysis. It plays an important role in cancer metabolism. Here we show that certain amino acids stabilise the M2PYK tetramer over monomer. Additionally, certain amino acids regulate the activity of M2PYK allosterically, but in opposite ways, with some being inhibitors and others activators. In particular, the amino-acid modulators phenylalanine, alanine, and serine function at physiological concentrations.

X-ray structures and biophysical binding data of M2PYK complexes with alanine, phenylalanine, serine or tryptophan reveal an R- to T-state oscillating model of M2PYK modulated by amino acids. Hydrophobic amino acids such as alanine, phenylalanine and tryptophan, inhibit the enzymic activity by stabilising M2PYK in an inactive T-state. By contrast, other amino acids such as serine binding to the same site activate by rotating each subunit by 11° thereby stabilising the active R-state tetramer. A systematic comparison of the crystal structures of M2PYK in complex with different amino-acid modulators revealed its allosteric mechanism. Inhibitory and activating amino acids bind to the same allosteric pocket, but shift the N-terminal loop in opposite ways, and thereby re-organise the interface bonds and induce the rigid-body rotation of each subunit. In particular, the amino-acid triggered rigid-body rotation from R-state conformation to T-state conformation disrupts the inter-subunit stabilisation of the B-domains, which are responsible for the formation of complete active sites. The amino acids therefore modulate the enzymic activity of M2PYK. Metabolites as M2PYK regulatory factors are summarised in Figure 4.25.

These observations highlight the important effects of amino acids on M2PYK regulation. It also provides insights to the M2PYK activator design. However, current evidence regarding the effects M2PYK activity modulators on cell proliferation are

controversial—some M2PYK activators show limited inhibition on cell growth rate. Some literature suggest that the effect is dependent on amino acids provided in cell medium.

Moreover, a potential feedback regulation cycle of M2PYK/alanine/ALT is proposed herein: ALT converts the PYK product pyruvate to alanine, which is a strong inhibitor against M2PYK. This feedback regulation cycle could be physiologically relevant and may contribute to cell proliferation.

Work described in this chapter provides insight into two biological phenomenon: effect of M2PYK activator on cell growth depends on amino acids in cell medium; and the feedback regulation cycle of M2PYK/alanine/ALT. Further cellular experiments are required for confirmation. For instance, a ALT-null cell may reduce its alanine-production ability, thereby up-regulating the activity of M2PYK, which in turn could reduce cancer cell proliferation.

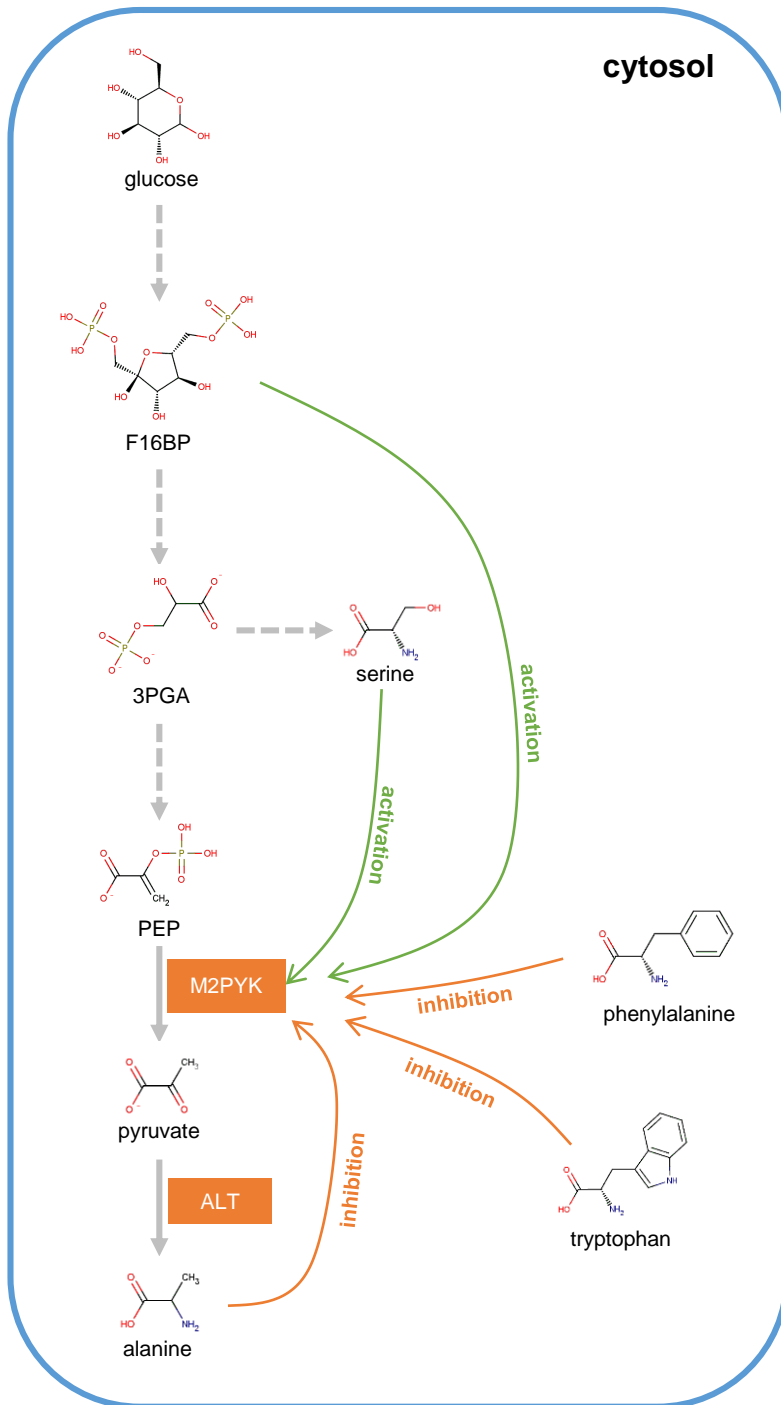


Figure 4.25 The regulation of M2PYK by metabolites in cytosol.

CHAPTER 5

Redox regulation of pyruvate kinase M2

CHAPTER 5. Redox regulation of pyruvate kinase M2

5.1 Background

In CHAPTER 3, it is demonstrated that M2PYK equilibrates between tetramer and monomer, which has little pyruvate kinase activity. In 2011, Anastasiou *et al.* discovered that the enzymic activity and oligomerisation state of M2PYK depends on its redox state (Anastasiou *et al.*, 2011). Here the effects of redox on the enzymic activity and structural properties are systematically investigated. Moreover, key residues involved in the redox-regulation are identified.

5.2 Methods

5.2.1 Enzymic activity assay

Briefly, an LDH-coupled enzyme assay was carried out for the investigation of the effects of redox on PYK activity. Fifty microlitres of 0.002 mg/ml of PYK in PBS-CM was incubated with or without 1 mM DTT and/or 0.5 mM F16BP in PBS-CM in each well of a 96-well microtitre plate at 37 °C at pH 7.4 for 5 min. Then the same volume of assay buffer [PBS-CM supplemented with 10 mM MgCl₂, 100 mM KCl, 1 mM NADH, 40 U/ml LDH, as well as saturating PEP (10 mM) and ADP (4 mM)] was added to each well to start the reaction. The decrease in absorbance at 340 nm (the absorbance of NADH) was measured for 5 min at 37 °C using a plate reader. More detailed description of the methods for the enzymic activity assay is shown in Section 2.5.1.

5.2.2 Analytical gel-filtration

Analytical gel-filtration assays were carried out to study the effects of redox on the oligomerisation state of M2PYK. Briefly, 0.1 mg/ml purified PYK was incubated with or without 1 mM DTT, 20 µM H₂O₂, or 1 mM CysNO in PBS-CM at room temperature

at pH 7.4 for 1 h or 12 h. After the incubation, samples were loaded independently onto the analytical gel-filtration column (Superdex[®] 200 PC 3.2/30). Twenty-five microlitres of samples were injected, and the column flow rate was maintained at 1 μ l/min. Protein peaks were monitored using absorbance at both 280 nm and 214 nm.). More detailed description of the methods for the analytical gel-filtration is shown in Section 2.4

5.2.3 Thermal shift assay

Thermal shift assay was carried out to show the effects of redox on the thermostability of pyruvate kinases. Briefly, 0.5 mg/ml PYK was incubated with or without 1 mM DTT or H₂O₂ in PBS-CM at room temperature at pH 7.4 for 1 h. Description of the methods for the thermal shift assay is given in Section 2.6.

5.2.4 Biotin-switch assay

The *in vitro* biotin-switch assay was carried out for the identification of *S*-nitrosylated proteins (Jaffrey & Snyder, 2001) (Figure 5.1). Protein samples (pre-incubated with or without 1 mM F16BP or 4 mM phenylalanine) were prepared by diluting to a concentration of 0.17 mg/ml in HEN buffer (250 mM HEPES, 1 mM EDTA, 0.1 mM neocuproine, pH 7.7). CysNO was used as the NO donor and was prepared by mixing 20 μ l 100 mM L-cysteine (dissolved in 200 mM HCl) with 20 μ l 100mM NaNO₂ (dissolved in H₂O) resulting in 50 mM solution of CysNO which was then added to protein samples to a final concentration of 1 mM for protein *S*-nitrosylation. The reaction incubated in the dark for 20 min at room temperature. The sample with an addition of 0.1% SDS for exposing all cysteine residues was used as a positive control. The sample without CysNO was used as a negative control.

After incubation, CysNO donor was removed by passing the samples through pre-equilibrated Zeba-spin columns and centrifuging at 1500 \times *g* for 2 min. N-Ethylmaleimide (NEM) blocking buffer (HEN buffer, 5% SDS, 50 mM NEM) was added to unfold the protein and block all unmodified cysteines and the reaction incubated at 50 $^{\circ}$ C for 30 min. Two volumes of -20 $^{\circ}$ C 100% acetone were then added

and the samples incubated at -20°C for 20 min. Precipitated protein was pelleted by centrifuging at 14,000× *g* for 5 min at 4 °C. Supernatant was removed. The protein pellet was washed for three times with -20 °C 70% acetone. Residual acetone allowed to evaporate by placing tubes uncapped in dark at room temperature.

Protein pellets were re-suspended in 85 µl HENS buffer (HEN buffer with 1% SDS). Biotin-labelling solution (final concentration: 25 mM ascorbate, 0.4 mM biotin-HPDP) was added and the samples were incubated for 1 h at room temperature. In this step, any nitrosylated cysteine can be reduced by ascorbate and thus biotinylated by biotin-HPDP. Non-nitrosylatable cysteines were blocked by NEM, and thus not biotinylated. After biotinylation, proteins were collected by acetone precipitation again: two volumes of -20 °C 100% acetone were then added and the samples incubated at -20°C for 20 min. Precipitated protein was pelleted by centrifuging at 14,000× *g* for 5 min at 4 °C. Supernatant was removed. The protein pellet was washed for three times with -20 °C 70% acetone. Residual acetone allowed to evaporate by placing tubes uncapped in dark at room temperature.

Each protein pellet sample was re-suspended with 300 µl H₂₅ENS buffer (with higher concentration of HEPES than HENS buffer, i.e. 25 mM HEPES, 1 mM EDTA, 1 mM neocuproine, and 1% SDS). Twenty microlitre per each sample was taken out as an 'input' control. For each of the rest of the 280 µl sample, 1.5 ml of neutralisation buffer (25 mM HEPES, 100 mM NaCl, 1 mM EDTA, 0.5% TritonX-100, pH 7.5) and 20 µl of streptavidin beads was added to pull-down the biotinylated (i.e., *S*-nitrosylated) proteins.

After an overnight-incubation at 4 °C, streptavidin beads conjugated with biotinylated proteins were centrifuged down 30 s at 5,000 rpm. Unbound proteins were washed out for five times with neutralisation buffer. Biotin-HPDP contains a disulfide bond. As a result, any biotinylated samples were eluted by elution buffer containing 1% β-mercaptoethanol (each sample was incubated with 20µL elution buffer for 30 min at room temperature). Eluted proteins were collected in the supernatant of each sample.

After SDS-PAGE was run for each eluted sample, the protein bands were transferred onto a nitrocellulose membrane at 80 V at 4 °C for 90 min for western-blot. The

membrane was blocked with PBST (PBS with 0.05% Tween 20) supplemented with 5% skimmed milk powder at room temperature for 1 h. The blocked membrane was then incubated with 1:2000 diluted HRP-linked anti-His-tag antibody overnight at 4 °C. After the membrane was washed three times with PBST with 5% skimmed milk powder followed by twice with PBS, ECL solutions were applied for luminescence exposure.

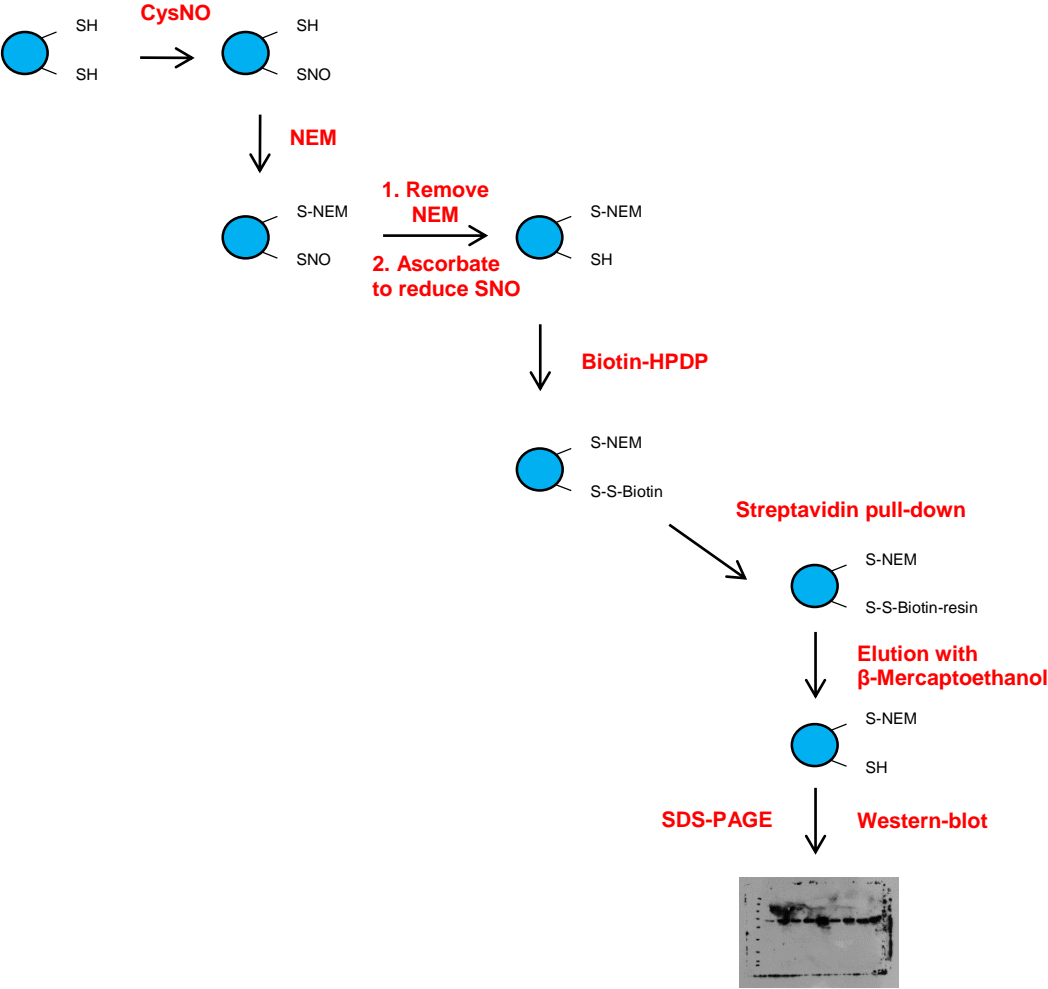


Figure 5.1 Biotin-switch assay workflow.

5.3 Results and discussion

5.3.1 Redox regulates the enzymic activity of M2PYK

It was reported that the enzymic activity of M2PYK is elevated in a reducing environment and that Cys358 is responsible for sensing the redox regulation (Anastasiou *et al.*, 2011, Mitchell, 2014). The enzyme assay carried out in this study showed that the enzymic activity of wild-type M2PYK was increased by approximately 30% in the presence of 1 mM DTT (Figure 5.2). An M2PYK mutant C358S, for the protection of Cys358 from oxidation, indeed reduced the effect of DTT. However, the reducing environment still retained some activation effect on the activity of M2PYK-C358S. This result suggests that Cys358 may not be the sole oxidisable residue on M2PYK. Mitchell *et al.* identified another residue, Cys326, that senses the redox-caused M2PYK activity regulation (Figure 5.3) (Mitchell, 2014). M2PYK-C326S adopts a monomeric conformation (Section 3.6). As expected, this monomeric M2PYK displayed low activity, but is able to be activated by the addition of DTT. This result implies that Cys326 is not the sole oxidisable cysteine, either. A systematic study of the effects of redox on M2PYK is shown in this chapter.

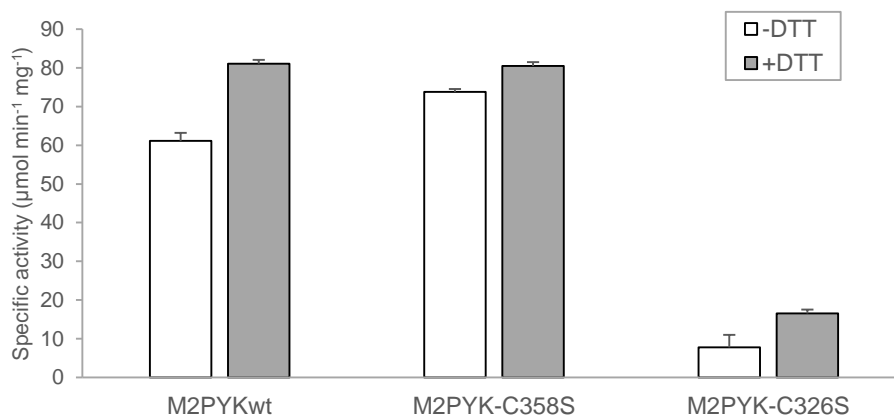


Figure 5.2 Effects of DTT on enzymic activity of M2PYK wild type and mutants.

Data represent the mean \pm SD of three experiments.

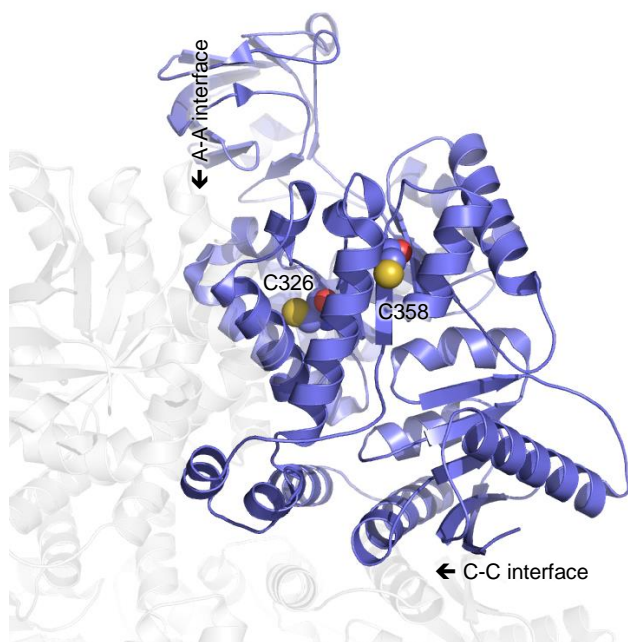


Figure 5.3 Positions of Cys326 and Cys358 of M2PYK.

5.3.2 Redox regulates the oligomerisation of M2PYK

Using analytical gel-filtration, it is shown that M2PYK can gradually dissociate from tetramer into monomers at 0.1 mg/ml (Figure 5.4). The tetramer:monomer ratio reached an equilibrium of about 1:4 (1:1 if consider a tetramer as one) at 12 h.

By comparison, M2PYK was also incubated in the presence of 1 mM DTT or 20 μ M H_2O_2 . Analytical gel-filtration showed a clear trend at 1 h (Figure 5.4A), that the proportion of monomeric M2PYK is higher when incubated with H_2O_2 , and is lower when incubated with DTT. After 12-h incubation when the dissociation of M2PYK reached the equilibrium, M2PYK incubated with H_2O_2 displayed more monomers in comparison with that without H_2O_2 (Figure 5.4B). By contrast, DTT maintained the majority of M2PYK as tetramers. This indicates that the oligomerisation/dissociation of M2PYK is redox-dependent. A reducing environment holds M2PYK as a tetramer, while oxidation can promote the dissociation of M2PYK. This result correlates with and helps explain previous observation, which demonstrated the enzymic activation effect of DTT (Figure 5.2).

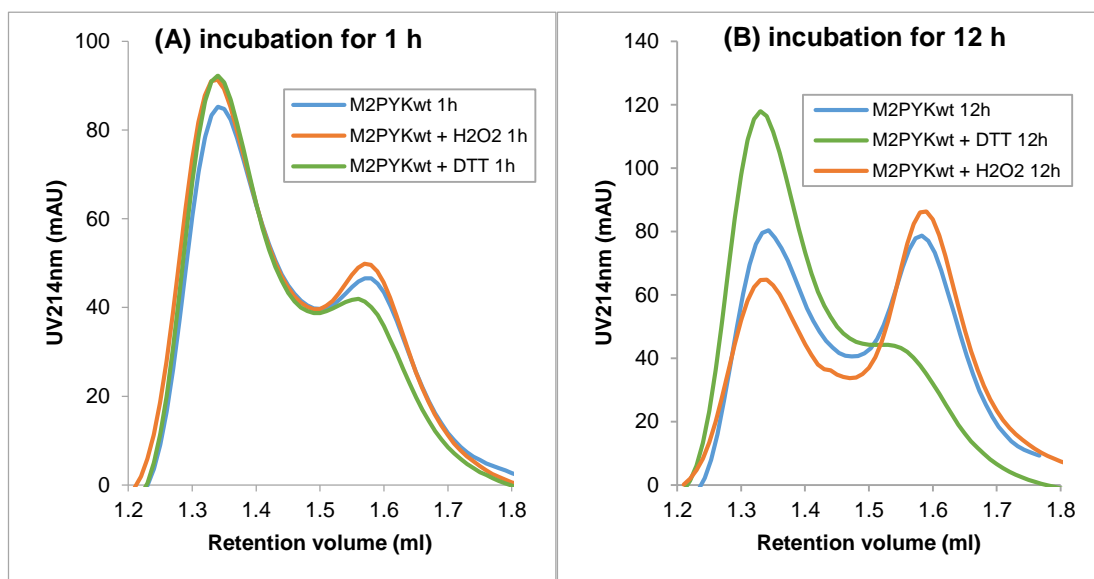


Figure 5.4 Effects of redox environments on the oligomerisation of M2PYK.

M2PYK was incubated at 0.1 mg/ml in PBS-CM in the absence and presence of 1 mM DTT or 20 μ M of H₂O₂ at room temperature for (A) 1 h and (B) 12 h. Analytical gel-filtration for M2PYK was carried out to determine the tetramer (left peaks) : monomer (right peaks) ratio with a Superdex[®] 200 PC 3.2/30 gel-filtration column. Twenty-five microlitres of sample was subjected to the assay each time.

5.3.3 Redox regulates the thermostability of M2PYK

It was shown that the thermal stability of M2PYK is affected by the binding of F16BP and amino-acid ligands (Section 3.7 and Section 4.4). Using a thermal shift assay for the determination of protein unfolding temperature and velocity, where the melting process of M2PYK in the absence and presence of 1 mM DTT or H₂O₂, it is shown that M2PYK is stabilised the addition of DTT by a 1-°C T_m increase (Figure 5.5). In contrast, the thermostability of M2PYK was significantly reduced in an oxidative environment. The melting temperature decreased by 3.5 °C.

These results suggest stabilisation and destabilisation effects of the reducing and oxidative environments on M2PYK, respectively. It correlates well with previous observations, that the reducing environment prevents M2PYK from dissociation, and thereby activates the enzymic activity of M2PYK. By contrast, the oxidative environment plays opposite roles. The results also indicate that tetrameric conformation of M2PYK is more stable (higher T_m) than the monomeric forms.

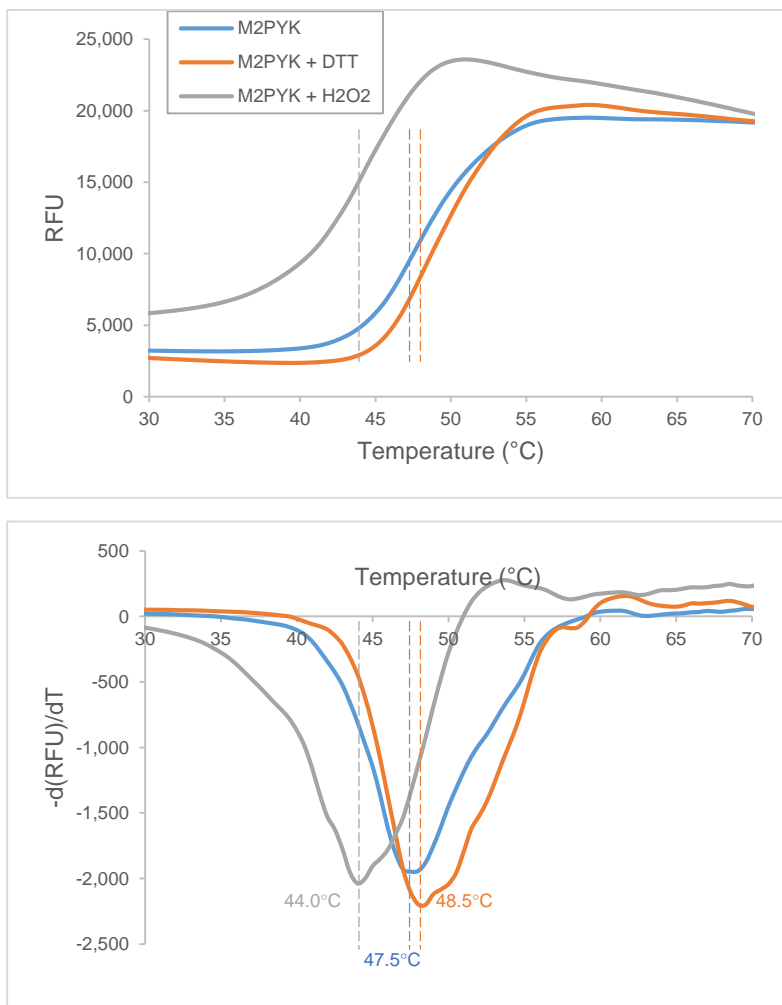


Figure 5.5 Thermal stability of M2PYK and the effects of redox environments.

Thermal shift assay results for 0.5 mg/ml M2PYK in the absence or presence of 1 mM DTT or H₂O₂. The bottom panel shows derivative calculations of the fluorescence readings.

5.3.4 Redox takes place on C326 on a tetramer interface of M2PYK

In this study, it is shown that oxidative environment promotes the dissociation of M2PYK, and thereby inhibits its enzymic activity. However, the reducing environment plays an opposite role.

In 2011, Anastasiou *et al.* reported that Cys358 was the main residue that can be oxidised by showing that the mutant M2PYK-C358S is free from effects of reducing agents or oxidants (Anastasiou *et al.*, 2011). In this study, it was shown that the C358S mutation indeed reduced the effect of DTT (Figure 5.2). However, the reducing environment still retained some activation effect on the activity of M2PYK-C358S. This result suggests that Cys358 may not be the sole oxidisable residue on M2PYK.

Moreover, the oxidation-preventing feature of M2PYK-C358S might be indirect. In Section 3.6, it was shown that the M2PYK-C358S is more tetrameric than the wild type (Figure 3.11). In this case, the way that M2PYK-C358S resists oxidation, might not be a direct effect of the mutation, but an indirect consequence of protecting some cysteines located on subunit interfaces (e.g. Cys326, etc.) from exposure to environmental oxidative factors and thus being oxidised and/or nitrosylated.

In 2014, Mitchell reported that Cys326 might be another main redox-sensitive residue in M2PYK (Mitchell, 2014). For confirmation, a mutant M2PYK-C326S is produced and characterised in this study. A further biotin-switch assay was carried out for the comparison of the cysteine *S*-nitrosylation effects on M2PYK, M2PYK-C326S, and M2PYK-C358S (Figure 5.6). Intensity of western-blot bands reflects the degree of *S*-nitrosylation.

In brief, M2PYK proteins were *S*-nitrosylated with an NO donor, followed by a step blocking un-nitrosylated cysteines (Figure 5.1). Afterwards, all nitrosylated residues were reduced by ascorbate, and then biotinylated by biotin-HPDP. Streptavidin-conjugated beads were adopted to pull-down all biotinylated proteins. SDS-PAGE and western-blot were used to characterise the degree of *S*-nitrosylation. In summary, all *S*-nitrosylated proteins were pulled-down and shown on the gel. By contrast, a less *S*-nitrosylated protein shows a lighter band. A sample without nitrosylation-treatment in

the first step was used as a negative control. An unfolded sample (and thus expose all cysteines to *S*-nitrosylation) was used as a positive control.

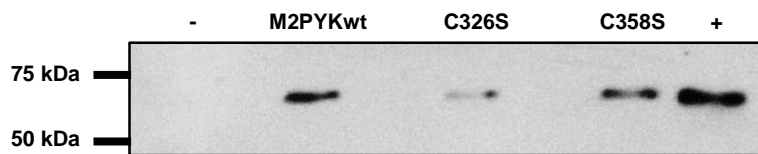


Figure 5.6 *S*-nitrosylation degree of M2PYK wild-type and mutants.

Intensity of western-blot bands reflects the degree of *S*-nitrosylation. The negative control (-) is a protein that was not *S*-nitrosylated. The positive control (+) is done with an unfolded protein (and thus expose all cysteines to *S*-nitrosylation).

The result shows no band and an intense band in the negative control and positive control lane, respectively, indicating the effectiveness of this experiment. Both M2PYK-C326S and M2PYK-C358S show lighter bands in comparison with that of the wild-type M2PYK. It suggests that both Cys326 and Cys358 were *S*-nitrosylated. However, neither of them was a sole nitrosylatable cysteine in M2PYK. M2PYK-C326S displays a lighter band than that of M2PYK-C358S, indicating that the degree of *S*-nitrosylation of Cys326 is higher.

5.3.5 M2PYK tetramerising agents prevent *S*-nitrosylation

Cys326 locates on the A-A interface of M2PYK (Figure 5.3). It is buried and is probably prevented from *S*-nitrosylation in a tetrameric M2PYK form. A dissociated M2PYK exposes Cys326 to the *S*-nitrosylating environment. Hence, the *S*-nitrosylation of Cys326 may be reduced in the presence of M2PYK tetramerising agents (e.g. F16BP, amino-acid modulators, etc.).

In this study, a biotin-switch assay was carried out for M2PYK in the absence or presence of F16BP and phenylalanine. The result showed that the degree of *S*-nitrosylation of M2PYK is significantly reduced by the addition of F16BP and phenylalanine (Figure 5.7). It suggests that by burying Cys326, a tetrameric conformation of M2PYK, regardless an R-state (stabilised by F16BP) or a T-state (stabilised by phenylalanine), is less sensitive to *S*-nitrosylation in comparison with a monomer. In other words, the dissociation of M2PYK promotes its degree of *S*-

nitrosylation (and presumably oxidation too). However, even in the presence of F16BP or phenylalanine there are bands that show nitrosylation/biotinylation of cysteine residues, which are approximately 70% weaker than the band of M2PYK without ligands (quantified with a software ImageJ). We suggest that the weaker bands are proportional to the monomer:tetramer equilibrium.

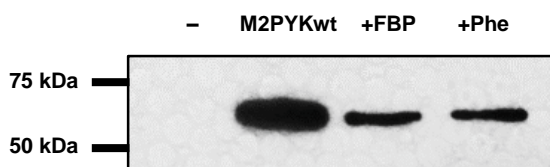


Figure 5.7 *S*-nitrosylation M2PYK is affected by modulators.

Intensity of western-blot bands reflects the degree of *S*-nitrosylation. The negative control (-) is a protein that was not *S*-nitrosylated.

5.4 Conclusion

It was demonstrated that a reducing environment holds M2PYK as a tetramer, increases its melting temperature, and thereby activates its enzymic activity. In contrast, an oxidising environment can promote the dissociation of M2PYK, and thus reduce its thermostability and enzymic activity. These effects are also shown by nitrosylation of cysteine. The question now remains to be whether oxidation or nitrosylation (or both) are of biological relevance in M2PYK regulation.

CHAPTER 6

Protein production and characterisation of *Leishmania* fructose-1,6-bisphosphatase

CHAPTER 6. Protein production and characterisation of *Leishmania* fructose-1,6-bisphosphatase

6.1 Background

The plasmid pET24a encoding C-terminal His₆-tagged *Lm*FBPase that was amplified by PCR using *L. major* (MHOM/SU/73/5-ASKH) genomic DNA was a gift from Professor Paul A. M. Michels. The amino acid sequence as well as the theoretical parameters of the bacterially expressed FBPase are shown in Table 6.1.

Table 6.1 Amino acid sequence and chemical parameters of expressed *Lm*FBPase.

Sequence of His ₆ - <i>Lm</i> FBPase						
1	MDVRRTPPT	TLTQYIIKSQ	PPHSRGDFTL	LMMAIQTSVK	VIEKNIRRAG	MKGMLGYIAG
61	QSANATGDHQ	AKLDVISNIA	FKAYLLSSTS	VCVLGSEEEE	QMIIAESGRR	GDYLIFFDPL
121	DGSSNIDANV	SVGSIWGVWR	LPKDTTINSV	EDANAVIRML	KGTMVSAGY	AVYGSATNLV
181	LTSGHGVDGF	TLDPNIGEFI	LTHPHISIPK	KRSIYSVNEG	NYGKWEPPFK	EYIDYLMNK
241	TTRYSAARYIG	SMVGDHRTL	LYGGIFCYPK	DANQVEGKLR	LLYEAAPMAM	IVEQAGGKAV
301	GNSGRILEQS	ITRLHQ RTPV	YFGSRQEVDL	CMAFRDRNVK	TEALAPTSSK	LRDPNSSSVD
361	<u>KLAAALEHHH</u>	<u>HHH</u>				
Number of residues	Theoretical molecular mass		Theoretical pI ^a		Theoretical extinction coefficient	
373	41,304 Dalton		8.56		45,840 M ⁻¹ cm ⁻¹	

^a The theoretical isoelectric point (pI), molecular mass and extinction coefficient were obtained from the ExPASy Server (Gasteiger *et al.*, 2005). The sequence corresponding to the C-terminal His tag is underlined. The mass of the Met corresponding to the start codon is included and is assumed to be translated as Met in the mature protein, but there is no experimental evidence that it is present in the mature enzyme.

Bacterial expression and purification, as well as thermal denaturation assays of *Lm*FBPase were first achieved in our laboratory by Dr Montserrat Vasquez-Valdivieso (Vasquez-Valdivieso, 2013). Further investigations on the study of *Lm*FBPase are carried out in this thesis. Results of protein production, preliminary biophysical characterisation and kinetic assays are shown in this chapter.

The methods of protein production and characterisation of *Lm*FBPase are briefly shown in CHAPTER 2.

6.2 Bioinformatic study suggests distinctive features of *Lm*FBPase

For the bioinformatic study of FBPases, amino acid sequences of 171 FBPases from different species [including eukaryotic (e.g. *Trypanosomatidae*, mammalian, plant, etc.), bacterial and archaea FBPases] were downloaded from the Uniprot database and aligned with ClustalW2 (Larkin *et al.*, 2007). Different colours show the level of conservation, where blue represents high conservation, green represents modest and red represents poor conservation (Figure 6.1). Big blue blocks indicate high ‘in-kingdom’ conservation. Some organisms have conserved isoenzymes of FBPases (e.g. human liver FBPase and muscle FBPase share 76% identical amino acids). In contrast, distant positions of plant cytosolic and chloroplast FBPases (highlighted in grey frames) suggest the sequence difference between isoforms is even larger than trans-kingdom differences, corresponding to their large structural and functional variation (discussed in detail in Section 1.3.5). The green colour in the small block of FBPases from three trypanosomatids (*T. brucei*, *T. cruzi*, and *L. major*, highlighted in a box with orange frames) indicates modest conservation (sequence identities approximately 60%) of these trypanosomatid gluconeogenic enzymes.

In 2014, Gao *et al.* made a series of sequence alignments, predicting the sequence-function relationship of Type-I FBPases (Gao *et al.*, 2014). The prediction results are shown in grey bars in Figure 6.1, which indicate the set of mandatory residues for the corresponding function is available in the FBPase sequence of that species. According to the prediction, AMP inhibition requires serine or threonine for residue 32, lysine or arginine for residue 113, and tyrosine for residue 114. Tetramer stability requires lysine or arginine for residue 43, and glutamate for residue 205. Anion activation requires glycine for residue 14, lysine or arginine for residue 38, and lysine or arginine for residue 88. The presence of a central cavity (that was predicted to be mandatory for the AMP/F26BP synergism) requires small side chains (glycine, alanine, cysteine, serine, or gap) for residue 45. The model proposed by Gao *et al.* predicts that trypanosomatid FBPases have stable tetramers, but that the anion activation and AMP/F26BP synergism are absent. Trypanosomatid FBPases lack Lys/Arg113 which was predicted to be essential for AMP inhibition. Actually, this alkaline residue that was shown to bind directly to the phospho group of AMP (Zarzycki *et al.*, 2011) is

replaced by an aspartic acid in *T. brucei* and *L. major* FBPases, and by histidine in *T. cruzi* FBPase. As a result, it was uncertain whether the inhibitory effect of AMP would also be observed in trypanosomatid FBPases.

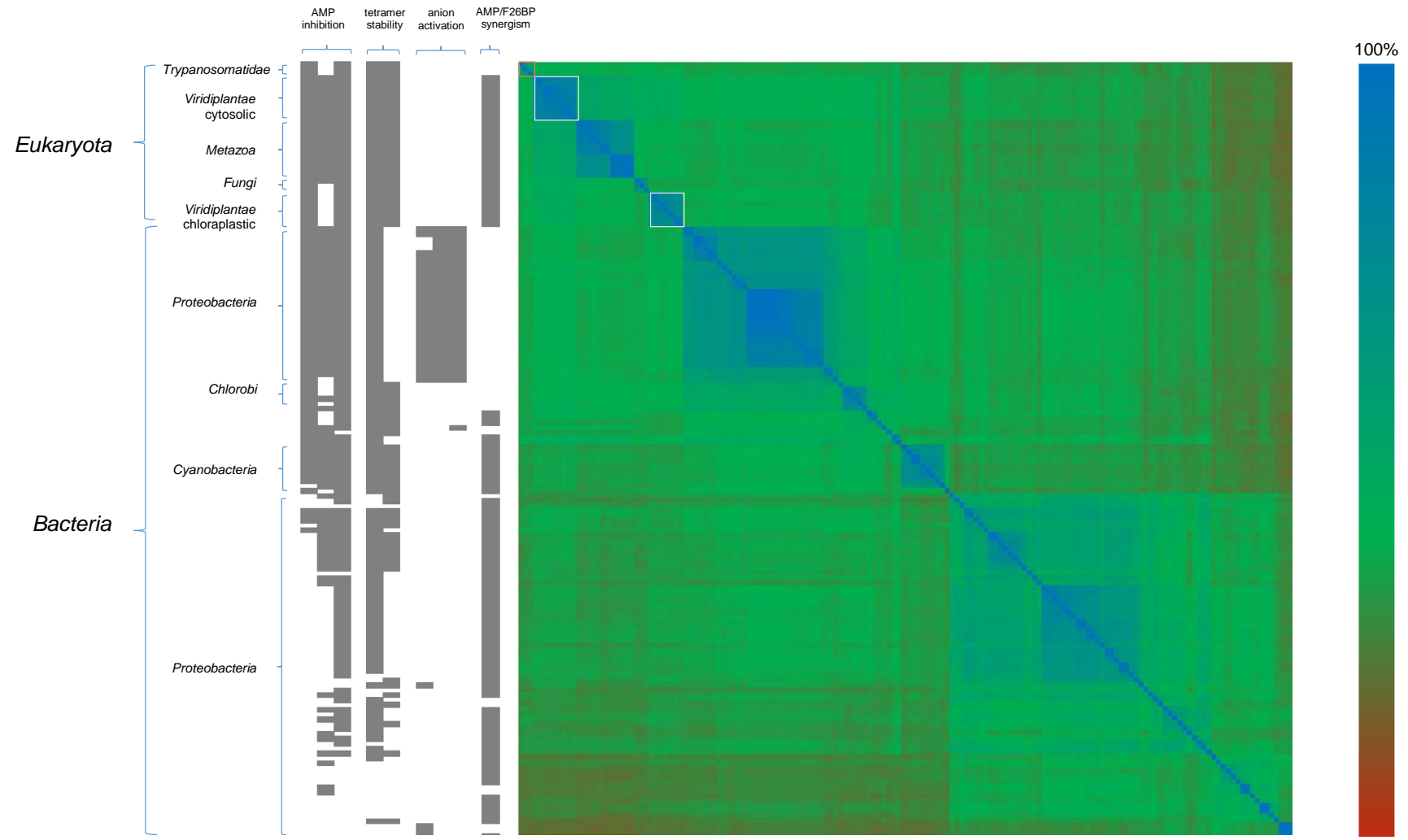


Figure 6.1 Similarity matrix of Type-I FBPase sequences among different species.

The level of conservation is represented by different colours, where blue represents high conservation, green represents modest and red represents poor conservation. All identity values are higher than a random sequence identity value of 6% (Chung & Subbiah, 1996). The colours are plotted with Microsoft Excel. The boxes with grey frames correlate to two isoforms of plant FBPases. The three trypanosomatid FBPases are in an orange box. Grey bars on the left of the figure indicate sequence-function relationship according to the prediction made by (Gao *et al.*, 2014). The prediction suggested that the AMP inhibition requires serine or threonine for residue 32, lysine or arginine for residue 113, and tyrosine for residue 114 (the availability of corresponding residues are shown in grey bars, same as below). Tetramer stability requires lysine or arginine for residue 43, and glutamate for residue 205. Anion activation requires glycine for residue 14, lysine or arginine for residue 38, and lysine or arginine for residue 88. The presence of a central cavity (that was predicted to be mandatory for the AMP/F26BP synergism) requires small side chains (glycine, alanine, cysteine, serine, or gap) for residue 45. Raw data of the matrix with sequence-identity values can be found in https://1drv.ms/x/s!An9gBV9AQR6hgY809t8N90_AWEIz-g.

6.3 Protein production of *L. major* FBPase

6.3.1 Overexpression and cell lysis of *Lm*FBPase

*Lm*FBPase was overexpressed in *E. coli* BL21(DE3) with a 24-h IPTG-induction at 30 °C. The harvested cells were lysed at 4 °C at 25 KPSI (equivalent to 1.72×10^5 KPa) with a constant cell disruptor. The lysate was centrifuged to remove the insoluble portion. The expression of *Lm*FBPase was characterised by SDS-PAGE (Figure 6.2). The presence of the band corresponding to *Lm*FBPase (expected molecular mass 41 KDa) in induced cells (Lanes 2 and 3) but its apparent absence in the pre-induction cells (Lane 1) indicates the successful expression of *Lm*FBPase. The band corresponding to *Lm*FBPase in the supernatant of the centrifuged cell lysate (Lane 4) indicates that soluble *Lm*FBPase was successfully obtained from the *E. coli* overexpression.

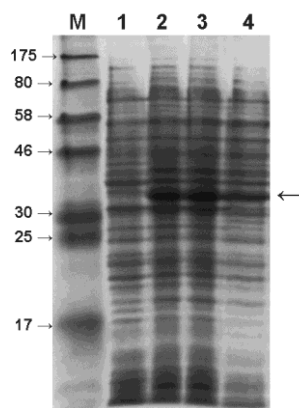


Figure 6.2 SDS-PAGE characterisation for the expression of *Lm*FBPase.

M: SDS-PAGE marker; 1: pre-induction; 2, 3: cell lysate; 4: supernatant of the centrifuged cell lysate. The arrow shows the band of *Lm*FBPase at the expected position.

6.3.2 The first purification step for *Lm*FBPase: IMAC

The cell lysate was then loaded onto a 5-ml cobalt-based IMAC column for metal-affinity purification. Unbound proteins were washed away in the flow-through fractions (Figure 6.3). Twenty millimolar imidazole was maintained in the initial loading buffer to remove weakly-bound proteins. His₆-*Lm*FBPase was eluted

gradually from the column by increasing the imidazole concentration using a linear gradient at a constant pH, where imidazole competed with the chelation of the His₆-tag on the cobalt column, and thereby eluted the target protein.

Two peaks were eluted from the IMAC column at different concentrations of Buffer B. The first peak came off at approximately 5% Buffer B (corresponding to about 45 mM imidazole), and showed mostly contaminations with only a tiny amount of *LmFBPase* according to the SDS-PAGE result (corresponding with the peak and SDS-PAGE lanes highlighted in cyan in Figure 6.3). A larger, second peak was eluted at about 50% Buffer B (corresponding to approximately 270 mM imidazole). These proteins analysed by SDS-PAGE showed that *LmFBPase* migrated as a single protein band (~37 kDa) with a few other protein bands indicating the presence of small amounts of contaminants. A second gel-filtration polishing step was required for the improvement of the protein purity.

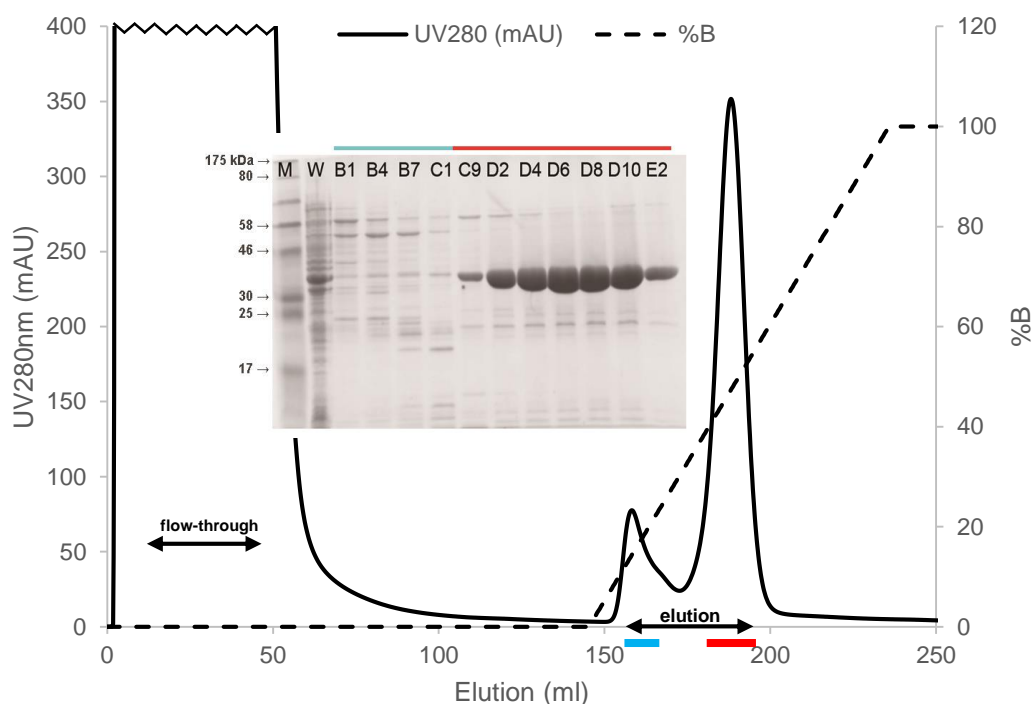


Figure 6.3 IMAC purification of His₆-*LmFBPase*.

The dashed line shows the percentage of Buffer B used for the purification. The elution of proteins from the IMAC column was monitored by a UV spectrometer at 280 nm (represented by the solid line), where two important fractions ‘flow-through’ and ‘elution’ are indicated with black arrows. Proteins from the two peaks of the elution were characterised by SDS-PAGE, where the lanes corresponding to each peak are highlighted in cyan and red lines, respectively.

For the labels of each lane, 'M' represents marker, 'W' represents whole cell, and other labels represent the fraction numbers.

6.3.3 The second purification step for *Lm*FBPase: gel filtration

The purified sample of *Lm*FBPase from the IMAC step of purification was concentrated to 2.5 ml with a Vivaspin[®] column. The concentrated sample was then loaded onto a size-exclusion column HiPrep 16/60 Sephacryl[®] S-200 HR (120 ml, separation range for globular proteins 5–250 kDa) that was pre-equilibrated with the size-exclusion buffer (20 mM TEA, 5 mM MgCl₂, 50 mM KCl, and 10% glycerol, pH 7.2) for a second-step polishing purification. The sample was purified at a constant flow rate of 0.5 ml/min, where *Lm*FBPase eluted predominantly as an asymmetric single peak at the retention volume of about 45 ml (Figure 6.4). It indicates that the *Lm*FBPase was most likely in a tetrameric form (~160 kDa). The prediction based on the calibration of this size-exclusion column with proteins at different sizes by GE Healthcare Ltd.¹ The trailing edge suggests a mixed conformation of the protein (e.g. mixed with R/T-state tetramers or dissociated *Lm*FBPase). Protein from each fraction of the peak was characterised by SDS-PAGE (highlighted with red lines), which shows a purity higher than 95%. Protein corresponding to the fractions labelled in green was pooled together and concentrated to 4.6 mg/ml with a Vivaspin[®] tube. The final yield was about 7.4 mg from 1 L of cell culture. The product in the size-exclusion buffer was flash frozen with liquid nitrogen and stored at -80 °C.

¹ Data file 18-1060-88 AD 'Sephacryl High Resolution media HiPrep Sephacryl HR columns', GE Healthcare.

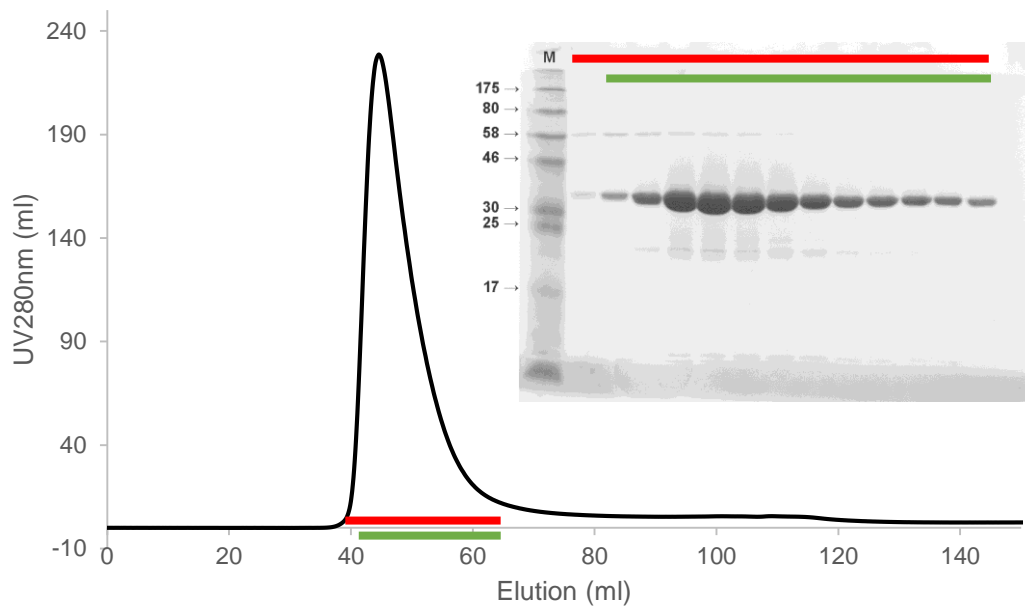


Figure 6.4 Size-exclusion purification of His₆-LmFBPase.

Elution of proteins from the size-exclusion column was monitored by a UV spectrometer at 280 nm. Proteins from the single peak (represented by the red lines) of the elution were characterised by SDS-PAGE. Fractions at the positions indicated by green lines were pooled together and collected as a final product. 'M' represents 'marker'.

6.4 Biophysical properties of *LmFBPase*

6.4.1 Determination of molecular size of *LmFBPase* by DLS

A DLS assay was carried out for the determination of the molecular size and aggregation of *LmFBPase*. Briefly, *LmFBPase* stored at $-80\text{ }^{\circ}\text{C}$ was thawed on ice and diluted to 1 mg/ml with the gel-filtration buffer. The sample was assayed immediately (Figure 6.5A, B, and C) and after incubation for five days at $4\text{ }^{\circ}\text{C}$ (Figure 6.5D).

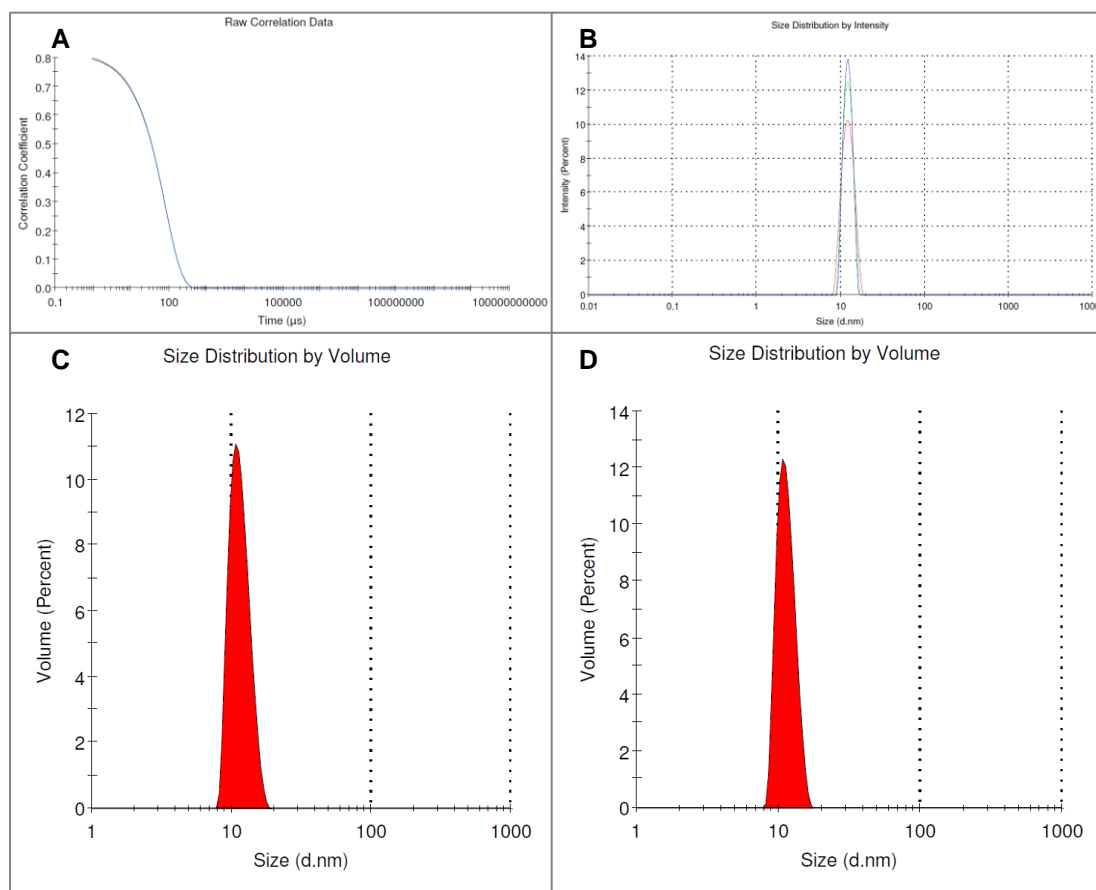


Figure 6.5 DLS analysis of *LmFBPase*.

A. Raw correlation data for the DLS analysis of freshly thawed *LmFBPase* (three repeats are presented in red, blue and green); B. a graph of the size distribution by intensity of freshly thawed *LmFBPase* (three repeats are presented in red, blue and green); C. a graph of the size distribution by volume of freshly thawed *LmFBPase*; D. a graph of the size distribution by volume of *LmFBPase* that has been stored at $4\text{ }^{\circ}\text{C}$ for five days.

The results showed that *LmFBPase* exists as a monodisperse protein. According to this assay, the mean hydrodynamic radius and molecular mass for *LmFBPase* are 11.46 nm and 200 kDa, respectively. These results suggest that *LmFBPase* exists as a tetramer in solution, which corresponds to the deduction based on its elution volume from the gel-filtration curve. No aggregation was detected in the samples. The consistency of the result using the sample that has been incubated at 4 °C for five days, where similar scattering signal and molecular size were detected, indicates the stability of *LmFBPase* under such conditions.

After its purity, molecular size and stability had been preliminarily characterised, *LmFBPase* was subjected to further biophysical, biochemical and structural investigations (e.g. enzymic activity assay, X-ray crystallography, etc.).

6.4.2 Thermostability of *LmFBPase*¹

LmFBPase unfolding in the absence and presence of different ligands and/or Mn²⁺ as a function of increasing temperature was determined with a thermal shift assay (i.e. thermal denaturation assay, TDA). The results showed that in the absence of ligands, the melting temperature [T_m , defined as the temperature midpoint for the protein unfolding transition (Morgan *et al.*, 2010)] of *LmFBPase* was 56.5 °C (Figure 6.6). Thermostability in the presence of the substrate F16BP was increased strikingly for *LmFBPase* with a ΔT_m of about 8 °C. In contrast, AMP caused only a modest change in the stability of the protein. Thermostability of *LmFBPase* was increased by more than 9 °C in the presence of Mn²⁺. Due to the strong stabilisation effect of Mn²⁺, it was used as a ‘silver bullet’ for the crystallisation of *LmFBPase*.

¹ The experiment regarding the thermostability investigation of *LmFBPase* described in this section was carried out by Dr Vasquez-Valdivieso in our laboratory [Vasquez-Valdivieso, M. G. (2013). Identification of selective inhibitors of phosphofructokinase and fructose biphosphatase as lead compounds against trypanosomatids, University of Edinburgh, Edinburgh.]

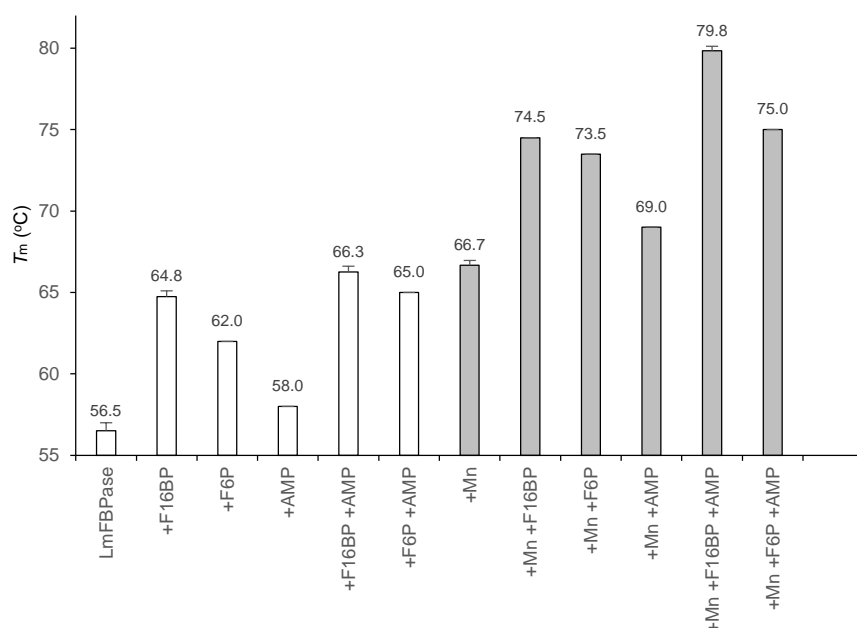


Figure 6.6 Melting temperatures (T_m) of *LmFBPase*.

Melting temperatures (T_m) of *LmFBPase* in the absence and presence of ligands (2 mM) and/or Mn^{2+} (10 mM). The shaded bars correspond to the presence of Mn^{2+} . The thermostability of *LmFBPase* and the effects of ligands and/or Mn^{2+} were determined with a thermal shift assay. Data represent the mean \pm SD of three experiments. This work was previously carried out by Dr Montserrat G. Vásquez-Valdivieso in our lab. More detailed methods and results can be found in her thesis (Vasquez-Valdivieso, 2013).

6.5 Kinetic properties of *LmFBPase*

A novel plate-based enzymic activity assay has been developed for trypanosomatid FBPsases by monitoring the formation of NADPH that was produced via the coupling enzymes PGI and G6PDH. The mechanism and detailed experimental procedure of this assay is described in Section 2.5. Briefly, the catalytic substrate F16BP was hydrolysed into phosphate and F6P, which was then isomerised to G6P by PGI in the presence of $NADP^+$. The latter was further catalysed by G6PDH into NADPH, which has an absorption at the wavelength of 340 nm.

6.5.1 *LmFBPase* is more active under mildly alkaline conditions

A preliminary assay was carried out for the determination of the optimal pH of the catalysis of *LmFBPase*. In this assay, the enzymic activity was tested in the presence of 10 mM Mg^{2+} and 100 mM K^+ with 150 μ M F16BP at 37 °C.

The enzyme shows an optimal F16BP-hydrolysis specific activity of about $18 \mu\text{mol min}^{-1} \text{mg}^{-1}$ under such conditions. Unlike most eukaryotic FBPases that exhibit highest activity at neutral pH (Gizak *et al.*, 2012, Liang *et al.*, 2013), *LmFBPase* is more active in a mildly alkaline environment (pH 8–8.5), where the specific activity is approximately 66% higher than that at pH 7.0 (Figure 6.7). This observation is similar to that of *E. coli* FBPase, which also exhibits an optimal activity at mildly alkaline conditions (pH 7.8) (Fraenkel *et al.*, 1966, Kelley-Loughnane *et al.*, 2002).

According to the optimization, pH 8.0 was used for further investigations in the following *LmFBPase* enzyme assays.

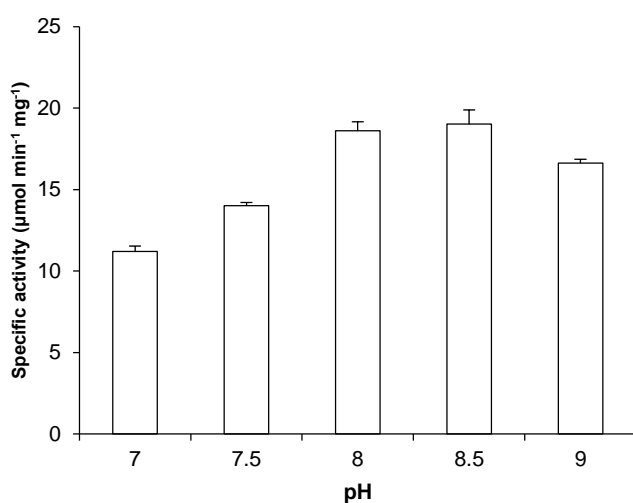


Figure 6.7 Enzyme activity of *LmFBPase* at different pH values.

6.5.2 Temperature optimisation for the enzyme assay of *LmFBPase*

The determination of an optimal temperature for the catalysis of *LmFBPase* was performed in the presence of 10 mM Mg^{2+} , 100 mM K^{+} with $150 \mu\text{M}$ F16BP at pH 8.0. The result shows that *LmFBPase* exhibits the highest activity at $37 \text{ }^{\circ}\text{C}$, which was used for further investigations in the following *LmFBPase* enzyme assays (Figure 6.8).

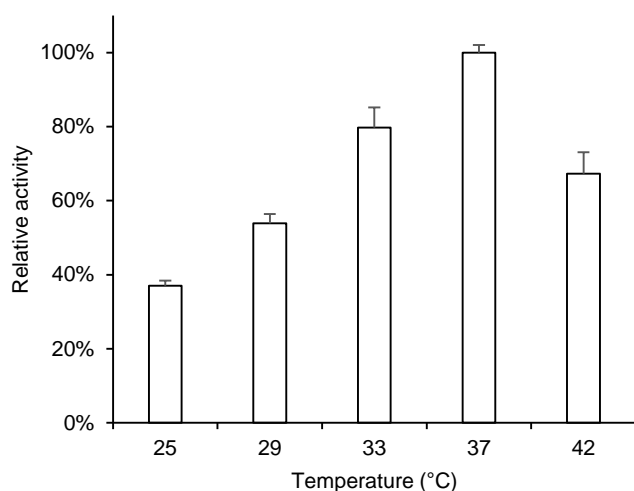


Figure 6.8 Enzyme activity of *LmFBPase* at different temperatures.

6.5.3 *LmFBPase* exhibits relatively weak substrate-binding

The enzyme assay for *LmFBPase* kinetics was carried out in the presence of 10 mM Mg^{2+} and 100 mM K^+ with a titration of F16BP at pH 8.0 at 37 °C. The result shows that the substrate F16BP binds to the enzyme with a $K_{0.5}$ value of 19.8 μM (Figure 6.9). This value is similar to the $K_{0.5}$ value of *E. coli* FBPase isotype I, but considerably larger than those of the mammalian FBPases, which are in the range of 1.2–2.1 μM (Table 6.2). This observation indicates that F16BP exhibits a weaker binding to FBPases from *L. major* and *E. coli* than to mammalian FBPases.

The sequence alignment of *L. major*, mammalian and *E. coli* FBPases is shown in Figure 1.13. Thirteen of the fourteen residues at the active site involved in substrate and/or metal binding are identical among *L. major* and mammalian FBPases (Choe *et al.*, 2000). The only difference is residue 221 which occurs as an asparagine in both *L. major* and *E. coli* FBPases but is a tyrosine in mammalian FBPases (Figure 1.13, all residues are numbered according to *LmFBPase* in this chapter, unless stated otherwise). Crystal structures of mammalian FBPases [e.g. structures of pig liver FBPase (PDB code: 1EYI) (Choe *et al.*, 2000), human liver FBPase (PDB code: 5FBP) (Ke *et al.*, 1991a), and human muscle FBPase (PDB code 4HE1) (Shi *et al.*, 2013)] show that the hydroxyl group on the side chain of this tyrosine is responsible for binding to the 1'-phospho group of F6P. The side chain of asparagine is shorter than tyrosine, so it might

not be able to bind to the substrate or the product. Consequently, the lack of stabilisation of the 1'-phospho group of the substrate or the product might be the reason for the weaker binding affinity ($K_{0.5}$ 19.8 μM) compared to the mammalian enzymes ($K_{0.5}$ 1.2–2.1 μM). The determination of the crystal structures of *Lm*FBPase allowed this point to be examined in detail, and is discussed in subsequent sections.

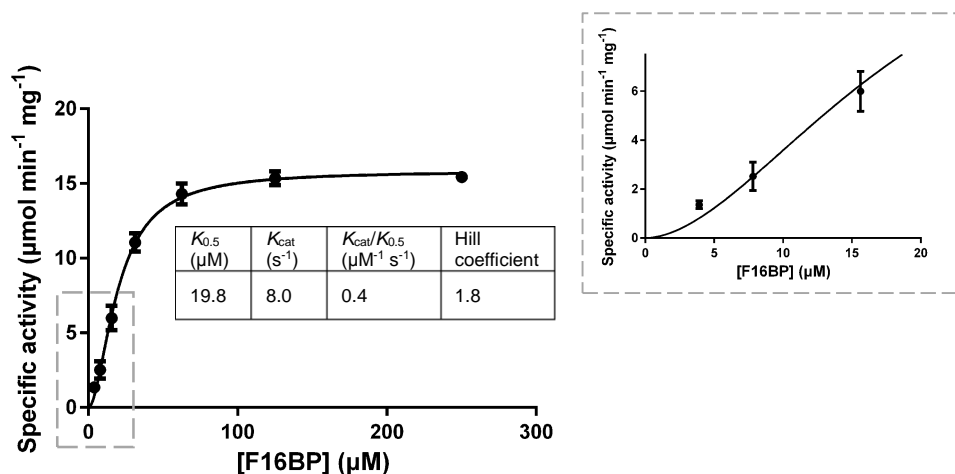


Figure 6.9 Kinetic characterisation of *Lm*FBPase.

The sigmoidal part of the curve that exhibits the cooperativity of *Lm*FBPase is highlighted with dashed lines, and the inset shows a zoomed in version. Data represent the mean \pm SD of three experiments.

Table 6.2 Kinetic parameters for *L. major*, mammalian and bacterial FBPases.

	k_{cat} (s^{-1})	$K_{0.5}$ (μM)	$K_a[\text{Mg}^{2+}]$ (mM)	K_i [AMP] (μM)	n_{H} [AMP]	reference
<i>L. major</i>	8.0	19.8	1.2	63.8	1.4	this study
Human liver	20.8	2.1	0.2	4.4	2.1	(Rakus <i>et al.</i> , 2005)
Human muscle	23.4	1.3	0.2	0.1	1.8	(Rakus <i>et al.</i> , 2005)
Pig liver	20.0	1.2	0.8	0.6	2.2	(Iancu <i>et al.</i> , 2005)
<i>E. coli</i> isotype I	14.6	15.4	0.6	2.7	1.1	(Kelley-Loughnane <i>et al.</i> , 2002)

6.5.4 F16BP exhibits homotropic allosteric regulation for *Lm*FBPase

The sigmoid curve (Figure 6.9) also shows that the substrate F16BP exhibits homotropic allosteric regulation for *Lm*FBPase with positive cooperativity of $n_H=1.8$. It indicates that the more substrate is bound to FBPase, the easier it is for additional substrate to bind until all binding sites are saturated. The effect of substrate on the thermostability of *Lm*FBPase showed that F16BP is able to stabilise the enzyme in the presence of Mg^{2+} and K^+ (Figure 6.6), which is likely due to the stabilisation of the dynamic loop (residues 50–71). In this case, the observation of the homotropic allosteric effect with positive cooperativity of F16BP implies that engaging the dynamic loop into the active site in one subunit may transmit to another subunit. The Hill coefficients are similar for *L. major*, human, pig and *E. coli* FBPases.

6.5.5 *Lm*FBPase requires magnesium for activity

The effect of Mg^{2+} on *Lm*FBPase was studied in the presence of 100 mM K^+ and a saturating concentration of F16BP (150 μ M) at pH 8.0 at 37 °C. Magnesium was shown to be mandatory for the catalytic activity of *Lm*FBPase. As shown in Figure 6.10, *Lm*FBPase has no activity in the absence of Mg^{2+} , for which the association constant was determined as 1.2 mM.

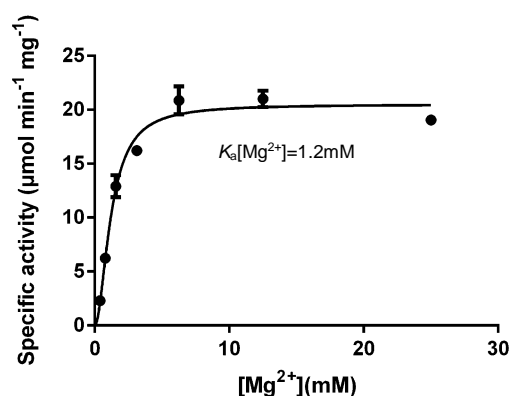


Figure 6.10 Effects of Mg^{2+} on *Lm*FBPase enzymic activity.

Data represent the mean \pm SD of three experiments.

6.5.6 Manganese inhibits the activity of *Lm*FBPase

In the enzyme assay where 10 mM Mg²⁺, 100 mM K⁺, and a sub-saturating concentration of F16BP (40 μM) were present, manganese exhibited an inhibitory effect on *Lm*FBPase activity with a *IC*₅₀ of 44.3 μM (Figure 6.11), which is substantially higher than the 1 μM cytosolic manganese in *T. brucei* (Fuad *et al.*, 2011). In this case, the inhibitory effect of manganese on *Lm*FBPase might not be physiologically relevant. A thermal shift assay comparing the thermostability of *Lm*FBPase in the absence/presence of manganese demonstrates its strong stabilisation effect (Figure 6.6). As a consequence, it was used as a ‘silver bullet’ for the crystallisation of *Lm*FBPase. More detailed structural comparisons and discussion are in Section 7.3.6.

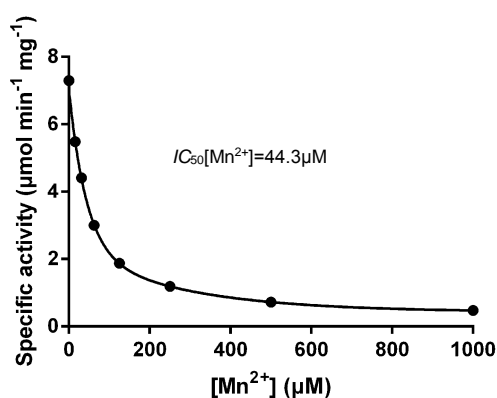


Figure 6.11 Effects of Mn²⁺ on *Lm*FBPase enzymic activity.

6.5.7 AMP is an allosteric inhibitor of *Lm*FBPase

AMP is a well-characterised allosteric inhibitor of mammalian FBPases (Gao *et al.*, 2014), and binds to an effector site about 30 Å distant from the active site. Sequence alignment of mammalian and *L. major* FBPases shows that the residues involved in AMP binding are poorly conserved (Figure 1.13), with five of eight residues different (residues 16, 25, 27, 28 and 112). Gao *et al.* (2014) showed a regular pattern in mammalian FBPases such that AMP inhibition requires serine or threonine at residue 31 (residue no. 29 in *Lm*FBPase), lysine or arginine at residue 112, and tyrosine at residue 113 (Gao *et al.*, 2014). *Lm*FBPase retains Thr29 and Tyr113, but has an aspartic acid at position 112 instead of an alkaline residue. The lack of sequence conservation at the effector site correlates well with the weaker binding of AMP to *Lm*FBPase than to mammalian FBPases (K_i 63.8 μ M instead of 0.1–4 μ M) (Figure 6.12).

The determined inhibitor constant is in the physiological range of the overall cellular AMP concentration (0.25 ± 0.06 mM) in trypanosomatids (Graven *et al.*, 2014). As a result, the fact that the K_i value for AMP is relatively high compared to those of mammalian FBPases may be of physiological relevance. Moreover, it may be related to the compartmentalisation of the glycolytic and gluconeogenic pathways of trypanosomatids inside glycosomes and the proposal that the glycosomal membrane is impermeable to adenine nucleotides (Professor Paul A. M. Michels, personal communication). The result suggests that FBPase activity and thus gluconeogenesis is under AMP regulation in trypanosomatids.

The kinetic characterisation of *Lm*FBPase was also carried out in the presence of different concentrations of AMP (Figure 6.13). This shows that AMP inhibits the activity of *Lm*FBPase without changing the $K_{0.5}$ of the substrate F16BP, thereby indicating that AMP is a non-competitive inhibitor against *Lm*FBPase. Further, the increase of AMP concentration reduces the Hill coefficient of F16BP. The AMP binding turns the positive cooperativity of F16BP to a negative cooperativity. More details of AMP binding to *Lm*FBPase were further investigated by protein crystallography.

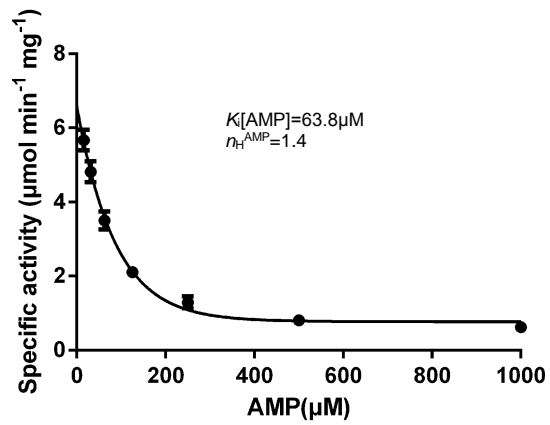


Figure 6.12 The inhibitory effect of AMP on *LmFBPase* activity.

Data represent the mean \pm SD of three experiments.

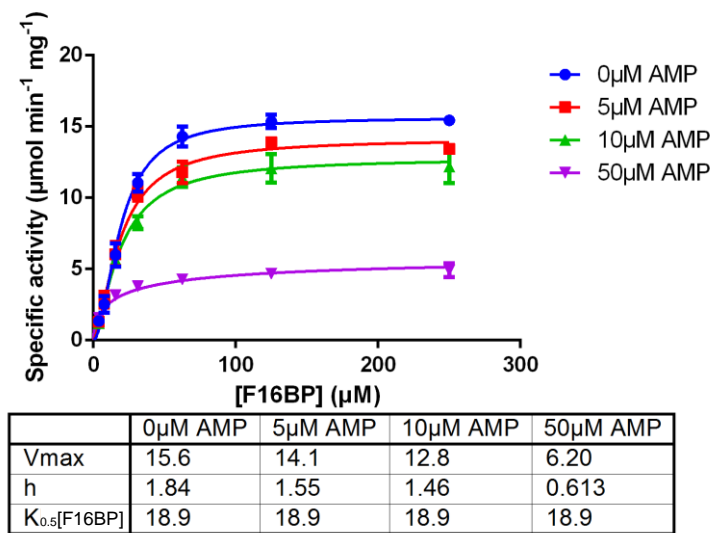


Figure 6.13 Kinetic characterisation of *LmFBPase* in the presence of different concentrations of AMP.

“h” represents the Hill coefficient. Data represent the mean \pm SD of three experiments.

6.5.8 F26BP is a competitive inhibitor of *Lm*FBPase

Fructose 2,6-bisphosphate (F26BP) is found to bind to the active site, and thereby serves as a competitive inhibitor of both liver and muscle isoforms of mammalian FBPases with inhibitor constants of 0.5 μM and 0.2 μM , respectively (Pilkis *et al.*, 1981, Van Schaftingen & Hers, 1981, Ke *et al.*, 1989b, Ke *et al.*, 1989a, Rakus *et al.*, 2000). In this study, F26BP also shows an inhibitory effect on *Lm*FBPase.

In the enzyme assay where 10 mM Mg^{2+} , 100 mM K^+ , and sub-saturating concentration of F16BP (30 μM) were present, F26BP exhibited an inhibitory effect on *Lm*FBPase activity with a K_i of 1.9 μM (Figure 6.14), which is a magnitude higher than that of mammalian FBPase. A kinetic characterisation of *Lm*FBPase in the presence of different F26BP concentrations demonstrates that F26BP reduces the substrate binding affinity without altering the maximum activity (Figure 6.15). This observation confirms that F26BP is a competitive inhibitor of *Lm*FBPase activity.

However, concerning the inhibitor constant of F26BP against *Lm*FBPase, it is questionable whether this inhibition is of physiological importance. F26BP is synthesised (and hydrolysed) in the cytosol of a trypanosomatid parasite, where it activates PYK at $K_{0.5}$ values of 0.056 μM (*T. brucei* PYK) or 0.290 μM (*L. mexicana* PYK) (Zhong *et al.*, 2013, Morgan *et al.*, 2010). F26BP almost certainly diffuses freely through the pores in the glycosomal membrane (Achcar *et al.*, 2013). Therefore, the cellular concentration of F26BP in *Leishmania* is unlikely to be higher than 1 μM . Hence, it seems the micromolar-level of F26BP required for *Lm*FBPase inhibition is unlikely to be a realistic concentration in *Leishmania* glycosomes.

F26BP is currently not commercially available to the author's best knowledge. The sample of F26BP available in the laboratory in Edinburgh was a gift from Dr David A. Okar at the Veterans Administration Medical Center (USA). As a step of quality control for the F26BP stock that had been stored at 10 mM in water at $-80\text{ }^\circ\text{C}$ for more than five years, an LDH-coupled enzyme assay for the kinetics of F26BP against *T. brucei* PYK was carried out. The $K_{0.5}$ of F26BP (defined as the concentration demonstrating 50% activation, 18 nM) shown in this assay is similar to that reported in the literature (13 nM) (Ernest *et al.*, 1998). This result indicates that F26BP was

stable under the storage conditions, and thereby eliminated the possibility that the questionable F26BP affinity against *Lm*FBPase was due to a faulty reagent.

In 2007, Rigden reported a kinetic result on *Tb*FBPase, showing that 50 μM F26BP inhibits 50% activity of *Tb*FBPase purified from *E. coli* expression (Rigden, 2007). This inhibitor constant of F26BP against *Tb*FBPase is close to that of *Lm*FBPase, and thereby further confirms this result which is presumably physiologically irrelevant under such conditions. Nevertheless, the physiological irrelevance might be true (in other words, it is only a biochemical observation *in vitro* but not realistic *in vivo*), given by the fact that F26BP was also shown to be able to inhibit the activity of FBPase from *E. coli*, an organism lacking F26BP (Hines *et al.*, 2007b).

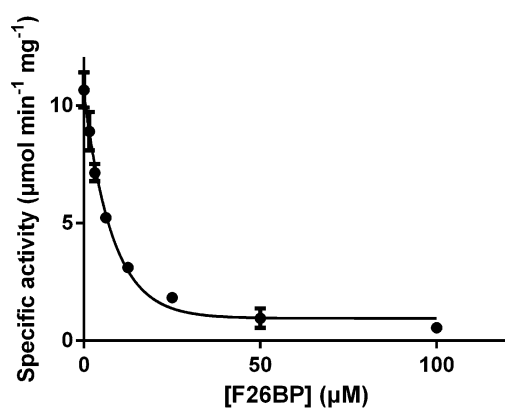


Figure 6.14 The inhibitory effect of F26BP on *Lm*FBPase activity.

Data represent the mean \pm SD of three experiments.

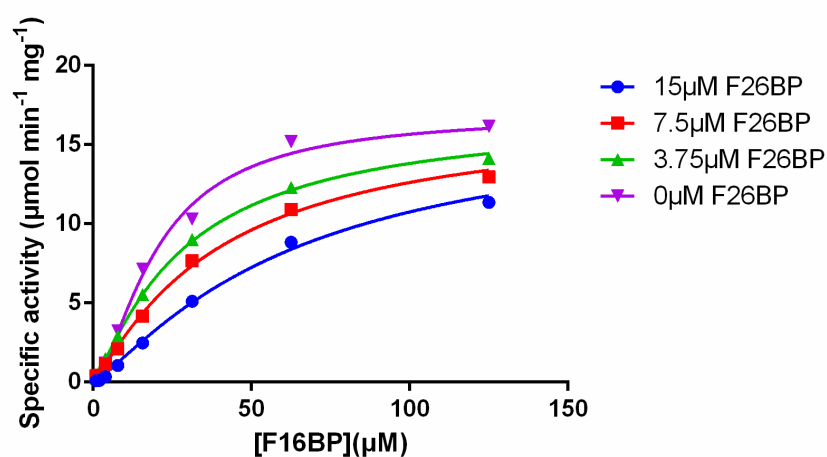


Figure 6.15 Kinetic characterisation of *Lm*FBPase in the presence of different concentrations of F26BP.

6.5.9 AMP and F26BP show synergistic inhibition against FBPases

F26BP and AMP are inhibitors of mammalian FBPase, and both also serve as activators of mammalian PFK (Blangy *et al.*, 1968, Pilkis *et al.*, 1981, Taketa & Pogell, 1965, Van Schaftingen & Hers, 1981). During starvation, glucagon is secreted and a downstream bifunctional enzyme fructose-6-phosphate-2-kinase/fructose-2,6-bisphosphatase (PFK-2/FBPase-2) is phosphorylated, which leads to the degradation of F26BP; whereas in the fed state, insulin reverses the effect of glucagon and raises the level of F26BP (Pilkis *et al.*, 1988, Christophe, 1995, Pilkis *et al.*, 1995, Okar *et al.*, 2001). The increment in F26BP level is not enough to inhibit mammalian FBPase completely by itself; however, AMP inhibition is enhanced up to ten fold in the presence of F26BP, which is termed AMP/F26BP synergism (Pilkis *et al.*, 1981, Van Schaftingen & Hers, 1981). Thus, even though AMP concentration is relatively constant *in vivo*, the fluctuation of F26BP levels can dynamically alter FBPase activity (Okar & Lange, 1999).

An enzyme assay for the kinetics of AMP inhibition of *Lm*FBPase was carried out in the presence of sub-saturating concentrations of F16BP (30 μ M) and a series of concentrations of F26BP (0–75 μ M) at pH 8.0 at 37 °C. The result demonstrates that less AMP is required for half inhibition of *Lm*FBPase activity in the presence of higher concentrations of F26BP, and *vice versa* (Figure 6.16A). A K_i [AMP]-vs-F26BP graph generated from Figure 6.16A more clearly shows the trend that the AMP inhibitory effect is F26BP-dependent. In the presence of F26BP, the K_i for the AMP falls up to 13 fold. In 2014, Gao *et al.* demonstrated that the presence of a central cavity (that was predicted to be mandatory for the AMP/F26BP synergism) requires small side chains (glycine, alanine, cysteine, serine, or gap) for residue 45 (Gao *et al.*, 2014) (discussed in detail in Section 6.2). Here the AMP/F26BP synergism of *Lm*FBPase with polar/long residues at its tetramer centre suggests a counterexample, where the structural mechanism of this synergism may be more complicated than the “small-residue45 theory”.

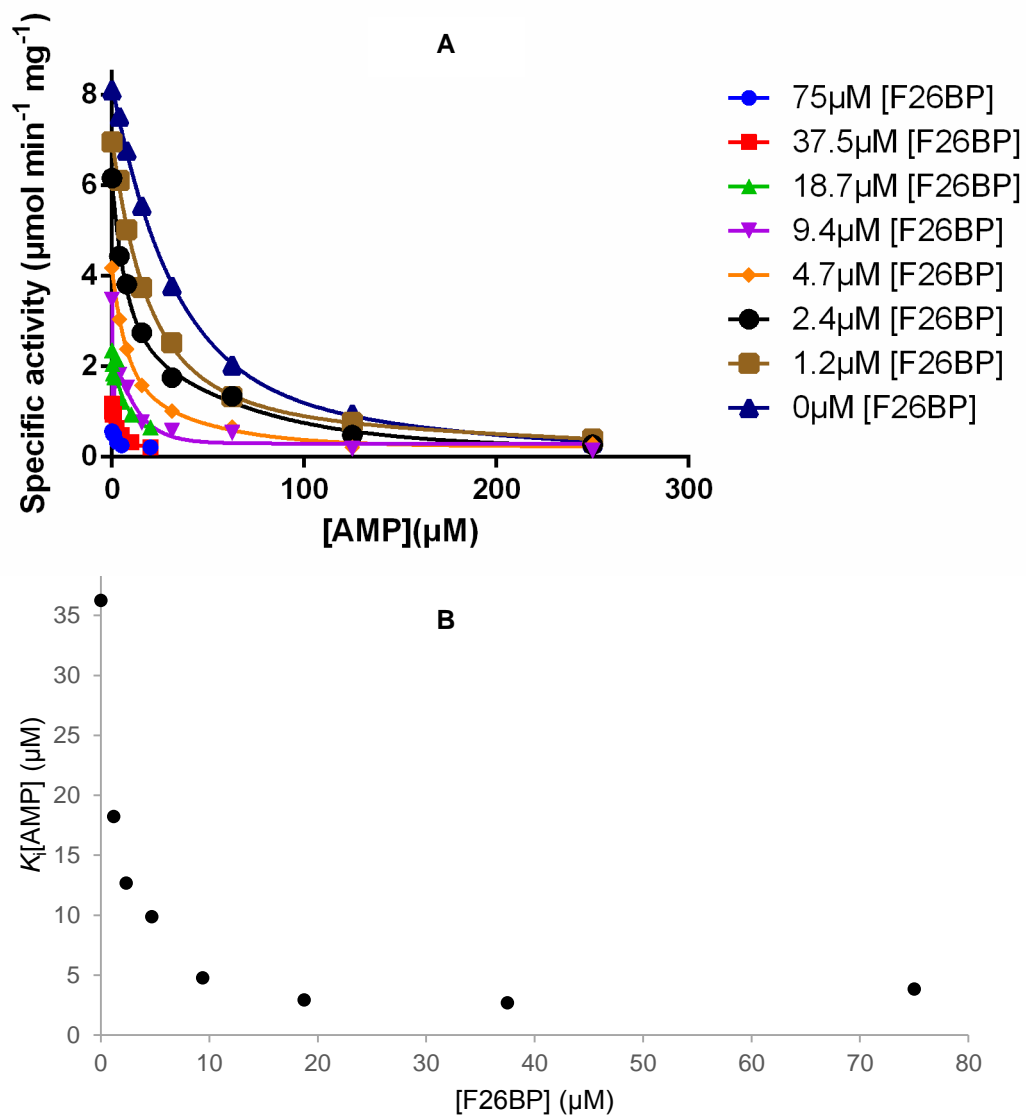


Figure 6.16 The AMP/F26BP synergistic inhibitory effect on *LmFBPase*.

A. The effect of AMP titration on the specific activity of *LmFBPase* in the presence of different concentrations of F26BP.

B. The K_i of AMP for *LmFBPase* decreases when higher concentrations of F26BP are present.

6.6 Conclusions

FBPase is a gluconeogenic enzyme that catalyses the hydrolysis of F16BP. It has been shown as a promising drug target against *Leishmania*. In this study, an enzyme assay was developed to characterise the kinetics and modulators of *Lm*FBPase. It is shown that the enzymic activity is pH, temperature, and divalent metal dependent. AMP is shown as a non-competitive inhibitor of *Lm*FBPase, and F26BP exhibits competitive inhibition. Combining AMP and F26BP shows a synergistically inhibitory effect on *Lm*FBPase activity.

CHAPTER 7

Crystal structure of *Leishmania* fructose-1,6-bisphosphatase and its allosteric mechanism

CHAPTER 7. Crystal structure of *Leishmania* fructose-1,6-bisphosphatase and its allosteric mechanism

7.1 Background

Fructose-1,6-bisphosphatase (FBPase) is a gluconeogenic enzyme that catalyses the transformation of fructose 1,6-bisphosphate (F16BP) to fructose 6-phosphate (F6P) and phosphate. The observation that *Leishmania* FBPase is important for parasite proliferation (Naderer *et al.*, 2006) renders it a potential drug target and thus gives impetus to the requirement for further detailed biochemical and structural characterisation of this enzyme.

A preliminary study has been carried out previously in our laboratory, mainly by Dr Montserrat Vásquez-Valdivieso who solved the crystal structures of the *apoenzyme* and *holoenzyme* forms of *Lm*FBPase (Vasquez-Valdivieso, 2013).

An *apoenzyme* crystal structure of the C-terminal His₆-tagged *Lm*FBPase diffracted at 2.7 Å was obtained from an initial crystallisation trial based on Hampton PEG/Ion 2 screening in the presence of 1 mM F16BP, 5 mM magnesium and 50 mM potassium (Vasquez-Valdivieso, 2013). The crystal structure showed a homotetramer, with no substrate/product/metal found in the density map. Moreover, residues 50–71 that correspond to an important dynamic loop in mammalian FBPases were not observed in the electron density map.

In the *holoenzyme* structure of *Lm*FBPase which was co-crystallised with manganese and the substrate F16BP, a catalytic product P_i and manganese atoms were found in each active site of the homotetramer. Its overall planar conformation is very similar to the *apoenzyme* structure, which also adopts a planar topology. The dynamic loop was found to be stabilised around the active site, in contrast to the *apoenzyme* structure where the dynamic loop was invisible in the electron density map. This observation highlights the catalytic importance of the dynamic loop of *Lm*FBPase.

The new *Lm*FBPase structure presented in this thesis is a complex of FBPase with AMP and F6P. It has been shown that AMP is an allosteric inhibitor against *Lm*FBPase (Section 6.5.7). Sequence alignment among *Leishmania* and mammalian FBPases has demonstrated the presence of a distinctive effector site in *Lm*FBPase (Section 6.2), which may provide a different allosteric mechanism and potential drug target. Structural studies of *Lm*FBPase in complex with AMP were carried out and are discussed in this chapter.

7.2 Methods

7.2.1 Crystallisation, data collection and processing

Purified His₆-*Lm*FBPase samples were used for the crystallisation experiments. Frozen protein samples were thawed on ice before using. Single crystals of *Lm*FBPase were obtained by vapour diffusion using the hanging-drop technique. *Lm*FBPase was pre-incubated in solution at 4 °C for 20 min (with the following final concentrations: 3.45 mg/ml *Lm*FBPase, 20 mM TEA, 5 mM MgCl₂, 50 mM KCl, 10% glycerol, 1 mM F16BP, 10 mM MnCl₂ and 1–2 mM AMP, pH 7.2). The incubation was followed by centrifugation at 14,000×*g* at 4 °C for 10 min to remove any trace amount of precipitations. To obtain crystals of the *Lm*FBPase/AMP complex, the drops were set up by mixing 1.5 µl of this mixed solution with 1.5 µl of reservoir solution [19%–24% w/v PEG 3,350 plus 0%–20% glycerol plus 56%–81% well buffer (0.05 M citric acid, 0.05 M Bis-Tris propane, pH 6.0)]. Two drops with same conditions (except for 1 mM AMP in one drop and 2 mM AMP in the other) were placed on the cover slip of each well. The temperatures of 4 °C and 17 °C were tried for crystal growth. The optimum crystallisation condition was found where 19% PEG 3,350 and 5% glycerol were used for the reservoir solution. Further details and the results of the crystallisation are shown in Section 7.3.1.

The crystallisation conditions previously used (Vasquez-Valdivieso, 2013) to obtain crystals of the *apoenzyme* structure and the *Lm*FBPase/Mn²⁺/P₁ structure are as follows: (1) The crystals of the *apoenzyme* structure were formed by mixing 1.5 µl of *Lm*FBPase (3.8 mg/ml of enzyme in 20 mM TEA, 5 mM MgCl₂, 50 mM KCl, 10%

glycerol, 1 mM F16BP, pH 7.0 solution) with 1.5 μ l reservoir solution [20% w/v PEG 3,350 (0.05 M citric acid, 0.05 M Bis-Tris propane, pH 5.0) and ‘silver bullet 85’ in crystal growth kit HR2-096 from Hampton Research Co., Ltd. (19 amino acids excluding cysteine in 0.02 M sodium HEPES, pH 6.8)]. The crystals were grown at 17 °C. Plate-like crystals appeared after three days. (2) The crystals of *LmFBPase*/Mn²⁺/P_i were crystallized by mixing 1.5 μ l of *LmFBPase* (4.0 mg/ml of enzyme in 20 mM TEA, 5 mM MgCl₂, 50 mM KCl, 10% glycerol, 1 mM F16BP, and 10 mM MnCl₂, pH 7.0) with 1.5 μ l reservoir solution [20% w/v PEG 3,350 (0.05 M citric acid, 0.05 M Bis-Tris propane, pH 6.0)]. Crystals were grown in three weeks at 17 °C. Twenty percent PEG 400 plus 10% glycerol were used as cryoprotectants.

The X-ray diffraction datasets were collected on Beamline I03 at the Diamond synchrotron radiation facility in Oxfordshire, United Kingdom. Each dataset was obtained from a single crystal flash-frozen in liquid nitrogen. Data were then processed with iMOSFLM (Battye *et al.*, 2011) and scaled with SCALA (Evans, 2006), or processed automatically with xia2 (Winter, 2009).

The structure determination and refinement strategy for the *LmFBPase* structure was similar to that of M2PYK structures (Section 4.2.3). One monomer of a *LmFBPase* apoenzyme homotetrameric crystal structure that was previously determined in our lab (Vasquez-Valdivieso, 2013) was used as a search model for the molecular replacement. Four subunits were found in each asymmetric unit. Structure refinement was performed with REFMAC, and COOT. No NCS restraint was defined due to the small differences among subunits. Detailed data collection and refinement statistics for *LmFBPase* structure are summarised in Table 7.3.

7.2.2 Virtual screening of small molecular inhibitors against *LmFBPase*

The pharmacophore-searching software LIDAEUS (Taylor *et al.*, 2008) was used as a drug discovery strategy to identify small molecular inhibitors against the AMP binding site of *LmFBPase*. Briefly, the *LmFBPase*/AMP complex structure was used for the screening, and the structure of the protein (*LmFBPase*) and ligand (AMP) were separately submitted to LIDAEUS for the definition of the coordinates of each

molecule. Energy maps and site points were calculated by LIDAEUS, followed by a screening against a compound database (CAMELSICK2, a multi-conformer database containing one million compounds with four million conformers).

7.3 Results and discussion

As described above, the *apoenzyme* crystal structure of *LmFBPase* and a complex structure of *LmFBPase*/ Mn^{2+} / P_i were previously solved in our laboratory (Vasquez-Valdivieso, 2013). The enzyme assay developed in this thesis shows that AMP allosterically inhibits *LmFBPase* (Section 6.5.7). Further, a novel crystal structure of *LmFBPase* in complex with AMP demonstrated a homotetramer that adopts a distinct topology. Comparisons and structural analyses of the three crystal structures of *LmFBPase* (the *apoenzyme* structure, *LmFBPase*/ Mn^{2+} / P_i , and the *LmFBPase*/AMP complex) as well as three corresponding mammalian FBPs are shown in the following sections.

7.3.1 Crystal structure of *LmFBPase*/AMP

Crystallisation conditions for the *LmFBPase*/AMP complex were optimised as below. Briefly, AMP was incubated with *LmFBPase* at pH 7.2. This solution (1.5 μl) was mixed with 1.5 μl of reservoir solution containing different concentrations of PEG 3,350 and glycerol (Table 7.1). Different crystal plates were placed at 4 °C (upper table) and 17 °C (lower table) respectively for the optimisation of crystal growth temperature. The crystal quality is represented by red colour in the table.

The best crystallisation conditions were found where 19% PEG 3,350 and 5% glycerol were used for the reservoir solution (highlighted in dark red in Table 7.1 and summarised in Table 7.2). Crystals under such conditions grew to approximately 200 $\mu\text{m} \times 5 \mu\text{m} \times 5 \mu\text{m}$ bar-shaped crystals in five days, and were subjected to X-ray diffraction (Figure 7.1). The crystal diffracted to a resolution of 2.6 Å with an X-ray beamline at the wavelength of 0.9700 nm (Beamline I03, Diamond synchrotron). To obtain the crystal structure of *LmFBPase*, molecular replacement was performed using the crystal structure of *apoenzyme LmFBPase*. The crystal structure is in space group

P2₁2₁2₁ in an orthorhombic lattice, with four *Lm*FBPase chains (approximately 41.3 kDa for each monomer) in each asymmetric unit, showing the homotetrameric conformations. More detailed information concerning data collection and structure refinement is summarised in Table 7.3.

Table 7.1 Conditions for crystallisation screening for *Lm*FBPase/AMP complex.

PEG glycerol		19%	20%	21%	22%	23%	24%
0%	Drop 1	0.38ml PEG 0.62ml well buffer	0.4ml PEG 0.6ml well buffer	0.42ml PEG 0.58ml well buffer	0.44ml PEG 0.56ml well buffer	0.46ml PEG 0.54ml well buffer	0.48ml PEG 0.52ml well buffer
	Drop 2	0.38ml PEG 0.62ml well buffer	0.4ml PEG 0.6ml well buffer	0.42ml PEG 0.58ml well buffer	0.44ml PEG 0.56ml well buffer	0.46ml PEG 0.54ml well buffer	0.48ml PEG 0.52ml well buffer
5%	Drop 1	0.38ml PEG 0.52ml well buffer 0.1ml 50% GOL	0.4ml PEG 0.5ml well buffer 0.1ml 50% GOL	0.42ml PEG 0.48ml well buffer 0.1ml 50% GOL	0.44ml PEG 0.46ml well buffer 0.1ml 50% GOL	0.46ml PEG 0.44ml well buffer 0.1ml 50% GOL	0.48ml PEG 0.52ml well buffer 0.1ml 50% GOL
	Drop 2	0.38ml PEG 0.52ml well buffer 0.1ml 50% GOL	0.4ml PEG 0.5ml well buffer 0.1ml 50% GOL	0.42ml PEG 0.48ml well buffer 0.1ml 50% GOL	0.44ml PEG 0.46ml well buffer 0.1ml 50% GOL	0.46ml PEG 0.44ml well buffer 0.1ml 50% GOL	0.48ml PEG 0.52ml well buffer 0.1ml 50% GOL
10%	Drop 1	0.38ml PEG 0.42ml well buffer 0.2ml 50% GOL	0.4ml PEG 0.4ml well buffer 0.2ml 50% GOL	0.42ml PEG 0.38ml well buffer 0.2ml 50% GOL	0.44ml PEG 0.56ml well buffer 0.2ml 50% GOL	0.46ml PEG 0.44ml well buffer 0.2ml 50% GOL	0.48ml PEG 0.42ml well buffer 0.2ml 50% GOL
	Drop 2	0.38ml PEG 0.42ml well buffer 0.2ml 50% GOL	0.4ml PEG 0.4ml well buffer 0.2ml 50% GOL	0.42ml PEG 0.38ml well buffer 0.2ml 50% GOL	0.44ml PEG 0.56ml well buffer 0.2ml 50% GOL	0.46ml PEG 0.44ml well buffer 0.2ml 50% GOL	0.48ml PEG 0.42ml well buffer 0.2ml 50% GOL
20%	Drop 1	0.38ml PEG 0.22ml well buffer 0.4ml 50% GOL	0.4ml PEG 0.2ml well buffer 0.4ml 50% GOL	0.42ml PEG 0.18ml well buffer 0.4ml 50% GOL	0.44ml PEG 0.16ml well buffer 0.4ml 50% GOL	0.46ml PEG 0.14ml well buffer 0.4ml 50% GOL	0.48ml PEG 0.12ml well buffer 0.4ml 50% GOL
	Drop 2	0.38ml PEG 0.22ml well buffer 0.4ml 50% GOL	0.4ml PEG 0.2ml well buffer 0.4ml 50% GOL	0.42ml PEG 0.18ml well buffer 0.4ml 50% GOL	0.44ml PEG 0.16ml well buffer 0.4ml 50% GOL	0.46ml PEG 0.14ml well buffer 0.4ml 50% GOL	0.48ml PEG 0.12ml well buffer 0.4ml 50% GOL
PEG glycerol		19%	20%	21%	22%	23%	24%
0%	Drop 1	0.38ml PEG 0.62ml well buffer	0.4ml PEG 0.6ml well buffer	0.42ml PEG 0.58ml well buffer	0.44ml PEG 0.56ml well buffer	0.46ml PEG 0.54ml well buffer	0.48ml PEG 0.52ml well buffer
	Drop 2	0.38ml PEG 0.62ml well buffer	0.4ml PEG 0.6ml well buffer	0.42ml PEG 0.58ml well buffer	0.44ml PEG 0.56ml well buffer	0.46ml PEG 0.54ml well buffer	0.48ml PEG 0.52ml well buffer
5%	Drop 1	0.38ml PEG 0.52ml well buffer 0.1ml 50% GOL	0.4ml PEG 0.5ml well buffer 0.1ml 50% GOL	0.42ml PEG 0.48ml well buffer 0.1ml 50% GOL	0.44ml PEG 0.46ml well buffer 0.1ml 50% GOL	0.46ml PEG 0.44ml well buffer 0.1ml 50% GOL	0.48ml PEG 0.52ml well buffer 0.1ml 50% GOL
	Drop 2	0.38ml PEG 0.52ml well buffer 0.1ml 50% GOL	0.4ml PEG 0.5ml well buffer 0.1ml 50% GOL	0.42ml PEG 0.48ml well buffer 0.1ml 50% GOL	0.44ml PEG 0.46ml well buffer 0.1ml 50% GOL	0.46ml PEG 0.44ml well buffer 0.1ml 50% GOL	0.48ml PEG 0.52ml well buffer 0.1ml 50% GOL
10%	Drop 1	0.38ml PEG 0.42ml well buffer 0.2ml 50% GOL	0.4ml PEG 0.4ml well buffer 0.2ml 50% GOL	0.42ml PEG 0.38ml well buffer 0.2ml 50% GOL	0.44ml PEG 0.56ml well buffer 0.2ml 50% GOL	0.46ml PEG 0.44ml well buffer 0.2ml 50% GOL	0.48ml PEG 0.42ml well buffer 0.2ml 50% GOL
	Drop 2	0.38ml PEG 0.42ml well buffer 0.2ml 50% GOL	0.4ml PEG 0.4ml well buffer 0.2ml 50% GOL	0.42ml PEG 0.38ml well buffer 0.2ml 50% GOL	0.44ml PEG 0.56ml well buffer 0.2ml 50% GOL	0.46ml PEG 0.44ml well buffer 0.2ml 50% GOL	0.48ml PEG 0.42ml well buffer 0.2ml 50% GOL
20%	Drop 1	0.38ml PEG 0.22ml well buffer 0.4ml 50% GOL	0.4ml PEG 0.2ml well buffer 0.4ml 50% GOL	0.42ml PEG 0.18ml well buffer 0.4ml 50% GOL	0.44ml PEG 0.16ml well buffer 0.4ml 50% GOL	0.46ml PEG 0.14ml well buffer 0.4ml 50% GOL	0.48ml PEG 0.12ml well buffer 0.4ml 50% GOL
	Drop 2	0.38ml PEG 0.22ml well buffer 0.4ml 50% GOL	0.4ml PEG 0.2ml well buffer 0.4ml 50% GOL	0.42ml PEG 0.18ml well buffer 0.4ml 50% GOL	0.44ml PEG 0.16ml well buffer 0.4ml 50% GOL	0.46ml PEG 0.14ml well buffer 0.4ml 50% GOL	0.48ml PEG 0.12ml well buffer 0.4ml 50% GOL

Cells shown in darker colour represent better crystals. The upper table shows crystal growth conditions at 4 °C, and the bottom table shows for those at 17 °C.

Table 7.2 The optimal condition for *Lm*FBPase/AMP crystal growth.

1.5 μ l protein solution	1.5 μ l reservoir solution	Temperature
3.45 mg/ml <i>Lm</i> FBPase, 20 mM TEA, 5 mM $MgCl_2$, 50 mM KCl, 10% glycerol, 1 mM F16BP, 10 mM $MnCl_2$ and 1 mM AMP, pH 7.2	19% w/v PEG 3,350, 5% glycerol, 79% well buffer (0.05 M citric acid, 0.05 M Bis-Tris propane, pH 6.0)	4 $^{\circ}C$

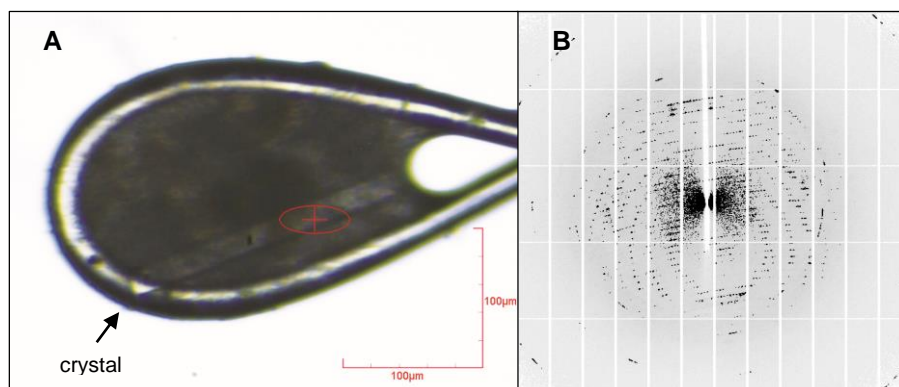


Figure 7.1 Crystal and its diffraction pattern for the *Lm*FBPase/AMP complex.

A. Crystallisation drop (trapped on a rod) containing conditions stated in Table 7.2 for the *Lm*FBPase/AMP complex. The red oval indicates the position of the beam spotting on the bar-shaped crystal.

B. Diffraction pattern from the *Lm*FBPase/AMP crystal.

Table 7.3 Crystallographic data collection and model refinement statistics for *Lm*FBPase/AMP complex.

Wavelength (Å)	0.9700
Resolution ^a (Å)	70.25–2.62 (2.714–2.62)
Space group	P2 ₁ 2 ₁ 2 ₁
Unit cell <i>a,b,c</i> (Å)	90.59 109.25 140.51
Total reflections	232518 (16569)
Unique reflections	42513 (4158)
Multiplicity	5.5 (5.4)
Completeness (%)	99.9 (99.6)
Mean <i>I</i> /σ(<i>I</i>)	12.4 (2.1)
Wilson B-factor (Å ²)	45.29
<i>R</i> _{merge} ^b (%)	10.2 (77.3)
<i>R</i> _{work} ^c	0.181
<i>R</i> _{free} ^d	0.231
Number of non-hydrogen atoms	10265
macromolecules	10123 (4×macromolecules)
waters	142
ligands	64 (4×F6P, 4×AMP)
Protein residues	1288
RMS (bonds, Å)	0.007
RMS (angles, °)	1.13
Ramachandran favored (%)	97
Ramachandran allowed (%)	3.2
Ramachandran outliers (%)	0
Rotamer outliers (%)	0.47
Average B-factor	57.09
macromolecules	57.26
ligands	64.17
solvent	41.64

^a Values in parentheses are for the highest resolution shell.

^b $R_{\text{merge}} = \frac{\sum_{hkl} |I - \langle I \rangle|}{\sum_{hkl} I}$.

^c $R_{\text{work}} = \frac{\sum |F_{\text{obs}} - F_{\text{calc}}|}{\sum |F_{\text{obs}}|}$, where F_{obs} and F_{calc} are the observed and the calculated structure factors, respectively.

^d R_{free} is calculated using 5% of total reflections randomly chosen and excluded from the refinement.

The terminal residues 1–7, 338–350, and the C-terminal His₆-tag, as well as a part of the dynamic loop (residues 60–70) were not built into the structure models due to the lack of electron density. The monomer core structure of *Lm*FBPase has an $\alpha/\beta/\alpha/\beta/\alpha$ ‘club sandwich’ topology, with two mixed β -sheets flanked by α -helices on both sides (Figure 7.2). The active site is located at the end of the B9 strand and adjacent to the H8 helix. The effector site is located between the termini of helices H1 and H2, and incorporates the seven-residue loop (residues 20–26, on the short interface of the tetramer) joining these two helices. The F_o-F_c density map (Figure 7.3A) clearly illustrates the AMP binding conformation in the effector site, where the main-chain atoms of Ile16, Thr29, Arg25, Asp27 as well as the side-chains of Arg25, Asp112, Tyr113 are directly involved in the electrostatic interactions with AMP. The effector site is approximately 32 Å distance from the active site, which incorporates the binding of a catalytic product F6P (Figure 7.3B). But the other catalytic product P_i is not found in the density map. More descriptions and discussions of the homotetrameric structure assemblies and structural comparisons among different *Lm*FBPase conformations are shown in subsequent sections.

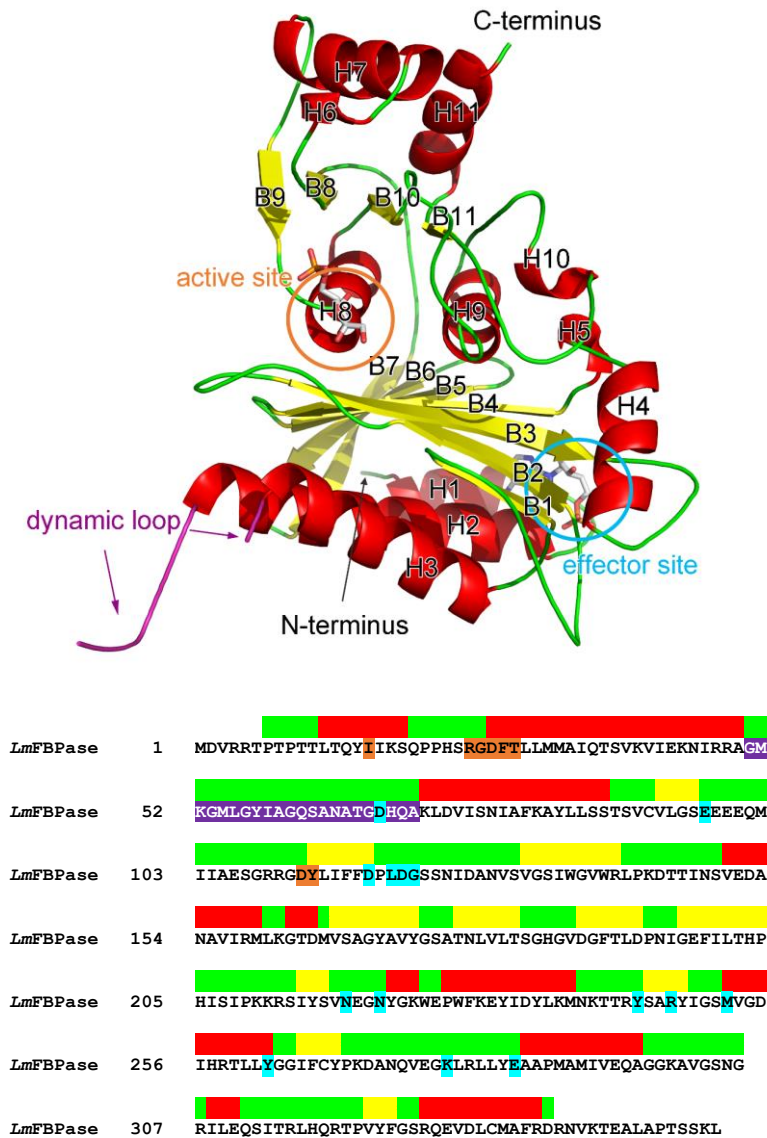


Figure 7.2 Overall structure and sequence of a monomer of *LmFBPase*.

The helices, strands, and loop regions are shown in red, yellow, and green cartoon ribbons, and the same colours are used to label the sequence. The positions of both ends of the ‘dynamic loop’ (residues 50–71) are shown with purple arrows in the figure, whereas its sequence is highlighted by purple background in the alignment. The position of the active site is shown with an orange circle in the structure, whereas its residue codes are highlighted by orange background in the alignment. Similarly, the effector site is shown in cyan. The terminal residues 1–7 and 338–350 as well as the C-terminal His-tag were not built into the structure models due to the lack of electron density.

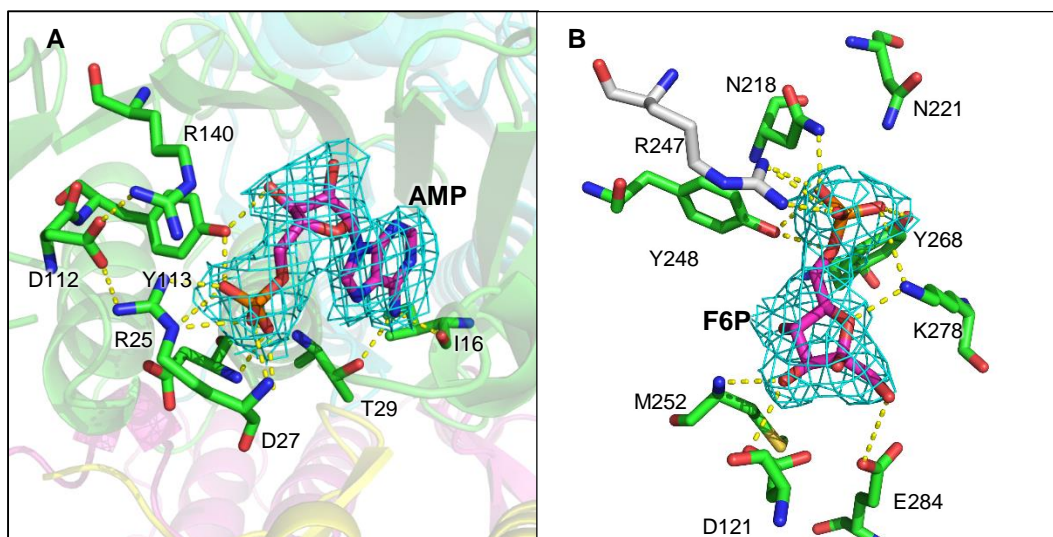


Figure 7.3 Conformation of the AMP and F6P binding sites in *LmFBPase*.

The electron density shown is from *Fo-Fc* maps contoured at the 3.0σ level using a cut-off radius of 1.65 \AA . The arginine from an adjacent chain is shown in grey.

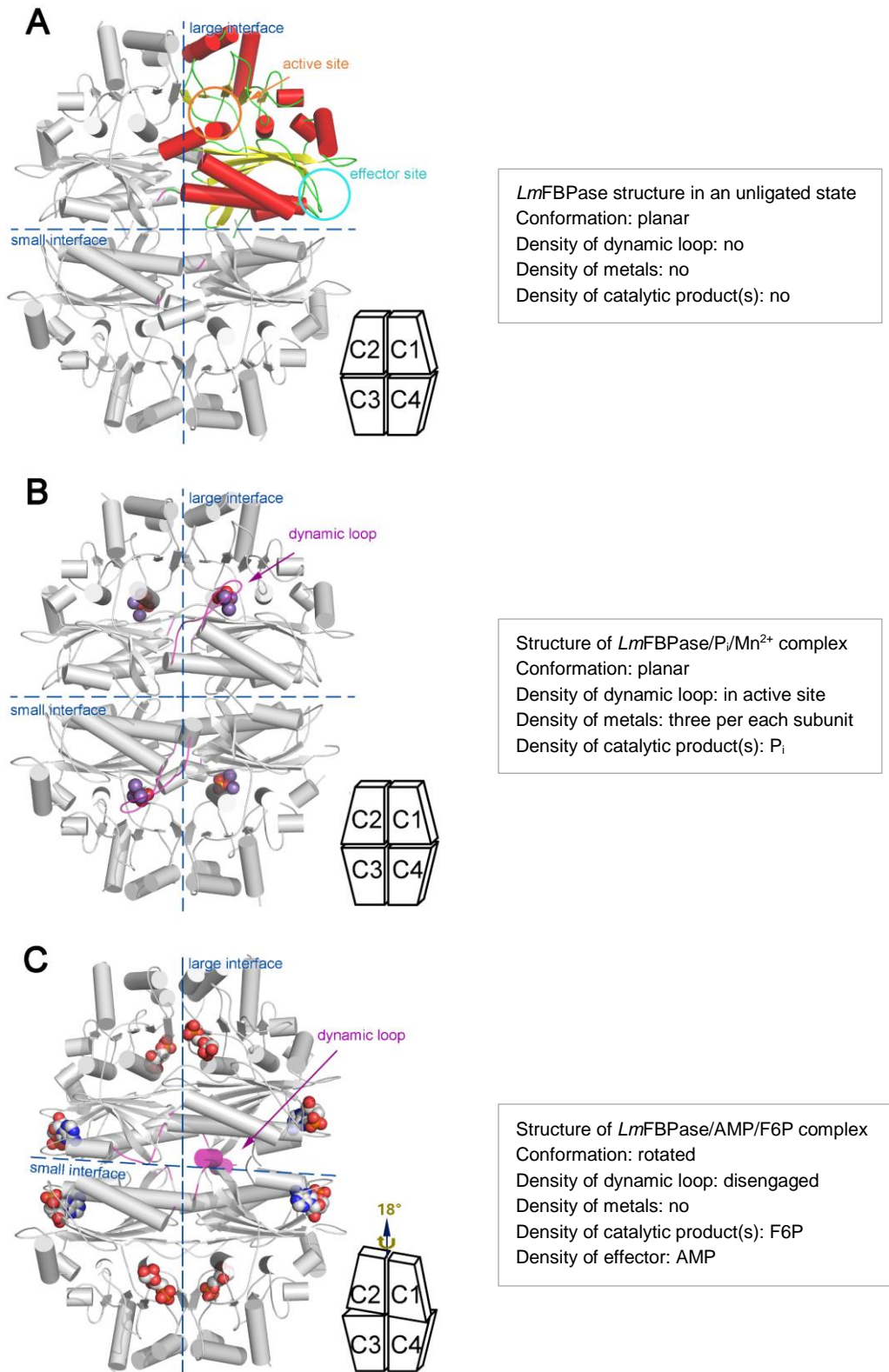


Figure 7.4 Overall structures of *LmFBPase*.

The large interface [between the Chain 1/Chain 4 (C1C4) dimer and the C2C3 dimer] and small interface (between the C1C2 dimer and the C3C4 dimer) are shown by dashed lines in each

homotetramer. The positions of active sites and effector sites are highlighted by arrows and circles in the first panel, where secondary structures are shown in different colours in Chain 1 (helices, β -strands and loop regions in red, yellow and green, respectively). Bound ligands are shown as spheres. The dynamic loops (residues 50–71) are indicated in purple. Schematic models [adapted from diagrams in (Gidh-Jain *et al.*, 1994)] are shown in the bottom right of each panel. A, *Lm*FBPase structure in an unligated state. B, Structure of *Lm*FBPase/phosphate/Mn²⁺ complex. C, Structure of *Lm*FBPase/AMP/F6P complex is in an allosterically inhibited conformation.

Table 7.4 Comparisons of structures of *L. major* and mammalian FBPases.

Structure name	<i>Lm</i> FBPase apoenzyme	<i>pl</i> FBPase apoenzyme	<i>Lm</i> FBPase/Mn/P _i	<i>pl</i> FBPase/F6P/P _i /Mg	<i>Lm</i> FBPase/F6P/P/AMP	<i>pl</i> FBPase/F6P/P _i /AMP/Mg
PDB code	ND ^b	2FBP	ND ^b	1EYI	ND ^b	1EYJ
Species/isoform	<i>L. major</i>	pig kidney ^a	<i>L. major</i>	pig liver	<i>L. major</i>	pig liver
Space group	P2 ₁ 2 ₁ 2 ₁	P3 ₂ 2 ₁	P2 ₁ 2 ₁ 2 ₁	I222	P2 ₁ 2 ₁ 2 ₁	P2 ₁ 2 ₁ 2
Topology	planar	planar	planar	planar	rotated	rotated
Ligand(s) in crystallisation drop	MgCl ₂ , KCl, F16BP	none	MgCl ₂ , MnCl ₂ , KCl, F16BP	MgCl ₂ , F6P, KP _i	MgCl ₂ , MnCl ₂ , KCl, F16BP, AMP	MgCl ₂ , F6P, KP _i , AMP
Ligand(s) in structure	none	none	P _i ; metal site 1: Mn; metal site 2: Mn; metal site 3: unknown blob	F6P; P _i ; metal site 1: Mg; metal site 2: Mg; metal site 3: unknown blob	F6P; AMP	F6P; P _i ; metal site 1: Mg; AMP
Dynamic loop	disordered	disordered	engaged	engaged	disengaged	disengaged
Reference	(Vasquez-Valdivieso, 2013)	(Ke <i>et al.</i> , 1989a)	(Vasquez-Valdivieso, 2013)	(Choe <i>et al.</i> , 2000)	this study	(Choe <i>et al.</i> , 2000)

^a Pig kidney and liver FBPase are essentially the same, as discussed in Section 1.3.5.1.

^b ND: not deposited yet.

Columns regarding *Lm*FBPase structures are shown in grey shade.

7.3.2 Secondary structure of *Lm*FBPase

Two interfaces are formed among the four monomers of the homotetramer of *Lm*FBPase, to constitute a small interface and a large interface (Figure 7.4). Small interface interactions mainly take place amid helices H1, H2, H3 and strands B6 and B7, as well as the loops between the two monomers (Figure 7.2). Moreover, this region, especially for the ‘locking loop’ ²⁰QPPHSRG²⁶ between helices H1 and H2, has more than one function, because it is also critical for the formation of the effector site (discussed in Section 7.3.4). This observation suggests that effector binding might affect the short interface interactions. The active site is located between two monomers in the position of the large interface, which highlights the catalytic importance of the formation and stability of the large interface. Intriguingly, not only interactions across

both the small and the large interfaces, but also interactions between diagonal chains (across the local 2-fold axis that define the 222 symmetry of the tetramer) were formed to stabilise the central position of the homotetramer (discussed in Section 7.3.6). For instance, the side chain of Asn195 in the loop region between strands B6 and B7 interacts with the side chain of another Asn195 belonging to the diagonal monomer (Figure 7.5C).

7.3.3 AMP changes the topology of the *Lm*FBPase tetramer but not the monomer

The monomer cores of the three structures of *Lm*FBPase are very similar, with an RMSD value lower than 1.0 Å. The binding of AMP significantly changes the overall tetramer structure of *Lm*FBPase. However, the overall conformations of the *apoenzyme* structure and the Mn²⁺-bound structure are very similar, with an RMSD value of only 0.99 Å (comparisons were made between two tetramers with Superpose, same as below) (Winn *et al.*, 2011). Both structures adopt a planar topology, which has no significant rotational movement of domains as analysed by Dyndom (Hayward & Lee, 2002). Structural superposition shows that these two planar tetramers adopt a similar topology to that of the active-state (namely R-state) mammalian FBPase (pig liver FBPase, PDB code: 1EYI), e.g. RMSD value of only 1.1 Å. However, the AMP-complexed structure shows a distinct topology, with an RMSD of 3.8 Å in comparison with a planar *Lm*FBPase structure. The difference is mainly because the binding of AMP induced an 18° pair-wise rotation along the small interface of the C1-C2 dimer relative to the C3-C4 dimer to yield a ‘rotated structure’ (Figure 7.4C).

7.3.4 Allosteric mechanism of *Lm*FBPase

A more detailed comparison between the planar and rotated structures enabled an allosteric mechanism to be proposed. As shown in Figure 7.5A, the conformational change from the planar conformation (represented by black solid trapezoid blocks) to the rotated conformation (represented by purple dashed blocks) mainly takes place along the short interface. In the planar structure (Figure 7.5B), where no AMP was bound, the position of the loop region between helices H1 and H2 (shown in green) is outward toward the C1-C4 short interface. Within this loop, His23 forms a hydrogen

bond with the main-chain oxygen of Gly108 across the short interface, and thereby locks the interface interaction. The AMP-binding pocket is in this region too (shown in purple), where its adenine interacts with Thr29 and its phospho group with Arg25, which are both on the same 'locking loop' as His23. Upon AMP binding to this pocket, the 'locking loop' is retracted, and the 'His23-lock' is pulled out from the interface interaction. Consequently, the unlocked chain (C4) becomes free to rotate. Likewise, the same 'unlock and rotate' effect also takes place on the other half (C2/C3) of the tetramer and the *Lm*FBPase tetramer adopts a 'rotated-state'. The sequence of the region in the mammalian enzymes corresponding to the locking loop in the *L. major* enzyme shows no conservation (residues 20–26) (Figure 1.13).

Moreover, in the planar structures (Figure 7.5C, green), the small interface is stabilised by electrostatic bonds across the small interface (e.g. Gln14-Ser87, Glu198-Thr37, Pro9-Tyr28, etc.). Upon dimer rotation, these bonds are disrupted to 'unzip' the short interface, and a new hydrogen bond Thr8-Ser87 is formed.

The hydrophilic centre of the tetramer is also re-organised upon AMP binding (Figure 7.5D). In the planar structure (left panel), a pair of salt bridges (Asp193-Lys44) are formed to lock both C1/C4 and C2/C3 short interfaces. The side-chain of Asn195 crosses the tetramer centre to interact with the Asn195 on the diagonally opposite chain. The low occupancies of Arg48 in both C2 and C4 suggest flexible side-chains. By contrast, residues in the centre of the tetramer of the rotated-state structure are completely re-organised (right panel). The flipped side chains of Arg48, with clear density, attracts the side chains of Asp193, thereby disrupting the small interface lock Asp193-Lys44. The diagonal trans-chain interaction between two Asn195 residues is also eliminated. In brief, the binding of AMP (a) pulls out and unlocks His23 from binding across the short interface, (b) unzips a series of interface bonds, (c) re-organises the tetramer centre, and (d) thereby induces the pairwise-rotation of *Lm*FBPase.

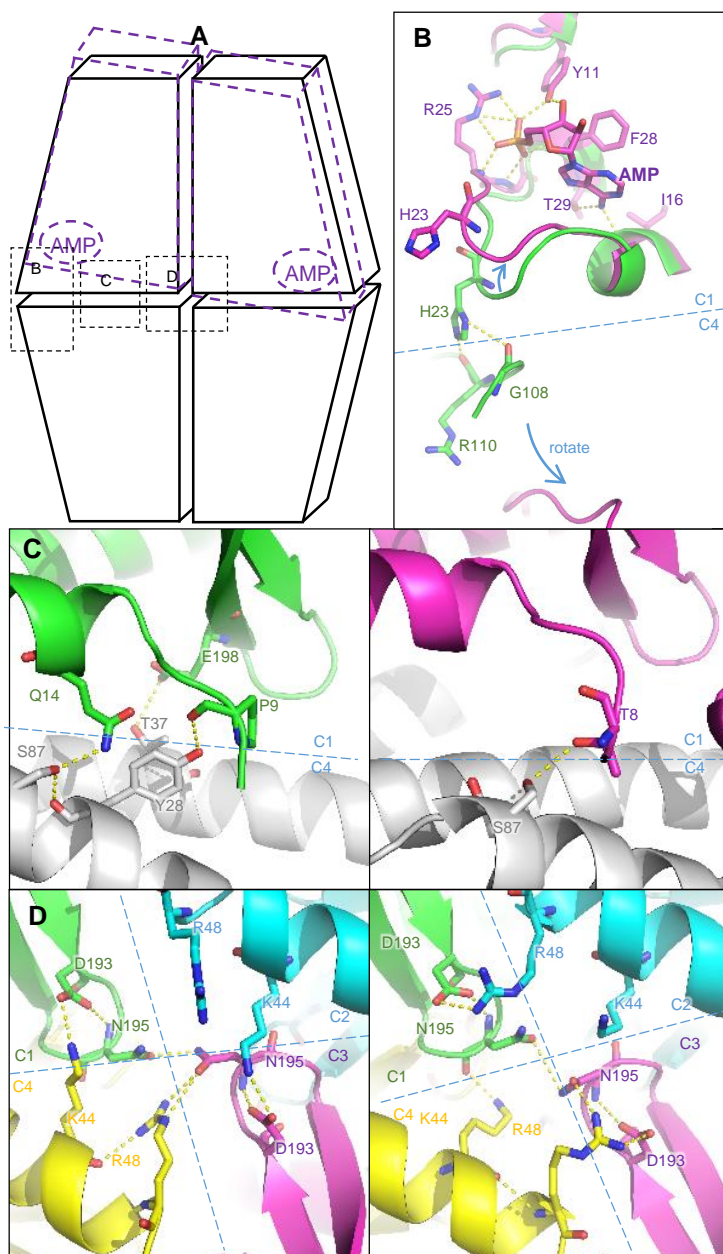


Figure 7.5 Crystal structures show allosteric effects of AMP on *LmFBPase*.

A. Schematic representations of the *LmFBPase* structures. Each trapezoid block represents a chain in this homotetramer [adapted from diagrams in (Gidh-Jain *et al.*, 1994)]. Black blocks show the planar topology, while the purple, rotated blocks represent the rotated state. AMP binding sites are indicated with purple ellipses. Positions corresponding to panels B, C and D are also indicated with black dashed rectangles.

B. Comparison of the AMP binding sites in the planar state structure (green) and the rotated state structure (purple). The planar state and the rotated state structures are superposed on Chain 1 (C1). The blue dashed line shows the short interface.

C. Comparison of the short interfaces of the planar state (left) and rotated state (right) structures. C1 chains are shown in green and purple for the planar and rotated state structures, respectively. C4 chains are shown in grey in each figure. The blue dashed line shows the short interface.

D. Comparison of the central interactions among chains in the planar state (left) and rotated state (right) structures. For each structure, C1, C2, C3 and C4 are represented in green, cyan, purple, and yellow, respectively. The blue dashed lines show chain interfaces.

7.3.5 Different conformations of the dynamic loop

Apart from the differences between planar and rotated structures caused by the binding of AMP, a second main difference among these three structures (the *LmFBPase apoenzyme* structure, *LmFBPase/P_i/Mn²⁺*, and *LmFBPase/F6P/AMP*) takes place within the dynamic loop (residues 50–71).

Dynamic loop of the *LmFBPase apoenzyme* structure. The hanging drop in which the *apoenzyme* structure was crystallised contained F16BP, K⁺ and Mg²⁺ (which are required for the activity of *LmFBPase*). However, none of the ligands (substrate, product, or metals) nor the dynamic loop was observed in the refined structure (Figure 7.4A). This is probably because during the crystallisation process, F16BP had been converted to F6P and P_i, which may dissociate under the crystallisation conditions. It also suggests that the dynamic loop is of greater flexibility under this catalytically active condition, which is required for the catalysis of *LmFBPase*. This observation corresponds to the *apoenzyme* structure of pig FBPase which is also in a planar topology (PDB code 2FBP), where the dynamic loop was also observed to be disordered (Ke *et al.*, 1989a).

Dynamic loop of the structure of *LmFBPase/P_i/Mn²⁺*. The dynamic loop of *LmFBPase* was found to be stabilised in an engaged conformation in the presence of P_i and manganese. This is consistent with the result that manganese dramatically increased the thermostability of *LmFBPase*. The catalytic product P_i is found in the active site, surrounded by two or three manganese atoms (Figure 7.8D).

Dynamic loop of the structure of *LmFBPase/F6P/AMP*. The hanging drop in which the AMP-complex structure was crystallised contained AMP, F16BP, Mn²⁺ and Mg²⁺. However, only AMP was found in the effector site, and one of the catalytic products F6P was found in the active site. The other catalytic product, phosphate ion, was not found in the complex structure. Apart from the 18°-pairwise rotation that takes place on the short interface upon binding of AMP (Figure 7.4C), the dynamic loop is also found extracted from the active site in a ‘disengaged conformation’, which is stabilised and interacted with by the diagonal subunit (Figure 7.6). In particular, the side chain

of Leu55 is trapped by a hydrophobic pocket in the diagonal subunit. Hence, the active site became incomplete and was thus catalytically inhibited.

The three conformations of the dynamic loop in the three different crystal structures — disordered, engaged with the active site, and disengaged — demonstrate its allosteric and catalytic importance.

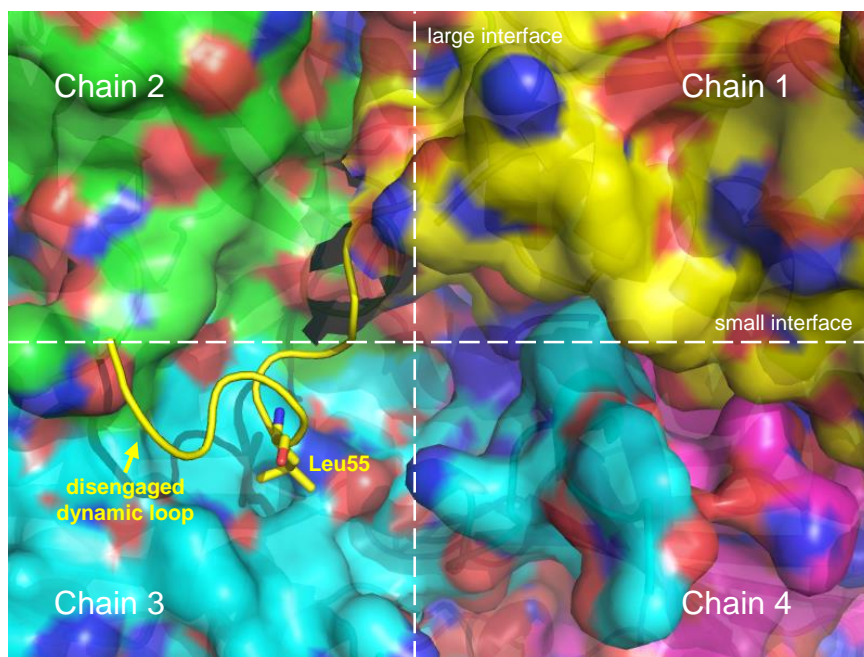


Figure 7.6 Interactions between disengaged dynamic loop and the diagonal subunit of *LmFBPase* in a rotated conformation.

This figure is generated from the *LmFBPase*/F6P/AMP (T-state) structure solved in this thesis. Chain 1, 2, 3, and 4 are shown in yellow, green, cyan, and purple, respectively. Blue and red surfaces represent nitrogen and oxygen atoms, respectively. Subunit interfaces are indicated with white dashed lines. The yellow loop represents the dynamic loop of Chain 1 (in a disengaged conformation).

7.3.6 Conformations of FBPase active sites under different conditions

Both mammalian and *Leishmania* FBPases require divalent metals like Mg^{2+} for catalysis (Section 6.5.5). The titration of Mg^{2+} against *Lm*FBPase exhibited a hyperbolic kinetic curve (Figure 6.10). In contrast, the enzymic activity of mammalian FBPases increases sigmoidally with the concentration of Mg^{2+} with the Hill coefficient for Mg^{2+} of approximately two (Nelson *et al.*, 2004, Rakus *et al.*, 2000, Rakus *et al.*, 2005). This corresponds with the observation that the divalent metal is retained at site I of each active site of the mammalian FBPase (Figure 7.7A), regardless of substrate/inhibitor binding (Choe *et al.*, 2000). However, the *Lm*FBPase structure that was crystallised under a similar condition, which also contains Mg^{2+} , K^+ and substrate in the crystal drop, shows an *apo*enzyme conformation where little density corresponding to the metal/substrate/product/dynamic loop position was found (Figure 7.7B). The correlation between the site-I Mg^{2+} binding observed in the crystal structures and the cooperativity of the divalent metals shown in the kinetic assay implies different metal-mediated cooperative mechanisms between mammalian and *L. major* FBPases, despite their similar active-site sequences (Figure 1.13) and similar conformations of the amino acids (Figure 7.7) involved in the metal/ P_i binding site. However, the mechanism of the different cooperative properties of Mg^{2+} is unknown.

In mammalian FBPase, three divalent metal ions are required for hydrolysis of F16BP (Choe *et al.*, 2000). Indeed, three blobs were found in each active site of the *Lm*FBPase/ Mn^{2+}/P_i structure (Figure 7.8D), but only manganese atoms at metal sites I and II can be confirmed as manganese according to the anomalous scattering at 1.89 Å at the absorption edge of manganese. There was little anomalous signal for site III. This probably arises from the binding of other atoms, e.g. magnesium, potassium, or water. Due to the lack of evidence, the site III ligand is labelled as an unknown ligand (UNK).

The reason for the presence of P_i is probably due to the remaining catalytic activity during crystallisation, despite the presumption that ~95% of the enzymic activity was inhibited by Mn^{2+} in the crystal drop (Figure 6.11). However, no density for the other catalytic product F6P was found in the active site, probably because of its relatively low affinity. Nevertheless, despite the similar crystallisation conditions to the

*apo*enzyme *Lm*FBPase structure where the dynamic loop was invisible in the electron density map, the dynamic loop in this Mn²⁺-stabilised structure was found to adopt an engaged conformation.

In the pig liver FBPase structure, catalytically important water molecule was found as a bridge between Asp74 and metal II (Figure 7.8C). This water molecule acts as a catalytic base in the abstraction of a proton from the second coordinated water molecule (coordinated with Glu98). However, this important water molecule is not found in the *Lm*FBPase/Mn/P_i structure. Instead, Asp74 adopts a closer position relative to metal II, which may form a direct ionic bond (3.4 Å) without mediation by a water molecule. Intriguingly, although manganese acts as a cofactor for mammalian FBPase activity (Benkovic & deMaine, 1982), here it was shown as a *Lm*FBPase inhibitor (Section 6.5.6 and Figure 6.11).

In mammalian FBPases, a divalent metal atom is retained at the metal site I (coordinated with F6P and P_i, as well as three acidic amino acids Asp118, Asp121, and Glu280) regardless of the conformational state. In contrast, no metal atoms are found in the active site in the *Lm*FBPase/F6P/AMP structure. This fits with the observation that magnesium shows no cooperative effect on *Lm*FBPase activity, whereas a positive cooperation was observed in mammalian FBPases (Nelson *et al.*, 2004). The overall *Lm*FBPase rotated structure adopts a similar topology to that of the T-state structure of pig liver FBPase (RMSD value of 0.85 Å). It also shows that formation of the complete active site is facilitated by Arg247 from the adjacent subunit across the large interface which forms an ionic interaction with the 6'-phospho group of the catalytic product F6P (Figure 7.8B). This interaction also demonstrates that the tetrameric form of *Lm*FBPase is necessary for catalysis.

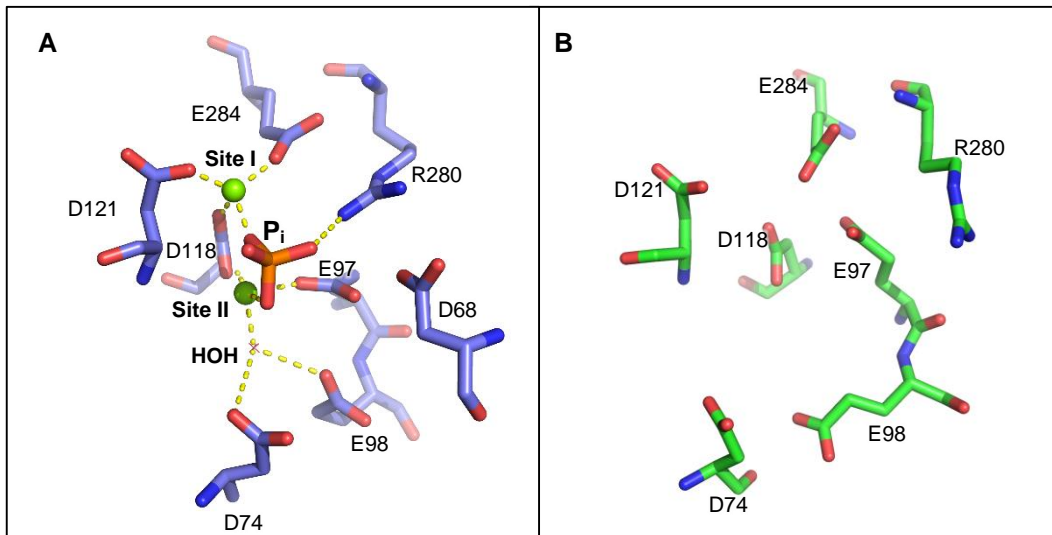


Figure 7.7 Comparison of active site conformations from mammalian and *Lm*FBPase structures crystallised with Mg^{2+} .

A. The active site of pig liver FBPase [blue, generated from the work by (Choe *et al.*, 2000), PDB code 1EYI]. This structure was co-crystallised with pig liver FBPase, magnesium, potassium, phosphate and F6P. Bound metal ions are shown in green spheres.
 B. The active site of *Lm*FBPase [green, generated from the work by (Vasquez-Valdivieso, 2013)]. This structure was co-crystallised with *Lm*FBPase, magnesium, potassium, and F16BP.

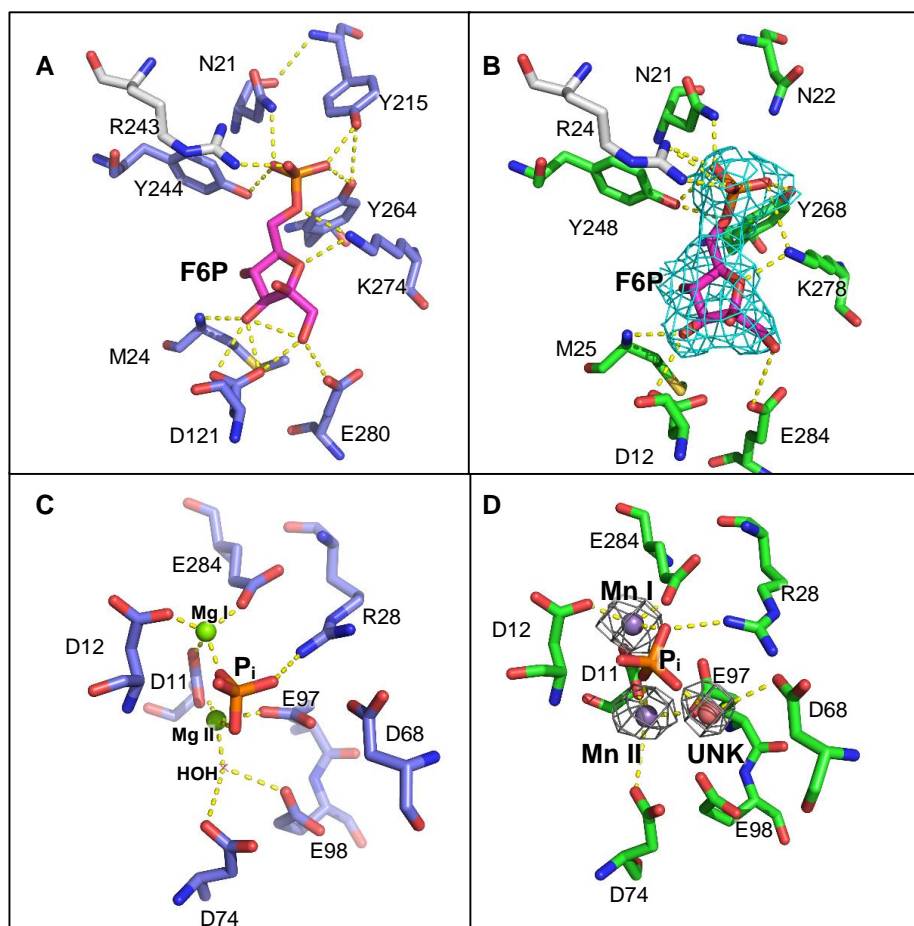


Figure 7.8 Comparison of the active sites of mammalian and *L. major* FBPsases.

Panels A and C, blue, pig liver FBPase, generated from the work by (Choe *et al.*, 2000), PDB code 1EYI. Panels B and D, green, *Lm*FBPase, generated from this study and (Vasquez-Valdivieso, 2013). F6P molecules are shown in magenta. Arginines from adjacent chains are shown in grey. The electron density of F6P in panel B (coloured in cyan) is from F_o-F_c maps contoured at the 3.0σ level using a cut-off radius of 1.65 Å. Electron density at the metal sites in panel D (grey mesh) is from $2F_o-F_c$ maps contoured at the 3.5σ level using a cut-off radius of 1.65 Å. The unknown cation at metal site III is labelled as 'UNK'.

7.3.7 Asn221 may be the reason for the low substrate affinity of *Lm*FBPase

Both the sequence alignment (Figure 1.13) and the structural comparison (Figure 7.8, A and B) show that the active sites among *Leishmania* and mammalian FBPases are conserved, except for a one-residue difference: the tyrosine that is responsible for binding to the 6'-phospho group of the catalytic substrate/product in mammalian FBPases, is replaced by Asn221 in *Lm*FBPase. This structure confirms our hypothesis that the side chain of Asn221 is not long enough to be able to interact with the ligand as the tyrosine does. This is also consistent with the observation that *Lm*FBPase has a weaker substrate binding affinity as well as lower turnover number compared to mammalian FBPases (Table 6.2). The similar kinetic parameters of *E. coli* FBPase which has a corresponding asparagine in its active site (Table 1.10) (Kelley-Loughnane *et al.*, 2002) may also strengthen the hypothesis.

F26BP is a competitive inhibitor against FBPases (shown in Section 6.5.8). The reason why F26BP binds more weakly to the active site of *Lm*FBPase (7.5 μM) than to those of mammalian FBPases (approximately 0.2 μM) also probably correlates with the tyrosine/asparagine replacement described above.

The crystal structure of pig liver FBPase in complex with F26BP binding in its active site was revealed by (Hines *et al.*, 2007a) (Figure 7.9A). In the current work, the F26BP was modelled into the active site of *Lm*FBPase, showing that it may adopt a similar binding conformation. The side chain of Asn221 is not long enough to be able to interact with the ligand as the tyrosine does. Therefore, the distance between the side chain of Asn221 and the closest atom on the 6'-phospho group of F26BP is too long (4.4 Å) for forming a hydrogen bond. This confirms our hypothesis that the Tyr \rightarrow Asn replacement may cause the lower inhibition *Lm*FBPase by F26BP.

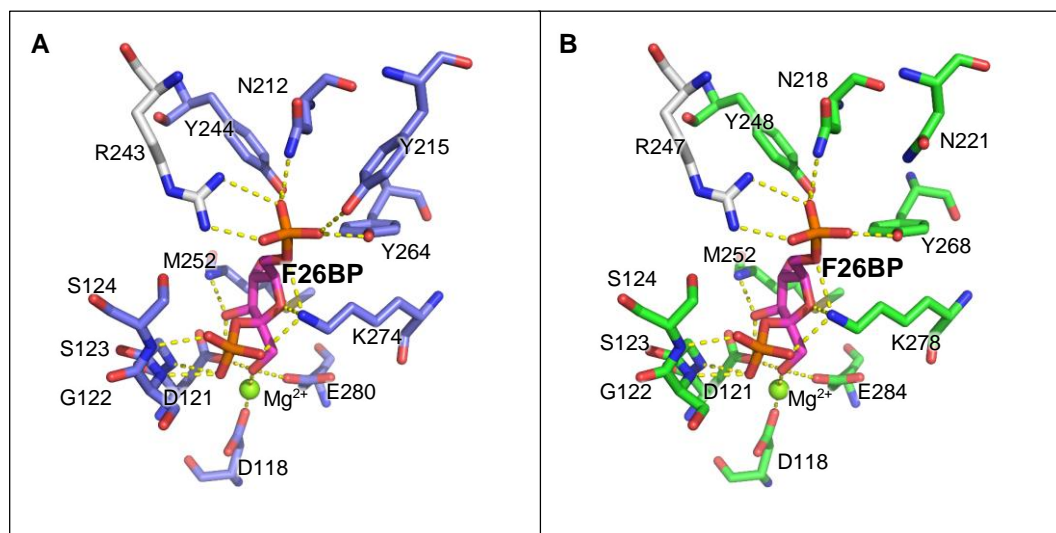


Figure 7.9 A modelled F26BP binding in the active site of *LmFBPase*.

A. Crystal structure of pig liver FBPase (PDB code: 2QVU) shows the binding mode of F26BP in its active site. B. The binding position of F26BP was modelled into the active site of *LmFBPase*. Arginines from adjacent chains are shown in grey.

7.3.8 Structurally distinct effector site offers a drug target against *LmFBPase*

Despite similar allosteric mechanisms between *Leishmania* and mammalian FBPsases (Section 1.3.5), both the sequence alignment (Figure 1.13) and the structural comparison (Figure 7.10) show that the AMP-binding sites of these FBPsases are poorly conserved. Zarzycki *et al.* (2011) solved a human FBPsase crystal structure in complex with AMP (Figure 7.10A) (Zarzycki *et al.*, 2011). It shows that seven residues are responsible for the electrostatic binding of AMP, whereas six residues are bound to AMP in *LmFBPase* (Figure 7.10B). Among the 7/6 residues with which AMP formed polar interactions, only two of them (the side-chain of Tyr113 and the main-chain oxygen of Thr29) are conserved. The conservation of Tyr113 and Thr29 suggests their potential evolutionary importance. A massive sequence alignment of 307 FBPsases from different organisms performed by Gao *et al.* (2014) also concluded the general importance of these two residues among all AMP-inhibited FBPsases (Gao *et al.*, 2014).

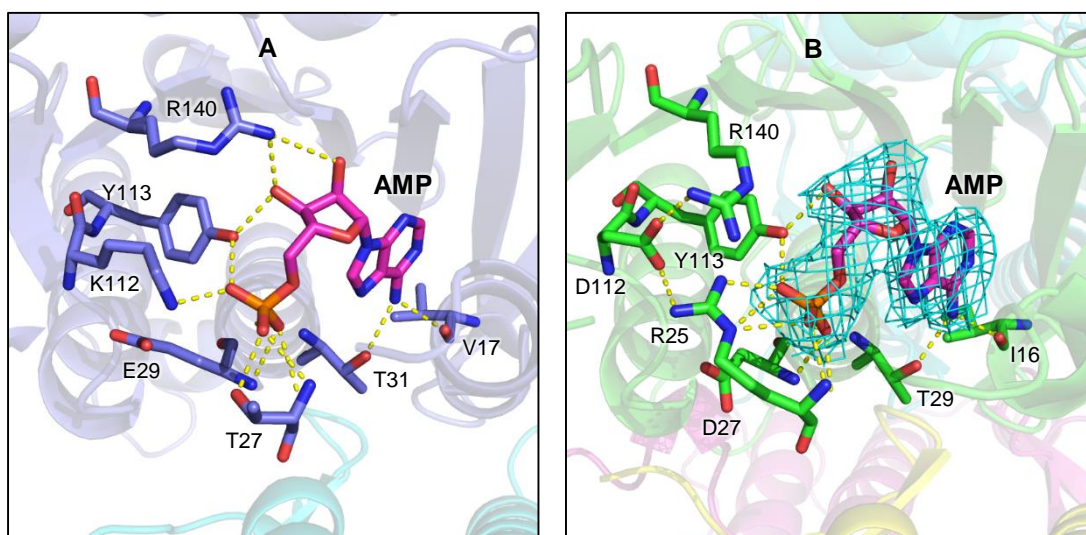


Figure 7.10 Comparison of AMP binding sites.

A. Conformation of the AMP binding site in human muscle FBPase (Zarzycki *et al.*, 2011) (blue, PDB code: 3IFA). B. Conformation of the AMP binding site in *LmFBPase* (green). The electron density shown is from $F_o - F_c$ maps contoured at the 3.0σ level using a cut-off radius of 1.65 \AA .

The side-chain of Thr27 in human FBPase forms a hydrogen bond with the phospho group of AMP. In *LmFBPase*, the corresponding residue is Arg25 which forms more and tighter interactions. Two relatively conserved differences are Val17 in human FBPase which is Ile16 in *LmFBPase*, while Glu29 is Asp27. The side chain of Arg140 in human FBPase interacts with the two hydroxyl groups of AMP. Arg140 remains conserved in *LmFBPase*, but is no longer able to bind with AMP. This is because of a significant change from a basic Lys112 in human FBPase to an acidic Asp112, which no longer interacts with AMP, but also attracts and twists the side-chain of Arg140 in *LmFBPase*, thereby disrupting its bonds to AMP. Hence, both bonds between AMP and Lys112/Arg140 are disrupted in *LmFBPase*, which is consistent with its weaker binding (Table 6.2).

LmFBPase can be considered as a potential drug target for diseases caused by *Leishmania* species. FBPase-null *L. major* lost both its ability to replicate in the macrophage phagolysosome, and to cause lesions in infected mice (Naderer *et al.*, 2006). In this study, it is shown that the structurally distinct effector site offers a promising target against *LmFBPase*. As shown in the *LmFBPase*/F6P/AMP complex crystal structure, the distinctive Asp112 provides an acidic, deeper pocket for inhibitor design.

Drugs targeting the AMP site of human FBPases have been extensively studied and designed for the treatment of type-2 diabetes (details shown in Section 1.3.5.2). For instance, benzoxazole benzenesulfonamides (Lai *et al.*, 2006), imidazole analogues (Dang *et al.*, 2007), and some tricyclic compounds (Tsukada *et al.*, 2009) have been demonstrated to bind to the effector site of human liver FBPases at the nanomolar level. Among these human FBPase inhibitors, some of them [e.g. CS-917 under clinical Phase 2b trials] have gained particular success (Erion *et al.*, 2005). These observations may also provide extensive insights into the design of drugs against *Lm*FBPase.

7.3.9 Structural mechanism of the AMP/F26BP synergistic inhibition of *Lm*FBPase

In 2007, Hines *et al.* revealed the first mammalian FBPase crystal structure co-crystallised with F26BP, showing that FBPase complexed with F26BP exhibits a 11° pairwise rotation of subunits along the small interface, which is similar to the T-state (Hines *et al.*, 2007a). F26BP binding induces a local structural rearrangement which is favourable for a disengaged dynamic loop rather than an engaged conformation. Both AMP and F26BP individually cause the structure to attain the T-state. But the mechanism of how the structural rearrangement on the large interface caused by F26BP binding affects the rotation along the small interface has remained unsolved. In 2014, Gao *et al.* demonstrated that the hydrophobic central cavity in FBPases, populated by water molecules, is an essential feature of the AMP/F26BP synergism (Gao *et al.*, 2014). *E. coli* FBPase with hydrophilic residues in this central cavity which is filled with hydrophilic side chains does not exhibit the AMP/F26BP synergism. By mutating the pig liver FBPase central residues to those of *E. coli* FBPase (i.e., Ser45→His, Thr46→Arg, Leu186→Tyr), the synergistic inhibitory effect on FBPase was diminished. Further, by comparing 307 eukaryotic and prokaryotic FBPase sequences¹, they showed that the side chain at position 45 is small in all compared eukaryotic FBPases, but large and hydrophilic in bacterial FBPases similar to *ec*FBPase. Therefore, they suggested an evolutionary pattern as well as a prediction model for the AMP/F26BP synergism based on the central residues, where glycine, alanine, cysteine, serine, or a gap are required for the synergistic effect. Unexpectedly,

¹ The 307 sequences compared by Gao *et al.* (2014) can be found in <https://1drv.ms/u/s!An9gBV9AQR6hgY840fbegVEGM5aTRQ>.

it is shown here that the AMP/F26BP synergistic inhibitory effect does function for *Lm*FBPase (Figure 6.16), despite its long, acidic glutamic acid at its position 45 (Figure 1.13).

Gao *et al.* showed that the organisation of water molecules within the hydrophobic central cavity of pig liver FBPase is important for the pairwise rotation of subunits. Unlike an R-state pig liver FBPase, a T-state FBPase changes its structure at both the dynamic loop and the central water molecules. The order-to-disorder transition of water molecules within the central cavity, caused by the movement of the dynamic loop from its engaged conformation, provides the requisite motive force for subunit pair rotation. In the case of *Lm*FBPase, which has a hydrophilic, filled centre, the pairwise rotation may be achieved by the re-arrangement of the central residues (Figure 7.5D). In the future, residue mutagenesis and molecular dynamic simulation may provide further information on the mechanism of the tetramer-centre-dependent pairwise rotation and the AMP/F26BP synergism.

The AMP/F26BP synergism can reduce the K_i of F26BP in the presence of AMP. Under this circumstance, the nanomolar-level of F26BP (concentration fluctuates at different cell stages) can realistically regulate the activity of *Lm*FBPase and thus gluconeogenesis.

7.3.10 Virtual screening for inhibitors against the effector site of *Lm*FBPase

Virtual screening is a computational approach that is able to analyse millions of compounds stored in databases using high-throughput computational docking onto ligand binding sites of proteins, thereby providing a focussed database for experimental high-throughput screening. Ligand Discovery At Edinburgh University (LIDAEUS) (Wu *et al.*, 2003, Taylor *et al.*, 2008) is our in-house high-throughput virtual screening program that uses a database of small-molecule 3D structures by fitting ligand atoms of each test structure onto site points representing the physicochemical properties and structure of the potential binding site. The strength of protein-ligand binding depends on the complementarity of shape and charge between

the ligand and the binding site, as well as a number of entropic factors. The program also applies a fast flexible conformational search to each ligand.

The effector sites between *L. major* and human FBPases are shown to be structurally distinct (Section 7.3.8), therefore offering a potential drug target against leishmaniases. For the virtual screening of small molecular compounds against the *Lm*FBPase effector site, the crystal structure of the *Lm*FBPase/AMP complex revealed in this study was subjected to LIDEAUS for compound screening against CAMELSICK2 (a multi-conformer database containing one million compounds with four million conformers). Conformations of the 500 top-scored compounds bound in this pocket were obtained and sorted according to the binding scores. Among these compounds, a family of dimethoxyphenyl pyrimidines were identified binding potently in the effector site (Figure 7.11). They show specific bonds to Arg25 of *Lm*FBPase, which is replaced by a threonine in mammalian FBPases. Experimental assays are to be carried out for the validation of the potency of these compounds. Moreover, the CS-917 series of inhibitors (under clinical Phase 2b trials) targeting this effector site of human FBPase are also worth trying for the inhibition of *Lm*FBPase.

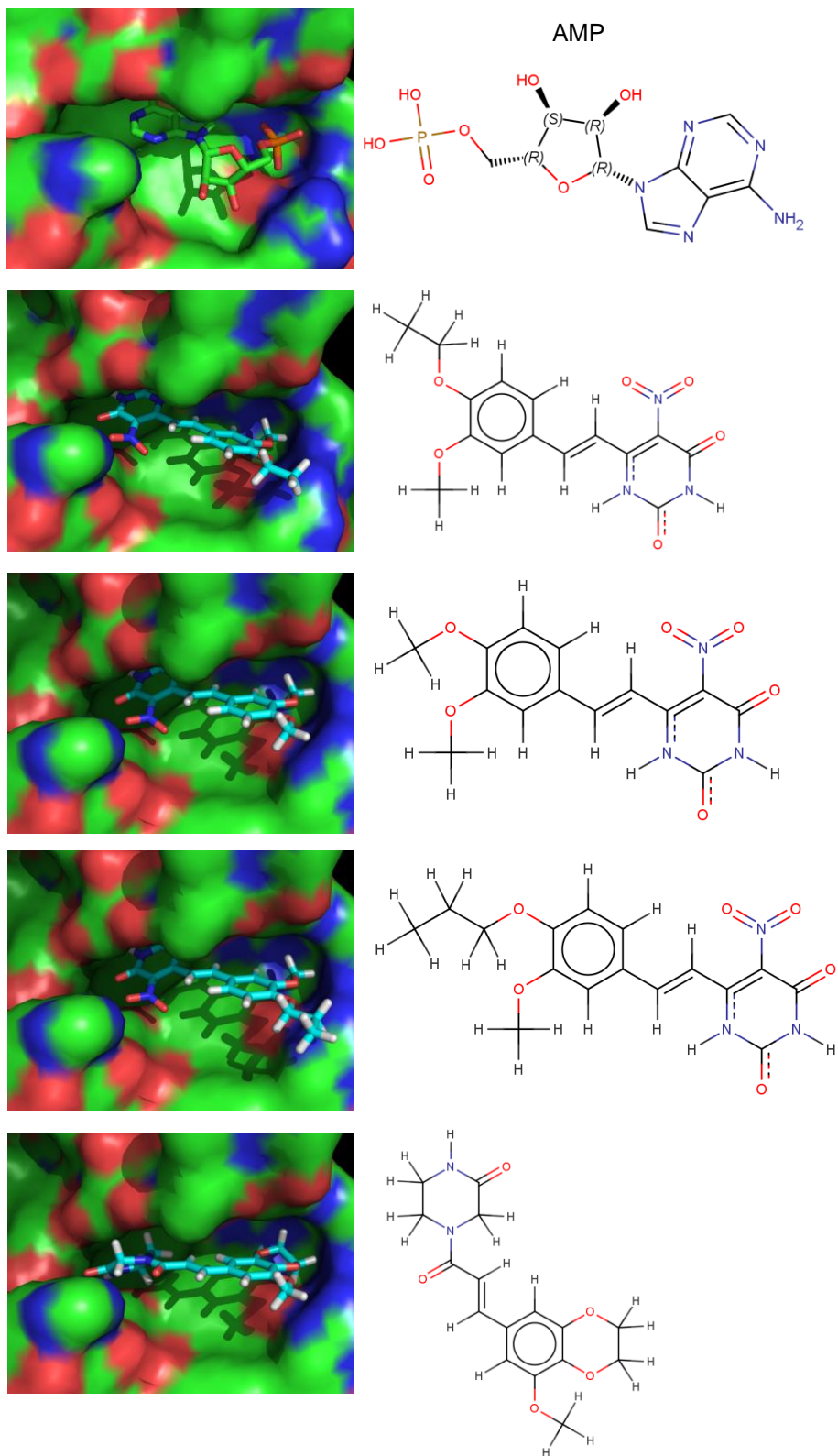


Figure 7.11 A series of potential inhibitors identified by LIDAEUS bound in the *Lm*FBPase effector site.

The first panel shows the natural ligand AMP for comparison.

7.3.11 A cocktail of PFK and FBPase inhibitors could be the ‘magic bullet’ for the treatment of diseases caused by *Leishmania*

L. major FBPase-null amastigotes were demonstrated to be able to survive the FBPase deletion (Naderer *et al.*, 2006). But they were shown to be unable to grow in the absence of hexose, and suspension in glycerol-containing medium resulted in rapid depletion of internal carbohydrate reserves. Further, *L. major* FBPase-null promastigotes were internalised by macrophages and able to differentiate into amastigotes but were unable to replicate in the macrophage phagolysosome. Similarly, the mutant persisted in mice but failed to generate normal lesions. It is likely that *Leishmania* amastigotes survive FBPase deletion (but are not able to proliferate anymore and form lesions), because of the possibility of reversal of the PFK reaction (Creek *et al.*, 2015). In this case, targeting of *Lm*FBPase alone to block gluconeogenesis might not be sufficient to eliminate all the parasites.

In another project carried out in our lab, a new series of nanomolar inhibitors have been discovered against PFK, a validated drug target in *T. brucei* (Albert *et al.*, 2005, McNae *et al.*, 2009). They are demonstrated to be potent *in vitro* inhibitors of *T. brucei* proliferation (unpublished data). Although these compounds are potent inhibitors of the PFKs of all three trypanosomatids, we do not expect them to kill the amastigotes of *T. cruzi* and *Leishmania* spp. This is because in contrast to bloodstream-form *T. brucei* which almost entirely relies on glycolysis for its ATP generation, the latter two species rely more on other metabolic processes for their free energy. But maybe the energy metabolic pathways of *T. cruzi* and *Leishmania* spp. can be inhibited when administered with other inhibitors. In that case, a cocktail of PFK and FBPase inhibitors could be the ‘magic bullet’ against *Leishmania* (and *T. cruzi*). (Professor Paul A. M. Michels, personal communication).

7.4 Conclusions

X-ray crystallographic studies show that the dynamic loop of *Lm*FBPase (residues 50–71) is flexible and of catalytic importance. Crystal structures reveal the allosteric mechanism of *Lm*FBPase in the presence of AMP. R-state structures adopt a planar

conformation, with disordered dynamic loops. The T-state structure forms upon AMP binding at effector sites, with dimers rotated along the short interface. This is because the binding of AMP displaces His23 and the associated 'locking loop' from binding across the short interface, and thereby unlocks the rotation of *Lm*FBPase. The rotation also unzips the short-interface bonds, re-organises bonds in the centre of the tetramer, disengages the dynamic loop, and therefore inhibits the enzymic activity.

The structure of the AMP site is poorly conserved between *Lm*FBPase and human FBPase. This provides an opportunity for structure-based drug discovery particularly against this binding site. As FBPase is a potential drug target against leishmaniases, proved to eliminate the replication and lesion effect of *Leishmania*, the structurally distinctive inhibitor binding site might be of particular therapeutic importance.

CHAPTER 8

Summary and forward look

CHAPTER 8. Summary and forward look

8.1 Summary of thesis

This thesis has described biochemical and structural studies of the M2-isoenzyme of human pyruvate kinase (M2PYK) and *Leishmania major* fructose-1,6-bisphosphatase (*Lm*FBPase) from. In particular, free amino acids and redox environments were discovered as regulatory factors of the oligomerisation state, conformation, and enzymic activity of M2PYK. Likewise, the allosteric inhibitory effect of AMP on *Leishmania* FBPase was revealed.

8.1.1 Pyruvate kinase

- Pyruvate kinase catalyses the final step of glycolysis, the conversion of ADP and PEP to ATP and pyruvate. It controls metabolic reprogramming for cell proliferation, and is thus a potential cancer therapeutic target. (0)
- Production of high-quality pure and active enzymes (wild-type M1PYK, wild-type M2PYK, M2PYK-C326S, and M2PYK-C358S) from *E. coli* were carried out, and the protocols proved to be robust and reproducible. (CHAPTER 3)
- Kinetic and biophysical properties of M1PYK and M2PYK were characterised. By combining the techniques of enzyme assay and analytical gel-filtration, it was demonstrated that M2PYK equilibrates between tetramer and monomer. In contrast, M1PYK is an intrinsic tetramer. (CHAPTER 3)
- Free amino acids stabilise the M2PYK tetramer over monomer. Certain amino acids regulate the activity of M2PYK allosterically, but in opposite ways, with some being inhibitors (e.g. alanine, phenylalanine, tryptophan, etc.) and others activators (e.g. serine, etc.). (CHAPTER 4)
- The allosteric mechanism of amino-acid modulation was studied by crystal structures of M2PYK in complex with amino-acid inhibitors and activator.

Inhibitory amino acids inhibit the enzymic activity by stabilising M2PYK in an inactive T-state. By contrast, other amino acids such as serine binding to the same site activate by rotating each subunit by 11° thereby stabilising the active R-state tetramer, where the complete active sites were formed with the assistance of adjacent subunits (Figure 8.1). (CHAPTER 4)

- Oxidative environments promote the dissociation of M2PYK, and thus reduce its enzymic activity. Reducing environments have the opposite effect. Cys326 is the most sensitive residue to the redox regulation. Because Cys326 is located on the interface of the tetramer, the oxidation of M2PYK can be prevented by holding it as a tetramer. (CHAPTER 5)
- Regulatory factors of M2PYK are summarised in Figure 8.1.

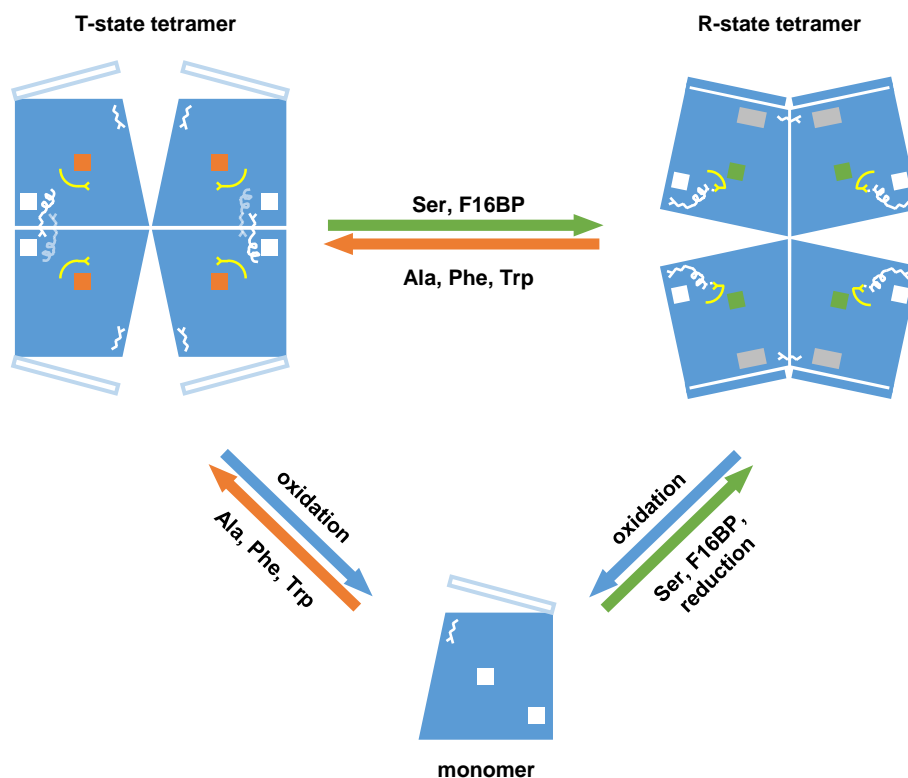


Figure 8.1 Regulatory factors of M2PYK.

Activation factors are shown with green arrows. Inhibitory factors are shown with blue and orange arrows. Detailed description is shown in CHAPTER 4, especially in Figure 4.17.

8.1.2 Fructose-1,6-bisphosphatase

- *Leishmania* are parasites that cause a spectrum of diseases, responsible for up to 40,000 deaths annually. The gluconeogenic enzyme fructose-1,6-bisphosphatase is a potential drug target against *Leishmania*. (0)
- Production of high-quality pure and active *Lm*FBPase from *E. coli* was carried out, and proved to be robust and reproducible. (CHAPTER 6)
- Kinetic properties of *Lm*FBPase were characterised. AMP was identified as an allosteric inhibitor of *Lm*FBPase. Fructose-2,6-bisphosphate is a competitive inhibitor. AMP and fructose-2,6-bisphosphate display synergistically inhibitory effects on *Lm*FBPase. (CHAPTER 6)
- X-ray crystallographic structures of *Lm*FBPase were studied. *Lm*FBPase was identified as a homotetramer. An important ‘dynamic loop’ that is stabilised in the active site, was proved to be of catalytic importance. Binding of AMP unlocks the dimer interface bonds, and thereby induces an 18° pairwise rotation between the two dimers (Figure 8.2). The rotation pulls the ‘dynamic loop’ out from the active site, disrupts the complete active site, and thereby inhibits the enzymic activity of *Lm*FBPase.
- The structure of the AMP site of *Lm*FBPase shows a different conformation from human FBPsases, thereby offering a potentially specific drug target.

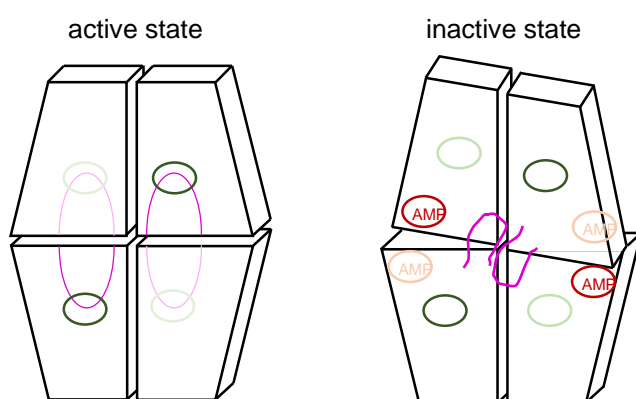


Figure 8.2 Allosteric models of *Lm*FBPase.

The active site, AMP site, and the dynamic loop are in green, red, and purple, respectively.

8.2 Forward look

8.2.1 Activator discovery against the amino-acid binding site of M2PYK

Activation of M2PYK is an effective strategy for the treatment of cancer, because it inhibits the Warburg effect in proliferative cells. Several activators of M2PYK have been discovered for the increase of its enzymic activity by binding to the F16BP pocket located on the A-A interface. In this study, it is shown that the amino acid binding site, located between the A-domain and the C-domain of M2PYK, is also a good target for the regulation of M2PYK activity. Therefore, this amino acid binding site is a potential target for the discovery of novel activators.

Potential activators have already been discovered by an initial virtual screening using a combination of similarity searching and docking to identify commercially available chemicals. Further experimental screenings will be carried out for the identification of M2PYK activators based on this virtual screening result. Identified hits will be subjected to cellular studies for the determination of their effects on cancer cell growth.

8.2.2 M2PYK activity and alanine biosynthesis: a rheostat-like relationship?

In this study, it is shown that alanine is a physiological inhibitor against M2PYK. Alanine transaminase (ALT), a metabolic enzyme that catalyses pyruvate to alanine in the presence of L-glutamate (and reverse), was found to be elevated in cancer patients (Chougule *et al.*, 2008). As a result, the inhibition of ALT activity is expected to reduce the production of alanine, which would be able to release the activity of M2PYK. This expectation was demonstrated in fish, by stimulating the PYK activity by dietary ALT inhibitors (Gonzalez *et al.*, 2012).

Deductively, M2PYK activity and alanine biosynthesis may interact as a rheostat-like relationship. In other words, the inhibition of M2PYK activity by alanine reduces the production of pyruvate, and thus alanine, thereby allowing greater M2PYK activity. The feedback regulation cycle of M2PYK/alanine/ALT seems physiologically realistic and contributive to cell proliferation. Further cellular studies may reveal its therapeutic importance.

8.2.3 T-state M2PYK may promote tumorigenesis

Inhibition of pyruvate kinase activity facilitates the biosynthesis of biomaterials, and thereby promotes the Warburg effect and tumorigenesis (Chaneton & Gottlieb, 2012). For example, it has been observed that a single switch from M1PYK (fully active) to M2PYK (less active) shifts cellular metabolism to aerobic glycolysis and that this promotes tumorigenesis (Christofk *et al.*, 2008a). Moreover, the dissociation of M2PYK from tetramers to dimers/monomers, which display little enzymic activity, has been shown to promote tumorigenesis and has been used as a cancer marker (Mazurek *et al.*, 2005). However, some studies have shown that M2PYK is the dominant isoform, regardless of the tissue type (Bluemlein *et al.*, 2011); and dissociated M2PYK is not always a good cancer marker (Li *et al.*, 2012). In this thesis, it is shown that M2PYK can be stabilised as a T-state inactive tetramer by metabolites, e.g. hydrophobic free amino acids. It provides another possible explanation to these observations, where the enzymic activity of non-dissociated M2PYK is inhibited and capable of promoting tumorigenesis. Once this hypothesis is confirmed, it may be possible to use the T-state tetrameric M2PYK as a cancer marker and therapeutic target.

8.2.4 Oxidation and dissociation of M2PYK, a chicken and egg situation

Oxidative environments promote the dissociation of M2PYK, and thus reduce its enzymic activity. The dissociation from tetramer to monomer exposes the redox-sensitive residue Cys326 on the A-A interface of M2PYK, which further facilitates the oxidation of M2PYK, i.e., the oxidation and dissociation of M2PYK promote each other. As a matter of fact, the oxidation and the dissociation of M2PYK is likely a chicken and egg situation. As a result, the discovery of new M2PYK tetramerising agents may prevent M2PYK from being a redox sensor.

8.2.5 Experimental screening of *Lm*FBPase inhibitors

The structure of the AMP site of *Lm*FBPase shows a different conformation from human FBPsases, thereby offering a potential specific drug target. Virtual screening of inhibitors against the AMP site of *Lm*FBPase has been carried out and identified

promising hits. Further experimental screening for *Lm*FBPase inhibitory compounds targeting the specific AMP site will be carried out. X-ray crystallography may be used to obtain co-crystal structures of *Lm*FBPase in complex with inhibitors, which can be further subjected to structure-activity relationship (SAR) studies to generate more potent inhibitors. *In vitro* studies can be carried out for the characterisation of the leishmanicidal activity of the discovered FBPase inhibitors.

References

- Achcar, F., Barrett, M. P. & Breitling, R. (2013). Explicit consideration of topological and parameter uncertainty gives new insights into a well-established model of glycolysis. *FEBS J.* **280**, 4640-4651.
- Aft, R., Zhang, F. & Gius, D. (2002). Evaluation of 2-deoxy-D-glucose as a chemotherapeutic agent: mechanism of cell death. *Br. J. Cancer* **87**, 805-812.
- Akhtar, K., Gupta, V., Koul, A., Alam, N., Bhat, R. & Bamezai, R. N. (2009). Differential behavior of missense mutations in the intersubunit contact domain of the human pyruvate kinase M2 isozyme. *J. Biol. Chem.* **284**, 11971-11981.
- Alam, A., Neyaz, M. K. & Ikramul Hasan, S. (2014). Exploiting unique structural and functional properties of malarial glycolytic enzymes for antimalarial drug development. *Malaria research and treatment* **2014**, 451065.
- Albert, M. A., Haanstra, J. R., Hannaert, V., Van Roy, J., Opperdoes, F. R., Bakker, B. M. & Michels, P. A. (2005). Experimental and in silico analyses of glycolytic flux control in bloodstream form *Trypanosoma brucei*. *J. Biol. Chem.* **280**, 28306-28315.
- Alvar, J., Croft, S. & Olliaro, P. (2006). Chemotherapy in the treatment and control of leishmaniasis. *Adv. Parasitol.* **61**, 223-274.
- Alvar, J., Velez, I. D., Bern, C., Herrero, M., Desjeux, P., Cano, J., Jannin, J. & den Boer, M. (2012). Leishmaniasis worldwide and global estimates of its incidence. *PLoS ONE* **7**, e35671.
- Anastasiou, D., Pouligiannis, G., Asara, J. M., Boxer, M. B., Jiang, J. K., Shen, M., Bellinger, G., Sasaki, A. T., Locasale, J. W., Auld, D. S., Thomas, C. J., Vander Heiden, M. G. & Cantley, L. C. (2011). Inhibition of pyruvate kinase M2 by reactive oxygen species contributes to cellular antioxidant responses. *Science* **334**, 1278-1283.
- Anastasiou, D., Yu, Y., Israelsen, W. J., Jiang, J. K., Boxer, M. B., Hong, B. S., Tempel, W., Dimov, S., Shen, M., Jha, A., Yang, H., Mattaini, K. R., Metallo, C. M., Fiske, B. P., Courtney, K. D., Malstrom, S., Khan, T. M., Kung, C., Skoumbourdis, A. P., Veith, H., Southall, N., Walsh, M. J., Brimacombe, K. R., Leister, W., Lunt, S. Y., Johnson, Z. R., Yen, K. E., Kunii, K., Davidson, S. M., Christofk, H. R., Austin, C. P., Inglese, J., Harris, M. H., Asara, J. M., Stephanopoulos, G., Salituro, F. G., Jin, S., Dang, L., Auld, D. S., Park, H. W., Cantley, L. C., Thomas, C. J. & Vander Heiden, M. G. (2012). Pyruvate kinase M2 activators promote tetramer formation and suppress tumorigenesis. *Nat. Chem. Biol.* **8**, 839-847.
- Anitha, M., Kaur, G., Baquer, N. Z. & Bamezai, R. (2004). Dominant negative effect of novel mutations in pyruvate kinase-M2. *DNA Cell Biol.* **23**, 442-449.

- Ashizawa, K., Willingham, M., Liang, C. & Cheng, S.-Y. (1991). In vivo regulation of monomer-tetramer conversion of pyruvate kinase subtype M2 by glucose is mediated via fructose 1, 6-bisphosphate. *J. Biol. Chem.* **266**, 16842-16846.
- Aykin-Burns, N., Ahmad, I. M., Zhu, Y., Oberley, L. W. & Spitz, D. R. (2009). Increased levels of superoxide and H₂O₂ mediate the differential susceptibility of cancer cells versus normal cells to glucose deprivation. *Biochem. J.* **418**, 29-37.
- Barciszewski, J., Wisniewski, J., Kolodziejczyk, R., Jaskolski, M., Rakus, D. & Dzugaj, A. (2016). T-to-R switch of muscle fructose-1,6-bisphosphatase involves fundamental changes of secondary and quaternary structure. *Acta crystallographica. Section D, Structural biology* **72**, 536-550.
- Barrett, M. P. & Croft, S. L. (2012). Management of trypanosomiasis and leishmaniasis. *Br. Med. Bull.* **104**, 175-196.
- Barros-Alvarez, X., Gualdron-Lopez, M., Acosta, H., Caceres, A. J., Graminha, M. A., Michels, P. A., Concepcion, J. L. & Quinones, W. (2014). Glycosomal targets for anti-trypanosomatid drug discovery. *Curr. Med. Chem.* **21**, 1679-1706.
- Battye, T. G., Kontogiannis, L., Johnson, O., Powell, H. R. & Leslie, A. G. (2011). iMOSFLM: a new graphical interface for diffraction-image processing with MOSFLM. *Acta Crystallogr. D Biol. Crystallogr.* **67**, 271-281.
- Benkovic, S. J. & deMaine, M. M. (1982). *Adv. Enzymol. Relat. Areas Mol. Biol.*, pp. 45-82: John Wiley & Sons, Inc.
- Bhardwaj, A. & Das, S. (2016). SIRT6 deacetylates PKM2 to suppress its nuclear localization and oncogenic functions. *Proc. Natl. Acad. Sci. U. S. A.* **113**, E538-547.
- Bie, J., Liu, S., Zhou, J., Xu, B. & Shen, Z. (2014). Design, synthesis and biological evaluation of 7-nitro-1H-indole-2-carboxylic acid derivatives as allosteric inhibitors of fructose-1,6-bisphosphatase. *Bioorg. Med. Chem.* **22**, 1850-1862.
- Blangy, D., Buc, H. & Monod, J. (1968). Kinetics of the allosteric interactions of phosphofructokinase from Escherichia coli. *J. Mol. Biol.* **31**, 13-35.
- Bluemlein, K., Gruning, N. M., Feichtinger, R. G., Lehrach, H., Kofler, B. & Ralser, M. (2011). No evidence for a shift in pyruvate kinase PKM1 to PKM2 expression during tumorigenesis. *Oncotarget* **2**, 393-400.
- Bollenbach, T. J., Mesecar, A. D. & Nowak, T. (1999). Role of lysine 240 in the mechanism of yeast pyruvate kinase catalysis. *Biochemistry* **38**, 9137-9145.
- Boxer, M. B., Jiang, J. K., Vander Heiden, M. G., Shen, M., Skoumbourdis, A. P., Southall, N., Veith, H., Leister, W., Austin, C. P., Park, H. W., Inglese, J., Cantley, L. C., Auld, D. S. & Thomas, C. J. (2010). Evaluation of substituted N,N'-diarylsulfonamides as activators of the tumor cell specific M2 isoform of pyruvate kinase. *J. Med. Chem.* **53**, 1048-1055.
- Brimacombe, K. R., Walsh, M. J., Liu, L., Vasquez-Valdivieso, M. G., Morgan, H. P., McNae, I., Fothergill-Gilmore, L. A., Michels, P. A., Auld, D. S., Simeonov, A.,

- Walkinshaw, M. D., Shen, M. & Boxer, M. B. (2014). Identification of ML251, a Potent Inhibitor of *T. brucei* and *T. cruzi* Phosphofructokinase. *ACS Med Chem Lett* **5**, 12-17.
- Brinck, U., Eigenbrodt, E., Oehmke, M., Mazurek, S. & Fischer, G. (1994). L-Pyruvate and M(2)-Pyruvate Kinase Expression in Renal-Cell Carcinomas and Their Metastases. *Virchows Arch. Int. J. Pathol.* **424**, 177-185.
- Brown, G., Singer, A., Lunin, V. V., Proudfoot, M., Skarina, T., Flick, R., Kochinyan, S., Sanishvili, R., Joachimiak, A., Edwards, A. M., Savchenko, A. & Yakunin, A. F. (2009). Structural and biochemical characterization of the type II fructose-1,6-bisphosphatase GlpX from *Escherichia coli*. *J. Biol. Chem.* **284**, 3784-3792.
- Burchmore, R. J. & Hart, D. T. (1995). Glucose transport in amastigotes and promastigotes of *Leishmania mexicana mexicana*. *Mol. Biochem. Parasitol.* **74**, 77-86.
- Burton, V. A., Chen, M., Ong, W. C., Ling, T., Fromm, H. J. & Stayton, M. M. (1993). High-level expression of porcine fructose-1,6-bisphosphatase in *Escherichia coli*: purification and characterization of the enzyme. *Biochem. Biophys. Res. Commun.* **192**, 511-517.
- Cairns, R. A., Harris, I. S. & Mak, T. W. (2011). Regulation of cancer cell metabolism. *Nat. Rev. Cancer* **11**, 85-95.
- Carminatti, H., de Asúa, L. J., Leiderman, B. & Rozengurt, E. (1971). Allosteric properties of skeletal muscle pyruvate kinase. *J. Biol. Chem.* **246**, 7284-7288.
- Centers for Disease Control and Prevention (2011). *Neglected Tropical Diseases*, <http://www.cdc.gov/globalhealth/ntd/diseases/index.html>.
- Chaneton, B. & Gottlieb, E. (2012). Rocking cell metabolism: revised functions of the key glycolytic regulator PKM2 in cancer. *Trends Biochem. Sci.* **37**, 309-316.
- Chaneton, B., Hillmann, P., Zheng, L., Martin, A. C., Maddocks, O. D., Chokkathukalam, A., Coyle, J. E., Jankevics, A., Holding, F. P., Vousden, K. H., Frezza, C., O'Reilly, M. & Gottlieb, E. (2012). Serine is a natural ligand and allosteric activator of pyruvate kinase M2. *Nature* **491**, 458-462.
- Chen, C., Wang, T., Wu, F., Huang, W., He, G., Ouyang, L., Xiang, M., Peng, C. & Jiang, Q. (2014). Combining structure-based pharmacophore modeling, virtual screening, and in silico ADMET analysis to discover novel tetrahydro-quinoline based pyruvate kinase isozyme M2 activators with antitumor activity. *Drug Des. Devel. Ther.* **8**, 1195-1210.
- Chen, J., Jiang, Z., Wang, B., Wang, Y. & Hu, X. (2012). Vitamin K(3) and K(5) are inhibitors of tumor pyruvate kinase M2. *Cancer Lett.* **316**, 204-210.

- Chen, J., Xie, J., Jiang, Z., Wang, B., Wang, Y. & Hu, X. (2011). Shikonin and its analogs inhibit cancer cell glycolysis by targeting tumor pyruvate kinase-M2. *Oncogene* **30**, 4297-4306.
- Chen, Z., Lu, W., Garcia-Prieto, C. & Huang, P. (2007). The Warburg effect and its cancer therapeutic implications. *J. Bioenerg. Biomembr.* **39**, 267-274.
- Cheng, X., Friesen, R. H. & Lee, J. C. (1996). Effects of conserved residues on the regulation of rabbit muscle pyruvate kinase. *J. Biol. Chem.* **271**, 6313-6321.
- Chiadmi, M., Navaza, A., Miginiac-Maslow, M., Jacquot, J. P. & Cherfils, J. (1999). Redox signalling in the chloroplast: structure of oxidized pea fructose-1,6-bisphosphate phosphatase. *EMBO J.* **18**, 6809-6815.
- Choe, J. Y., Fromm, H. J. & Honzatko, R. B. (2000). Crystal structures of fructose 1,6-bisphosphatase: mechanism of catalysis and allosteric inhibition revealed in product complexes. *Biochemistry* **39**, 8565-8574.
- Choe, J. Y., Nelson, S. W., Arienti, K. L., Axe, F. U., Collins, T. L., Jones, T. K., Kimmich, R. D., Newman, M. J., Norvell, K., Ripka, W. C., Romano, S. J., Short, K. M., Slee, D. H., Fromm, H. J. & Honzatko, R. B. (2003). Inhibition of fructose-1,6-bisphosphatase by a new class of allosteric effectors. *J. Biol. Chem.* **278**, 51176-51183.
- Choe, J. Y., Poland, B. W., Fromm, H. J. & Honzatko, R. B. (1998). Role of a dynamic loop in cation activation and allosteric regulation of recombinant porcine fructose-1,6-bisphosphatase. *Biochemistry* **37**, 11441-11450.
- Chougule, A., Hussain, S. & Agarwal, D. P. (2008). Prognostic and diagnostic value of serum pseudocholinesterase, serum aspartate transaminase, and serum alinine transaminase in malignancies treated by radiotherapy. *J. Cancer Res. Ther.* **4**, 21-25.
- Christofk, H. R., Vander Heiden, M. G., Harris, M. H., Ramanathan, A., Gerszten, R. E., Wei, R., Fleming, M. D., Schreiber, S. L. & Cantley, L. C. (2008a). The M2 splice isoform of pyruvate kinase is important for cancer metabolism and tumour growth. *Nature* **452**, 230-233.
- Christofk, H. R., Vander Heiden, M. G., Wu, N., Asara, J. M. & Cantley, L. C. (2008b). Pyruvate kinase M2 is a phosphotyrosine-binding protein. *Nature* **452**, 181-186.
- Christophe, J. (1995). Glucagon receptors: from genetic structure and expression to effector coupling and biological responses. *Biochim. Biophys. Acta* **1241**, 45-57.
- Chung, S. Y. & Subbiah, S. (1996). A structural explanation for the twilight zone of protein sequence homology. *Structure* **4**, 1123-1127.
- Clower, C. V., Chatterjee, D., Wang, Z. X., Cantley, L. C., Heiden, M. G. V. & Krainer, A. R. (2010). The alternative splicing repressors hnRNP A1/A2 and PTB influence pyruvate kinase isoform expression and cell metabolism. *Proc. Natl. Acad. Sci. U. S. A.* **107**, 1894-1899.

- Consler, T. G., Jennewein, M. J., Cai, G. Z. & Lee, J. C. (1990). Synergistic effects of proton and phenylalanine on the regulation of muscle pyruvate kinase. *Biochemistry* **29**, 10765-10771.
- Consler, T. G., Jennewein, M. J., Cai, G. Z. & Lee, J. C. (1992). Energetics of allosteric regulation in muscle pyruvate kinase. *Biochemistry* **31**, 7870-7878.
- Cotton, C. A., Kabasakal, B. V., Miah, N. A. & Murray, J. W. (2015). Structure of the dual-function fructose-1,6/sedoheptulose-1,7-bisphosphatase from *Thermosynechococcus elongatus* bound with sedoheptulose-7-phosphate. *Acta crystallographica. Section F, Structural biology communications* **71**, 1341-1345.
- Creek, D. J., Mazet, M., Achcar, F., Anderson, J., Kim, D. H., Kamour, R., Morand, P., Millerioux, Y., Biran, M., Kerkhoven, E. J., Chokkathukalam, A., Weidt, S. K., Burgess, K. E., Breitling, R., Watson, D. G., Bringaud, F. & Barrett, M. P. (2015). Probing the metabolic network in bloodstream-form *Trypanosoma brucei* using untargeted metabolomics with stable isotope labelled glucose. *PLoS Pathog.* **11**, e1004689.
- Cull, B., Prado Godinho, J. L., Fernandes Rodrigues, J. C., Frank, B., Schurigt, U., Williams, R. A., Coombs, G. H. & Mottram, J. C. (2014). Glycosome turnover in *Leishmania major* is mediated by autophagy. *Autophagy* **10**, 2143-2157.
- Daie, J. (1993). Cytosolic fructose-1,6-bisphosphatase: A key enzyme in the sucrose biosynthetic pathway. *Photosynth. Res.* **38**, 5-14.
- Dang, Q., Brown, B. S., Liu, Y., Rydzewski, R. M., Robinson, E. D., van Poelje, P. D., Reddy, M. R. & Erion, M. D. (2009). Fructose-1,6-bisphosphatase inhibitors. 1. Purine phosphonic acids as novel AMP mimics. *J. Med. Chem.* **52**, 2880-2898.
- Dang, Q., Kasibhatla, S. R., Reddy, K. R., Jiang, T., Reddy, M. R., Potter, S. C., Fujitaki, J. M., van Poelje, P. D., Huang, J., Lipscomb, W. N. & Erion, M. D. (2007). Discovery of potent and specific fructose-1,6-bisphosphatase inhibitors and a series of orally-bioavailable phosphoramidase-sensitive prodrugs for the treatment of type 2 diabetes. *J. Am. Chem. Soc.* **129**, 15491-15502.
- Dang, Q., Kasibhatla, S. R., Xiao, W., Liu, Y., Dare, J., Taplin, F., Reddy, K. R., Scarlato, G. R., Gibson, T., van Poelje, P. D., Potter, S. C. & Erion, M. D. (2010). Fructose-1,6-bisphosphatase inhibitors. 2. design, synthesis, and structure-activity relationship of a series of phosphonic acid containing benzimidazoles that function as 5'-adenosinemonophosphate (AMP) mimics. *J. Med. Chem.* **53**, 441-451.
- Dang, Q., Kasibhatla, S. R., Jiang, T., Taplin, F., Gibson, T., Potter, S. C., van Poelje, P. D. & Erion, M. D. (2011a). Oxazole phosphonic acids as fructose 1,6-bisphosphatase inhibitors with potent glucose-lowering activity. *Medchemcomm* **2**, 287-290.
- Dang, Q., Liu, Y., Cashion, D. K., Kasibhatla, S. R., Jiang, T., Taplin, F., Jacintho, J. D., Li, H., Sun, Z., Fan, Y., DaRe, J., Tian, F., Li, W., Gibson, T., Lemus, R., van Poelje, P. D., Potter, S. C. & Erion, M. D. (2011b). Discovery of a series of phosphonic acid-containing thiazoles and orally bioavailable diamide prodrugs that

lower glucose in diabetic animals through inhibition of fructose-1,6-bisphosphatase. *J. Med. Chem.* **54**, 153-165.

Dang, Q., Van Poelje, P. D. & Erion, M. D. (2012). *New Therapeutic Strategies for Type 2 Diabetes: Small Molecule Approaches*, pp. 306-323: The Royal Society of Chemistry.

Das, M., Bag, A., Saha, S., Ghosh, A., Dey, S., Das, P., Mandal, C., Ray, S., Chakrabarti, S., Ray, M. & Jana, S. (2016). Molecular association of glucose-6-phosphate isomerase and pyruvate kinase M2 with glyceraldehyde-3-phosphate dehydrogenase in cancer cells. *BMC Cancer* **16**, 152.

David, C. J., Chen, M., Assanah, M., Canoll, P. & Manley, J. L. (2010). HnRNP proteins controlled by c-Myc deregulate pyruvate kinase mRNA splicing in cancer. *Nature* **463**, 364-368.

de la Paz Santangelo, M., Gest, P. M., Guerin, M. E., Coincon, M., Pham, H., Ryan, G., Puckett, S. E., Spencer, J. S., Gonzalez-Juarrero, M., Daher, R., Lenaerts, A. J., Schnappinger, D., Therisod, M., Ehrt, S., Sygusch, J. & Jackson, M. (2011). Glycolytic and non-glycolytic functions of *Mycobacterium tuberculosis* fructose-1,6-bisphosphate aldolase, an essential enzyme produced by replicating and non-replicating bacilli. *J. Biol. Chem.* **286**, 40219-40231.

Dell'Antone, P. (2009). Targets of 3-bromopyruvate, a new, energy depleting, anticancer agent. *Med. Chem.* **5**, 491-496.

Desai, S., Ding, M., Wang, B., Lu, Z., Zhao, Q., Shaw, K., Yung, W. K., Weinstein, J. N., Tan, M. & Yao, J. (2014). Tissue-specific isoform switch and DNA hypomethylation of the pyruvate kinase PKM gene in human cancers. *Oncotarget* **5**, 8202-8210.

Dombrackas, J. D., Santarsiero, B. D. & Mesecar, A. D. (2005). Structural basis for tumor pyruvate kinase M2 allosteric regulation and catalysis. *Biochemistry* **44**, 9417-9429.

Donahue, J. L., Bownas, J. L., Niehaus, W. G. & Larson, T. J. (2000). Purification and characterization of glpX-encoded fructose 1, 6-bisphosphatase, a new enzyme of the glycerol 3-phosphate regulon of *Escherichia coli*. *J. Bacteriol.* **182**, 5624-5627.

Dziewulska-Szwajkowska, D. & Dżugaj, A. (2010). Kinetic properties of Pelophylax esculentus muscle FBPase. *Comparative Biochemistry and Physiology Part B: Biochemistry and Molecular Biology* **157**, 294-300.

Eigenbrodt, E. & Glossmann, H. (1980). Glycolysis—one of the keys to cancer? *Trends Pharmacol. Sci.* **1**, 240-245.

Eigenbrodt, E., Leib, S., Kramer, W., Friis, R. R. & Schoner, W. (1983). Structural and kinetic differences between the M2 type pyruvate kinases from lung and various tumors. *Biomed. Biochim. Acta* **42**, S278-282.

- Eigenbrodt, E., Reinacher, M., Scheefers-Borchel, U., Scheefers, H. & Friis, R. (1992). Double role for pyruvate kinase type M2 in the expansion of phosphometabolite pools found in tumor cells. *Crit. Rev. Oncog.* **3**, 91-115.
- El-Maghrabi, M. R., Claus, T., McGrane, M. & Pilkis, S. (1982). Influence of phosphorylation on the interaction of effectors with rat liver pyruvate kinase. *J. Biol. Chem.* **257**, 233-240.
- Elf, S. E. & Chen, J. (2014). Targeting glucose metabolism in patients with cancer. *Cancer* **120**, 774-780.
- Elia, S., Massoud, R., Guggino, G., Cristino, B., Cortese, C., De Massimi, A. R. & Zenobi, R. (2008). Tumor type M2-pyruvate-kinase levels in pleural fluid versus plasma in cancer patients: a further tool to define the need for invasive procedures. *Eur. J. Cardiothorac. Surg.* **33**, 723-727.
- Emsley, P. & Cowtan, K. (2004). Coot: model-building tools for molecular graphics. *Acta Crystallogr. D Biol. Crystallogr.* **60**, 2126-2132.
- Entian, K. D., Vogel, R. F., Rose, M., Hofmann, L. & Mecke, D. (1988). Isolation and primary structure of the gene encoding fructose-1,6-bisphosphatase from *Saccharomyces cerevisiae*. *FEBS Lett.* **236**, 195-200.
- Erion, M. D., van Poelje, P. D., Dang, Q., Kasibhatla, S. R., Potter, S. C., Reddy, M. R., Reddy, K. R., Jiang, T. & Lipscomb, W. N. (2005). MB06322 (CS-917): A potent and selective inhibitor of fructose 1,6-bisphosphatase for controlling gluconeogenesis in type 2 diabetes. *Proc. Natl. Acad. Sci. U. S. A.* **102**, 7970-7975.
- Ernest, I., Callens, M., Uttaro, A. D., Chevalier, N., Opperdoes, F. R., Muirhead, H. & Michels, P. A. (1998). Pyruvate kinase of *Trypanosoma brucei*: overexpression, purification, and functional characterization of wild-type and mutated enzyme. *Protein Expr. Purif.* **13**, 373-382.
- Evans, P. (2006). Scaling and assessment of data quality. *Acta Crystallogr. D Biol. Crystallogr.* **62**, 72-82.
- Fatela-Cantillo, D., Fernandez-Suarez, A., Moreno, M. A. M., Gutierrez, J. J. P. & Iglesias, J. M. D. (2012). Prognostic value of plasmatic tumor M2 pyruvate kinase and carcinoembryonic antigen in the survival of colorectal cancer patients. *Tumor Biol.* **33**, 825-832.
- Feasey, N., Wansbrough-Jones, M., Mabey, D. C. W. & Solomon, A. W. (2010). Neglected tropical diseases. *Br. Med. Bull.* **93**, 179-200.
- Feksa, L. R., Cornelio, A. R., Rech, V. C., Dutra, C. S., Wyse, A. T. S., Wajner, M. & Wannmacher, C. M. D. (2002). Alanine prevents the reduction of pyruvate kinase activity in brain cortex of rats subjected to chemically induced hyperphenylalaninemia. *Neurochem. Res.* **27**, 947-952.
- Feng, C., Gao, Y., Wang, C., Yu, X., Zhang, W., Guan, H., Shan, Z. & Teng, W. (2013). Aberrant overexpression of pyruvate kinase M2 is associated with aggressive

- tumor features and the BRAF mutation in papillary thyroid cancer. *J. Clin. Endocrinol. Metab.* **98**, E1524-1533.
- Fenton, A. W., Johnson, T. A. & Holyoak, T. (2010). The pyruvate kinase model system, a cautionary tale for the use of osmolyte perturbations to support conformational equilibria in allostery. *Protein Sci.* **19**, 1796-1800.
- Fraenkel, D. G. & Horecker, B. L. (1965). Fructose-1, 6-diphosphatase and acid hexose phosphatase of *Escherichia coli*. *J. Bacteriol.* **90**, 837-842.
- Fraenkel, D. G., Pontremoli, S. & Horecker, B. L. (1966). The specific fructose diphosphatase of *Escherichia coli*: Properties and partial purification. *Arch. Biochem. Biophys.* **114**, 4-12.
- Fuad, F. A., Fothergill-Gilmore, L. A., Nowicki, M. W., Eades, L. J., Morgan, H. P., McNae, I. W., Michels, P. A. & Walkinshaw, M. D. (2011). Phosphoglycerate mutase from *Trypanosoma brucei* is hyperactivated by cobalt in vitro, but not in vivo. *Metallomics* **3**, 1310-1317.
- Ganapathy, U., Marrero, J., Calhoun, S., Eoh, H., de Carvalho, L. P., Rhee, K. & Ehrt, S. (2015). Two enzymes with redundant fructose bisphosphatase activity sustain gluconeogenesis and virulence in *Mycobacterium tuberculosis*. *Nat. Commun.* **6**, 7912.
- Gao, X., Wang, H., Yang, J. J., Chen, J., Jie, J., Li, L., Zhang, Y. & Liu, Z. R. (2013a). Reciprocal regulation of protein kinase and pyruvate kinase activities of pyruvate kinase M2 by growth signals. *J. Biol. Chem.* **288**, 15971-15979.
- Gao, X., Wang, H., Yang, J. J., Liu, X. & Liu, Z. R. (2012). Pyruvate kinase M2 regulates gene transcription by acting as a protein kinase. *Mol. Cell* **45**, 598-609.
- Gao, Y. (2013). Allosteric regulation of mammalian fructose-1,6-bisphosphatase, Iowa State University, Ames, Iowa, US.
- Gao, Y., Iancu, C. V., Mukind, S., Choe, J. Y. & Honzatko, R. B. (2013b). Mechanism of displacement of a catalytically essential loop from the active site of mammalian fructose-1,6-bisphosphatase. *Biochemistry* **52**, 5206-5216.
- Gao, Y., Shen, L. & Honzatko, R. B. (2014). Central cavity of fructose-1,6-bisphosphatase and the evolution of AMP/fructose 2,6-bisphosphate synergism in eukaryotic organisms. *J. Biol. Chem.* **289**, 8450-8461.
- Gasteiger, E., Hoogland, C., Gattiker, A., Duvaud, S. e., Wilkins, M. R., Appel, R. D. & Bairoch, A. (2005). *Protein identification and analysis tools on the ExPASy server*. Springer.
- Gidh-Jain, M., Zhang, Y., van Poelje, P. D., Liang, J. Y., Huang, S., Kim, J., Elliott, J. T., Erion, M. D., Pilkis, S. J., Raafat el-Maghrabi, M. & et al. (1994). The allosteric site of human liver fructose-1,6-bisphosphatase. Analysis of six AMP site mutants based on the crystal structure. *J. Biol. Chem.* **269**, 27732-27738.

- Gilbert, I. H. (2013). Drug discovery for neglected diseases: molecular target-based and phenotypic approaches. *J. Med. Chem.* **56**, 7719-7726.
- Gizak, A., Sok, A. J., Lipinska, A., Zarzycki, M., Rakus, D. & Dzugaj, A. (2012). A comparative study on the sensitivity of *Cyprinus carpio* muscle and liver FBPase toward AMP and calcium. *Comparative Biochemistry and Physiology Part B: Biochemistry and Molecular Biology* **162**, 51-55.
- Gonzalez, J. D., Caballero, A., Viegas, I., Meton, I., Jones, J. G., Barra, J., Fernandez, F. & Baanante, I. V. (2012). Effects of alanine aminotransferase inhibition on the intermediary metabolism in *Sparus aurata* through dietary amino-oxyacetate supplementation. *Br. J. Nutr.* **107**, 1747-1756.
- Graven, P., Tambalo, M., Scapozza, L. & Perozzo, R. (2014). Purine metabolite and energy charge analysis of *Trypanosoma brucei* cells in different growth phases using an optimized ion-pair RP-HPLC/UV for the quantification of adenine and guanine pools. *Exp. Parasitol.* **141**, 28-38.
- Gualdrón-López, M., Brennard, A., Hannaert, V., Quiñones, W., Cáceres, A. J., Bringaud, F., Concepción, J. L. & Michels, P. A. M. (2012). When, how and why glycolysis became compartmentalised in the Kinetoplastea. A new look at an ancient organelle. *Int. J. Parasitol.* **42**, 1-20.
- Guo, C. X., Linton, A., Jalaie, M., Kephart, S., Ornelas, M., Pairish, M., Greasley, S., Richardson, P., Maegley, K., Hickey, M., Li, J., Wu, X., Ji, X. D. & Xie, Z. (2013). Discovery of 2-((1H-benzo[d]imidazol-1-yl) methyl)-4H-pyrido [1,2-a]pyrimidin-4-ones as novel PKM2 activators. *Bioorg. Med. Chem. Lett.* **23**, 3358-3363.
- Gupta, V., Kalaiarasan, P., Faheem, M., Singh, N., Iqbal, M. A. & Bamezai, R. N. (2010). Dominant negative mutations affect oligomerization of human pyruvate kinase M2 isozyme and promote cellular growth and polyploidy. *J. Biol. Chem.* **285**, 16864-16873.
- Gutka, H. J., Franzblau, S. G., Movahedzadeh, F. & Abad-Zapatero, C. (2011a). Crystallization and preliminary X-ray characterization of the glpX-encoded class II fructose-1,6-bisphosphatase from *Mycobacterium tuberculosis*. *Acta Crystallogr Sect F Struct Biol Cryst Commun* **67**, 710-713.
- Gutka, H. J., Rukseree, K., Wheeler, P. R., Franzblau, S. G. & Movahedzadeh, F. (2011b). glpX gene of *Mycobacterium tuberculosis*: heterologous expression, purification, and enzymatic characterization of the encoded fructose 1,6-bisphosphatase II. *Appl. Biochem. Biotechnol.* **164**, 1376-1389.
- Gutka, H. J., Wang, Y., Franzblau, S. G. & Movahedzadeh, F. (2015). glpx Gene in *Mycobacterium tuberculosis* Is Required for In Vitro Gluconeogenic Growth and In Vivo Survival. *PLoS ONE* **10**, e0138436.
- Haanstra, J. R., González-Marcano, E. B., Gualdrón-López, M. & Michels, P. A. M. (2016). Biogenesis, maintenance and dynamics of glycosomes in trypanosomatid parasites. *Biochimica et Biophysica Acta (BBA) - Molecular Cell Research* **1863**, 1038-1048.

Hardt, P. D. & Ewald, N. (2008). Tumor M2 pyruvate kinase: a tumor marker and its clinical application in gastrointestinal malignancy. *Expert Rev. Mol. Diagn.* **8**, 579-585.

Hardt, P. D., Mazurek, S., Toepler, M., Schlierbach, P., Bretzel, R. G., Eigenbrodt, E. & Kloer, H. U. (2004). Faecal tumour M2 pyruvate kinase: a new, sensitive screening tool for colorectal cancer. *Br. J. Cancer* **91**, 980-984.

Hardt, P. D., Ngoumou, B. K., Rupp, J., Schnell-Kretschmer, H. & Kloer, H. U. (2000). Tumor M2-pyruvate kinase: A promising tumor marker in the diagnosis of gastro-intestinal cancer. *Anticancer Res.* **20**, 4965-4968.

Hardt, P. D., Toepler, M., Ngoumou, B., Rupp, J. & Kloer, H. U. (2003). Measurement of fecal pyruvate kinase type M2 (Tumor M2-PK) concentrations in patients with gastric cancer, colorectal cancer, colorectal adenomas and controls. *Anticancer Res.* **23**, 851-853.

Hart, D. T., Misset, O., Edwards, S. W. & Opperdoes, F. R. (1984). A comparison of the glycosomes (microbodies) isolated from *Trypanosoma brucei* bloodstream form and cultured procyclic trypomastigotes. *Mol. Biochem. Parasitol.* **12**, 25-35.

Hathurusinghe, H. R. & Goonetilleke, K. S. (2007). Current status of tumor M2 pyruvate kinase (tumor M2-PK) as a biomarker of gastrointestinal malignancy. *Ann. Surg. Oncol.* **14**, 2714-2720.

Haug, U., Hundt, S. & Brenner, H. (2008). Sensitivity and specificity of faecal tumour M2 pyruvate kinase for detection of colorectal adenomas in a large screening study. *Br. J. Cancer* **99**, 133-135.

Haug, U., Rothenbacher, D., Wentz, M., Seiler, C., Stegmaier, C. & Brenner, H. (2007). Tumour M2-PK as a stool marker for colorectal cancer: comparative analysis in a large sample of unselected older adults vs colorectal cancer patients. *Br. J. Cancer* **96**, 1329-1334.

Haug, U., Wentz, M. N., Seiler, C. M., Rothenbacher, D., Buchler, M. W. & Brenner, H. (2006). Tumor M2 pyruvate kinase as a stool marker for colorectal cancer: Stability at room temperature and implications for application in the screening setting. *Clin. Chem.* **52**, 782-784.

Hayward, S. & Lee, R. A. (2002). Improvements in the analysis of domain motions in proteins from conformational change: DynDom version 1.50. *J. Mol. Graph. Model.* **21**, 181-183.

He, C. L., Bian, Y. Y., Xue, Y., Liu, Z. X., Zhou, K. Q., Yao, C. F., Lin, Y., Zou, H. F., Luo, F. X., Qu, Y. Y., Zhao, J. Y., Ye, M. L., Zhao, S. M. & Xu, W. (2016). Pyruvate kinase M2 activates mTORC1 by phosphorylating AKT1S1. *Sci Rep* **6**, 21524.

Hebeisen, P., Haap, W., Kuhn, B., Mohr, P., Wessel, H. P., Zutter, U., Kirchner, S., Ruf, A., Benz, J., Joseph, C., Alvarez-Sanchez, R., Gubler, M., Schott, B., Benardeau, A., Tozzo, E. & Kitas, E. (2011). Orally active aminopyridines as

inhibitors of tetrameric fructose-1,6-bisphosphatase. *Bioorg. Med. Chem. Lett.* **21**, 3237-3242.

Hebeisen, P., Kuhn, B., Kohler, P., Gubler, M., Huber, W., Kitas, E., Schott, B., Benz, J., Joseph, C. & Ruf, A. (2008). Allosteric FBPase inhibitors gain 10(5) times in potency when simultaneously binding two neighboring AMP sites. *Bioorg. Med. Chem. Lett.* **18**, 4708-4712.

Herman, P. & Lee, J. C. (2009). Functional energetic landscape in the allosteric regulation of muscle pyruvate kinase. 1. Calorimetric study. *Biochemistry* **48**, 9448-9455.

Herzog, B., Stitt, M. & Heldt, H. W. (1984). Control of Photosynthetic Sucrose Synthesis by Fructose 2,6-Bisphosphate : III. Properties of the Cytosolic Fructose 1,6-Bisphosphatase. *Plant Physiol.* **75**, 561-565.

Hines, J. K., Chen, X., Nix, J. C., Fromm, H. J. & Honzatko, R. B. (2007a). Structures of mammalian and bacterial fructose-1,6-bisphosphatase reveal the basis for synergism in AMP/fructose 2,6-bisphosphate inhibition. *J. Biol. Chem.* **282**, 36121-36131.

Hines, J. K., Fromm, H. J. & Honzatko, R. B. (2006). Novel allosteric activation site in Escherichia coli fructose-1,6-bisphosphatase. *J. Biol. Chem.* **281**, 18386-18393.

Hines, J. K., Fromm, H. J. & Honzatko, R. B. (2007b). Structures of activated fructose-1,6-bisphosphatase from Escherichia coli. Coordinate regulation of bacterial metabolism and the conservation of the R-state. *J. Biol. Chem.* **282**, 11696-11704.

Hines, J. K., Kruesel, C. E., Fromm, H. J. & Honzatko, R. B. (2007c). Structure of inhibited fructose-1,6-bisphosphatase from Escherichia coli: distinct allosteric inhibition sites for AMP and glucose 6-phosphate and the characterization of a gluconeogenic switch. *J. Biol. Chem.* **282**, 24697-24706.

Hitosugi, T., Kang, S., Vander Heiden, M. G., Chung, T. W., Elf, S., Lythgoe, K., Dong, S., Lonial, S., Wang, X., Chen, G. Z., Xie, J., Gu, T. L., Polakiewicz, R. D., Roesel, J. L., Boggon, T. J., Khuri, F. R., Gilliland, D. G., Cantley, L. C., Kaufman, J. & Chen, J. (2009). Tyrosine phosphorylation inhibits PKM2 to promote the Warburg effect and tumor growth. *Sci. Signal.* **2**, ra73.

Holyoak, T., Zhang, B., Deng, J., Tang, Q., Prasannan, C. B. & Fenton, A. W. (2013). Energetic coupling between an oxidizable cysteine and the phosphorylatable N-terminus of human liver pyruvate kinase. *Biochemistry* **52**, 466-476.

Hotez, P. J., Alvarado, M., Basanez, M. G., Bolliger, I., Bourne, R., Boussinesq, M., Brooker, S. J., Brown, A. S., Buckle, G., Budke, C. M., Carabin, H., Coffeng, L. E., Fevre, E. M., Furst, T., Halasa, Y. A., Jasrasaria, R., Johns, N. E., Keiser, J., King, C. H., Lozano, R., Murdoch, M. E., O'Hanlon, S., Pion, S. D., Pullan, R. L., Ramaiah, K. D., Roberts, T., Shepard, D. S., Smith, J. L., Stolk, W. A., Undurraga, E. A., Utzinger, J., Wang, M., Murray, C. J. & Naghavi, M. (2014). The global burden of disease study 2010: interpretation and implications for the neglected tropical diseases. *PLoS Negl. Trop. Dis.* **8**, e2865.

- Hotez, P. J., Bottazzi, M. E. & Strych, U. (2016). New Vaccines for the World's Poorest People. *Annu. Rev. Med.* **67**, 405-417.
- Hotez, P. J., Dumonteil, E., Heffernan, M. J. & Bottazzi, M. E. (2013). Innovation for the 'bottom 100 million': eliminating neglected tropical diseases in the Americas. *Adv. Exp. Med. Biol.* **764**, 1-12.
- Hotez, P. J., Molyneux, D. H., Fenwick, A., Kumaresan, J., Sachs, S. E., Sachs, J. D. & Savioli, L. (2007). Control of Neglected Tropical Diseases. *N. Engl. J. Med.* **357**, 1018-1027.
- Hsu, M. C., Hung, W. C., Yamaguchi, H., Lim, S. O., Liao, H. W., Tsai, C. H. & Hung, M. C. (2016). Extracellular PKM2 induces cancer proliferation by activating the EGFR signaling pathway. *American journal of cancer research* **6**, 628-638.
- Hugo, F., Fischer, G. & Eigenbrodt, E. (1999). Quantitative detection of tumor M2-PK in serum and plasma. *Anticancer Res.* **19**, 2753-2757.
- Iancu, C. V., Mukund, S., Fromm, H. J. & Honzatko, R. B. (2005). R-state AMP complex reveals initial steps of the quaternary transition of fructose-1,6-bisphosphatase. *J. Biol. Chem.* **280**, 19737-19745.
- Imamura, K. & Tanaka, T. (1972). Multimolecular forms of pyruvate kinase from rat and other mammalian tissues. I. Electrophoretic studies. *J Biochem* **71**, 1043-1051.
- Iqbal, M. A., Gupta, V., Gopinath, P., Mazurek, S. & Bamezai, R. N. (2014a). Pyruvate kinase M2 and cancer: an updated assessment. *FEBS Lett.* **588**, 2685-2692.
- Iqbal, M. A., Siddiqui, F. A., Chaman, N., Gupta, V., Kumar, B., Gopinath, P. & Bamezai, R. N. (2014b). Missense mutations in pyruvate kinase M2 promote cancer metabolism, oxidative endurance, anchorage independence, and tumor growth in a dominant negative manner. *J. Biol. Chem.* **289**, 8098-8105.
- Jacobs, R. T., Nare, B., Wring, S. A., Orr, M. D., Chen, D., Sligar, J. M., Jenks, M. X., Noe, R. A., Bowling, T. S. & Mercer, L. T. (2011). SCYX-7158, an orally-active benzoxaborole for the treatment of stage 2 human African trypanosomiasis. *PLoS Negl. Trop. Dis.* **5**, e1151.
- Jacquot, J. P., Lopez-Jaramillo, J., Chueca, A., Cherfils, J., Lemaire, S., Chedozeau, B., Miginiac-Maslow, M., Decottignies, P., Wolosiuk, R. & Lopez-Gorge, J. (1995). High-level expression of recombinant pea chloroplast fructose-1,6-bisphosphatase and mutagenesis of its regulatory site. *Eur. J. Biochem.* **229**, 675-681.
- Jacquot, J. P., Lopez-Jaramillo, J., Miginiac-Maslow, M., Lemaire, S., Cherfils, J., Chueca, A. & Lopez-Gorge, J. (1997). Cysteine-153 is required for redox regulation of pea chloroplast fructose-1,6-bisphosphatase. *FEBS Lett.* **401**, 143-147.
- Jaffrey, S. R. & Snyder, S. H. (2001). The biotin switch method for the detection of S-nitrosylated proteins. *Sci. Signal.* **2001**, p11.
- Jiang, J. K., Boxer, M. B., Vander Heiden, M. G., Shen, M., Skoumbourdis, A. P., Southall, N., Veith, H., Leister, W., Austin, C. P., Park, H. W., Inglesse, J., Cantley,

- L. C., Auld, D. S. & Thomas, C. J. (2010). Evaluation of thieno[3,2-b]pyrrole[3,2-d]pyridazinones as activators of the tumor cell specific M2 isoform of pyruvate kinase. *Bioorg. Med. Chem. Lett.* **20**, 3387-3393.
- Jiang, Y., Li, X., Yang, W., Hawke, D. H., Zheng, Y., Xia, Y., Aldape, K., Wei, C., Guo, F., Chen, Y. & Lu, Z. (2014a). PKM2 regulates chromosome segregation and mitosis progression of tumor cells. *Mol. Cell* **53**, 75-87.
- Jiang, Y., Wang, Y., Wang, T., Hawke, D. H., Zheng, Y., Li, X., Zhou, Q., Majumder, S., Bi, E., Liu, D. X., Huang, S. & Lu, Z. (2014b). PKM2 phosphorylates MLC2 and regulates cytokinesis of tumour cells. *Nat. Commun.* **5**, 5566.
- Karachaliou, N., Papadaki, C., Lagoudaki, E., Trypaki, M., Sfakianaki, M., Koutsopoulos, A., Mavroudis, D., Stathopoulos, E., Georgoulas, V. & Souglakos, J. (2013). Predictive value of BRCA1, ERCC1, ATP7B, PKM2, TOPOI, TOPOmicron-IIA, TOPOIIB and C-MYC genes in patients with small cell lung cancer (SCLC) who received first line therapy with cisplatin and etoposide. *PLoS ONE* **8**, e74611.
- Karl, S., Jones, M. K., Gutierrez, L., Moore, B., Kattenberg, E. & Lacerda, M. (2015). Challenges for Diagnosis of Malaria and Neglected Tropical Diseases in Elimination Settings. *Biomed Res Int* **2015**, 270756.
- Kato, H., Fukuda, T., Parkison, C., McPhie, P. & Cheng, S. Y. (1989). Cytosolic thyroid hormone-binding protein is a monomer of pyruvate kinase. *Proc. Natl. Acad. Sci. U. S. A.* **86**, 7861-7865.
- Kaura, B., Bagga, R. & Patel, F. D. (2004). Evaluation of the Pyruvate Kinase isoenzyme tumor (Tu M2 - PK) as a tumor marker for cervical carcinoma. *J. Obstet. Gynaecol. Res.* **30**, 193-196.
- Ke, H. M., Liang, J. Y., Zhang, Y. P. & Lipscomb, W. N. (1991a). Conformational transition of fructose-1,6-bisphosphatase: structure comparison between the AMP complex (T form) and the fructose 6-phosphate complex (R form). *Biochemistry* **30**, 4412-4420.
- Ke, H. M., Thorpe, C. M., Seaton, B. A., Lipscomb, W. N. & Marcus, F. (1989a). Structure refinement of fructose-1,6-bisphosphatase and its fructose 2,6-bisphosphate complex at 2.8 Å resolution. *J. Mol. Biol.* **212**, 513-539.
- Ke, H. M., Thorpe, C. M., Seaton, B. A., Marcus, F. & Lipscomb, W. N. (1989b). Molecular-structure of fructose-1,6-Bisphosphatase at 2.8-Å resolution. *Proc. Natl. Acad. Sci. U. S. A.* **86**, 1475-1479.
- Ke, H. M., Zhang, Y. P., Liang, J. Y. & Lipscomb, W. N. (1991b). Crystal structure of the neutral form of fructose-1,6-bisphosphatase complexed with the product fructose 6-phosphate at 2.1-Å resolution. *Proc. Natl. Acad. Sci. U. S. A.* **88**, 2989-2993.
- Kefas, B., Comeau, L., Erdle, N., Montgomery, E., Amos, S. & Purow, B. (2010). Pyruvate kinase M2 is a target of the tumor-suppressive microRNA-326 and regulates the survival of glioma cells. *Neuro-oncol.* **12**, 1102-1112.

- Keller, K. E., Doctor, Z. M., Dwyer, Z. W. & Lee, Y. S. (2014). SAICAR induces protein kinase activity of PKM2 that is necessary for sustained proliferative signaling of cancer cells. *Mol. Cell* **53**, 700-709.
- Keller, K. E., Tan, I. S. & Lee, Y. S. (2012). SAICAR stimulates pyruvate kinase isoform M2 and promotes cancer cell survival in glucose-limited conditions. *Science* **338**, 1069-1072.
- Kelley-Loughnane, N., Biolsi, S. A., Gibson, K. M., Lu, G., Hehir, M. J., Phelan, P. & Kantrowitz, E. R. (2002). Purification, kinetic studies, and homology model of *Escherichia coli* fructose-1,6-bisphosphatase. *Biochim. Biophys. Acta* **1594**, 6-16.
- Kelly, G. J., Zimmermann, G. & Latzko, E. (1982). Fructose-bisphosphatase from spinach leaf chloroplast and cytoplasm. *Methods Enzymol.* **90 Pt E**, 371-378.
- Kim, D. J., Park, Y. S., Kim, N. D., Min, S. H., You, Y. M., Jung, Y., Koo, H., Noh, H., Kim, J. A., Park, K. C. & Yeom, Y. I. (2015). A novel pyruvate kinase M2 activator compound that suppresses lung cancer cell viability under hypoxia. *Mol. Cells* **38**, 373-379.
- Kim, J. W. & Dang, C. V. (2006). Cancer's molecular sweet tooth and the Warburg effect. *Cancer Res.* **66**, 8927-8930.
- Kitas, E., Mohr, P., Kuhn, B., Hebeisen, P., Wessel, H. P., Haap, W., Ruf, A., Benz, J., Joseph, C., Huber, W., Sanchez, R. A., Paehler, A., Benardeau, A., Gubler, M., Schott, B. & Tozzo, E. (2010). Sulfonylureido thiazoles as fructose-1,6-bisphosphatase inhibitors for the treatment of type-2 diabetes. *Bioorg. Med. Chem. Lett.* **20**, 594-599.
- Koss, K., Maxton, D. & Jankowski, J. A. Z. (2008). Faecal dimeric M2 pyruvate kinase in colorectal cancer and polyps correlates with tumour staging and surgical intervention. *Colorectal Dis.* **10**, 244-248.
- Kosugi, M., Ahmad, R., Alam, M., Uchida, Y. & Kufe, D. (2011). MUC1-C oncoprotein regulates glycolysis and pyruvate kinase M2 activity in cancer cells. *PLoS ONE* **6**, e28234.
- Kotz, J. (2012). Phenotypic screening, take two. *SciBX: Science-Business eXchange* **5**.
- Krissinel, E. & Henrick, K. (2004). Secondary-structure matching (SSM), a new tool for fast protein structure alignment in three dimensions. *Acta Crystallogr. D Biol. Crystallogr.* **60**, 2256-2268.
- Krissinel, E. & Henrick, K. (2005). *Computational Life Sciences: First International Symposium, CompLife 2005, Konstanz, Germany, September 25-27, 2005. Proceedings*, edited by M. R. Berthold, R. C. Glen, K. Diederichs, O. Kohlbacher & I. Fischer, pp. 163-174. Berlin, Heidelberg: Springer Berlin Heidelberg.

- Kumar, Y., Gurusamy, K., Pamecha, V. & Davidson, B. R. (2007a). Tumor M2-pyruvate kinase as tumor marker in exocrine pancreatic cancer - A meta-analysis. *Pancreas* **35**, 114-119.
- Kumar, Y., Tapuria, N., Kirmani, N. & Davidson, B. R. (2007b). Tumour M2-pyruvate kinase: a gastrointestinal cancer marker. *Eur. J. Gastroenterol. Hepatol.* **19**, 265-276.
- Kung, C., Hixon, J., Choe, S., Marks, K., Gross, S., Murphy, E., DeLaBarre, B., Cianchetta, G., Sethumadhavan, S. & Wang, X. (2012). Small molecule activation of PKM2 in cancer cells induces serine auxotrophy. *Chem. Biol.* **19**, 1187-1198.
- Kuznetsova, E., Xu, L., Singer, A., Brown, G., Dong, A., Flick, R., Cui, H., Cuff, M., Joachimiak, A., Savchenko, A. & Yakunin, A. F. (2010). Structure and activity of the metal-independent fructose-1,6-bisphosphatase YK23 from *Saccharomyces cerevisiae*. *J. Biol. Chem.* **285**, 21049-21059.
- Lai, C., Gum, R. J., Daly, M., Fry, E. H., Hutchins, C., Abad-Zapatero, C. & von Geldern, T. W. (2006). Benzoxazole benzenesulfonamides as allosteric inhibitors of fructose-1,6-bisphosphatase. *Bioorg. Med. Chem. Lett.* **16**, 1807-1810.
- Landt, S., Jeschke, S., Koeninger, A., Thomas, A., Heusner, T., Korlach, S., Ulm, K., Schmidt, P., Blohmer, J. U., Lichtenegger, W., Sehouli, J. & Kuemmel, S. (2010). Tumor-specific correlation of tumor M2 pyruvate kinase in pre-invasive, invasive and recurrent cervical cancer. *Anticancer Res.* **30**, 375-381.
- Larkin, M. A., Blackshields, G., Brown, N., Chenna, R., McGettigan, P. A., McWilliam, H., Valentin, F., Wallace, I. M., Wilm, A. & Lopez, R. (2007). Clustal W and Clustal X version 2.0. *Bioinformatics* **23**, 2947-2948.
- Laskowski, R. A., Hutchinson, E. G., Michie, A. D., Wallace, A. C., Jones, M. L. & Thornton, J. M. (1997). PDBsum: a Web-based database of summaries and analyses of all PDB structures. *Trends Biochem. Sci.* **22**, 488-490.
- Lee, J., Kim, H. K., Han, Y. M. & Kim, J. (2008). Pyruvate kinase isozyme type M2 (PKM2) interacts and cooperates with Oct-4 in regulating transcription. *Int. J. Biochem. Cell Biol.* **40**, 1043-1054.
- Li, J., Yang, Z., Zou, Q., Yuan, Y., Li, J., Liang, L., Zeng, G. & Chen, S. (2014a). PKM2 and ACVR 1C are prognostic markers for poor prognosis of gallbladder cancer. *Clin. Transl. Oncol.* **16**, 200-207.
- Li, L., Zhang, Y., Qiao, J., Yang, J. J. & Liu, Z. R. (2014b). Pyruvate kinase M2 in blood circulation facilitates tumor growth by promoting angiogenesis. *J. Biol. Chem.* **289**, 25812-25821.
- Li, N., Feng, L., Liu, H., Wang, J., Kasembeli, M., Tran, M. K., Twardy, D. J., Lin, S. H. & Chen, J. (2016). PARP Inhibition Suppresses Growth of EGFR-Mutant Cancers by Targeting Nuclear PKM2. *Cell Rep.*

- Li, R., Liu, J. J., Xue, H. P. & Huang, G. (2012). Diagnostic value of fecal tumor M2-pyruvate kinase for CRC screening: A systematic review and meta-analysis. *Int. J. Cancer* **131**, 1837-1845.
- Li, Z., Yang, P. & Li, Z. (2014c). The multifaceted regulation and functions of PKM2 in tumor progression. *Biochim. Biophys. Acta* **1846**, 285-296.
- Liang, P., Sun, J., Huang, Y., Zhang, F., Zhou, J., Hu, Y., Wang, X., Liang, C., Zheng, M., Xu, Y., Mao, Q., Hu, X., Li, X., Xu, J., Lu, G. & Yu, X. (2013). Biochemical characterization and functional analysis of fructose-1,6-bisphosphatase from *Clonorchis sinensis*. *Mol. Biol. Rep.* **40**, 4371-4382.
- Liao, B. R., He, H. B., Yang, L. L., Gao, L. X., Chang, L., Tang, J., Li, J. Y., Li, J. & Yang, F. (2014). Synthesis and structure-activity relationship of non-phosphorus-based fructose-1,6-bisphosphatase inhibitors: 2,5-Diphenyl-1,3,4-oxadiazoles. *European journal of medicinal chemistry* **83**, 15-25.
- Liu, A. M., Xu, Z., Shek, F. H., Wong, K. F., Lee, N. P., Poon, R. T., Chen, J. & Luk, J. M. (2014). miR-122 targets pyruvate kinase M2 and affects metabolism of hepatocellular carcinoma. *PLoS ONE* **9**, e86872.
- Liu, F. & Fromm, H. J. (1990). Kinetic studies on the mechanism and regulation of rabbit liver fructose-1,6-bisphosphatase. *J. Biol. Chem.* **265**, 7401-7406.
- Liu, J., Zhu, H., Jiang, H., Zhang, H., Wu, D., Hu, X. & Zhang, H. (2015). Tumor M2 pyruvate kinase in diagnosis of nonsmall cell lung cancer: A meta-analysis based on Chinese population. *J Cancer Res Ther* **11 Suppl**, c104-106.
- Liu, Y., Cao, Y., Zhang, W., Bergmeier, S., Qian, Y., Akbar, H., Colvin, R., Ding, J., Tong, L., Wu, S., Hines, J. & Chen, X. (2012). A small-molecule inhibitor of glucose transporter 1 downregulates glycolysis, induces cell-cycle arrest, and inhibits cancer cell growth in vitro and in vivo. *Mol. Cancer Ther.* **11**, 1672-1682.
- Lonhienne, T. G. & Winzor, D. J. (2002). Calorimetric demonstration of the potential of molecular crowding to emulate the effect of an allosteric activator on pyruvate kinase kinetics. *Biochemistry* **41**, 6897-6901.
- Lu, G., Stec, B., Giroux, E. L. & Kantrowitz, E. R. (1996). Evidence for an active T-state pig kidney fructose 1,6-bisphosphatase: interface residue Lys-42 is important for allosteric inhibition and AMP cooperativity. *Protein Sci.* **5**, 2333-2342.
- Lüftner, D., Mesterharm, J., Akrivakis, C., Geppert, R., Petrides, P., Wernecke, K. & Possinger, K. (1999). Tumor type M2 pyruvate kinase expression in advanced breast cancer. *Anticancer Res.* **20**, 5077-5082.
- Luo, W., Hu, H., Chang, R., Zhong, J., Knabel, M., O'Meally, R., Cole, R. N., Pandey, A. & Semenza, G. L. (2011). Pyruvate kinase M2 is a PHD3-stimulated coactivator for hypoxia-inducible factor 1. *Cell* **145**, 732-744.
- Lv, L., Li, D., Zhao, D., Lin, R., Chu, Y., Zhang, H., Zha, Z., Liu, Y., Li, Z. & Xu, Y. (2011). Acetylation targets the M2 isoform of pyruvate kinase for degradation

- through chaperone-mediated autophagy and promotes tumor growth. *Mol. Cell* **42**, 719-730.
- Lv, L., Xu, Y. P., Zhao, D., Li, F. L., Wang, W., Sasaki, N., Jiang, Y., Zhou, X., Li, T. T., Guan, K. L., Lei, Q. Y. & Xiong, Y. (2013). Mitogenic and oncogenic stimulation of K433 acetylation promotes PKM2 protein kinase activity and nuclear localization. *Mol. Cell* **52**, 340-352.
- Magnusson, I., Rothman, D. L., Katz, L. D., Shulman, R. G. & Shulman, G. I. (1992). Increased rate of gluconeogenesis in type II diabetes mellitus. A ¹³C nuclear magnetic resonance study. *J. Clin. Invest.* **90**, 1323-1327.
- Majumdar, D., Thornton, M., Irving, G., Soliman, A. & Kapur, K. (2010). Faecal Tumour M2 Pyruvate Kinase - a Non-Invasive Marker for Identifying High-Risk Patients Undergoing Colorectal Investigations in a District General Hospital. *Gut* **59**, A125-A126.
- Marie, J., Buc, H., Simon, M. P. & Kahn, A. (1980). Phosphorylation of human erythrocyte pyruvate kinase by soluble cyclic - AMP - dependent protein kinases. *Eur. J. Biochem.* **108**, 251-260.
- Marie, J., Tichonicky, L., Dreyfus, J.-C. & Kahn, A. (1979). Endogenous, cyclic 3' -2-5' AMP-dependent phosphorylation of human red cell pyruvate kinase. *Biochem. Biophys. Res. Commun.* **87**, 862-866.
- Martinez-Oyanedel, J., McNae, I. W., Nowicki, M. W., Keillor, J. W., Michels, P. A., Fothergill-Gilmore, L. A. & Walkinshaw, M. D. (2007). The first crystal structure of phosphofructokinase from a eukaryote: *Trypanosoma brucei*. *J. Mol. Biol.* **366**, 1185-1198.
- Mazurek, S. (2011). Pyruvate kinase type M2: a key regulator of the metabolic budget system in tumor cells. *Int. J. Biochem. Cell Biol.* **43**, 969-980.
- Mazurek, S., Boschek, C. B., Hugo, F. & Eigenbrodt, E. (2005). Pyruvate kinase type M2 and its role in tumor growth and spreading. *Semin. Cancer Biol.* **15**, 300-308.
- Mazurek, S., Grimm, H., Boschek, C. B., Vaupel, P. & Eigenbrodt, E. (2002). Pyruvate kinase type M2: a crossroad in the tumor metabolome. *Br. J. Nutr.* **87**, S23-S29.
- Mazurek, S., Scheefers-Borchel, U., Scheefers, H., Michel, A., Basenau, D., Fischer, G., Dahlmann, N., Laumen, R. & Eigenbrodt, E. (1993). Die Bedeutung der Pyruvatkinase in der Onkologie. *Notabene Med* **3**, 97-103.
- McCoy, A. J., Grosse-Kunstleve, R. W., Adams, P. D., Winn, M. D., Storoni, L. C. & Read, R. J. (2007). Phaser crystallographic software. *J. Appl. Crystallogr.* **40**, 658-674.
- McGrane, M. M., El-Maghrabi, M. R. & Pilkis, S. J. (1983). The interaction of fructose 2,6-bisphosphate and AMP with rat hepatic fructose 1,6-bisphosphatase. *J. Biol. Chem.* **258**, 10445-10454.

- McNae, I. W., Martinez-Oyanedel, J., Keillor, J. W., Michels, P. A., Fothergill-Gilmore, L. A. & Walkinshaw, M. D. (2009). The crystal structure of ATP-bound phosphofructokinase from *Trypanosoma brucei* reveals conformational transitions different from those of other phosphofructokinases. *J. Mol. Biol.* **385**, 1519-1533.
- Michels, P. A., Bringaud, F., Herman, M. & Hannaert, V. (2006). Metabolic functions of glycosomes in trypanosomatids. *Biochimica et Biophysica Acta (BBA)-Molecular Cell Research* **1763**, 1463-1477.
- Mitchell, R. (2014). The Regulation of Human M2 Pyruvate Kinase, The University of Edinburgh.
- Mor, I., Carlessi, R., Ast, T., Feinstein, E. & Kimchi, A. (2012). Death-associated protein kinase increases glycolytic rate through binding and activation of pyruvate kinase. *Oncogene* **31**, 683-693.
- Morgan, H. P., McNae, I. W., Nowicki, M. W., Hannaert, V., Michels, P. A., Fothergill-Gilmore, L. A. & Walkinshaw, M. D. (2010). Allosteric mechanism of pyruvate kinase from *Leishmania mexicana* uses a rock and lock model. *J. Biol. Chem.* **285**, 12892-12898.
- Morgan, H. P., O'Reilly, F. J., Wear, M. A., O'Neill, J. R., Fothergill-Gilmore, L. A., Hupp, T. & Walkinshaw, M. D. (2013). M2 pyruvate kinase provides a mechanism for nutrient sensing and regulation of cell proliferation. *Proc. Natl. Acad. Sci. U. S. A.* **110**, 5881-5886.
- Morgan, H. P., Walsh, M. J., Blackburn, E. A., Wear, M. A., Boxer, M. B., Shen, M., Veith, H., McNae, I. W., Nowicki, M. W., Michels, P. A., Auld, D. S., Fothergill-Gilmore, L. A. & Walkinshaw, M. D. (2012). A new family of covalent inhibitors block nucleotide binding to the active site of pyruvate kinase. *Biochem. J.* **448**, 67-72.
- Mulder, S. A., Van Leerdam, M. E., van Vuuren, A. J., Francke, J., van Toorenenbergen, A. W., Kuipers, E. J. & Ouwendijk, R. J. T. (2007). Tumor pyruvate kinase isoenzyme type M2 and immunochemical fecal occult blood test: performance in screening for colorectal cancer. *Eur. J. Gastroenterol. Hepatol.* **19**, 878-882.
- Munoz, M. E. & Ponce, E. (2003). Pyruvate kinase: current status of regulatory and functional properties. *Comp. Biochem. Physiol. B Biochem. Mol. Biol.* **135**, 197-218.
- Murshudov, G. N., Vagin, A. A. & Dodson, E. J. (1997). Refinement of macromolecular structures by the maximum-likelihood method. *Acta Crystallogr. D Biol. Crystallogr.* **53**, 240-255.
- Naderer, T., Ellis, M. A., Sernee, M. F., De Souza, D. P., Curtis, J., Handman, E. & McConville, M. J. (2006). Virulence of *Leishmania major* in macrophages and mice requires the gluconeogenic enzyme fructose-1,6-bisphosphatase. *Proc. Natl. Acad. Sci. U. S. A.* **103**, 5502-5507.

- Nakatsu, D., Horiuchi, Y., Kano, F., Noguchi, Y., Sugawara, T., Takamoto, I., Kubota, N., Kadowaki, T. & Murata, M. (2015). L-cysteine reversibly inhibits glucose-induced biphasic insulin secretion and ATP production by inactivating PKM2. *Proc. Natl. Acad. Sci. U. S. A.* **112**, E1067-1076.
- Nelson, S. W., Honzatko, R. B. & Fromm, H. J. (2004). Origin of cooperativity in the activation of fructose-1,6-bisphosphatase by Mg^{2+} . *J. Biol. Chem.* **279**, 18481-18487.
- Nelson, S. W., Iancu, C. V., Choe, J. Y., Honzatko, R. B. & Fromm, H. J. (2000). Tryptophan fluorescence reveals the conformational state of a dynamic loop in recombinant porcine fructose-1,6-bisphosphatase. *Biochemistry* **39**, 11100-11106.
- Netzker, R., Greiner, E., Eigenbrodt, E., Noguchi, T., Tanaka, T. & Brand, K. (1992). Cell cycle-associated expression of M2-type isozyme of pyruvate kinase in proliferating rat thymocytes. *J. Biol. Chem.* **267**, 6421-6424.
- Nishimasu, H., Fushinobu, S., Shoun, H. & Wakagi, T. (2004). The first crystal structure of the novel class of fructose-1,6-bisphosphatase present in thermophilic archaea. *Structure* **12**, 949-959.
- Noguchi, T., Inoue, H. & Tanaka, T. (1986a). The M1-type and M2-type isozymes of rat pyruvate-kinase are produced from the same gene by alternative RNA splicing. *J. Biol. Chem.* **261**, 3807-3812.
- Noguchi, T., Inoue, H. & Tanaka, T. (1986b). The M1- and M2-type isozymes of rat pyruvate kinase are produced from the same gene by alternative RNA splicing. *J. Biol. Chem.* **261**, 13807-13812.
- Noguchi, T., Yamada, K., Inoue, H., Matsuda, T. & Tanaka, T. (1987). The L-type and R-type isozymes of rat pyruvate-kinase are produced from a single gene by use of different promoters. *J. Biol. Chem.* **262**, 14366-14371.
- Okar, D. A. & Lange, A. J. (1999). Fructose-2,6-bisphosphate and control of carbohydrate metabolism in eukaryotes. *Biofactors* **10**, 1-14.
- Okar, D. A., Manzano, A., Navarro-Sabate, A., Riera, L., Bartrons, R. & Lange, A. J. (2001). PFK-2/FBPase-2: maker and breaker of the essential biofactor fructose-2,6-bisphosphate. *Trends Biochem. Sci.* **26**, 30-35.
- Opperdoes, F. R. & Borst, P. (1977). Localization of nine glycolytic enzymes in a microbody-like organelle in *Trypanosoma brucei*: the glycosome. *FEBS Lett.* **80**, 360-364.
- Opperdoes, F. R. & Michels, P. A. (2001). Enzymes of carbohydrate metabolism as potential drug targets. *Int. J. Parasitol.* **31**, 482-490.
- Opperdoes, F. R. & Michels, P. A. (2008). The metabolic repertoire of *Leishmania* and implications for drug discovery. *Leishmania, after the genome, 1st edn.* Caister Academic Press, Norfolk, UK, 123-158.

- Oremek, G., Teigelkamp, S., Kramer, W., Eigenbrodt, E. & Usadel, K. (1998). The pyruvate kinase isoenzyme tumor M2 (Tu M2-PK) as a tumor marker for renal carcinoma. *Anticancer Res.* **19**, 2599-2601.
- Oremek, G. M., Teigelkamp, S., Kramer, W., Eigenbrodt, E. & Usadel, K. H. (1999). The pyruvate kinase isoenzyme tumor M2 (Tu M2-PK) as a tumor marker for renal carcinoma. *Anticancer Res.* **19**, 2599-2601.
- Palmer, T. N. & Odedra, B. R. (1982). L-Phenylalanine inhibition of muscle pyruvate kinase. *Biosci. Rep.* **2**, 825-833.
- Palsson-McDermott, E. M., Curtis, A. M., Goel, G., Lauterbach, M. A., Sheedy, F. J., Gleeson, L. E., van den Bosch, M. W., Quinn, S. R., Domingo-Fernandez, R., Johnston, D. G., Jiang, J. K., Israelsen, W. J., Keane, J., Thomas, C., Clish, C., Vander Heiden, M., Xavier, R. J. & O'Neill, L. A. (2015). Pyruvate kinase M2 regulates Hif-1alpha activity and IL-1beta induction and is a critical determinant of the warburg effect in LPS-activated macrophages. *Cell Metab.* **21**, 65-80.
- Papadaki, C., Sfakianaki, M., Lagoudaki, E., Ioannidis, G., Tsakalaki, E., Trypaki, M., Giagkas, G., Pontikakis, S., Stathopoulos, E., Mavroudis, D., Georgoulas, V. & Souglakos, J. (2011). PKM2 as a biomarker for chemosensitivity to cisplatin-based chemotherapy in metastatic/advanced non-small cell lung cancer (Nslc). *J. Thorac. Oncol.* **6**, S998-S998.
- Park, S. H., Ozden, O., Liu, G., Song, H. Y., Zhu, Y., Yan, Y., Zou, X., Kang, H. J., Jiang, H., Principe, D. R., Cha, Y. I., Roh, M., Vassilopoulos, A. & Gius, D. (2016). SIRT2-Mediated Deacetylation and Tetramerization of Pyruvate Kinase Directs Glycolysis and Tumor Growth. *Cancer Res.* **76**, 3802-3812.
- Parnell, K. M., Foulks, J. M., Nix, R. N., Clifford, A., Bullough, J., Luo, B., Senina, A., Vollmer, D., Liu, J., McCarthy, V., Xu, Y., Saunders, M., Liu, X. H., Pearce, S., Wright, K., O'Reilly, M., McCullar, M. V., Ho, K. K. & Kanner, S. B. (2013). Pharmacologic activation of PKM2 slows lung tumor xenograft growth. *Mol. Cancer Ther.* **12**, 1453-1460.
- Pilkis, S. J., Claus, T. H., Kurland, I. J. & Lange, A. J. (1995). 6-Phosphofructo-2-kinase/fructose-2,6-bisphosphatase: a metabolic signaling enzyme. *Annu. Rev. Biochem.* **64**, 799-835.
- Pilkis, S. J., el-Maghrabi, M. R. & Claus, T. H. (1988). Hormonal regulation of hepatic gluconeogenesis and glycolysis. *Annu. Rev. Biochem.* **57**, 755-783.
- Pilkis, S. J., El-Maghrabi, M. R., Pilkis, J. & Claus, T. (1981). Inhibition of fructose-1,6-bisphosphatase by fructose 2,6-bisphosphate. *J. Biol. Chem.* **256**, 3619-3622.
- Pilkis, S. J., McGrane, M. M., Kountz, P. D., el-Maghrabi, M. R., Pilkis, J., Maryanoff, B. E., Reitz, A. B. & Benkovic, S. J. (1986). The effect of arabinose 1,5-bisphosphate on rat hepatic 6-phosphofructo-1-kinase and fructose-1,6-bisphosphatase. *Biochem. Biophys. Res. Commun.* **138**, 159-166.

- Plowman, K. M. & Krall, A. R. (1965). A kinetic study of nucleotide interactions with pyruvate kinase. *Biochemistry* **4**, 2809-2814.
- Porter, D. H. & Cardenas, J. M. (1980). L-Phenylalanine stereospecifically inhibits the renaturation of muscle pyruvate kinase. *Arch. Biochem. Biophys.* **202**, 54-62.
- Prasannan, C. B., Tang, Q. & Fenton, A. W. (2012). Allosteric regulation of human liver pyruvate kinase by peptides that mimic the phosphorylated/dephosphorylated N-terminus. *Methods Mol. Biol.* **796**, 335-349.
- Prasannan, C. B., Villar, M. T., Artigues, A. & Fenton, A. W. (2013). Identification of regions of rabbit muscle pyruvate kinase important for allosteric regulation by phenylalanine, detected by H/D exchange mass spectrometry. *Biochemistry* **52**, 1998-2006.
- Rakus, D., Maciaszczyk, E., Wawrzycka, D., Ulaszewski, S., Eschrich, K. & Dzugaj, A. (2005). The origin of the high sensitivity of muscle fructose 1,6-bisphosphatase towards AMP. *FEBS Lett.* **579**, 5577-5581.
- Rakus, D., Skalecki, K. & Dzugaj, A. (2000). Kinetic properties of pig (*Sus scrofa domestica*) and bovine (*Bos taurus*) D-fructose-1,6-bisphosphate 1-phosphohydrolase (F1,6BPase): liver-like isozymes in mammalian lung tissue. *Comp. Biochem. Physiol. B Biochem. Mol. Biol.* **127**, 123-134.
- Rakus, D., Tillmann, H., Wysocki, R., Ulaszewski, S., Eschrich, K. & Dzugaj, A. (2003). Different sensitivities of mutants and chimeric forms of human muscle and liver fructose-1,6-bisphosphatases towards AMP. *Biol. Chem.* **384**, 51-58.
- Ralton, J. E., Naderer, T., Piraino, H. L., Bashtannyk, T. A., Callaghan, J. M. & McConville, M. J. (2003). Evidence that intracellular beta1-2 mannan is a virulence factor in *Leishmania* parasites. *J. Biol. Chem.* **278**, 40757-40763.
- Rempel, A., Mathupala, S. P., Griffin, C. A., Hawkins, A. L. & Pedersen, P. L. (1996). Glucose catabolism in cancer cells: amplification of the gene encoding type II hexokinase. *Cancer Res.* **56**, 2468-2471.
- Rice, P., Longden, I. & Bleasby, A. (2000). EMBOSS: the European Molecular Biology Open Software Suite. *Trends Genet.* **16**, 276-277.
- Rigden, D. J. (2007). Fructose-1,6-bisphosphatase, a surprising yet promising drug target in *Leishmania*, 39th Microsymposium 'Glycosomes, trypanosomatid metabolism and drug discovery', Brussels, Belgium.
- Riou, J. P., Claus, T. H. & Pilkis, S. (1978). Stimulation of glucagon of in vivo phosphorylation of rat hepatic pyruvate kinase. *J. Biol. Chem.* **253**, 656-659.
- Rittmann, D., Schaffer, S., Wendisch, V. & Sahm, H. (2003). Fructose-1,6-bisphosphatase from *Corynebacterium glutamicum*: expression and deletion of the *fbp* gene and biochemical characterization of the enzyme. *Arch. Microbiol.* **180**, 285-292.

Rodriguez-Contreras, D. & Hamilton, N. (2014). Gluconeogenesis in *Leishmania mexicana*: contribution of glycerol kinase, phosphoenolpyruvate carboxykinase, and pyruvate phosphate dikinase. *J. Biol. Chem.* **289**, 32989-33000.

Rodriguez-Contreras, D. & Landfear, S. M. (2006). Metabolic changes in glucose transporter-deficient *Leishmania mexicana* and parasite virulence. *J. Biol. Chem.* **281**, 20068-20076.

Rodriguez-Suarez, R. J., Mora-Garcia, S. & Wolosiuk, R. A. (1997). Characterization of cysteine residues involved in the reductive activation and the structural stability of rapeseed (*Brassica napus*) chloroplast fructose-1,6-bisphosphatase. *Biochem. Biophys. Res. Commun.* **232**, 388-393.

Roigas, J., Deger, S., Schroeder, J., Wille, A., Turk, I., Brux, B., Jung, K., Schnorr, D. & Loening, S. A. (2003). Tumor type M2 pyruvate kinase expression in metastatic renal cell carcinoma. *Urol. Res.* **31**, 358-362.

Rudnitskaya, A., Borkin, D. A., Huynh, K., Torok, B. & Stieglitz, K. (2010). Rational design, synthesis, and potency of N-substituted indoles, pyrroles, and triarylpyrazoles as potential fructose 1,6-bisphosphatase inhibitors. *Chemmedchem* **5**, 384-389.

Rudnitskaya, A., Huynh, K., Torok, B. & Stieglitz, K. (2009). Novel heteroaromatic organofluorine inhibitors of fructose-1,6-bisphosphatase. *J. Med. Chem.* **52**, 878-882.

Saito, S., Furuno, A., Sakurai, J., Sakamoto, A., Park, H. R., Shin-Ya, K., Tsuruo, T. & Tomida, A. (2009). Chemical genomics identifies the unfolded protein response as a target for selective cancer cell killing during glucose deprivation. *Cancer Res.* **69**, 4225-4234.

Sanchez-Moreno, M., Lasztity, D., Coppens, I. & Opperdoes, F. R. (1992). Characterization of carbohydrate metabolism and demonstration of glycosomes in a *Phytomonas* sp. isolated from *Euphorbia characias*. *Mol. Biochem. Parasitol.* **54**, 185-199.

Scatena, R., Bottoni, P., Pontoglio, A. & Giardina, B. (2010). Revisiting the Warburg effect in cancer cells with proteomics. The emergence of new approaches to diagnosis, prognosis and therapy. *PROTEOMICS-Clinical Applications* **4**, 143-158.

Schneider, J., Bitterlich, N. & Schulze, G. (2005). Improved sensitivity in the diagnosis of gastro-intestinal tumors by fuzzy logic-based tumor marker profiles including the tumor M2-PK. *Anticancer Res.* **25**, 1507-1515.

Schneider, J., Morr, H., Velcovsky, H., Weisse, G. & Eigenbrodt, E. (1999). Quantitative detection of tumor M2-pyruvate kinase in plasma of patients with lung cancer in comparison to other lung diseases. *Cancer Detect. Prev.* **24**, 531-535.

Schneider, J., Morr, H., Velcovsky, H. G., Weisse, G. & Eigenbrodt, E. (2000). Quantitative detection of Tumor M2-pyruvate kinase in plasma of patients with lung cancer in comparison to other lung diseases. *Cancer Detect. Prev.* **24**, 531-535.

- Schneider, J., Neu, K., Grimm, H., Velcovsky, H. G., Weisse, G. & Eigenbrodt, E. (2002). Tumor M2-pyruvate kinase in lung cancer patients: Immunohistochemical detection and disease monitoring. *Anticancer Res.* **22**, 311-318.
- Schneider, J., Neu, K., Velcovsky, H. G., Morr, H. & Eigenbrodt, E. (2003a). Tumor M2-pyruvate kinase in the follow-up of inoperable lung cancer patients: a pilot study. *Cancer Lett.* **193**, 91-98.
- Schneider, J., Peltri, G., Bitterlich, N., Neu, K., Velcovsky, H.-G., Morr, H., Katz, N. & Eigenbrodt, E. (2003b). Fuzzy logic-based tumor marker profiles including a new marker tumor M2-PK improved sensitivity to the detection of progression in lung cancer patients. *Anticancer Res.* **23**, 899.
- Schneider, J. & Schulze, G. (2003). Comparison of tumor M2-pyruvate kinase (tumor M2-PK), carcinoembryonic antigen (CEA), carbohydrate antigens CA 19-9 and CA 72-4 in the diagnosis of gastrointestinal cancer. *Anticancer Res.* **23**, 5089-5093.
- Schulze, G. (1999). The tumor marker tumor M2-PK: an application in the diagnosis of gastrointestinal cancer. *Anticancer Res.* **20**, 4961-4964.
- Shastri, Y. M., Loitsch, S., Hoepffner, N., Povse, N., Hanisch, E., Rosch, W., Mossner, J. & Stein, J. M. (2008). Comparison of an established simple office-based immunological FOBT with fecal tumor pyruvate kinase type M2 (M2-PK) for colorectal cancer screening: Prospective multicenter study. *Am. J. Gastroenterol.* **103**, 1496-1504.
- Shastri, Y. M., Naumann, M., Oremek, G. M., Hanisch, E., Rosch, W., Mossner, J., Caspary, W. F. & Stein, J. M. (2006). Prospective multicenter evaluation of fecal tumor pyruvate kinase type M2 (M2-PK) as a screening biomarker for colorectal neoplasia. *Int. J. Cancer* **119**, 2651-2656.
- Shastri, Y. M. & Stein, J. (2007). Fecal tumor M2 pyruvate kinase is not a specific biomarker for colorectal cancer screening. *World J. Gastroenterol.* **13**, 2768-2769.
- Shastri, Y. M. & Stein, J. M. (2008). Faecal tumour pyruvate kinase M2: not a good marker for the detection of colorectal adenomas. *Br. J. Cancer* **99**, 1366-1366.
- Shi, R., Chen, Z. Y., Zhu, D. W., Li, C., Shan, Y., Xu, G. & Lin, S. X. (2013). Crystal structures of human muscle fructose-1,6-bisphosphatase: novel quaternary states, enhanced AMP affinity, and allosteric signal transmission pathway. *PLoS ONE* **8**, e71242.
- Shimada, N., Shinagawa, T. & Ishii, S. (2008). Modulation of M2-type pyruvate kinase activity by the cytoplasmic PML tumor suppressor protein. *Genes Cells* **13**, 245-254.
- Shingyoji, M., Iizasa, T., Higashiyama, M., Imamura, F., Saruki, N., Imaizumi, A., Yamamoto, H., Daimon, T., Tochikubo, O. & Mitsushima, T. (2013). The significance and robustness of a plasma free amino acid (PFAA) profile-based multiplex function for detecting lung cancer. *BMC Cancer* **13**, 77.

Sievers, F., Wilm, A., Dineen, D., Gibson, T. J., Karplus, K., Li, W. Z., Lopez, R., McWilliam, H., Remmert, M., Soding, J., Thompson, J. D. & Higgins, D. G. (2011). Fast, scalable generation of high-quality protein multiple sequence alignments using Clustal Omega. *Mol. Syst. Biol.* **7**.

Siriwardana, P., Mason, J. M., Goonetilleke, K., King, N. K., France, M. W. & Sirwardena, A. K. (2006). Tumour-M2-pyruvate kinase (Tu-M2-PK): A novel biomarker of adverse prognosis in pancreatic cancer. *Gastroenterology* **130**, A149-A149.

Sithambaram, S., Hilmi, I. & Goh, K. L. (2015). The Diagnostic Accuracy of the M2 Pyruvate Kinase Quick Stool Test--A Rapid Office Based Assay Test for the Detection of Colorectal Cancer. *PLoS ONE* **10**, e0131616.

Sparmann, G., Schulz, J. & Hofmann, E. (1973). Effects of L-alanine and fructose (1,6-diphosphate) on pyruvate kinase from ehrlich ascites tumour cells. *FEBS Lett.* **36**, 305-308.

Spoden, G. A., Morandell, D., Ehehalt, D., Fiedler, M., Jansen-Dürr, P., Hermann, M. & Zwerschke, W. (2009). The SUMO-E3 ligase PIAS3 targets pyruvate kinase M2. *J. Cell. Biochem.* **107**, 293-302.

Stec, B., Yang, H., Johnson, K. A., Chen, L. & Roberts, M. F. (2000). MJ0109 is an enzyme that is both an inositol monophosphatase and the 'missing' archaeal fructose-1,6-bisphosphatase. *Nat. Struct. Biol.* **7**, 1046-1050.

Steinmann, B. & Santer, R. (2012). *Inborn metabolic diseases*, pp. 157-165: Springer.

Stieglitz, K. A., Johnson, K. A., Yang, H., Roberts, M. F., Seaton, B. A., Head, J. F. & Stec, B. (2002). Crystal structure of a dual activity IMPase/FBPase (AF2372) from *Archaeoglobus fulgidus*. The story of a mobile loop. *J. Biol. Chem.* **277**, 22863-22874.

Stitt, M. (1990). Fructose-2,6-Bisphosphate as a Regulatory Molecule in Plants. *Annual Review of Plant Physiology and Plant Molecular Biology* **41**, 153-185.

Stitt, M. & Heldt, H. W. (1985). Control of photosynthetic sucrose synthesis by fructose 2,6-bisphosphate : VI. regulation of the cytosolic fructose 1,6-bisphosphatase in spinach leaves by an interaction between metabolic intermediates and fructose 2,6-bisphosphate. *Plant Physiol.* **79**, 599-608.

Stolzenberger, J., Lindner, S. N., Persicke, M., Brautaset, T. & Wendisch, V. F. (2013). Characterization of fructose 1,6-bisphosphatase and sedoheptulose 1,7-bisphosphatase from the facultative ribulose monophosphate cycle methylotroph *Bacillus methanolicus*. *J. Bacteriol.* **195**, 5112-5122.

Sun, Q. A., Chen, X. X., Ma, J. H., Peng, H. Y., Wang, F., Zha, X. J., Wang, Y. N., Jing, Y. L., Yang, H. W., Chen, R. R., Chang, L., Zhang, Y., Goto, J., Onda, H., Chen, T., Wang, M. R., Lu, Y. Y., You, H., Kwiatkowski, D. & Zhang, H. B. (2011). Mammalian target of rapamycin up-regulation of pyruvate kinase isoenzyme type

- M2 is critical for aerobic glycolysis and tumor growth. *Proc. Natl. Acad. Sci. U. S. A.* **108**, 4129-4134.
- Szöör, B., Haanstra, J. R., Gualdrón-López, M. & Michels, P. A. M. (2014). Evolution, dynamics and specialized functions of glycosomes in metabolism and development of trypanosomatids. *Curr. Opin. Microbiol.* **22**, 79-87.
- Tai, W. T., Hung, M. H., Chu, P. Y., Chen, Y. L., Chen, L. J., Tsai, M. H., Chen, M. H., Shiau, C. W., Boo, Y. P. & Chen, K. F. (2016). SH2 domain-containing phosphatase 1 regulates pyruvate kinase M2 in hepatocellular carcinoma. *Oncotarget*.
- Takenaka, M., Noguchi, T., Sadahiro, S., Hirai, H., Yamada, K., Matsuda, T., Imai, E. & Tanaka, T. (1991). Isolation and characterization of the human pyruvate kinase M gene. *Eur. J. Biochem.* **198**, 101-106.
- Taketa, K. & Pogell, B. M. (1965). Allosteric inhibition of rat liver fructose 1,6-diphosphatase by Adenosine 5'-monophosphate. *J. Biol. Chem.* **240**, 651-662.
- Taylor, P., Blackburn, E., Sheng, Y. G., Harding, S., Hsin, K. Y., Kan, D., Shave, S. & Walkinshaw, M. D. (2008). Ligand discovery and virtual screening using the program LIDAEUS. *Br. J. Pharmacol.* **153 Suppl 1**, S55-67.
- Tejwani, G. A. (1983). Regulation of fructose-bisphosphatase activity. *Adv. Enzymol. Relat. Areas Mol. Biol.* **54**, 121-194.
- Tillmann, H. & Eschrich, K. (1998). Isolation and characterization of an allelic cDNA for human muscle fructose-1,6-bisphosphatase. *Gene* **212**, 295-304.
- Tonus, C., Sellinger, M., Koss, K. & Neupert, G. (2012). Faecal pyruvate kinase isoenzyme type M2 for colorectal cancer screening: A meta-analysis. *World journal of gastroenterology: WJG* **18**, 4004.
- Torreele, E., Bourdin Trunz, B., Tweats, D., Kaiser, M., Brun, R., Mazue, G., Bray, M. A. & Pecoul, B. (2010). Fexinidazole—a new oral nitroimidazole drug candidate entering clinical development for the treatment of sleeping sickness. *PLoS Negl. Trop. Dis.* **4**, e923.
- Traut, T. (2008). *Allosteric Regulatory Enzymes*, edited by T. Traut, pp. 201-207. Chapel Hill, NC: Springer US.
- Tsukada, T., Kanno, O., Yamane, T., Tanaka, J., Yoshida, T., Okuno, A., Shiiki, T., Takahashi, M. & Nishi, T. (2010a). Discovery of potent and orally active tricyclic-based FBPase inhibitors. *Bioorg. Med. Chem.* **18**, 5346-5351.
- Tsukada, T., Takahashi, M., Takemoto, T., Kanno, O., Yamane, T., Kawamura, S. & Nishi, T. (2009). Synthesis, SAR, and X-ray structure of tricyclic compounds as potent FBPase inhibitors. *Bioorg. Med. Chem. Lett.* **19**, 5909-5912.
- Tsukada, T., Takahashi, M., Takemoto, T., Kanno, O., Yamane, T., Kawamura, S. & Nishi, T. (2010b). Structure-based drug design of tricyclic 8H-indeno[1,2-

- d][1,3]thiazoles as potent FBPase inhibitors. *Bioorg. Med. Chem. Lett.* **20**, 1004-1007.
- Tsukada, T., Tamaki, K., Tanaka, J., Takagi, T., Yoshida, T., Okuno, A., Shiiki, T., Takahashi, M. & Nishi, T. (2010c). A prodrug approach towards the development of tricyclic-based FBPase inhibitors. *Bioorg. Med. Chem. Lett.* **20**, 2938-2941.
- Ugurel, S., Bell, N., Sucker, A., Zimpfer, A., Rittgen, W. & Schadendorf, D. (2005). Tumor type M2 pyruvate kinase (TuM2 - PK) as a novel plasma tumor marker in melanoma. *Int. J. Cancer* **117**, 825-830.
- Uppara, M., Adaba, F., Askari, A., Clark, S., Hanna, G., Athanasiou, T. & Faiz, O. (2015). A systematic review and meta-analysis of the diagnostic accuracy of pyruvate kinase M2 isoenzymatic assay in diagnosing colorectal cancer. *World J. Surg. Oncol.* **13**, 48.
- Urness, J. M., Clapp, K. M., Timmons, J. C., Bai, X., Chandrasoma, N., Buszek, K. R. & Fenton, A. W. (2013). Distinguishing the chemical moiety of phosphoenolpyruvate that contributes to allostery in muscle pyruvate kinase. *Biochemistry* **52**, 1-3.
- Valentini, G., Chiarelli, L. R., Fortin, R., Dolzan, M., Galizzi, A., Abraham, D. J., Wang, C. Q., Bianchi, P., Zanella, A. & Mattevi, A. (2002). Structure and function of human erythrocyte pyruvate kinase - Molecular basis of nonspherocytic hemolytic anemia. *J. Biol. Chem.* **277**, 23807-23814.
- van Niekerk, D. D., Penkler, G. P., du Toit, F. & Snoep, J. L. (2016). Targeting glycolysis in the malaria parasite *Plasmodium falciparum*. *FEBS J.* **283**, 634-646.
- van Poelje, P. D., Dang, Q. & Erion, M. D. (2007). Fructose-1,6-bisphosphatase as a therapeutic target for type 2 diabetes. *Drug Discovery Today: Therapeutic Strategies* **4**, 103-109.
- van Poelje, P. D., Potter, S. C. & Erion, M. D. (2011). Fructose-1, 6-Bisphosphatase Inhibitors for Reducing Excessive Endogenous Glucose Production in Type 2 Diabetes, Vol. 203, *Diabetes - Perspectives in Drug Therapy*, edited by M. Schwanstecher, pp. 279-301. Berlin, Heidelberg: Springer Berlin Heidelberg.
- Van Schaftingen, E. & Hers, H. G. (1981). Inhibition of fructose-1,6-bisphosphatase by fructose 2,6-biphosphate. *Proc. Natl. Acad. Sci. U. S. A.* **78**, 2861-2863.
- van Veelen, C. W., Staal, G. E., Verbiest, H. & Vlug, A. M. (1977). Alanine inhibition of pyruvate kinase in gliomas and meningiomas. A diagnostic tool in surgery for gliomas? *Lancet* **2**, 384-385.
- Vander Heiden, M. G., Cantley, L. C. & Thompson, C. B. (2009). Understanding the Warburg effect: the metabolic requirements of cell proliferation. *Science* **324**, 1029-1033.

- Vander Heiden, M. G., Christofk, H. R., Schuman, E., Subtelny, A. O., Sharfi, H., Harlow, E. E., Xian, J. & Cantley, L. C. (2010). Identification of small molecule inhibitors of pyruvate kinase M2. *Biochem. Pharmacol.* **79**, 1118-1124.
- Varga, Z., Hegele, A., Stief, T., Heidenreich, A. & Hofmann, R. (2002). Determination of pyruvate kinase type tumor M2 in human renal cell carcinoma: a suitable tumor marker? *Urol. Res.* **30**, 122-125.
- Vasquez-Valdivieso, M. G. (2013). Identification of selective inhibitors of phosphofruktokinase and fructose biphosphatase as lead compounds against trypanosomatids, University of Edinburgh, Edinburgh.
- Ventrucci, M., Cipolla, A., Racchini, C., Casadei, R., Simoni, P. & Gullo, L. (2004). Tumor M2-pyruvate kinase, a new metabolic marker for pancreatic cancer. *Dig. Dis. Sci.* **49**, 1149-1155.
- Verlinde, C. L. M., Hannaert, V., Blonski, C., Willson, M., Perie, J. J., Fothergill-Gilmore, L. A., Opperdoes, F. R., Gelb, M. H., Hol, W. G. J. & Michels, P. A. M. (2001). Glycolysis as a target for the design of new anti-trypanosome drugs. *Drug Resist. Updat.* **4**, 50-65.
- Villeret, V., Huang, S., Zhang, Y., Xue, Y. & Lipscomb, W. N. (1995). Crystal structure of spinach chloroplast fructose-1,6-bisphosphatase at 2.8 Å resolution. *Biochemistry* **34**, 4299-4306.
- von Geldern, T. W., Lai, C., Gum, R. J., Daly, M., Sun, C., Fry, E. H. & Abad-Zapatero, C. (2006). Benzoxazole benzenesulfonamides are novel allosteric inhibitors of fructose-1,6-bisphosphatase with a distinct binding mode. *Bioorg. Med. Chem. Lett.* **16**, 1811-1815.
- Walsh, M. J., Brimacombe, K. R., Anastasiou, D., Yu, Y., Israelsen, W. J., Hong, B. S., Tempel, W., Dimov, S., Veith, H., Yang, H., Kung, C., Yen, K. E., Dang, L., Salituro, F., Auld, D. S., Park, H. W., Vander Heiden, M. G., Thomas, C. J., Shen, M. & Boxer, M. B. (2010a). *Probe Reports from the NIH Molecular Libraries Program*. Bethesda (MD): National Center for Biotechnology Information (US).
- Walsh, M. J., Brimacombe, K. R., Vasquez-Valdivieso, M. G., Auld, D. S., Simeonov, A., Morgan, H. P., Fothergill-Gilmore, L. A., Michels, P. A. M., Walkinshaw, M. D., Shen, M. & Boxer, M. B. (2010b). *Probe Reports from the NIH Molecular Libraries Program*. Bethesda (MD): National Center for Biotechnology Information (US).
- Walsh, M. J., Brimacombe, K. R., Veith, H., Bougie, J. M., Daniel, T., Leister, W., Cantley, L. C., Israelsen, W. J., Vander Heiden, M. G., Shen, M., Auld, D. S., Thomas, C. J. & Boxer, M. B. (2011). 2-Oxo-N-aryl-1,2,3,4-tetrahydroquinoline-6-sulfonamides as activators of the tumor cell specific M2 isoform of pyruvate kinase. *Bioorg. Med. Chem. Lett.* **21**, 6322-6327.
- Wang, C., Chiarelli, L. R., Bianchi, P., Abraham, D. J., Galizzi, A., Mattevi, A., Zanella, A. & Valentini, G. (2001). Human erythrocyte pyruvate kinase:

- characterization of the recombinant enzyme and a mutant form (R510Q) causing nonspherocytic hemolytic anemia. *Blood* **98**, 3113-3120.
- Wang, H.-J., Hsieh, Y.-J., Cheng, W.-C., Lin, C.-P., Lin, Y.-s., Yang, S.-F., Chen, C.-C., Izumiya, Y., Yu, J.-S., Kung, H.-J. & Wang, W.-C. (2014). JMJD5 regulates PKM2 nuclear translocation and reprograms HIF-1 α -mediated glucose metabolism. *Proceedings of the National Academy of Sciences* **111**, 279-284.
- Wang, P., Sun, C., Zhu, T. & Xu, Y. (2015). Structural insight into mechanisms for dynamic regulation of PKM2. *Protein Cell* **6**, 275-287.
- Wang, Z., Chatterjee, D., Jeon, H. Y., Akerman, M., Vander Heiden, M. G., Cantley, L. C. & Krainer, A. R. (2012). Exon-centric regulation of pyruvate kinase M alternative splicing via mutually exclusive exons. *J. Mol. Cell Biol.* **4**, 79-87.
- Warburg, O., Wind, F. & Negelein, E. (1927). The metabolism of tumors in the body. *The Journal of general physiology* **8**, 519-530.
- Warner, S. L., Carpenter, K. J. & Bearss, D. J. (2014). Activators of PKM2 in cancer metabolism. *Future Med Chem* **6**, 1167-1178.
- Wechsel, H. W., Petri, E., Bichler, K. H. & Feil, G. (1999). Marker for renal cell carcinoma (RCC): The dimeric form of pyruvate kinase type M-2 (Tu M2-PK). *Anticancer Res.* **19**, 2583-2590.
- Weeks, C. M., Roszak, A. W., Erman, M., Kaiser, R., Jornvall, H. & Ghosh, D. (1999). Structure of rabbit liver fructose 1,6-bisphosphatase at 2.3 Å resolution. *Acta Crystallogr. D Biol. Crystallogr.* **55**, 93-102.
- Weinberger, R., Appel, B., Stein, A., Metz, Y., Neheman, A. & Barak, M. (2007). The pyruvate kinase isoenzyme M2 (Tu M2-PK) as a tumour marker for renal cell carcinoma. *Eur. J. Cancer Care (Engl.)* **16**, 333-337.
- WHO (2010). *First WHO report on neglected tropical diseases: Working to overcome the global impact of neglected tropical diseases*: World Health Organization.
- WHO (2012). *Accelerating work to overcome the global impact of neglected tropical diseases. A road map for implementation*. Washington, DC: WHO.
- World Health Organization (2015a). *Fact sheets relating to NTD*, http://www.who.int/neglected_diseases/mediacentre/factsheet/en/.
- WHO (2015b). *Investing to overcome the global impact of neglected tropical diseases: third WHO report on neglected diseases 2015*. World Health Organization.
- Williams, R., Holyoak, T., McDonald, G., Gui, C. & Fenton, A. W. (2006). Differentiating a ligand's chemical requirements for allosteric interactions from those for protein binding. Phenylalanine inhibition of pyruvate kinase. *Biochemistry* **45**, 5421-5429.

Winn, M. D., Ballard, C. C., Cowtan, K. D., Dodson, E. J., Emsley, P., Evans, P. R., Keegan, R. M., Krissinel, E. B., Leslie, A. G. W., McCoy, A., McNicholas, S. J., Murshudov, G. N., Pannu, N. S., Potterton, E. A., Powell, H. R., Read, R. J., Vagin, A. & Wilson, K. S. (2011). Overview of the CCP4 suite and current developments. *Acta Crystallographica Section D* **67**, 235-242.

Winter, G. (2009). xia2: an expert system for macromolecular crystallography data reduction. *Journal of Applied Crystallography* **43**, 186-190.

Wolf, A., Agnihotri, S., Micallef, J., Mukherjee, J., Sabha, N., Cairns, R., Hawkins, C. & Guha, A. (2011). Hexokinase 2 is a key mediator of aerobic glycolysis and promotes tumor growth in human glioblastoma multiforme. *J. Exp. Med.* **208**, 313-326.

Wong, N., Ojo, D., Yan, J. & Tang, D. (2015). PKM2 contributes to cancer metabolism. *Cancer Lett.* **356**, 184-191.

Wong, T. S., Liu, X. B., Ho, A. C. W., Yuen, A. P. W., Ng, R. W. M. & Wei, W. I. (2008). Identification of pyruvate kinase type M2 as potential oncoprotein in squamous cell carcinoma of tongue through microRNA profiling. *Int. J. Cancer* **123**, 251-257.

Wright, S. W., Carlo, A. A., Carty, M. D., Danley, D. E., Hageman, D. L., Karam, G. A., Levy, C. B., Mansour, M. N., Mathiowetz, A. M., McClure, L. D., Nestor, N. B., McPherson, R. K., Pandit, J., Pustilnik, L. R., Schulte, G. K., Soeller, W. C., Treadway, J. L., Wang, I. K. & Bauer, P. H. (2002). Anilinoquinazoline inhibitors of fructose 1,6-bisphosphatase bind at a novel allosteric site: synthesis, in vitro characterization, and X-ray crystallography. *J. Med. Chem.* **45**, 3865-3877.

Wright, S. W., Carlo, A. A., Danley, D. E., Hageman, D. L., Karam, G. A., Mansour, M. N., McClure, L. D., Pandit, J., Schulte, G. K., Treadway, J. L., Wang, I. K. & Bauer, P. H. (2003). 3-(2-Carboxyethyl)-4,6-dichlor-1H-indole-2-carboxylic acid: An allosteric inhibitor of fructose-1,6-bisphosphatase at the AMP site. *Bioorg. Med. Chem. Lett.* **13**, 2055-2058.

Wu, S. Y., McNae, I., Kontopidis, G., McClue, S. J., McInnes, C., Stewart, K. J., Wang, S., Zheleva, D. I., Marriage, H., Lane, D. P., Taylor, P., Fischer, P. M. & Walkinshaw, M. D. (2003). Discovery of a novel family of CDK inhibitors with the program LIDAEUS: structural basis for ligand-induced disordering of the activation loop. *Structure* **11**, 399-410.

Xie, X., Wang, M., Mei, J., Hu, F., Ding, F. & Lv, L. (2015). Pyruvate kinase M2 interacts with DNA damage-binding protein 2 and reduces cell survival upon UV irradiation. *Biochem. Biophys. Res. Commun.* **467**, 427-433.

Xu, Y., Liu, X.-H., Saunders, M., Pearce, S., Foulks, J. M., Parnell, K. M., Clifford, A., Nix, R. N., Bullough, J., Hendrickson, T. F., Wright, K., McCullar, M. V., Kanner, S. B. & Ho, K.-K. (2014). Discovery of 3-(trifluoromethyl)-1H-pyrazole-5-carboxamide activators of the M2 isoform of pyruvate kinase (PKM2). *Bioorg. Med. Chem. Lett.* **24**, 515-519.

- Yacovan, A., Ozeri, R., Kehat, T., Mirilashvili, S., Sherman, D., Aizikovitch, A., Shitrit, A., Ben-Zeev, E., Schutz, N., Bohana-Kashtan, O., Konson, A., Behar, V. & Becker, O. M. (2012). 1-(sulfonyl)-5-(arylsulfonyl)indoline as activators of the tumor cell specific M2 isoform of pyruvate kinase. *Bioorg. Med. Chem. Lett.* **22**, 6460-6468.
- Yamey, G. & Hotez, P. (2007). Neglected tropical diseases. *BMJ : British Medical Journal* **335**, 269-270.
- Yan, X. & Maier, C. S. (2009). Hydrogen/deuterium exchange mass spectrometry. *Methods Mol. Biol.* **492**, 255-271.
- Yang, W. & Lu, Z. (2013). Nuclear PKM2 regulates the Warburg effect. *Cell Cycle* **12**, 0-4.
- Yang, W. & Lu, Z. (2015). Pyruvate kinase M2 at a glance. *J. Cell Sci.*
- Yang, W., Xia, Y., Hawke, D., Li, X., Liang, J., Xing, D., Aldape, K., Hunter, T., Alfred Yung, W. & Lu, Z. (2012a). PKM2 phosphorylates histone H3 and promotes gene transcription and tumorigenesis. *Cell* **150**, 685-696.
- Yang, W., Xia, Y., Ji, H., Zheng, Y., Liang, J., Huang, W., Gao, X., Aldape, K. & Lu, Z. (2011). Nuclear PKM2 regulates beta-catenin transactivation upon EGFR activation. *Nature* **480**, 118-122.
- Yang, W., Zheng, Y., Xia, Y., Ji, H., Chen, X., Guo, F., Lyssiotis, C. A., Aldape, K., Cantley, L. C. & Lu, Z. (2012b). ERK1/2-dependent phosphorylation and nuclear translocation of PKM2 promotes the Warburg effect. *Nat. Cell Biol.* **14**, 1295-1304.
- York, J. D., Ponder, J. W. & Majerus, P. W. (1995). Definition of a metal-dependent/Li(+)-inhibited phosphomonoesterase protein family based upon a conserved three-dimensional core structure. *Proceedings of the National Academy of Sciences* **92**, 5149-5153.
- Yu, Z., Zhao, X., Huang, L., Zhang, T., Yang, F., Xie, L., Song, S., Miao, P., Zhao, L., Sun, X., Liu, J. & Huang, G. (2013). Proviral insertion in murine lymphomas 2 (PIM2) oncogene phosphorylates pyruvate kinase M2 (PKM2) and promotes glycolysis in cancer cells. *J. Biol. Chem.* **288**, 35406-35416.
- Zarzycki, M., Kolodziejczyk, R., Maciaszczyk-Dziubinska, E., Wysocki, R., Jaskolski, M. & Dzugaj, A. (2011). Structure of E69Q mutant of human muscle fructose-1,6-bisphosphatase. *Acta Crystallographica Section D-Biological Crystallography* **67**, 1028-1034.
- Zhan, C., Shi, Y., Lu, C. & Wang, Q. (2013). Pyruvate kinase M2 is highly correlated with the differentiation and the prognosis of esophageal squamous cell cancer. *Dis. Esophagus* **26**, 746-753.
- Zhang, B., Chen, J. Y., Chen, D. D., Wang, G. B. & Shen, P. (2004). Tumor type M-2 pyruvate kinase expression in gastric cancer, colorectal cancer and controls. *World J. Gastroenterol.* **10**, 1643-1646.

Zhang, Y., Liu, B., Wu, X., Li, R., Ning, X., Liu, Y., Liu, Z., Ge, Z., Li, R. & Yin, Y. (2015). New pyridin-3-ylmethyl carbamodithioic esters activate pyruvate kinase M2 and potential anticancer lead compounds. *Bioorg. Med. Chem.*

Zhao, Q. H., Cao, Y., Wang, Y., Hu, C. L., Hu, A. L., Ruan, L., Bo, Q. L., Liu, Q. F., Chen, W. J., Tao, F. B., Ren, M., Ge, Y. S., Chen, A. G. & Li, L. (2014). Plasma and tissue free amino acid profiles and their concentration correlation in patients with lung cancer. *Asia Pac. J. Clin. Nutr.* **23**, 429-436.

Zhao, Y., Butler, E. B. & Tan, M. (2013). Targeting cellular metabolism to improve cancer therapeutics. *Cell Death Dis.* **4**, e532.

Zhao, Y., Coloff, J. L., Ferguson, E. C., Jacobs, S. R., Cui, K. & Rathmell, J. C. (2008). Glucose metabolism attenuates p53 and Puma-dependent cell death upon growth factor deprivation. *J. Biol. Chem.* **283**, 36344-36353.

Zhong, W. (2013). Biochemical and Structural Studies on Trypanosomatid Pyruvate Kinases, University of Edinburgh, Edinburgh.

Zhong, W., Morgan, H. P., Nowicki, M. W., McNae, I. W., Yuan, M., Bella, J., Michels, P. A., Fothergill-Gilmore, L. A. & Walkinshaw, M. D. (2014). Pyruvate kinases have an intrinsic and conserved decarboxylase activity. *Biochem. J.* **458**, 301-311.

Zhong, W. H., Morgan, H. P., McNae, I. W., Michels, P. A. M., Fothergill-Gilmore, L. A. & Walkinshaw, M. D. (2013). 'In crystallo' substrate binding triggers major domain movements and reveals magnesium as a co-activator of *Trypanosoma brucei* pyruvate kinase. *Acta Crystallographica Section D-Biological Crystallography* **69**, 1768-1779.

Zimmermann, G., Kelly, G. J. & Latzko, E. (1978). Purification and properties of spinach leaf cytoplasmic fructose-1,6-bisphosphatase. *J. Biol. Chem.* **253**, 5952-5956.

Zoraghi, R., See, R. H., Axerio-Cilies, P., Kumar, N. S., Gong, H., Moreau, A., Hsing, M., Kaur, S., Swayze, R. D., Worrall, L., Amandoron, E., Lian, T., Jackson, L., Jiang, J., Thorson, L., Labriere, C., Foster, L., Brunham, R. C., McMaster, W. R., Finlay, B. B., Strynadka, N. C., Cherkasov, A., Young, R. N. & Reiner, N. E. (2011a). Identification of pyruvate kinase in methicillin-resistant *Staphylococcus aureus* as a novel antimicrobial drug target. *Antimicrob. Agents Chemother.* **55**, 2042-2053.

Zoraghi, R., Worrall, L., See, R. H., Strangman, W., Popplewell, W. L., Gong, H., Samaai, T., Swayze, R. D., Kaur, S., Vuckovic, M., Finlay, B. B., Brunham, R. C., McMaster, W. R., Davies-Coleman, M. T., Strynadka, N. C., Andersen, R. J. & Reiner, N. E. (2011b). Methicillin-resistant *Staphylococcus aureus* (MRSA) pyruvate kinase as a target for bis-indole alkaloids with antibacterial activities. *J. Biol. Chem.* **286**, 44716-44725.

